AD

USAAVLABS TECHNICAL REPORT 68-72

SOFT IN-PLANE MATCHED-STIFFNESS/FLEXURE-ROOT-BLADE ROTOR SYSTEM SUMMARY REPORT

By

Salvatore V. Cardinale

August 1968

U. S. ARMY AVIATION MATERIEL LABORATORIES
FORT EUSTIS, VIRGINIA

CONTRACT DA 44-177-AMC-244(T)
LOCKHEED-CALIFORNIA COMPANY
A DIVISION OF LOCKHEED AIRCRAFT CORPORATION
BURBANK, CALIFORNIA

179

DEPARTMENT OF THE ARMY
U. S. ARMY AVIATION MATERIEL LABORATORIES
FORT EUSTIS, VIRGINIA 23604

This report has been reviewed by the U. S. Army Aviation Materiel Laboratories and is considered to be technically sound. It is published for exchange of information and stimulation of ideas.

Task 1F16[illegible]04A13903
Contract DA 44-177-AMC-244(T)
USAAVLABS Technical Report 68-72
August 1969

SOFT IN-PLANE MATCHED-STIFFNESS/FLEXURE-ROOT-BLADE ROTOR SYSTEM SUMMARY REPORT

Final Report

Lockheed Report 19556

Prepared by

Lockheed-California Company
A Division of Lockheed Aircraft Corporation
Burbank, California

for

U.S. ARMY AVIATION MATERIEL LABORATORIES
FORT EUSTIS, VIRGINIA

SUMMARY

A flight research program was conducted to explore the feasibility and operating characteristics of a matched-stiffness rigid rotor which was designed to have sufficient torsional flexibility to eliminate the need for feathering bearings. The desired stiffness characteristics were obtained by use of a low in-plane stiffness, equal to the flapping stiffness. The result was a rotor which had a first in-plane frequency lower than its rotational frequency (.65P at the normal operating rpm).

An analytical and experimental program was conducted in which the soft in-plane matched-stiffness rigid rotor was test flown on an XH-51A helicopter. This report discusses the design, analysis, and testing aspects of the program. Also included in the report is a discussion which reviews the features of a matched-stiffness rotor that make it attractive.

The particular system tested had satisfactory rotational speed margins for on-the-ground mechanical stability (ground resonance), when takeoffs and landings were performed from and onto a smooth prepared surface. In free flight, however, the system had marginal mechanical stability at a rotational speed 11 percent below normal operating speed, a condition which is given the name "air resonance".

An extensive on-the-ground test program was conducted prior to flight testing. Whirl tower tests were made to assess rotational speed boundaries relative to on-the-ground and in-flight mechanical instabilities (the whirl tower included a gimbaled inertia frame). Ground tests were conducted to assess the effects of various landing gear contact and rotor lift conditions.

A goal of the program was to demonstrate satisfactory mechanical stability in flight at rotor rotational speeds below the normal operating speed; at rotor speeds reduced to values associated with autorotation maneuvers. During flight tests, however, stability became marginal at 89 percent of the normal operating speed, a higher value than had been expected. This high value was concluded to leave an inadequate margin for flight safety and was cause for stopping the flight program.

Mechanical coupling was introduced into the rotor during the program. It was the intention that the coupling would produce beneficial aerodynamic damping that would improve the stability margin. The particular coupling geometry that was tested did not prove fruitful, however. Contrary to this experience, analysis results indicated that the use of mechanical coupling could still be the answer, but it was concluded that extension of the analytical study was beyond the scope of this program.

The limited range of rotor rotational speeds that was established in this program is reason to conclude that the soft in-plane matched-stiffness concept is not yet developed to the extent necessary to consider it practical for use in the immediate future.

FOREWORD

The program was conducted by the Lockheed-California Company, under Contract DA 44-177-AMC-244(T), sponsored by the U.S. Army Aviation Materiel Laboratories (USAAVLABS), Fort Eustis, Virginia. Technical monitor was H.I. MacDonald of USAAVLABS.

Analytical studies were conducted at Lockheed under the direction of Dr. Richard M. Carlson, Division Engineer, Rotary Wing, during January to October, 1965. The design and test programs were conducted by a team of rotary-wing specialists in design, design analysis, rotor dynamics, and ground and flight testing under the direction of D.T. Sasaki, Project Leader. Technical consultation was provided by I.H. Culver and J.F. Johnston. D.R. Segner was the test pilot. Design and fabrication of the test rotor and ground and flight tests were done between October 1965 and July 1966.

The final report was prepared by S.V. Cardinale of Lockheed, in cooperation with R.E. Donham and I.B. Sachs of Lockheed and H.I. MacDonald of USAAVLABS.

TABLE OF CONTENTS

TABLE OF CONTENTS (Continued)

LIST OF ILLUSTRATIONS

LIST OF ILLUSTRATIONS (Continued)

LIST OF ILLUSTRATIONS (Continued)

LIST OF ILLUSTRATIONS (Continued)

LIST OF TABLES

LIST OF SYMBOLS

B_o	Flapping angular displacement due to static load
CF	Centrifugal force, lb
E	In-plane bending angular displacement due to static load; or, Modulus of elasticity, psi
F	Force, lb
f	Applied stress, psi; or, Frequency, cps or cpm
F_{su}	Ultimate allowable shear stress, psi
F_{tu}	Ultimate allowable tensile stress, psi
G	Shear modulus, psi
I	Area moment of inertia, $in.^4$
ΔI_ϕ	Increment of mass moment of inertia of vehicle in roll, $slug\text{-}feet^2$
K_β	Rotor stiffness at the hub, $\frac{\partial M}{\partial \beta}$, ft-lb/rad
K_{β_o}	Flapping stiffness of blade outboard of feathering bearing, $\frac{\partial M}{\partial \beta_o}$, ft-lb/rad
K_ϵ	In-plane stiffness of blade outboard of feathering bearing, $\frac{\partial M}{\partial \epsilon}$, ft-lb/rad
M	Bending moment, in.-lb
MS	Margin of safety
P	Rotor rotational frequency, cps or cpm; or, Load, lb
rpm	Revolutions per minute
S	Shear load, lb
shp	Shaft horsepower
Tan α_3	Pitch-lag coupling: mechanical coupling between in-plane and feathering motions. As used in this report, Tangent α_3 represents the ratio of feathering motion to in-plane motion occurring at the in-board end of the control torque tube. Positive α_3 is noseup feathering for aft in-plane bending.
$\bar{\beta}_o$	Flapping angular displacement due to perturbational load

δ	Deflection, in.
$\tan \delta_3$	Pitch-flap coupling: mechanical coupling between flapping and feathering motions. As used in this report, Tangent δ_3 represents the ratio of feathering motion to flapping motion occurring at the inboard end of the control torque tube. Positive δ_3 is noseup feathering for down flapwise bending.
$\bar{\epsilon}$	In-plane bending angular displacement due to perturbational load
ξ	Fraction of critical damping
θ	Blade pitch angle, radians or degrees; or, Torsional deflection, degrees
Ω	Rotor speed, radians per second
ω_{ip}	Blade first harmonic in-plane bending frequency, radians per second

SECTION 1

INTRODUCTION

1.1 BACKGROUND

A joint NASA-USAAVLABS-Lockheed program was established to explore the feasibility and potential benefits of the matched-stiffness flexure-root rigid-rotor concept, one which involves rotor blade in-plane stiffness reduced to a value nearly equal to flapping stiffness.

In an earlier study, under USAAVLABS Contract DA 44-177-TC-828, a 10-foot-diameter four-bladed matched-stiffness rotor was tested in the NASA-Langley wind tunnel. The results of this study encouraged additional research. A follow-on study, under Contract DA 44-177-AMC-78(T), was performed to explore dynamic and general characteristics of the matched-stiffness concept, which included the added feature of a torsionally soft flexure-root in lieu of feathering bearings. Wind tunnel model tests showed such a system to produce low in-plane loads and no indication of control coupling or rotor pitchup.

Based on the results of these earlier programs, USAAVLABS and the Lockheed-California Company entered into Contract DA 44-177-AMC-244(T) for a flight research program of a full-scale soft in-plane matched-stiffness/flexure-root rigid-rotor system. The objective was to determine the feasibility and operating characteristics of the rotor system in a program that included flight tests on an XH-51A helicopter. A photograph of the flight test vehicle is shown in Figure 1.

Results of preliminary analytical design studies, reported in Reference 1, indicated that an aircraft equipped with a soft in-plane matched-stiffness rotor should be designed to have both roll and pitch natural frequencies (in flight) at values below that defined by subtracting the first in-plane bending frequency from the rotational frequency of the rotor at normal operating speed. The test aircraft had this characteristic; it was also provided with an adjustable natural frequency through the use of an adjustable mass moment of inertia.

Flight tests included hover and flight at forward speeds up to 60 knots.

1.2 BASIC THEORY OF THE MATCHED-STIFFNESS CONCEPT

The XH-51A rigid-rotor helicopter, viewed from a dynamic behavior viewpoint, consists of a rotor which acts as a flexible gyroscope, connected

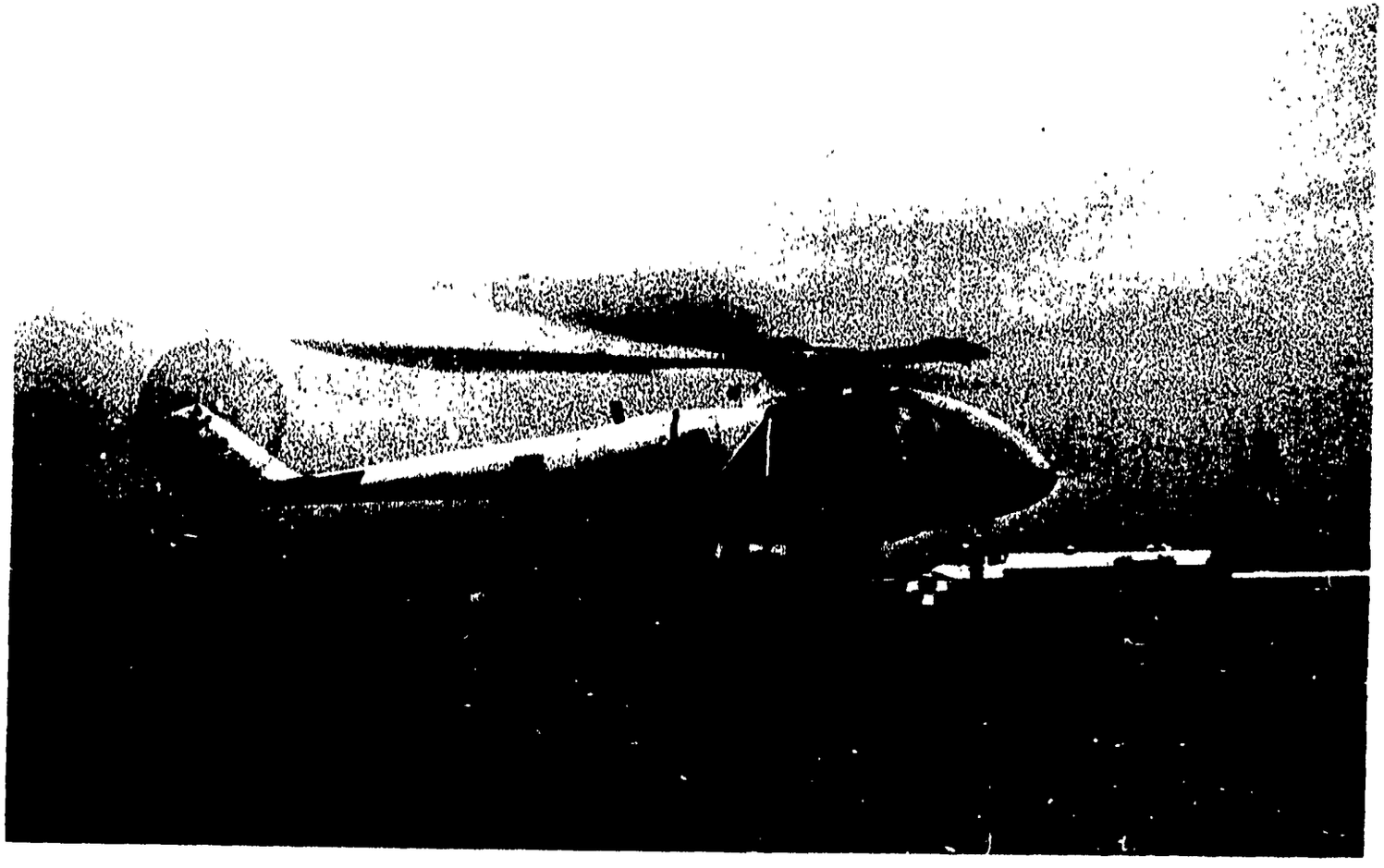

Figure 1. First Flight of the Test Aircraft With the Soft In-Plane Matched-Stiffness Rotor.

to a body, and slaved to a control gyroscope.* The control gyro is designed to receive command signals from the pilot and vehicle disturbance signals from the rotor and body. Associated with the disturbance signals (feed-back signals) is an undesirable characteristic: the magnitude of the feedback is sensitive to changes in mean levels of lift and power. Unwanted components of the feedback signal develop in the form of blade feathering moments due to coupling of steady and cyclic structural deformation of the rotor blades. It will be shown that the undesirable coupling can be eliminated by adjusting the stiffness characteristics of the rotor blades. A rotor system in which the coupling has been eliminated would generate the cyclic feedback signals necessary for maintaining aircraft stability separate from those associated with power or load factor changes.

A rotor designed to separate desirable and undesirable cyclic signals could conceivably have a number of benefits. Since a reduction of control system forces is implied, a small control gyro and small control system components are foreseen. The reduction of forces and elimination of cross coupling suggests improved stability characteristics. Other advantages could be: elimination of feathering bearings, low blade loads, low drag, low vibration, and general control system simplification.

The manner in which the undesirable feedback is eliminated by matching stiffnesses is qualitatively explained through use of the schematic representation of a rotor blade shown in Figure 2. The elastic blade is represented by two inelastic beams connected by springs, K_{β_o} and K_{ϵ}, which represent the flapping and in-plane stiffnesses, respectively.

The rotor blade is designed to have cone and sweep angles. Therefore, angular deflections of the outer beam in the flapping and in-plane directions will cause bending moments in each direction to develop feathering moments. These feathering moments generate feedback signals to the control gyro. The bending moments are expressed as functions of angular motions and spring rates, thus:

$$M_{FLAPPING} = K_{\beta_o} (B_o \pm \bar{\beta}_o)$$

$$M_{IN\text{-}PLANE} = K_{\epsilon} (E \pm \bar{\epsilon})$$

---

* Readers not familiar with the control gyroscope concept of the XH-51A rigid-rotor system may refer to "Response Characteristics of the Gyro-Controlled Lockheed Rotor System", by Dr. G. J. Sissingh, Vol 12, No. 14 of the Journal of the American Helicopter Society, October 1967.

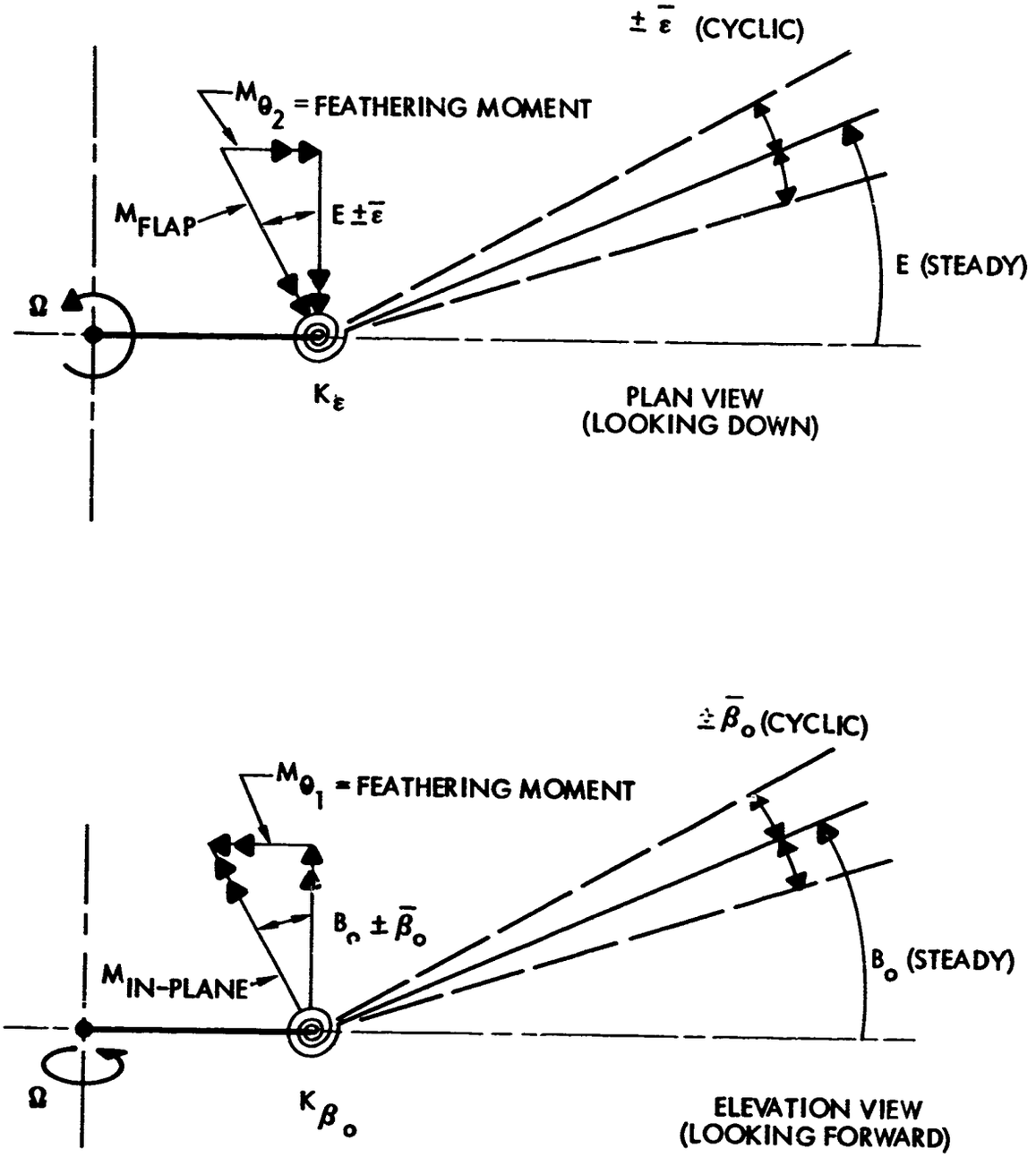

Figure 2. Schematic of Rotor Blade Showing Development of Feathering Moment Components From Flapping and In-Plane Structural (Elastic) Deflections.

The feathering moment components are expressed as

$$M_{\theta_1} = K_{\beta_o} (B_o \pm \bar{\beta}_o) \sin (E \pm \bar{\epsilon})$$

$$M_{\theta_2} = K_{\epsilon} (E \pm \bar{\epsilon}) \sin (B_o \pm \bar{\beta}_o)$$

The net feathering moment is the difference between M_{θ_1} and M_{θ_2}. Simplified per a small-angle assumption, the net feathering moment can be expressed as

$$M_{\theta} = K_{\epsilon} (E \pm \bar{\epsilon}) (B_o \pm \bar{\beta}_o) - K_{\beta_o} (\bar{B}_o + \bar{\beta}_o) (E \pm \bar{\epsilon})$$

This equation contains terms which are products of steady motions only, terms which are products of cyclic motions only, and terms which are products of both steady and cyclic motions. Since the main interest has been identified as the coupled motions, the character of the undesirable coupling can be studied by isolating and examining those terms containing the products of steady and cyclic motions. Extracting these increments of feathering moment from the preceding equation gives

$$\Delta M_{\theta} = K_{\epsilon} (\pm \bar{\beta}_o E \pm \bar{\epsilon} B_o) - K_{\beta_o} (\pm \bar{\beta}_o E \pm \bar{\epsilon} B_o)$$

$$= \pm \bar{\beta}_o E (K_{\epsilon} - K_{\beta_o}) \pm \bar{\epsilon} B_o (K_{\epsilon} - K_{\beta_o})$$

It can be seen that the coupled terms will disappear if K_{ϵ} and K_{β_o} are equal to each other; that is, by matching the flapping and in-plane stiffness coupling of steady and cyclic structural deformations is eliminated. This observation is the basis for considering the use of a matched-stiffness rotor for eliminating undesirable feedback signals.

In the original XH-51A rigid rotor, the in-plane stiffness is considerably larger than the flapping stiffness, the undesirable feedback signals due to coupling are tolerably small compared with desirable feedback signals. This is due to relatively large sweep and cone angles and a relatively large control gyroscope. These built-in angles, which are designed into the rotor (rather than induced by structural elasticity) are basic elements of the Lockheed rigid-rotor control and stabilization system. The system depends on sensing cyclic disturbances through a feedback from the rotor blade to the gyroscope. The sweep and cone angles are designed to produce relatively strong feedback signals, thus making the undesirable signals small by comparison.

SECTION 2

CONSIDERATIONS PERTINENT TO DEFINING THE TEST CONFIGURATION

Since the primary objective of the research was to determine the feasibility of providing an operational helicopter with a matched-stiffness rotor system having no feathering bearings, an initial task was to establish the design characteristics of a rotor system with the desired stiffness features sized to fit the test aircraft.

Attaining a matched-stiffness blade involves changing the relative proportions of flapping and in-plane stiffnesses from those which had been successfully used in the past; and attaining a low torsional stiffness to enable the blade to feather without the use of feathering bearings involves the use of low in-plane stiffness. The result is a blade with a first in-plane frequency below the operating rotational frequency. This introduces the possibility of developing mechanical instability in the form of ground or air resonance. The problem was to design a system which was tailored both to provide the highly desirable soft in-plane matched-stiffness feature and yet not be sensitive to ground and air resonance within selected operating rotational speed boundaries.

2.1 THE GROUND/AIR RESONANCE PROBLEM

The mechanical instability associated with softening the in-plane stiffness, identified in the literature as "ground resonance", can involve any body mode that includes in-plane hub motion and the first in-plane blade motion. It occurs when the value "rotor rpm minus the first in-plane frequency" $(\Omega - \omega_{ip})$ matches, or is close to, a body mode natural frequency. The instability is basically mechanical. It obtains driving energy from the rotating rotor and from power turning the rotor (shaft torque). It does not develop from aerodynamic forces. The following qualitative review is given to acquaint the reader with the phenomenon.

A particular in-plane oscillatory mode of the blades of a nonrotating four-bladed rotor is shown in Figure 3. If the frequency of this vibration mode is designated ω_{ip}, then,

$$\omega_{ip} = \frac{2\pi}{\tau} \text{ radians per second}$$

The center of gravity of the rotor disk can be said to whirl about the center of rotation at an angular velocity equal to ω_{ip}. Comparing the

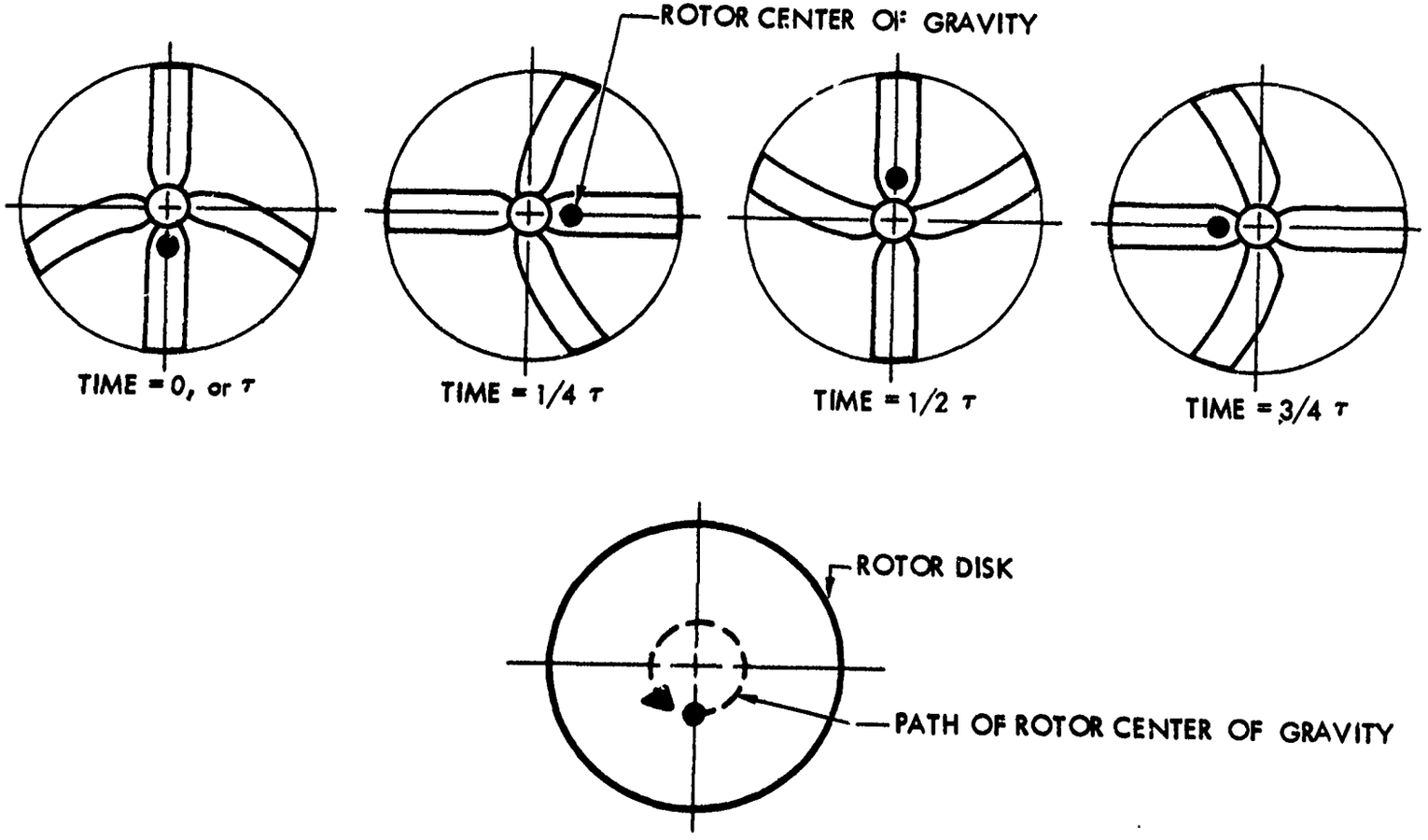

Figure 3. In-Plane Oscillatory Mode of Blades of a Nonrotating Rotor.

frequency of the oscillation mode with the rotor rotational speed, relative to the nonrotating helicopter body, the following are observed:

- At rotor speeds where $\Omega<\omega_{ip}$, the oscillation drives the rotor system. In this case the vibration energy is absorbed by the rotor/engine system.

- As rotor speed is increased to where $\Omega>\omega_{ip}$, the engine and whirling rotor hub feed energy into the vibrating system.

The oscillating rotor can excite the body's natural modes. Sketch (a) of Figure 4 illustrates how horizontal vibratory forces due to the oscillating rotor produce oscillatory pitching and rolling moments. The frequency of these moments is $\Omega-\omega_{ip}$.

The helicopter on the ground, shown schematically in sketch (b), is effectively a spring-supported mass having natural frequencies in pitch and roll related to the helicopter mass moments of inertia and the spring characteristics of the landing gear. When subjected to the oscillatory horizontal forces, the spring-mass system is subjected to a forced vibration. If $\Omega-\omega_{ip}$ is a value which causes the vibration to occur at a frequency near a natural frequency, a resonant condition severe enough to be catastrophic can result. This phenomenon is generally called "ground resonance". Classical analytical studies of ground resonance are reported in References 2, 3, and 4.

A similar instability can occur when the helicopter is airborne; this situation is referred to herein as "air resonance". The spring-mass system representing the airborne helicopter is shown in sketch (c).

The dynamic response of the structures can be modified by tailoring the stiffness to separate $\Omega-\omega_{ip}$ from natural frequencies, and by introducing damping. Dampers are generally included in landing gear and lead-lag motion systems of articulated rotors for the express purpose of preventing ground resonance. Air resonance is not a problem in articulated rotor systems since they have such low flapping stiffnesses, and corresponding low body natural frequencies.

A rigid-rotor system, which is very stiff in-plane, will not experience air or ground resonance because of the relative magnitudes of the driving frequency $\Omega-\omega_{ip}$ and body natural frequencies either in the air or on the ground. However, lowering the in-plane stiffness of the rigid rotor, to obtain the soft in-plane matched-stiffness characteristics, introduces potential mechanical instability both on the ground and in flight, unless means to avoid these phenomena are provided.

2.2 DESIGN CONSIDERATIONS FOR AVOIDING OR ATTENUATING RESONANCE

The qualitative review is continued, to illustrate the reasoning behind the choice of features for design of the test rotor. Relationships between the

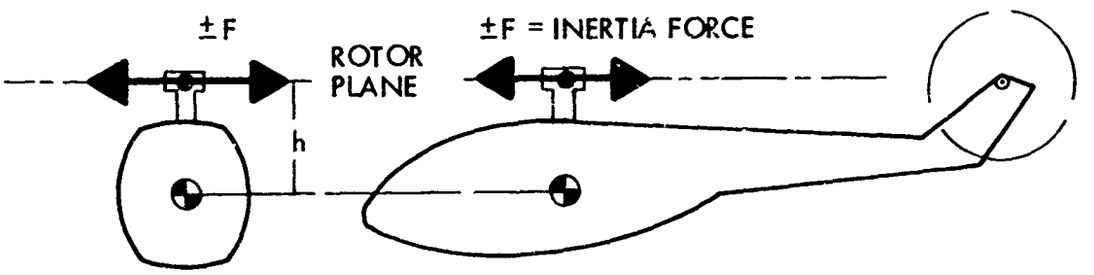

(a) HORIZONTAL VIBRATORY INERTIA FORCES PRODUCE OSCILLATORY PITCHING AND ROLLING MOMENTS ABOUT AIRCRAFT CENTER OF GRAVITY

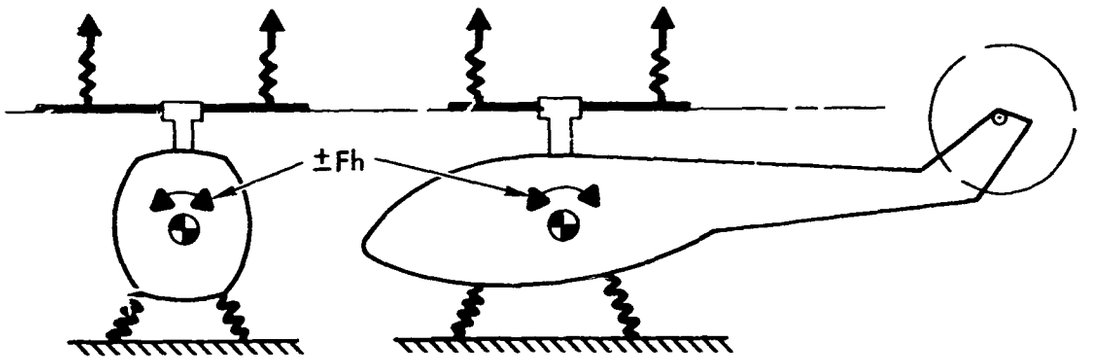

(b) ON THE GROUND - SPRINGS REPRESENT LANDING GEAR AND ROTOR FLAPPING STIFFNESSES

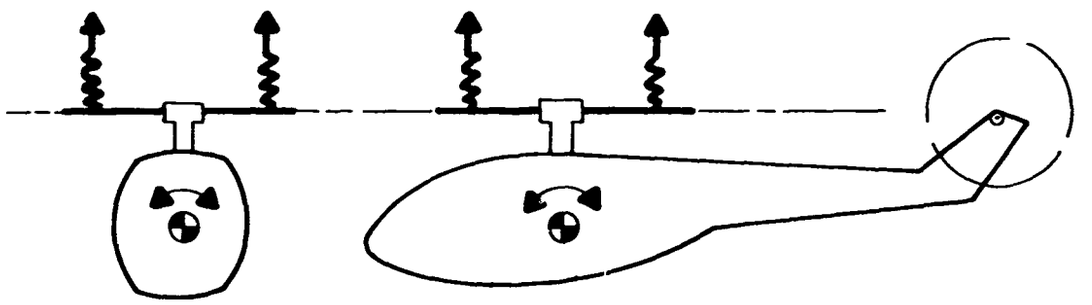

(c) IN THE AIR - SPRINGS REPRESENT ROTOR FLAPPING STIFFNESS

Figure 4. Schematic of Vibratory Moments and Spring-Mass Systems.

driving frequency and the rotor speed are examined. Figure 5 shows the basic relationship. For a rigid rotor, no driving energy is available in the region to the left of $\Omega = \omega_{ip}$, whereas to the right of this point the existence of a source of driving energy is indicated. This is simply a graphic representation of the mechanism described earlier in Section 2.1. The relationship between the driving frequency and the rotor speed for an articulated rotor is also shown for comparison.

How the $\Omega - \omega_{ip}$ curves relate to typical body frequencies is shown in Figure 6. Separate charts are shown for articulated rotor and stiff in-plane rigid-rotor helicopters. Note that for the articulated rotor helicopter a critical body frequency for an on-the-ground condition coincides with the driving frequency when the rotor speed is at some value below the operating speed. This coincidence implies the occurrence of ground resonance. For the stiff in-plane rigid-rotor helicopter, curve crossings occur only in that portion of the $\Omega - \omega_{ip}$ curve where no driving energy source exists; therefore, neither ground resonance nor air resonance is expected to occur.

The frequency relationships shown in Figure 7 for a soft in-plane rigid rotor show that a typical operating range is bounded by conditions that could result in ground resonance if the rotor overspeeds while on the ground, and in air resonance if the rotor is slowed in flight. Examination of Figure 7 for ways to avoid ground and air resonance suggests five approaches:

1. Increase the rotor in-plane stiffness so that the curve is changed to resemble that shown in Figure 6.

2. Decrease the rotor in-plane stiffness substantially so that crossings will occur at very low values of rpm, well below the operating range (also, the available driving energy will be small at the low rpm values). This would approach the articulated rotor relationships shown in Figure 6.

3. Introduce damping into the system.

4. Lower the in-flight natural frequency of the body in roll so that the air resonance crossing moves to a lower rpm; lower than a probable limit for an autorotation maneuver.

5. Raise the on-the-ground natural frequency of the body in pitch, so that the ground resonance crossing moves to a higher rpm, thus providing more margin against ground resonance. (The body roll stiffness of the XH-51A while on the ground was so high due to the nature of the landing gear design that it was considered not to be a problem.)

The first solution suggested above is contrary to the basic objectives of the program. To increase the in-plane stiffness without changing the flapping stiffness would destroy the matched-stiffness feature. To increase

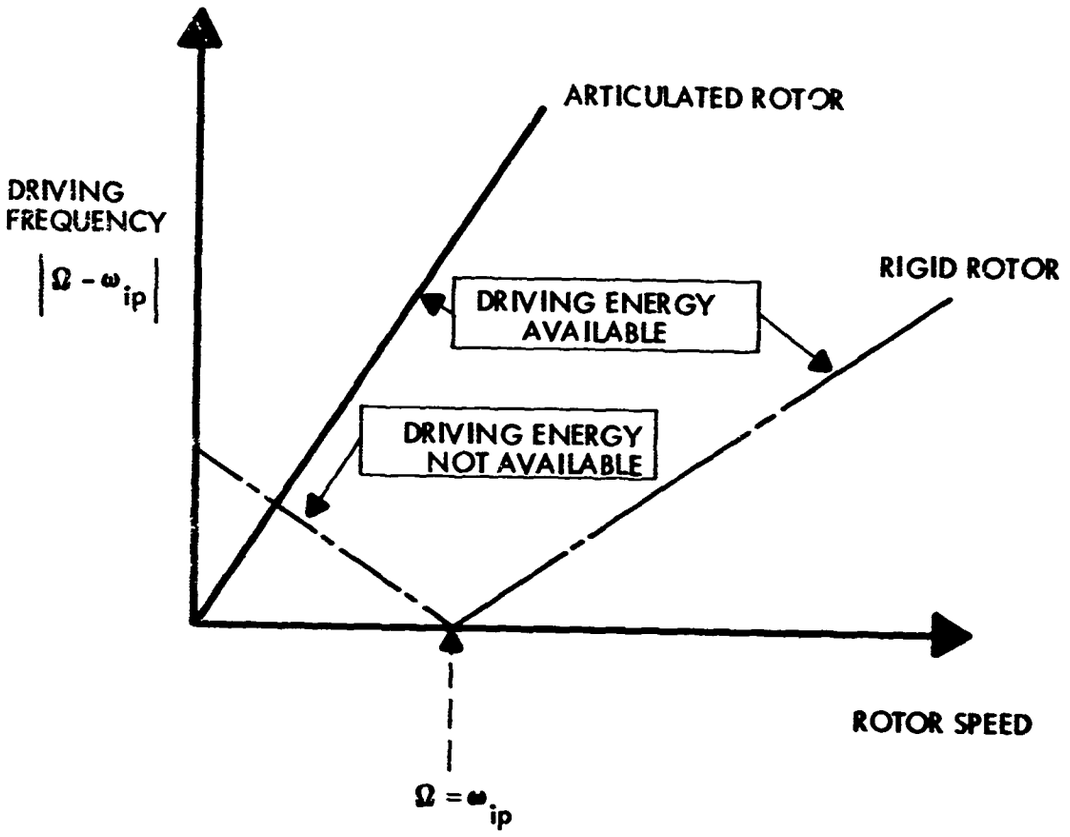

Figure 5. Relationships Between Exciting Frequencies and Rotor Speed.

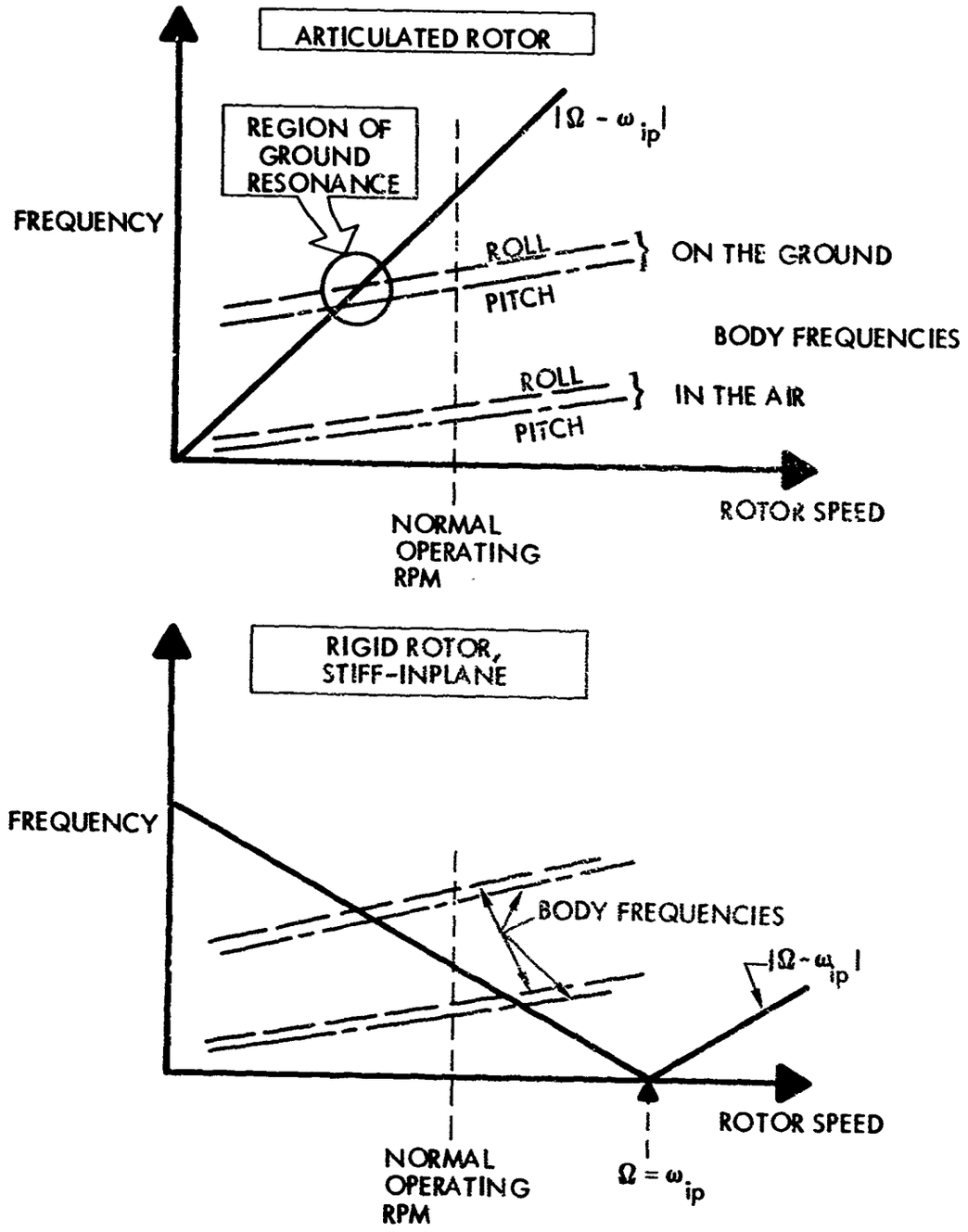

Figure 6. Relationship Between Driving Frequency and Body Frequencies for Articulated Rotor and Stiff In-Plane Rigid-Rotor Systems.

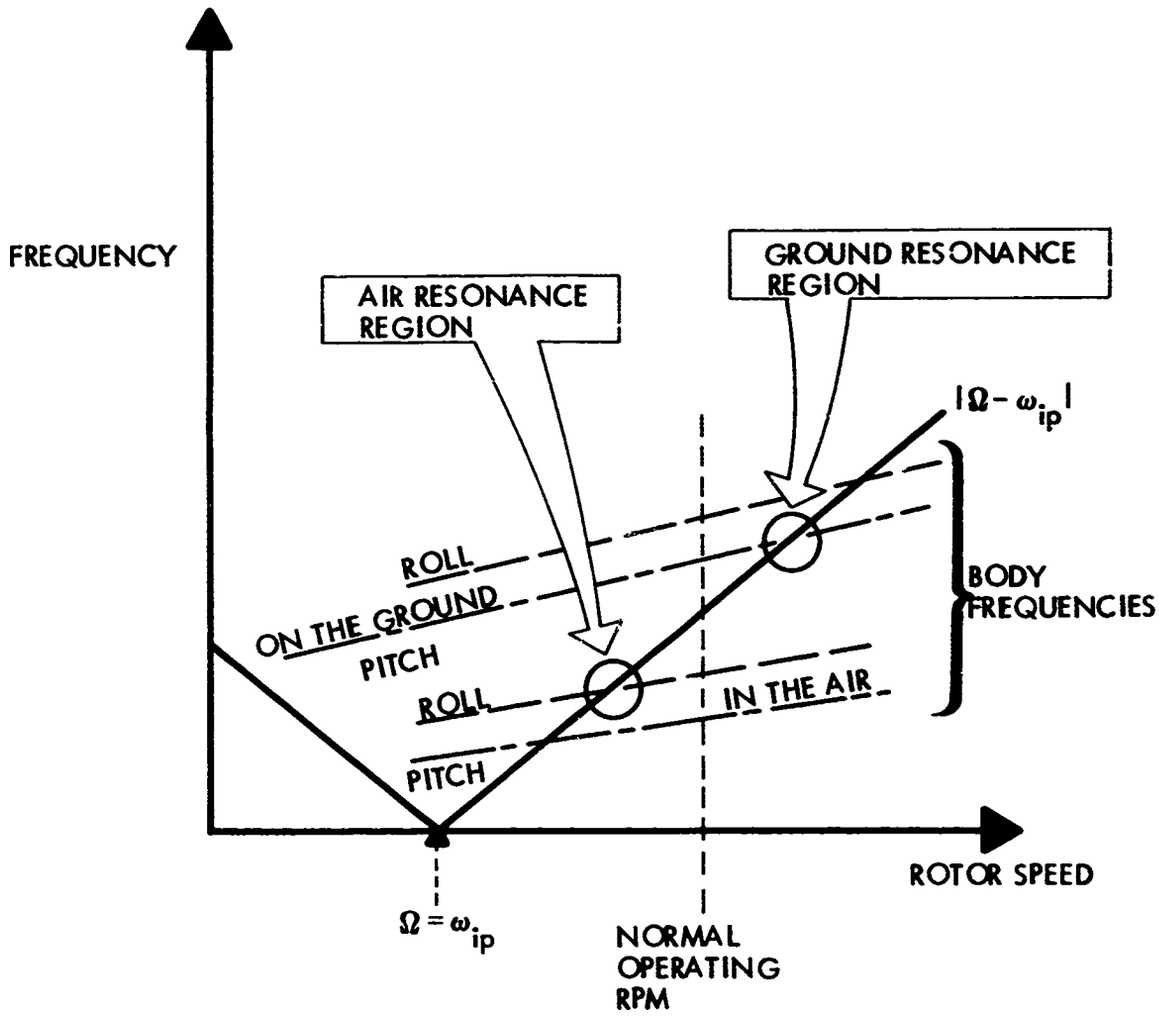

Figure 7. Relationship Between Driving Frequency and Body Frequencies for a Soft In-Plane Rigid-Rotor System.

stiffness in both directions (so that matched stiffness can be retained while in-plane stiffness is increased) would destroy the torsionally soft blade root feature.

The second solution listed above, to decrease the in-plane stiffness, was used to design the test rotor to the extent that it was practical. A practical lower limit is defined by strength requirements. The blades must be designed for at least the strength dictated by power and transient loads. This lower strength limit has a corresponding stiffness limit in a blade of practical construction. The philosophy applied to the design of the test rotor was to provide the lowest practical in-plane stiffness for an adequate level of in-plane strength while maintaining equal flapping and in-plane stiffnesses and the lowest possible torsional stiffness.

Later in the program attention was directed toward evaluating the aerodynamic damping characteristics of the rotor/gyro system. Aerodynamic damping is attractive because it is independent of functional integrity and operational reliability of auxiliary mechanical devices. Aerodynamic damping is derived from lift and drag generated by cyclic feathering and by blade flapping motion.

Lowering the body natural frequency in roll was provided for through provisions for adding mass to outriggers to vary the roll moment of inertia of the aircraft.

Damping in pitch was provided by adding mechanical dampers to the landing gear. Later, as a result of ground tests (discussed in Section 8), the pitch frequency was changed by replacing the aluminum landing gear skids with stiffened steel skids.

2.3 DESIGN CONSTRAINTS

In addition to designing the rotor to have the desired stiffness characteristics, and to have provisions for adjusting variables during the test program, design constraints were imposed by the desire to make the new hardware compatible with as much of the test aircraft's existing hardware as possible. No changes were to be made to the rotor shaft, the gyro mount/drive system, or the airframe. Changes to the control system were to be kept to a minimum. Dampers were to be added to the landing gear with a minimum of redesign.

It was learned during the ensuing design studies that it would be wise to modify the main rotor transmission support system to make the attachment between the transmission and the fuselage rigid. This arrangement would preclude the possibility of rotor/body modes becoming dependent on transmission support stiffness and of being vulnerable to sudden change if the supports "bottomed" during maneuvers or landings.

In the interest of maximum safety during the test program, a conservative approach was applied in selection of structural materials and in assessing working stresses. It was accepted that this approach would affect weight and design details.

SECTION 3

DESCRIPTION OF THE TEST CONFIGURATION

The rotor was designed to be tested on the XH-51A helicopter. Only minor modifications to the XH-51A were necessary to accommodate the new rotor system. The helicopter remained sufficiently unchanged to allow realistic comparisons of weight, vibration characteristics, control forces, and performance of the rigid-rotor system originally flown on the XH-51A and the new matched-stiffness rotor. General characteristics of the aircraft are given in Table XII (in the Appendix).*

3.1 ROTOR SYSTEM

The original XH-51A main rotor and its control gyro were replaced by the matched-stiffness rotor and its control gyro. The control gyros were similar except that the new one had a lower mass moment of inertia and was designed to permit changes of the moment of inertia during the program. The general arrangement of the unmodified XH-51A helicopter, which shows the original rotor system, is shown in Figure 68. Details of the matched-stiffness rotor are shown in Figures 69 through 75. Differences between the original rotor and the matched-stiffness rotor are:

- The short, stiff cuffs with feathering bearings were replaced by long, torsionally soft, flexure beams having polar symmetric bending stiffness.
- The aerodynamic span of each blade was shortened to accommodate the flexure beams. (The rotor diameter was not changed.)
- The feathering control system was extended to bridge the flexure beam. In the original rotor system the pitch control arm was designed to rotate the cuff on bearings. In the matched-stiffness system, feathering was accomplished by twisting the flexure beam.

The test rotor has four blades assembled from a central laminated flat plate steel hub, to which are joined four radially directed, mutually perpendicular, bonded steel flexure beams, each supporting a blade approximately 130 inches in span. Each blade is swept forward from the axis of the flexure beam. This assembly is illustrated in Figure 8 and detailed in Figures 70 through 72.

---

* Tables and drawings giving details of the test rotor and aircraft are accumulated in an appendix.

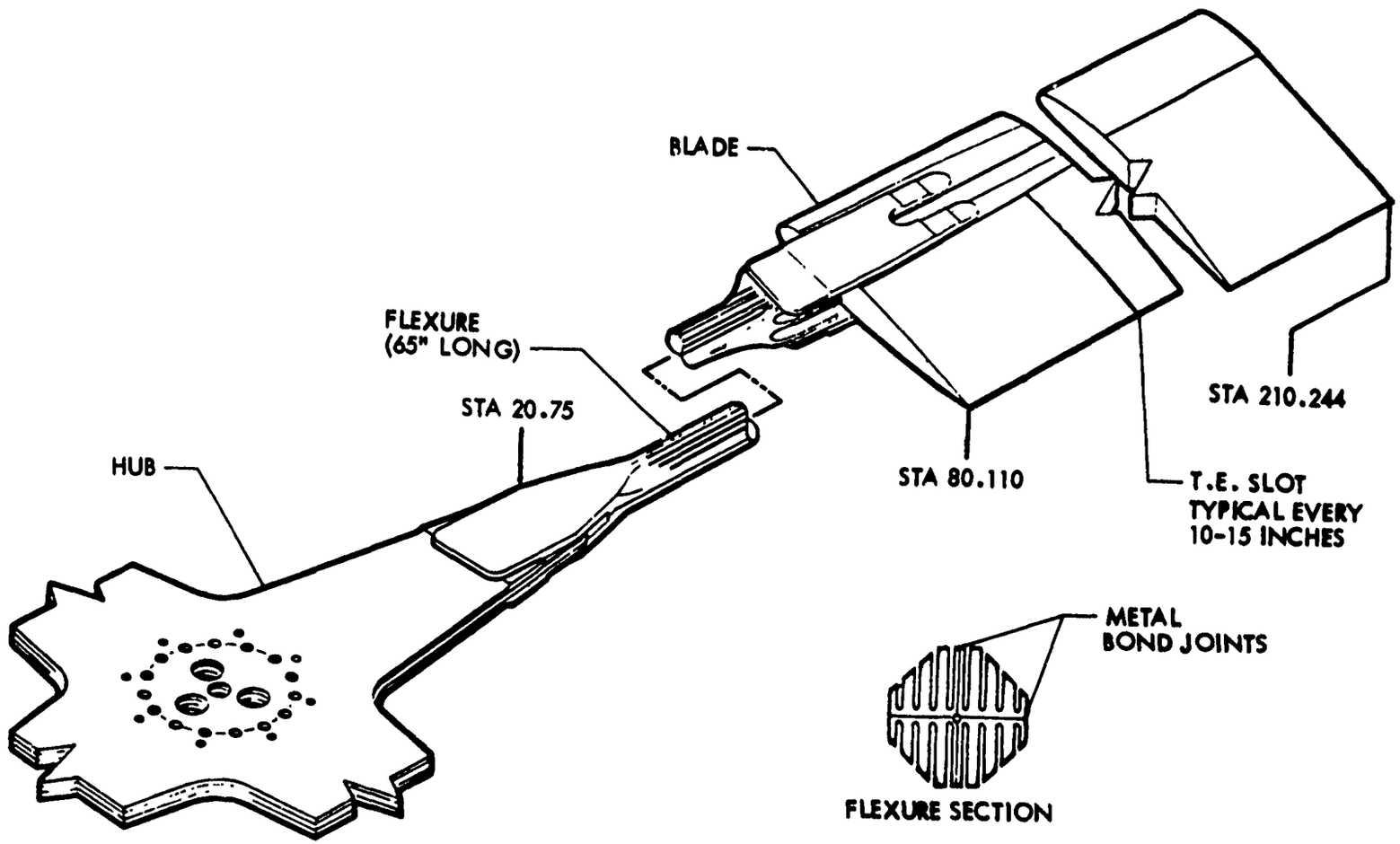

Figure 8. Hub, Flexure, and Blade of the Test Rotor.

3.1.1 Rotor Blade

The structural nose (the "D" spar) is similar to that of the original XH-51A blade. The leading-edge skins and channel beams are essentially the same as in the original blades. They are made of stainless steel and, together with the steel nose ballast bar, comprise the primary blade structure. The all-aluminum trailing edge serves primarily as aerodynamic fairing. The trailing edge is segmented at several spanwise locations; gaps between the segments are closed by sliding seals to maintain aerodynamic integrity without transmitting loads. This slotted trailing-edge construction is used to reduce in-plane bending stiffness as part of the tailoring procedure for stiffness matching and natural frequency control. The blade construction is shown in Figure 70.

The flexure-to-blade splice was designed to provide for varying the sweep and coning angles. Sweep could be varied from zero to three degrees forward, and the overcone angle from zero to one degree.

3.1.2 Rotor Hub

The rotor hub is made of bonded laminated steel plate. It is relatively thick where it attaches to the rotor shaft and has four radial arms which taper in thickness and planform. Each arm has a 3-degree cone angle, is relatively thick, and is profiled at the outboard end to provide for attachment to the flexure beam. The rotor hub is shown in Figure 71.

No attempt was made to match stiffnesses in the hub. The torsional stiffness of the hub is so much greater than that of the flexure beams that it does not become involved in the development of feathering signals from blade motion.

3.1.3 Flexure Beam

The flexure beam consists of four machined 17-4PH stainless steel bars bonded together. Each flexure beam is approximately 55 inches long and has end fittings for hub and blade attachments. This is the matched-stiffness element of the rotor. The bending stiffness of any cross section of the flexure is polar symmetric. The concept of a double-comb cross section (Figure 8) was selected because of its low bending stiffness, adequate bending strength, low torsional stiffness, adequate torsional strength, and fabrication simplicity. The bonds have centrally disposed glue lines which provide good fail-safe characteristics. Annular clamps at each end of the flexure prevent development of tension loads on the adhesive joints. The flexure beam length and cross-section size were selected as a result of an optimization study which was made to determine the best compromise between adequate strength and minimum torsional stiffness consistent with matched in-plane and flapping stiffnesses. Details of the flexure beam are shown in Figure 72.

3.1.4 Control Gyroscope

The control gyroscope for the test vehicle was a modified XH-51A control gyro. The hub, dome, and driving machinery of the original aircraft were not changed. Three new sets of arms were made to provide a choice of gyroscope mass moments of inertia of 1, 2, or 4 slug-feet^2. (The mass moment of inertia of the XH-51A gyro was 7.15 slug-feet^2.) Other values were obtained during tests by changing tip weight bars in the tubular arms. The rotor-to-gyro mechanical advantage and cant angle were the same as those of the XH-51A. The gyro assembly is shown in Figure 73.

3.1.5 Control System

Prior to Modification

The feathering control mechanism between the gyroscope and the rotor blades is shown in Figure 9. (Details of this system are shown in Figure 74.) The pitch link, a push-pull rod from a gyro arm, is attached to a pitch arm which is bearing-mounted on a supporting fulcrum bolted to the hub. The axis of rotation of the pitch arm is parallel to the feathering axis. The pitch arm is constrained against rotation about all other axes to provide support for horizontal components of pitch link loads and control system centrifugal forces.

A rigid steel torque tube which transmits feathering control moment from the gyro to the blade is attached to the pitch arm through a flexible coupling. The torque tube is located forward of and completely clear of the flexure beam. The coupling is stiff in twist and soft in bending, thus providing the characteristics of a universal joint without bearings. A spherical bearing, centered in the plane of the flexible coupling at the torque tube pivot point, transfers centrifugal forces of the torque tube and fittings into the pitch arm. The outboard end of the torque tube is attached to the flexure beam through another flexible coupling. This arrangement provides for bending and shear isolation while maintaining torsional continuity. The system was designed to be free of mechanical coupling (later modified as described in a following paragraph).

The torque tube was located away from the flexure, and no aerodynamically faired housing was used for the following reasons:

- Complete inspectability of the flexure beam was provided.
- Flexure beam and torque tube motions relative to each other are so large (the flexure bends while the torque tube hinges) that encapsulation of one by the other, or both by a faired housing, would have resulted in a configuration with drag equal to or greater than that of the selected design.
- To fair each of the members would have resulted in added weight that could not be justified.

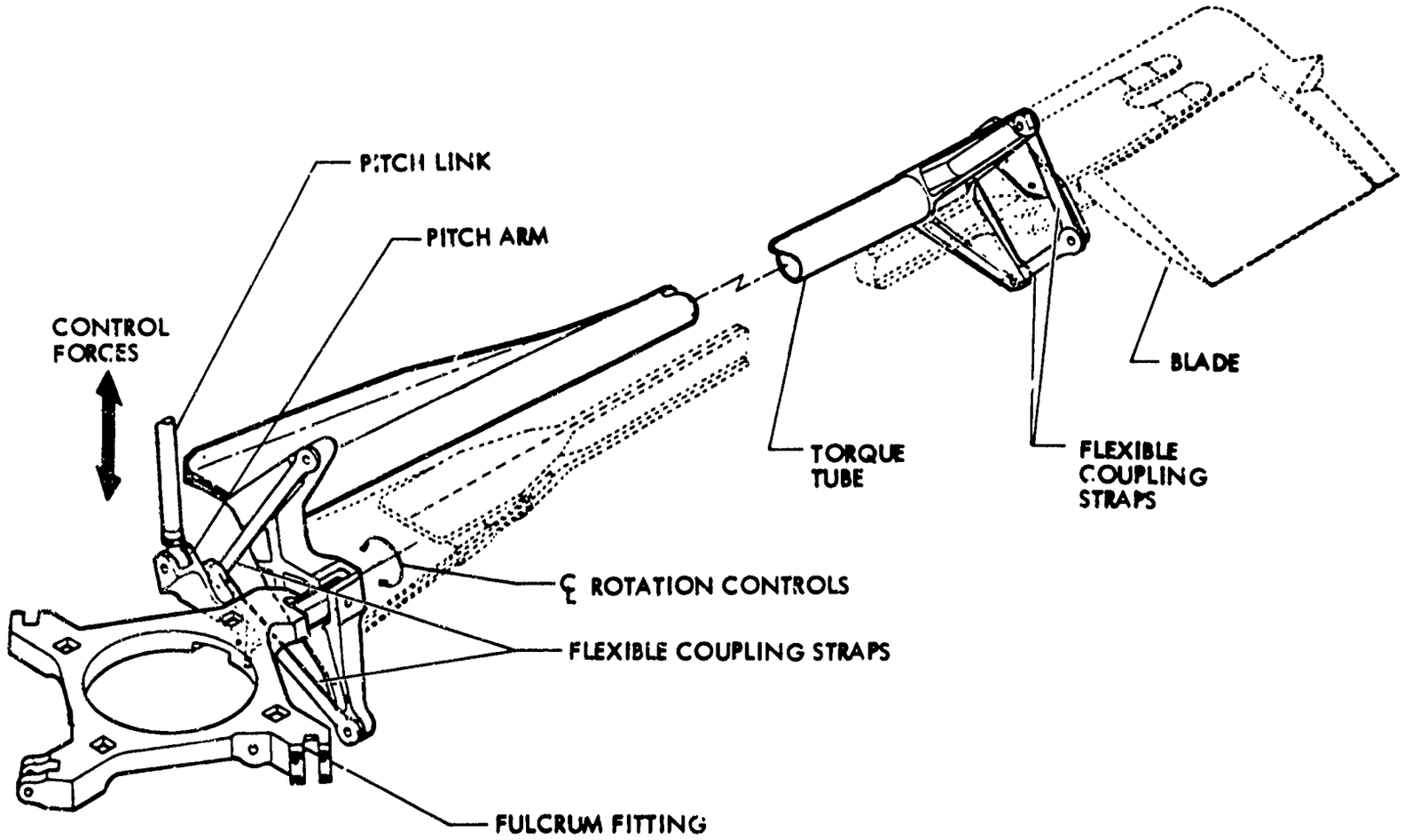

Figure 9. Feathering Control System.

Control System Modification

After several hours of testing on the whirl tower, difficulties were encountered with the spherical bearings. The system was modified to eliminate the 45-degree bearings, which were identified as the source of trouble due to the load path provided by their arrangement.

Analytical studies that preceded and paralleled the design effort had shown that mechanical coupling of feathering motion with flapping and in-plane motions would have a beneficial effect in relation to the mechanical instability problem. A geometry change to effect these coupled motions was designed into the modification concurrent with the bearing redesign. Details of the tests and a discussion of the mechanical coupling geometry are given in Section 7.3. The modified hardware is detailed in Figure 75.

3.2 LANDING GEAR

The XH-51A landing gear consists of two retractable, aluminum alloy, tubular skids, spaced approximately 4 feet apart. Each is attached to the fuselage by two steel struts, as shown in the following sketch.

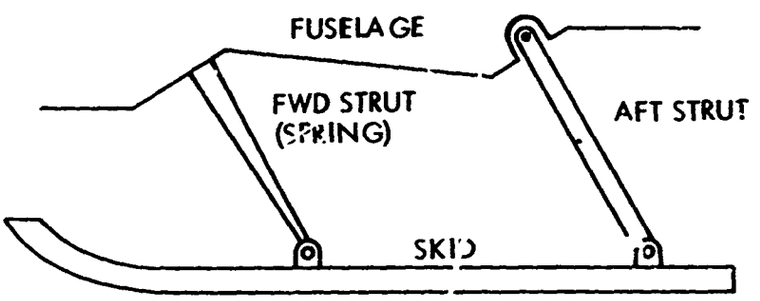

The forward strut is pin-connected to the skid and rigidly connected to the fuselage when the gear is extended. It serves as a spring for energy absorption in landing. The aft strut is pinned at both ends.

Initial Modification

The landing gear was first modified to include a linear viscous damper (in parallel with the forward strut) to provide a means of

increasing the margins against mechanical instability during on-the-ground testing. The modification is illustrated below.

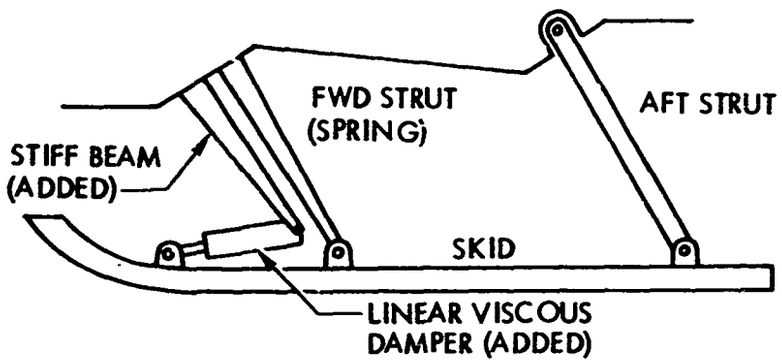

Final Modification

Preflight ground tests (discussed in Section 8) indicated a need to further modify the landing gear. The aluminum skids were replaced with stiffer steel skids. The new skids were similar to the original skids but included stiffeners welded to the aft portion. The viscous dampers were retained but were installed such that their use was optional. The steel skid and damper are shown in Figure 10.

3.3 WEIGHT AND BALANCE SUMMARY

Weight and balance characteristics of the test aircraft are summarized in Tables XIII and XIV (in the Appendix).

Figure 11 shows that shaft moments are within the selected flight limits (-15,200 and +7600 inch-pounds) for all conditions. These moments correspond to center-of-gravity position limits 4 inches forward and 2 inches aft of the rotor centerline at the design gross weight, 3800 pounds.

The matched-stiffness rotor group weight, 523 pounds (Table XIII), represents a weight fraction (rotor group weight/design gross weight) of 13.8 percent. The weight fraction for a stiff in-plane rotor of a size appropriate for the test aircraft is 15.5 percent. The matched-stiffness rotor group is 11 percent lighter than the stiff in-plane rigid-rotor group. Since the rotor was designed conservatively for test purposes, it is estimated that a matched-stiffness rotor system weight fraction of less than 12 percent is attainable.

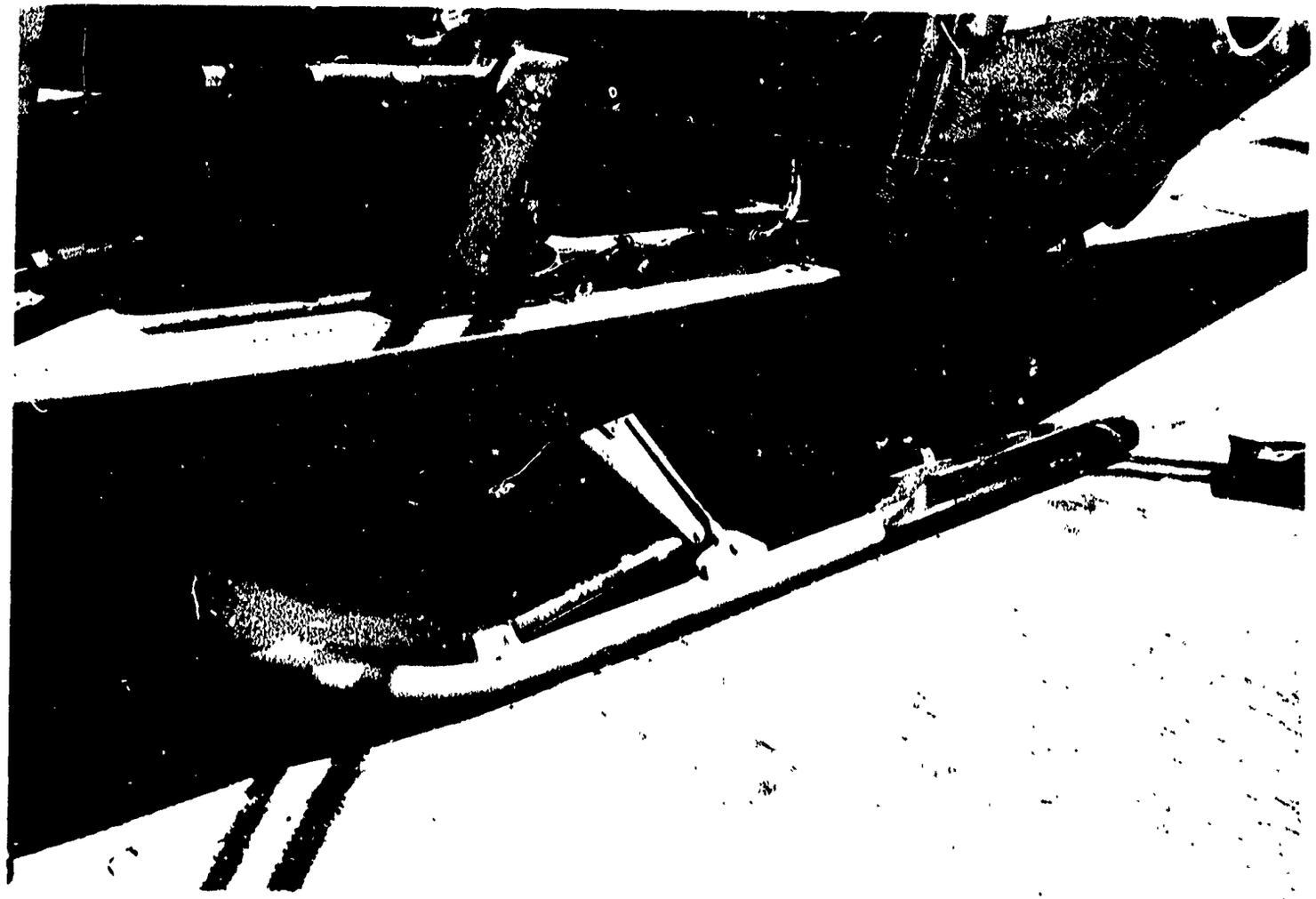

Figure 10. Final Landing Gear Configuration, Including Viscous Damper, Steel Skid, and Stiffeners.

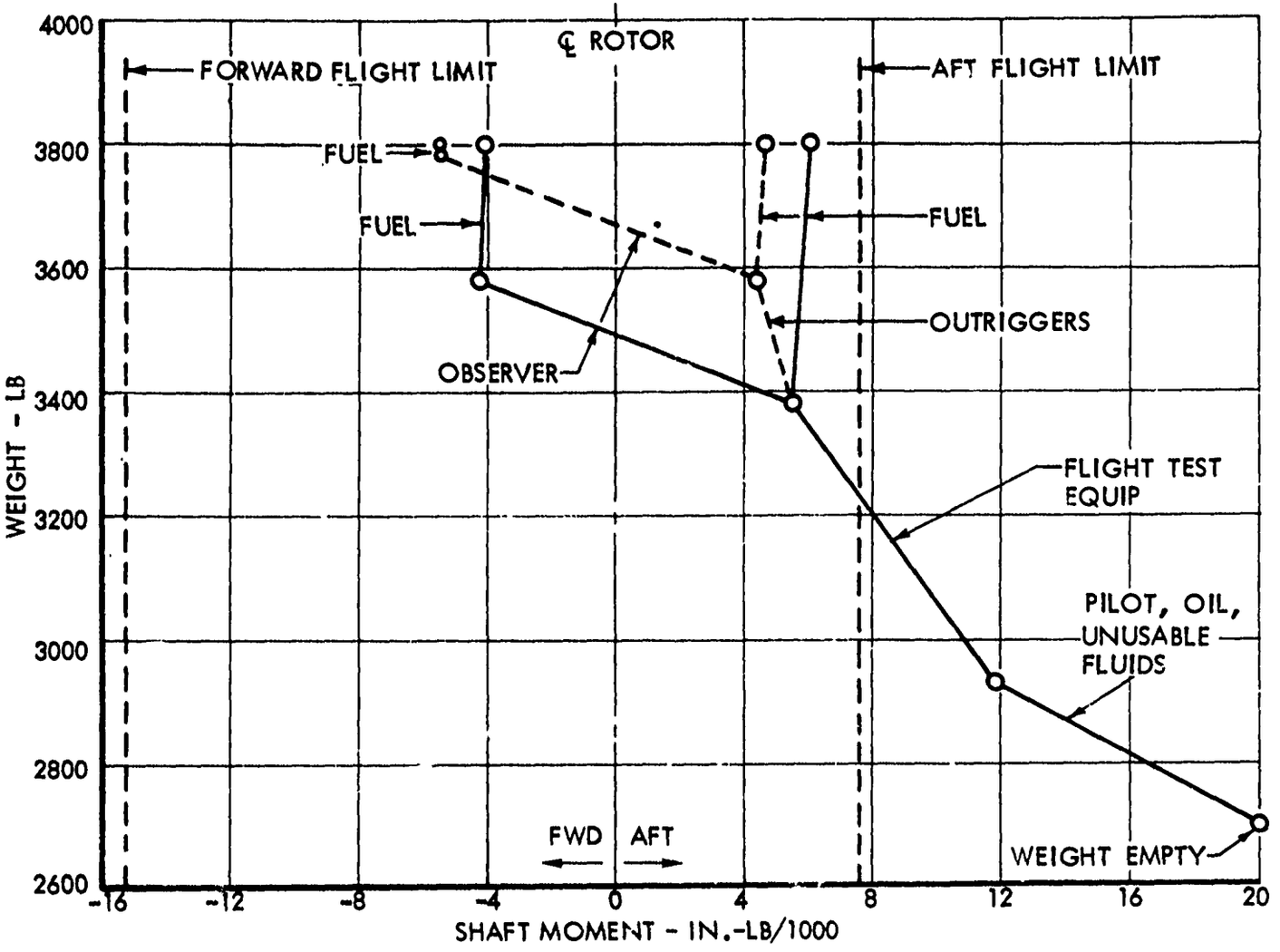

Figure 11. Balance Diagram.

SECTION 4

DESIGN ANALYSES

Analytical studies were conducted throughout the program to evaluate the test aircraft's mechanical stability characteristics. A cursory analysis was also made to predict flying qualities, stability and control characteristics, and performance.

4.1 FLYING QUALITIES

Flying qualities of gyro-controlled rigid-rotor helicopters, including the XH-51A, are primarily functions of:

(1) the tendency of the gyro to remain fixed in space orientation when the helicopter is disturbed

(2) the natural frequencies of pitch and roll modes (rotor stiffness and body moments of inertia)

(3) the precession rate of the control gyro due to cyclic stick displacement or to body pitch or roll moments

The characteristic of the gyro to tend to remain fixed in space orientation is influenced by friction in the control system, stiffness of the cyclic control system, and the gyro's mass moment of inertia. The matched-stiffness rotor flexure produced less friction but higher torsional stiffness than exists on a rigid-rotor with feathering bearings. Torsional stiffness was compensated by the action of a negative spring which was included in the XH-51A control system to govern forces. The gyro for the matched-stiffness rotor was selected to have a smaller mass moment of inertia than was used with the standard rotor, and the negative springs were adjusted to produce a ratio of gyro inertia to restraining forces equivalent to that of the original XH-51A system. Therefore, the effects of changing from a feathering bearing system to a root flexure were not expected to significantly change flying qualities.

The fact that the standard rigid rotor and the matched-stiffness rotor had different flapping stiffnesses was cause for a difference in the aircraft's natural frequencies. The standard rotor at normal rotational speed had a flapping stiffness, K_β, of 120,000 foot-pounds per radian. The flapping stiffness of the matched-stiffness rotor is 64,000 foot-pounds per radian. The corresponding natural frequencies are:

Motion	Standard Rigid Rotor	Matched-Stiffness Rotor
Pitch	7.3 radians per second	5.3 radians per second
Roll	14.0	10.2

This reduction in pitch and roll frequencies was not expected to change the flying qualities noticeably, since the frequencies remained high compared to conventional helicopters, where frequencies are as low as 0.19 radian per second.

The gyro precession rate due to stick displacement is related to the moment applied through the control system. The effectiveness of the control system is adjustable, however, so changes made to accommodate the test rotor were not expected to adversely affect flying qualities.

The gyro precession rate due to feedback of pitch and roll moments is a function of the forward sweep of the blades. Due to the length of the root flexure, the swept portion of the blade is more outboard on the matched-stiffness blade than on a standard XH-51A blade. Thus, in the case of the matched-stiffness blade, a smaller portion of blade bending moment is resolved into a feathering moment feedback signal. This means that the matched-stiffness rotor causes a lesser gyro precession rate per unit of blade flapping moment than does the rigid rotor, which means less damping and faster response to both control inputs and gust disturbances. The effect on flying qualities was expected to be seen as higher maneuverability and perhaps a rougher ride in turbulence. Neither effect was expected to be large enough to cause difficulties for the test program.

4.2 PERFORMANCE

Changes in performance of the test aircraft were expected to be minimal. Hover performance was predicted to be reduced slightly because the matched-stiffness hub requires more power; this can be visualized from Figure 12, which shows that the blade attachment fitting on the matched-stiffness rotor has a longer moment arm about the center of rotation than does the bearing housing of the standard rotor. Power required to rotate the test rotor was calculated to be 60 horsepower more for the standard hub (at normal operating speed).

No additional effect on forward flight performance was expected, since the frontal areas of the two rotors were essentially the same.

4.3 DYNAMIC STABILITY

Since mechanical stability had been identified as an area of concern, an extensive investigation was conducted to assess the dynamic characteristics of the test vehicle. Tests were included to establish validity of data used in analyses.

An analytical model was developed using the classical lumped-mass technique. The model describes the complete elastic rotor system, including the control gyro, a flexible shaft, and a transmission support system.

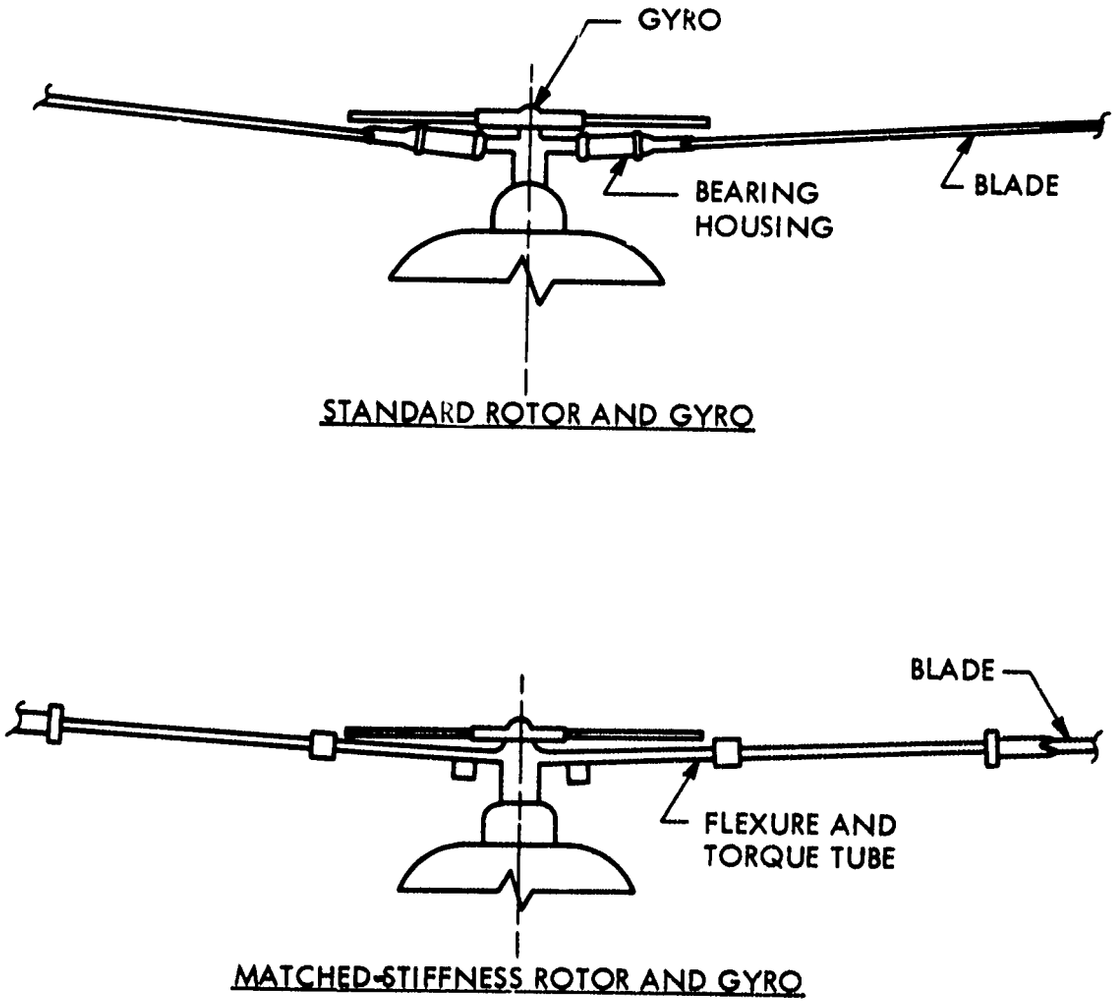

Figure 12. Frontal Area Comparison — Standard and Matched-Stiffness Rotors.

Each flexible blade contains 11 lumped-mass stations. Each mass has three degrees of freedom: vertical translation, in-plane translation, and pitch angle. Coupling of vertical bending, in-plane bending, and torsion (due to sweep, coning, collective, and twist) is included in the structural description. The model also includes the gyro control system with flexibilities of its components. The complete model originally had 80 degrees of freedom, however, to reduce the time required to solve the eigenvalue problem, the 80th order system was reduced to a 22nd order system using natural cantilever blade modes. The 80- and 22-degree-of-freedom systems are shown in Tables XV and XVI (in the Appendix). The reduction in model size had little effect on the results (this was demonstrated by solving a 50th order and a 20th order system and comparing results). The motions of all 80 coordinates were obtained from eigenvectors from the 22nd order solutions and their mode shapes.

Because the fuselage is anisotropic, the analytical model of the rotor system was transformed from rotating coordinates to stationary coordinates.

A simplified analysis using only 10 degrees of freedom was used for rapid parametric studies during preliminary design. This analysis aided the physical understanding of the solutions and provided a check on the analyses of the final design, which was made with the larger order description. The simplified model contained the first flapping bending, first in-plane bending, and feathering modes (including the gyro control system) of each blade, combined with four rigid-body motions of the vehicle. The equations of this method are shown in Tables XVII and XVIII (in the Appendix).

4.3.1 Stability Boundaries

Air Resonance

Stability boundaries were estimated using the 22-degree-of-freedom analysis for a preliminary configuration of the test rotor having the following characteristics:

Blade overcone angle = 1.0 degree

Blade forward sweep angle = 1.5 degrees

Blade tip weight = zero

Gyro inertia = 2 slug-feet^2

Control system coupling = zero ($\alpha_3 = \delta_3 = 0$)

Rotor stiffness = K_β = 64,000 foot-pounds per radian at nominal rpm

In-plane bending frequency = .64P

Roll inertia increment = 200 slug-feet^2

Support between transmission and fuselage assumed to be rigid.

Results of the analysis are shown in Figure 13. They show that the rotor must be operated above 300 rpm if air resonance is to be avoided. This limit represents a stability boundary at 85 percent of the normal operating speed of 355 rpm. This limit, seen in the lower chart, corresponds to the crossing of the driving and roll frequency curves at around 280 rpm, in the upper chart. The dashed line was added to illustrate the effectiveness of changing the aircraft's roll moment of inertia.

The effects of varying a number of rotor system characteristics were considered with respect to their possible effects on air-resonance boundaries. Many characteristics - gyro mechanical advantage, gyro control lead angle, blade sweep, blade overcone, gyro spring bias, and swash plate damper rate - were fixed at values estimated to provide good handling quality and control characteristics. Selected values were based on experience acquired in original development of the XH-51A helicopter.

Calculations were performed to assess the influence of these variables on the air resonance boundary. However, to the extent that such analyses were made, in most cases the effects were small. Since the reliability of the technique had not yet been established, and since a design objective was to keep control system changes to a minimum (Section 2.3), it was decided to stay with design values dictated by experience. This decision was also influenced by the fact that analyses indicated an interaction among some of the variables, so that it was difficult to judge the true effects of a single change.

An exception to the foregoing was gyro size. An expected benefit of the matched-system concept was cited earlier as a reduction in gyro polar moment of inertia. Wind tunnel tests (Section 1.1) had indicated that a small gyro would be adequate. This observation was borne out in analyses made during preliminary design in this program, and by whirl tower tests (Section 7.3). Therefore, a relatively small gyro was selected for the test rotor. The gyro size was later increased for rotor control reasons (Para 9.4.1), but still remained small compared with that used on a standard XH-51A.

The effects of using blade tip weights were also assessed by analysis. No appreciable improvement was noted. This conclusion can be reached intuitively: tip weights lower the rotor in-plane frequency and thus move the Ω-ω_{ip} curve in a direction to improve the stability margin. however, this effect is compensated for by the added rotor stiffness caused by centrifugal acceleration of the tip masses. Whirl tower tests (Section 7.3) bear out this conclusion.

The use of flexible supports between the transmission and body was considered as a means of lowering body frequencies and as a means of adding dampers across the support springs. However, this idea was not pursued for the following reasons.

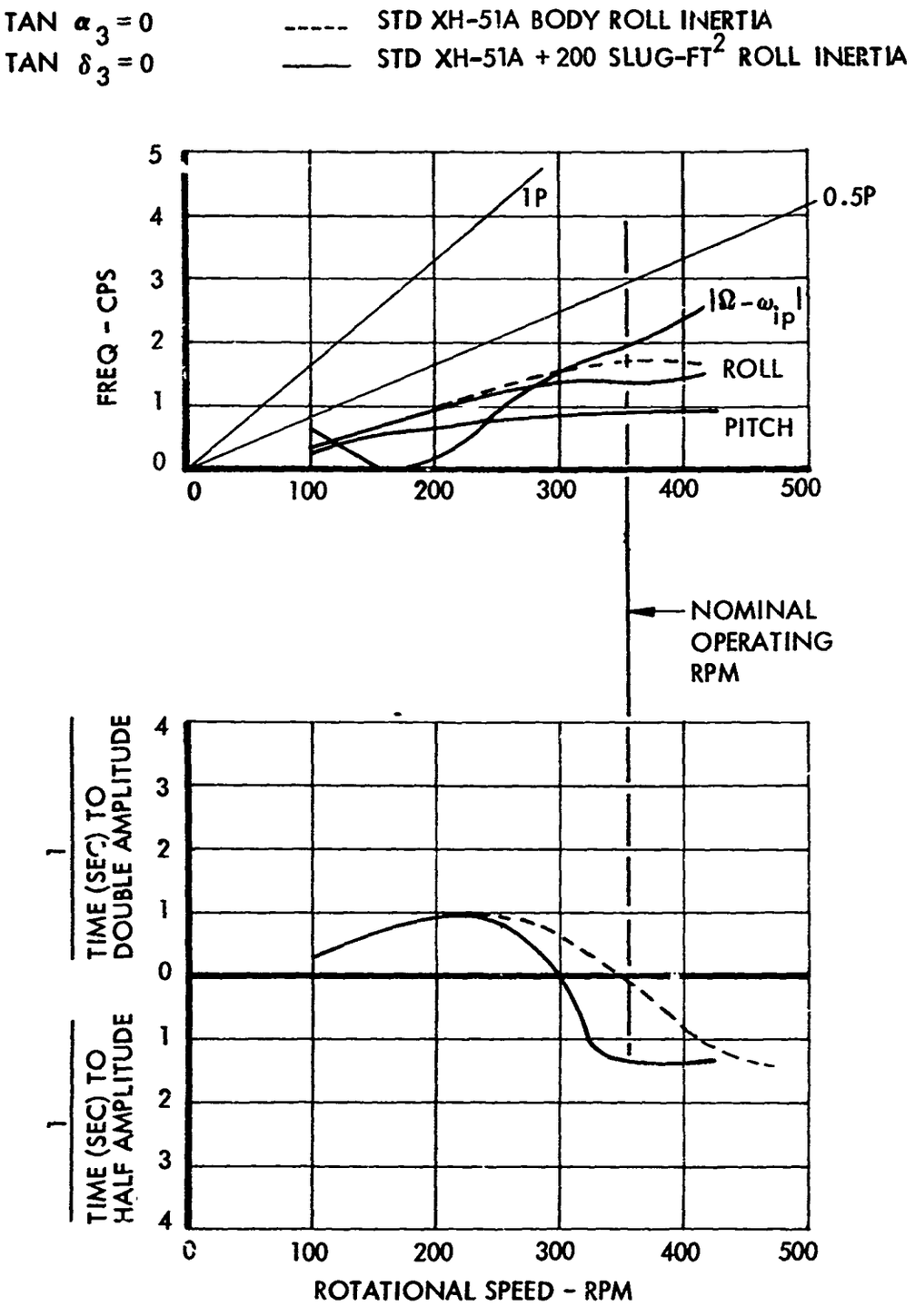

Figure 13. Results of a Flight Resonance Analysis for a Preliminary Design Configuration.

1. Softening the transmission supports would lower the body pitch frequency, and thereby reduce the margin against ground resonance.

2. Softening the transmission introduces a higher frequency roll mode which might be adversely affected by overspeeding the rotor.

3. The permissible travel of a soft mount has practical space limits, so the possibility of contacting the stops is introduced; this could result in sudden increase in body roll frequency, possibly leading to air resonance.

Calculations also were performed for a configuration which is essentially the same as that for which results are shown on Figure 13, except that the control system geometry was adjusted to produce mechanical couplings (tangent α_3 and tangent δ_3). Results are shown in Figure 14. A comparison of Figures 13 and 14 shows only a modest improvement in the rpm limit, but it shows that the use of coupling can provide damping that substantially reduces the instability level. This result suggests that it may be possible to suppress the instability to an extent to effect stability.

Ground Resonance - The margin of safety against ground resonance was evaluated by a study of test data instead of by analysis. Two methods were available to examine the probability of encountering ground resonance: the whirl tower model had the capability of varying spring rates and body inertias; shake tests were made to provide data for assessing the vehicle's dynamic characteristics at various levels of lift sharing between the rotor and the landing gear (Sections 6 and 7).

The shake tests showed the roll stiffness to be very high when the aircraft was supported by its landing gear. The roll mode was not considered to be a problem. Pitch frequency, on the other hand, was found to be low. From an analysis of the data it was deduced that the rotating rotor would probably add enough stiffness to satisfy the stability requirement. As a measure of safety, the landing gear damper described in Section 3 was added.

4.3.2 Blade Frequency Spectra

Natural frequencies of the rotating blades were calculated to aid in the study of dynamic characteristics of the rotor blades. The analytical model used for the calculations described the inertia and stiffness characteristics of each blade by 30 mass elements. The calculations included coupling of flapping, in-plane and torsional frequencies, mode shapes, and shear and moment distributions. Calculations were made for several collective angles. Figure 15 shows a typical set of results; these particular data are for the rotor at a collective setting of 10.88 degrees, for five rpm values (0, 100, 200, 355, and 500). Mode shapes for the 355 rpm case are shown on Figures 16 and 17.

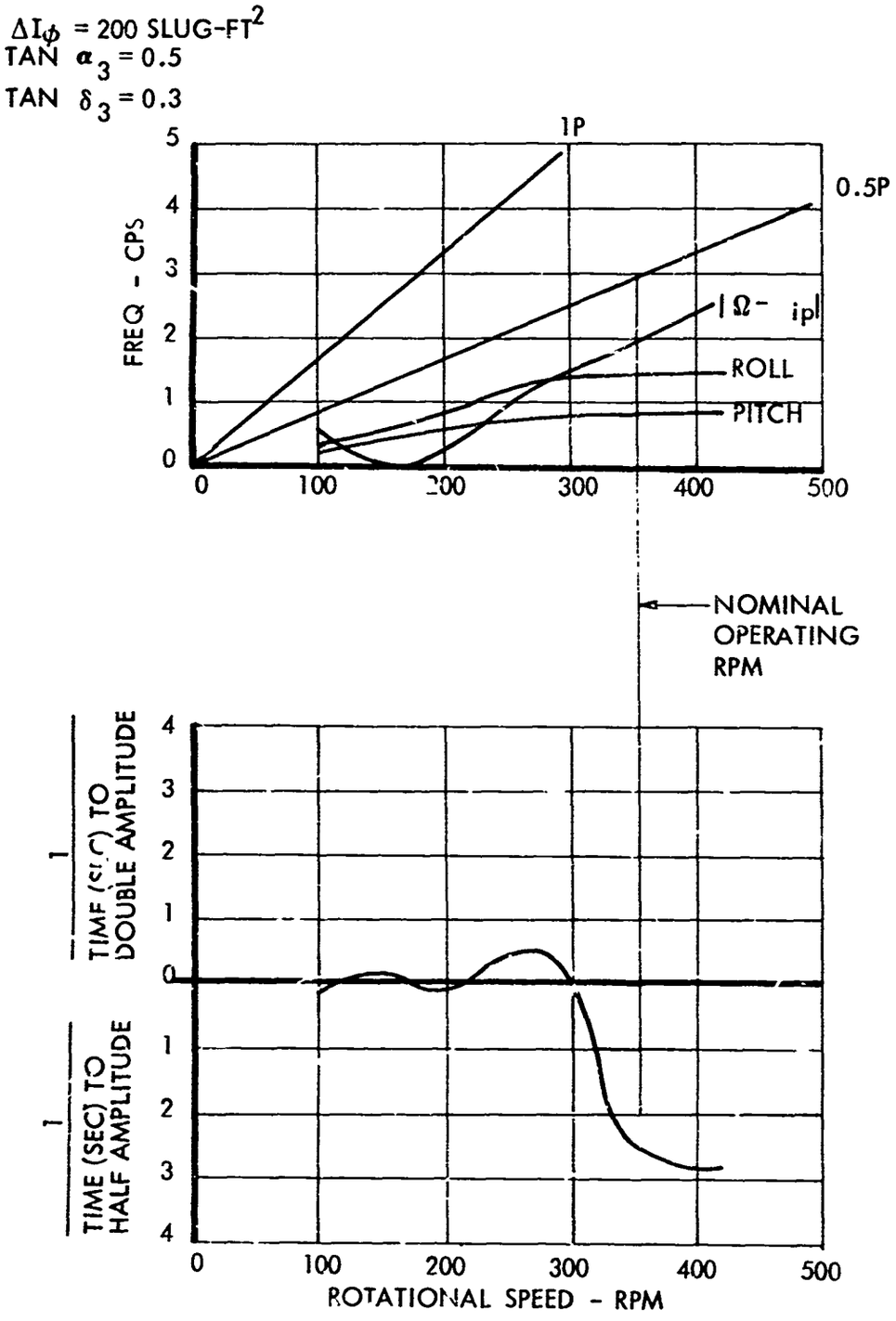

Figure 14. Results of Flight Resonance Analysis for a Configuration Which Includes Mechanical Coupling.

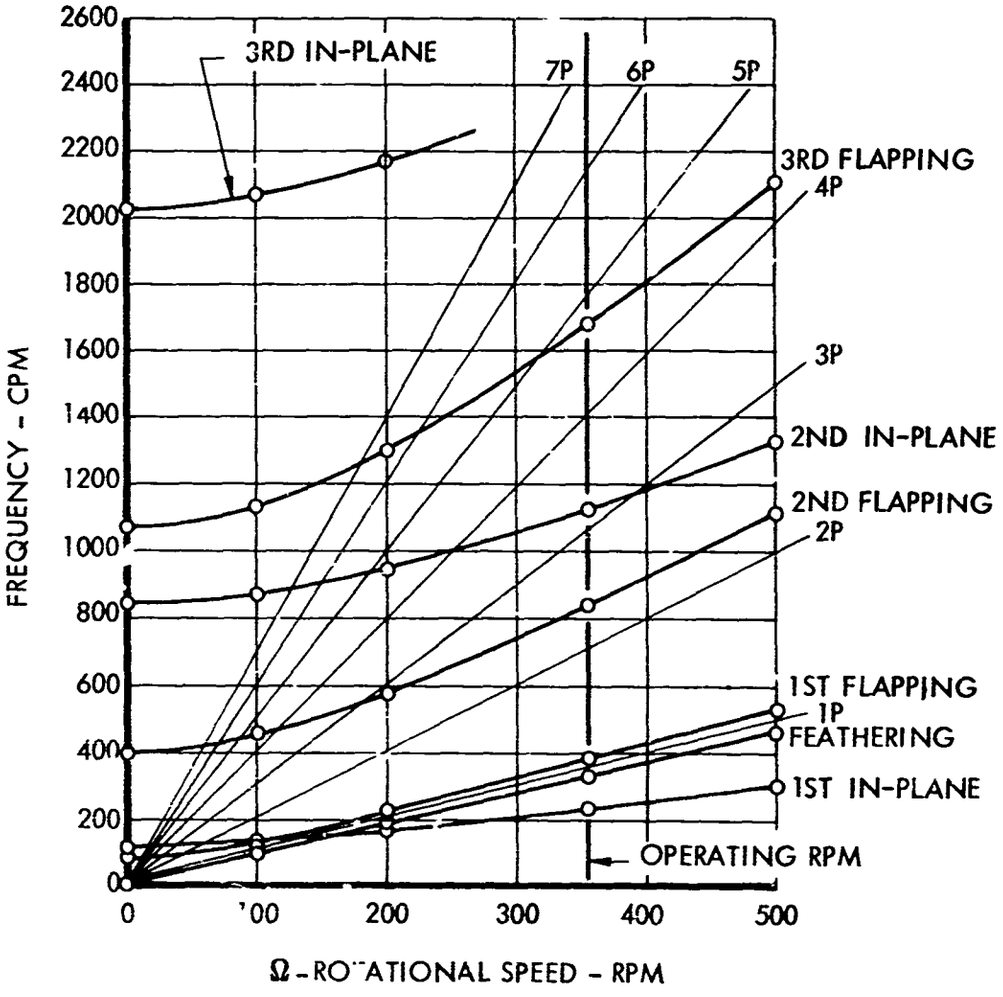

Figure 15. Rotating Coupled Blade Frequencies, θ_o = 10.88 Degrees.

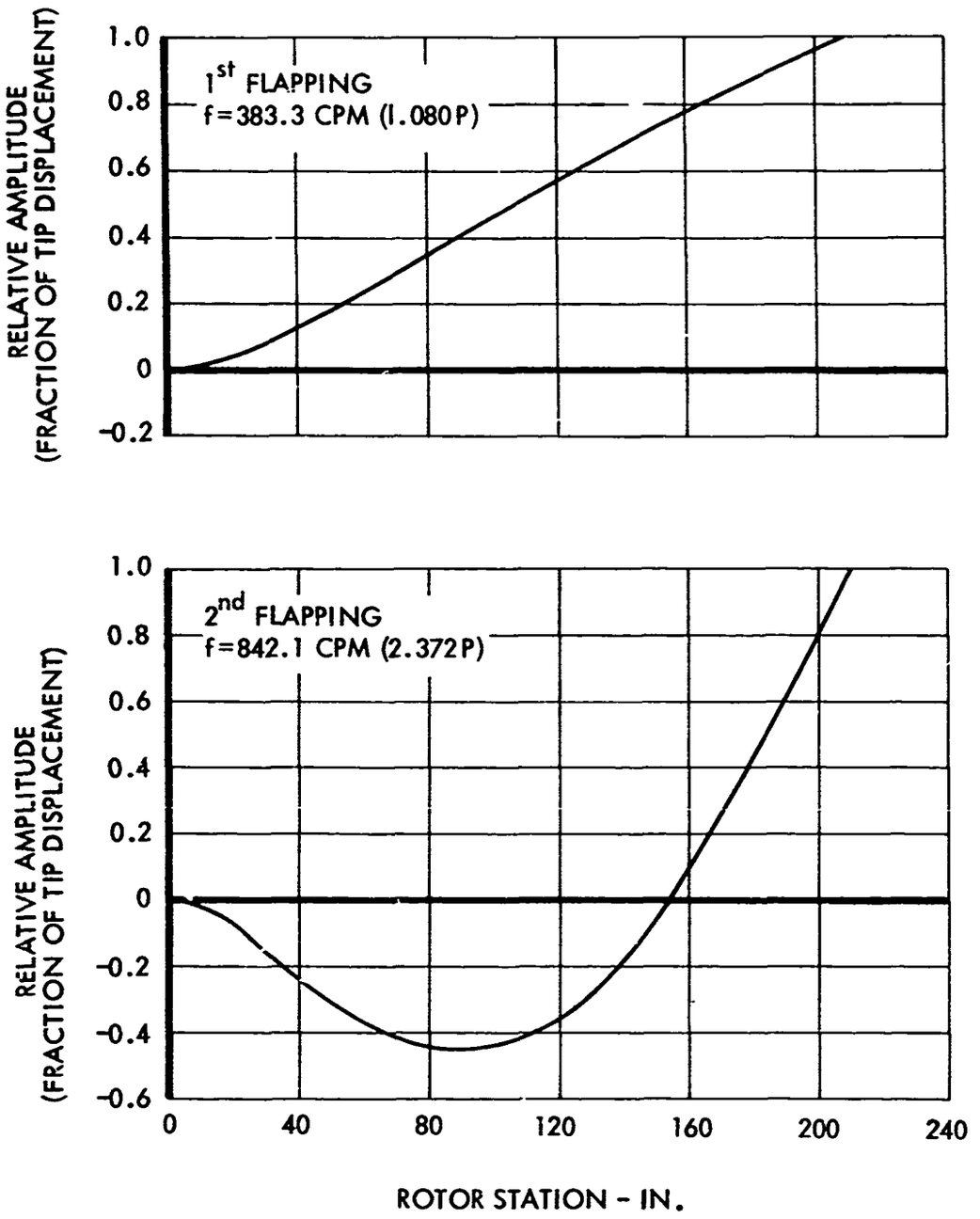

Figure 16. Rotating Blade Flapping Mode Shapes at Ω = 355 RPM Corresponding to Frequency Spectrum of Figure 15.

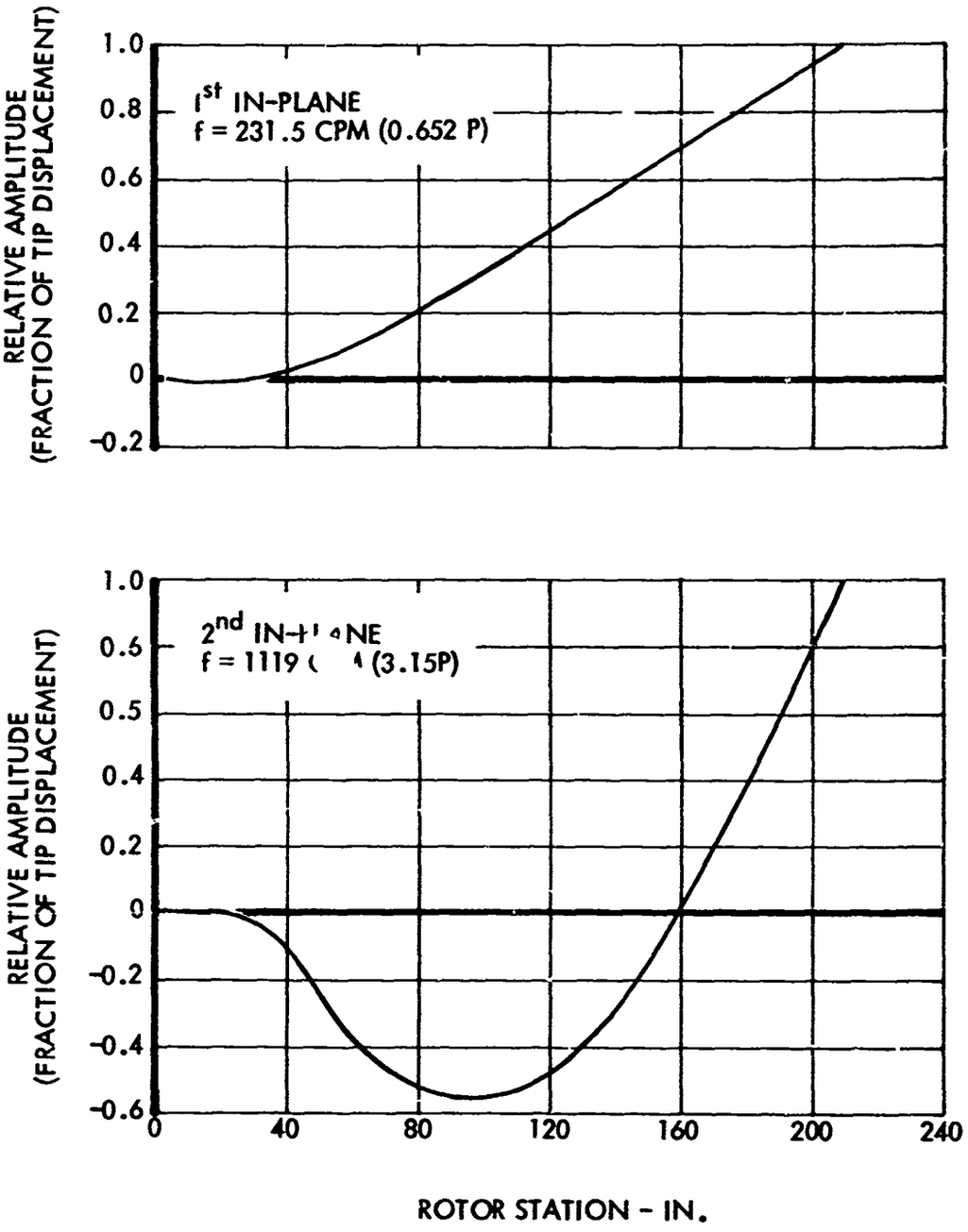

Figure 17. Rotating Blade In-Plane Mode Shapes at Ω = 355 RPM Corresponding to Frequency Spectrum of Figure 15.

Figure 15 shows that the first in-plane frequency is low as expected. The second in-plane bending frequency is close to 3P. It was rationalized that since the analysis did not include the in-plane stiffness of the trailing-edge box sections the apparent proximity of the second in-plane and 3P frequencies would probably not actually occur.

SECTION 5

STRUCTURAL SUBSTANTIATION

Strength analyses were performed to substantiate design of the test rotor and of the aircraft modification; these analyses are shown in Reference 1. This section briefly summarizes structural design criteria, strength analysis of the flexure, normal operating stresses in the rotor, and fatigue tests.

5.1 STRUCTURAL DESIGN CRITERIA

A brief statement of the primary elements of the criteria is presented. More detailed criteria and loads analyses are given in Reference 1.

5.1.1 Design Weight Data

The basic design gross weight was selected as 3800 pounds. The corresponding design center-of-gravity range is described in Section 3.3 and shown in Figure 11.

5.1.2 Design Flight Speeds

Forward Speed

Design loads were based on a level flight high speed (sea level standard atmosphere) of 140 knots and a design dive speed of 150 knots.

Rotor Speed

Design rotor speeds are summarized in Figure 18. A design goal was to attain freedom from air resonance at and above 75 percent of the normal operating rpm.

5.1.3 Design Load Factors

Design load factors are shown versus rotor speed in Figure 18 and versus flight speed in Figure 19.

5.2 STATIC STRENGTH ANALYSIS OF THE FLEXURE BEAM

A cross section of the flexure beam described in Section 3.13 is shown in the following sketch. This cross section is constant between rotor Stations 73 and 40; then it tapers to a larger size at Station 25.

The highest stress was determined to occur at Station 73.

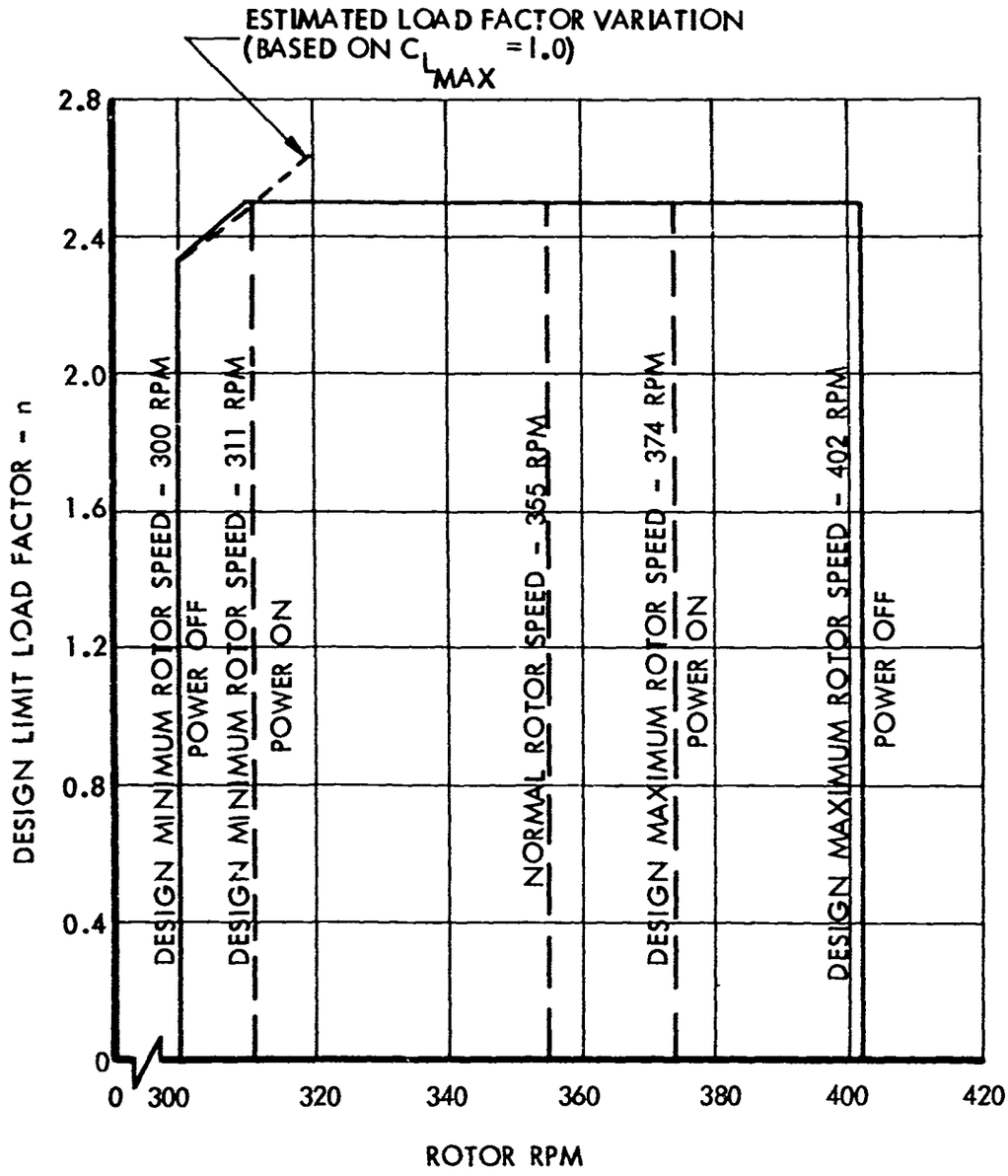

Figure 18. Design Limit Load Factor Versus RPM.

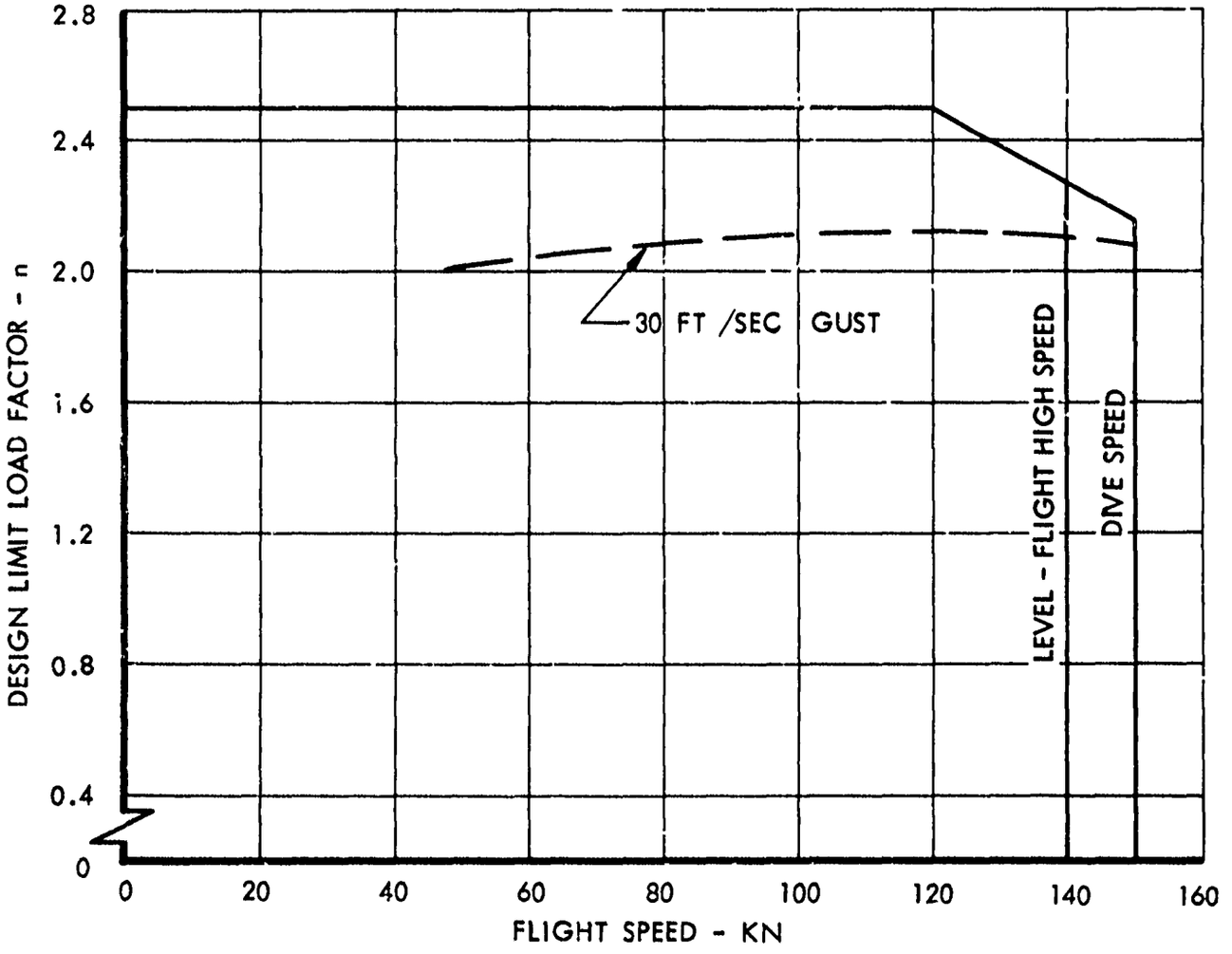

Figure 19. Design Limit Load Factor Versus Flight Speed.

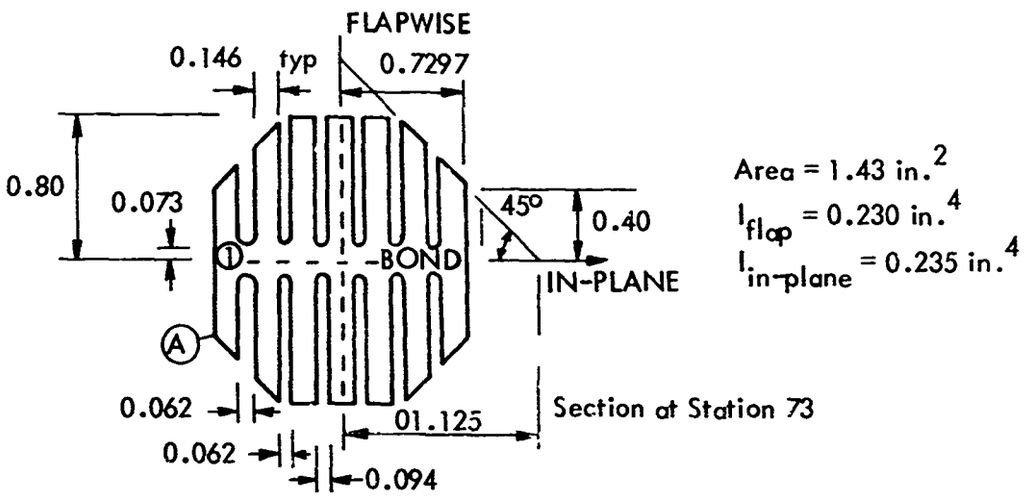

The design loads were for a condition where the load factor was 2.5 at a forward speed of 150 knots. It can be seen by reference to Figure 19 that the design condition is conservative since the design point falls outside the design envelope. Limit loads are reproduced from Reference 1 on Figure 20. Design limit loads are converted to ultimate loads as follows:

Flapwise bending moment

Steady = 1.5 X 6.100 = 9,150 in.-lb, ultimate

Cyclic = 1.5 X 5,000 = ±7,500 in.-lb, ultimate

In-plane bending moment

Steady = 1.5 X 8,400 = 12,600 in.-lb, ultimate

Cyclic = 1.5 X ±4,000 = ±6,000 in.-lb, ultimate

Centrifugal force (with 4 lb tip weight) from page 39 of Reference 1

CF = (1.5) (24,400) = 36,600 lb, ultimate

The maximum stress due to bending occurs at point 4 (see sketch). Cyclic flapping and in-plane stresses are conservatively combined, producing maximum stress due to flapping bending moment and centrifugal force thus:

$$f_{bu} + f_{tu} = \frac{0.40\ (9150 + 7500)}{0.230} + \frac{0.73\ (12600 + 6000)}{0.235} + \frac{36,600}{1.43} = 112500 \text{ psi}$$

Stresses due to torsion are conservatively based on the torsional deflection limit of the flexure beam, 21 degrees. Considering Element 1 in the

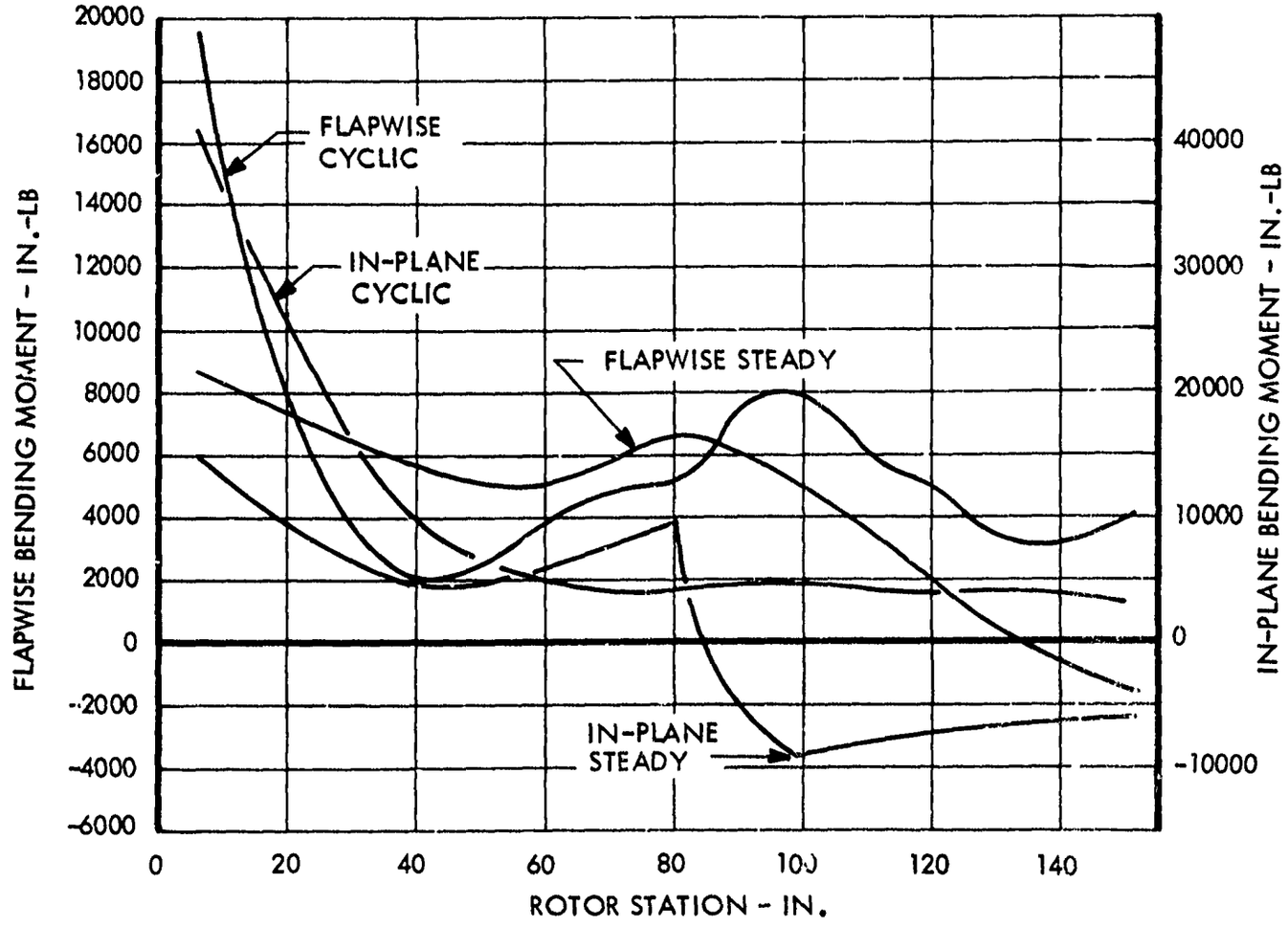

Figure 20. Rotor Blade Limit Loads, 2.5g at 150 Knots.

preceding sketch (shown isolated in the following sketch), stress due to rotation, to be added to the stresses shown above, is determined as follows. Stress is caused by rotation and vertical displacement of the element. An effective length of 40 inches was determined as appropriate for this analysis.

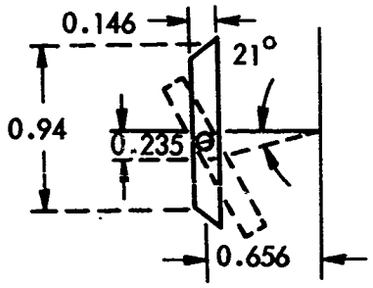

Properties of element:

$I = 0.0101 \text{ in.}^4$

$A = 0.137 \text{ in.}^2$

The vertical deflection is schematically represented thus:

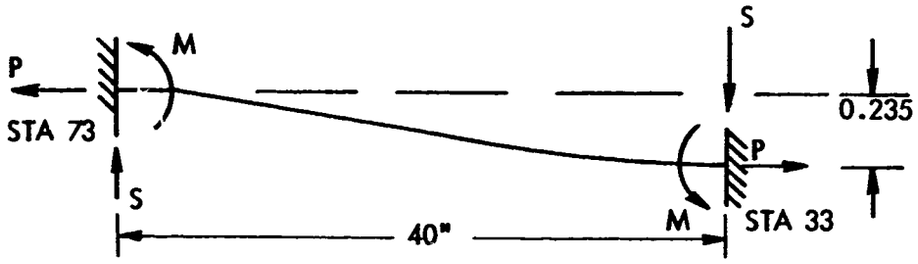

The centrifugal force loading is schematically represented thus:

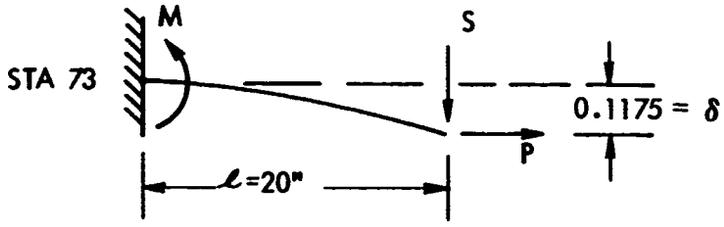

Centrifugal load $P = 24{,}400 \times \frac{0.137}{1.43} = 2{,}340$ lb (limit)

$\delta = \frac{S}{P}(\ell - J \text{ Tanh } U)$ (Reference 6, Table VI, Case 13)

$$J = \sqrt{\frac{EI}{P}} = \sqrt{\frac{(24 \times 10^6)\ (0.0101)}{2{,}340}} = 11.19$$

$$U = \frac{\ell}{J} = \frac{20}{11.19} = 1.79$$

$$\delta = 0.1175 = \frac{S}{2{,}340}\ (20 - 11.19 \tanh 1.79)$$

$$S = \frac{(0.1175)\ (2{,}340)}{9.42} = 29.2 \text{ lb}$$

$$M = (29.2)\ (20) - (2{,}340)\ (0.1175) = 310 \text{ in. lb}$$

$$f_{bu} = \frac{(310)\ (1.5)\ (0.47)}{0.0101} = 21{,}600 \text{ psi}$$

$$f_{bu} + f_{tu} = 21{,}600 + 112{,}500 = 134{,}100 \text{ psi}$$

F_{tu} = 190,000 psi (Reference 7)

$$\text{M.S. (Bending and tension)} = \frac{190{,}000}{134{,}100} - 1 = 0.42$$

Torsional Shear Stress for $\theta = 21^\circ$

(Interaction between torsional shear and bending stress is negligible).

$$f_s = \frac{\theta t G}{\ell} \quad \text{(Reference 8, page 270)}$$

$$f_{su} = \frac{(1.5)\ (0.367)\ (0.146)\ (11 \times 10^6)}{40}$$

$$= 22{,}000 \text{ psi}$$

F_{su} = 123,000 psi (Reference 7)

$$\text{M.S. (Torsion)} = \frac{123{,}000}{22{,}000} - 1 = 4.60$$

5.3 MAIN ROTOR 1g OPERATING STRESSES

The stresses calculated at several locations on the rotor, for flight at 140 knots and 355 rpm, are tabulated below. These data (from Reference 1) give a general indication of the fatigue strength of the rotor; all are below the calculated endurance limits.

TABLE I. SUMMARY OF 1g MAIN ROTOR OPERATING STRESSES (CALCULATED)

Member	Material	Station	Steady Stress (psi)	Cyclic Stress (psi)
Hub	4340 Steel 160,000 psi	9	19,800	17,200
Flexure	17-4 Steel H900	73	29,700	11,900
Blade	301 Steel 1/2 Hard	94	32,390	10,170
Blade	301 Steel 1/2 Hard	138	39,800	12,370

5.4 FATIGUE TESTS

The main components of the new rotor system were fatigue tested to demonstrate safe life for the planned flight tests. The components which were tested are:

- Hub and hub-to-flexure splice
- Flexure and flexure-to-blade splice
- Blade root and blade-to-flexure splice
- Pitch control system, from pitch arm to flexure
- Outer blade

A brief description of each test follows.

5.4.1 Tests of the Hub and Hub-to-Flexure Splice

An assembly consisting of the inboard portion of the flexure (simulated), a single-arm hub, and the hub-to-flexure splice was fatigue tested in a jig in which the hub was attached to a part of the jig which represented the rotor shaft. Loads were applied by hydraulic jacks in a manner that caused design bending and torsion moments and centrifugal forces to occur at Station 20. Figure 21 shows a typical load spectrum for a single flight.

Figures 22 and 23 show the test setup and the test programmer controlling the load spectrum by monitoring tape-recorded signals.

This component completed 1,331 simulated flights (322 hours), consisting of 3.08×10^6 cycles of the load spectrum and 1,400 start-stop cycles, without failure. A complete report is contained in Reference 9.

5.4.2 Tests of the Flexure and Flexure-to-Blade Splice

An assembly consisting of a flexure, splice plates, and a simulated blade fitting was tested. Hydraulic jacks were used to apply shear, tension, and torsion in a manner that design loads occurred at Station 73. The test setup is shown in Figure 24. The load spectrum was controlled in the manner described above.

The flexure completed 1,447 simulated flights (382 hours), consisting of 3.18×10^6 cycles of spectrum loading and 1,536 start-stop cycles, without failure.

5.4.3 Tests of the Blade Root and Blade-to-Flexure Splice

The test article consisted of the inboard part of the blade, the blade-to-flexure splice, and a simulated outboard end of the flexure. The setup for this test is shown in Figure 25.

The blade root and blade-to-flexure splice completed 1,377 simulated flights (344 hours), consisting of 3.11×10^6 cycles of spectrum loading and 1,501 start-stop cycles, without failure.

5.4.4 Tests of the Pitch Control System

A complete blade pitch control system, from the gyro pitch link to and including the gimbal on the outboard end of the flexure, was tested. Start-stop cycles were included in the load spectrum. The setup for this test is shown in Figure 26.

The system sustained 10.1×10^6 cycles of maximum feathering moment and 1,885 on-off cycles of centrifugal force without failure.

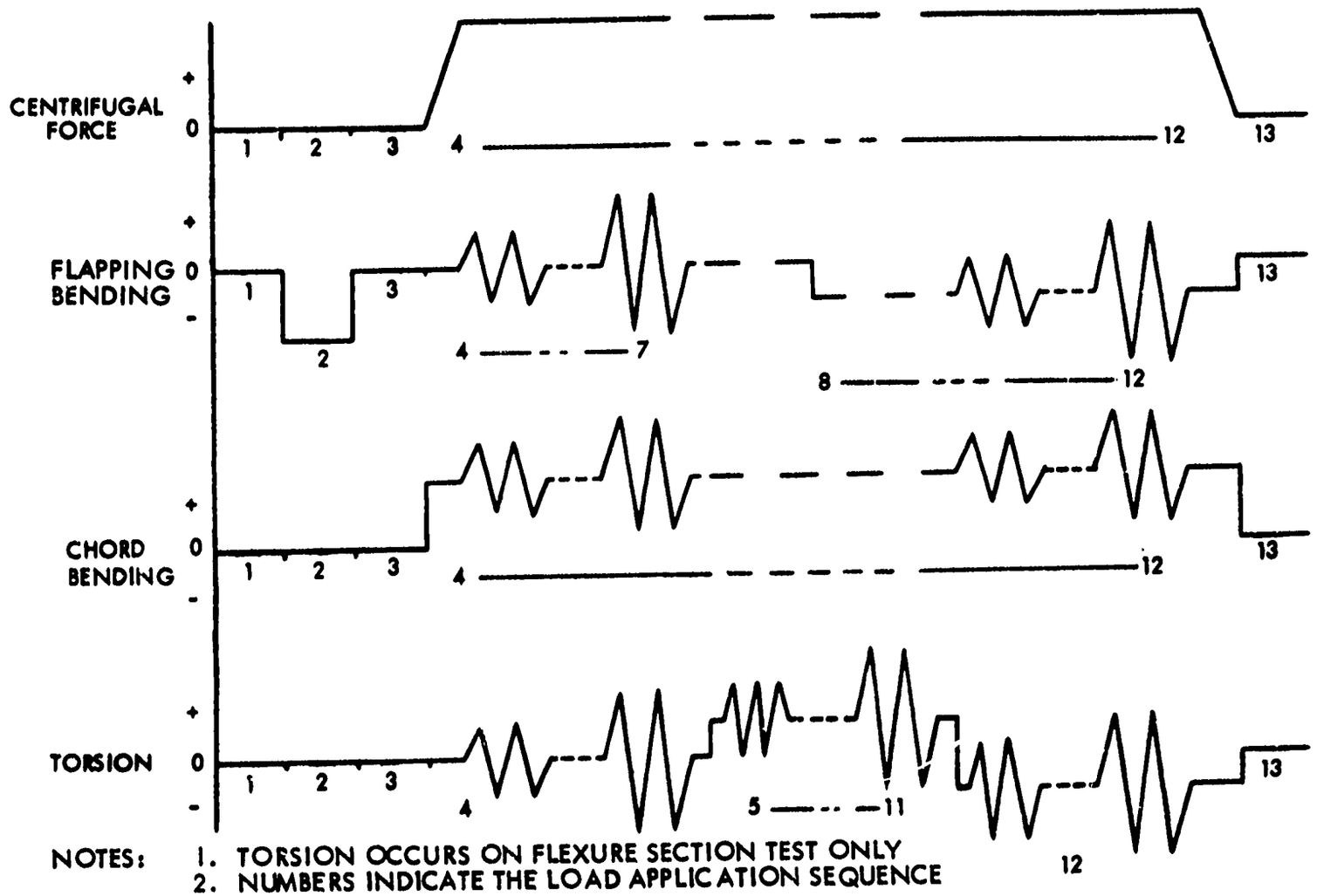

Figure 21. Typical Flight-by-Flight Load Spectrum.

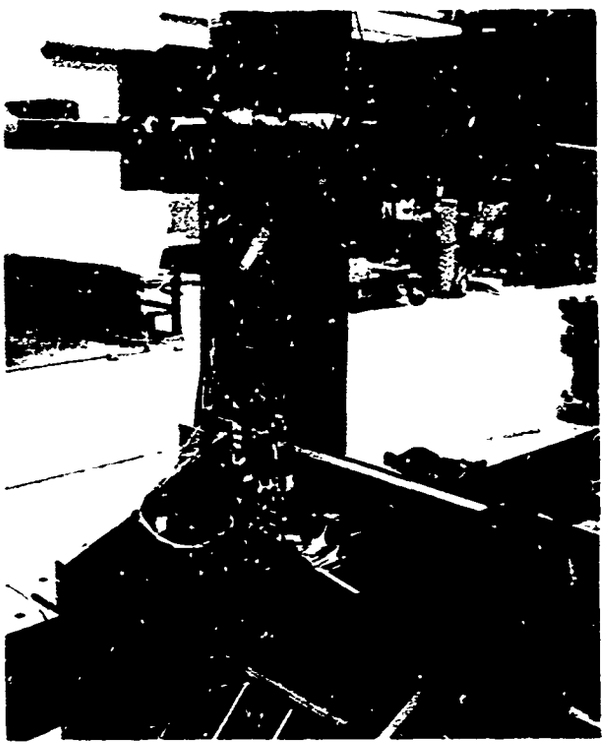

Figure 22. Hub Arm Fatigue Test Setup.

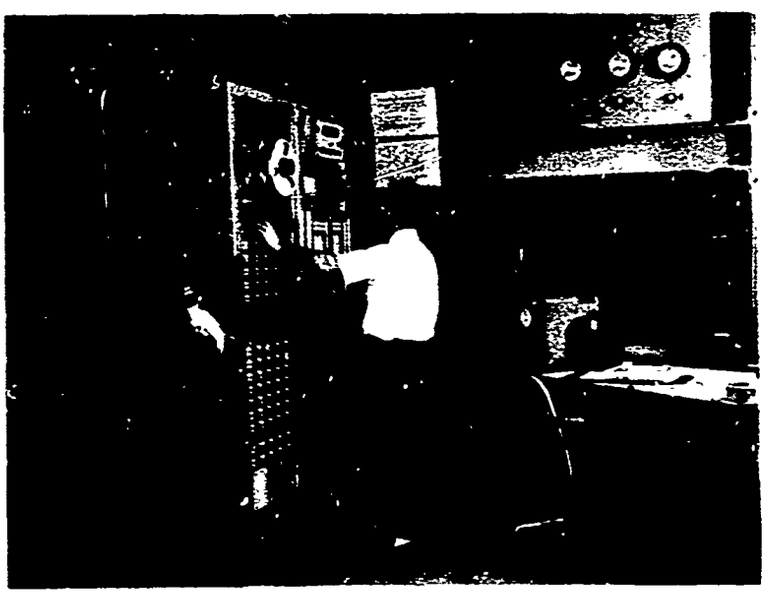

Figure 23. Test Load Application Programming Equipment.

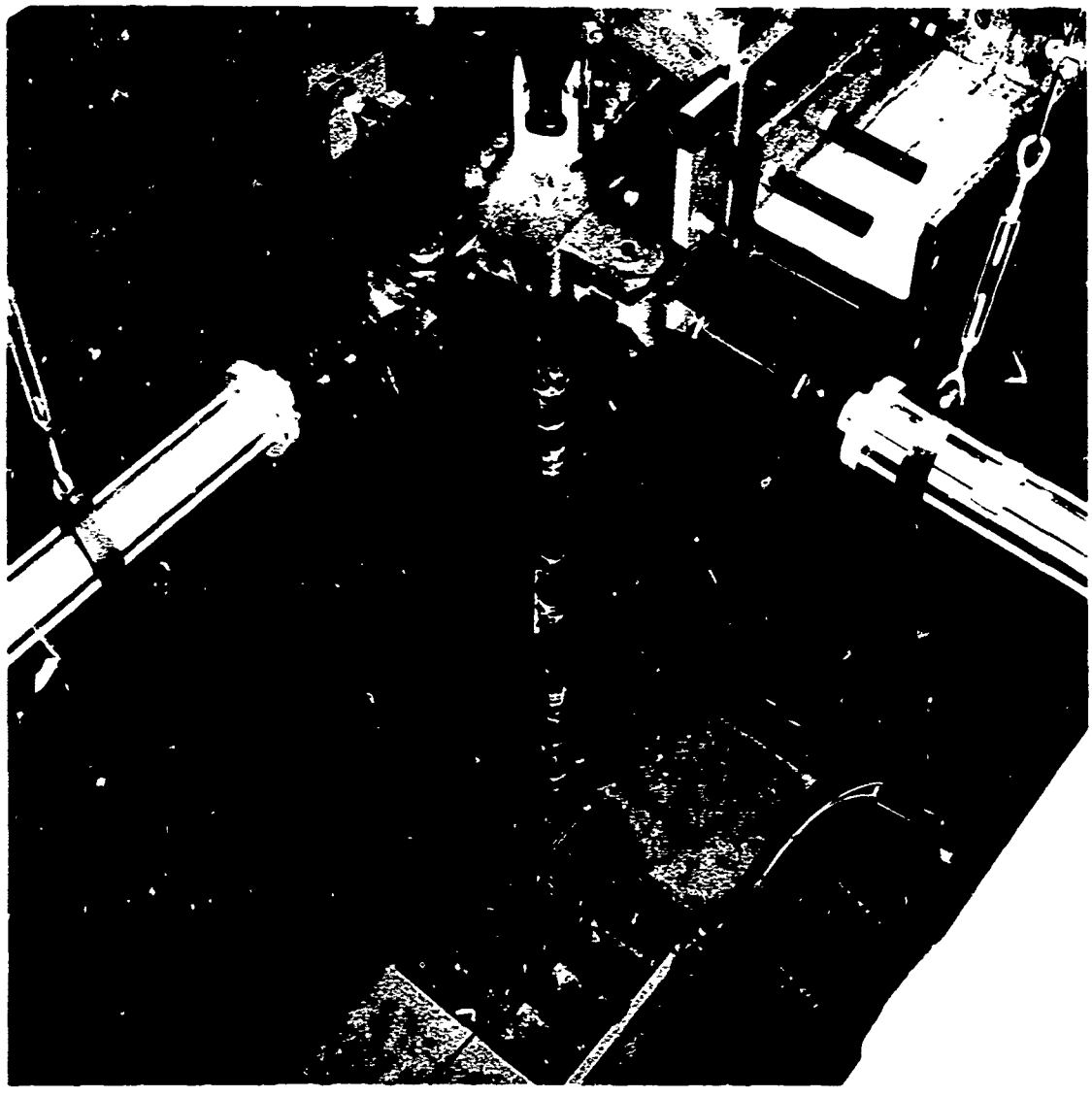

Figure 24. Flexure System Test Setup.

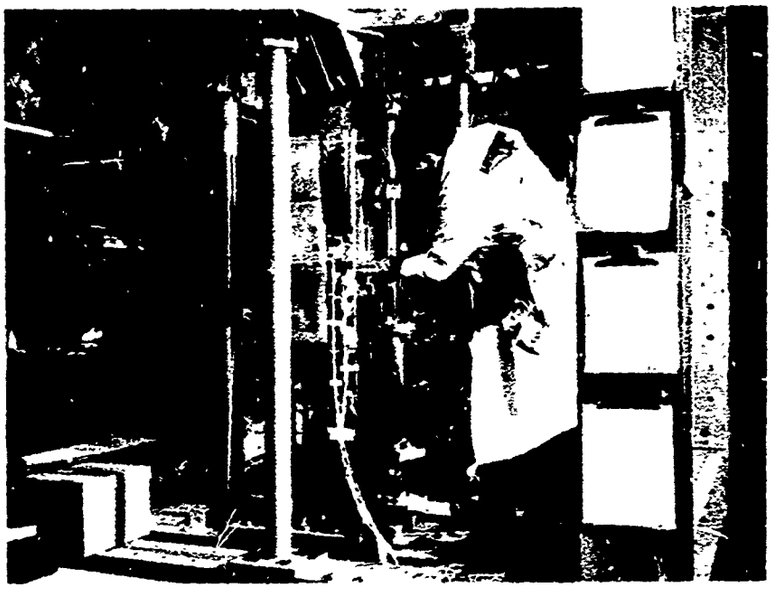

Figure 25. Blade Root End Fatigue Test Setup.

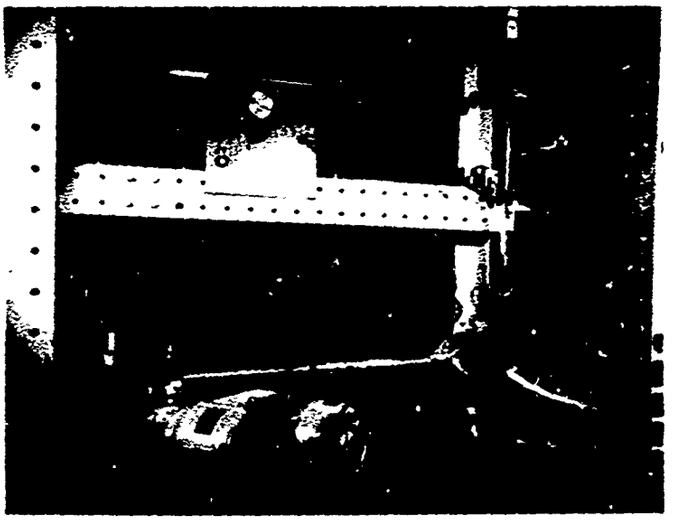

Figure 26. Control Torque Tube System Fatigue Test Setup.

5.4.5 Tests of the Outer Blade

Each test article consisted of a full length blade of typical construction except that only the longest doubler was included. The section which had been determined to be critical was outboard of this doubler. The specimen was supported on two slings. An oscillatory excitation was applied at the inboard end to produce the design stress level at the critical section. Each blade was instrumented and calibrated such that stresses could be monitored. Two samples were tested in the flap bending direction and another two in the in-plane bending direction.

One flap bending specimen completed 12.62×10^6 cycles of load without failure, the maximum stress was 44,000 psi. The second specimen completed 1.1×10^6 cycles with a maximum stress of 50,000 psi; failure occurred through the shear beam.

One chord bending specimen completed 17.9×10^6 cycles with a maximum stress of 49,000 psi with no primary structural failure. The aluminum trailing edge skin cracked in a spanwise direction at the aft edge of the shear beam, adjacent to a slot, after 2.3×10^6 cycles. The crack did not grow beyond 0.50 inch as load application continued to 170.9×10^6 cycles. The second specimen failed at 55,000 cycles due to 54,500 psi stress in the shear beam.

5.4.6 Conclusions Reached From Fatigue Tests

Conclusions were qualified since tests on the hub, flexure, and splices were stopped after 75 percent of the scheduled testing was successfully completed. This was done to allow for modification of the test load spectrum, should flight test measurements indicate this to be necessary. However, the early termination of the flight test program precluded completion of the fatigue tests. Based on the tests which were conducted, the following conclusions are made:

- The hub, flexure, blade root, and their attachments are predicted to have safe lives of at least 112 flight test hours (based on a test reduction factor of 3).
- The outer blade and pitch control system are predicted to have safe lives in excess of 1,000 hours.

SECTION 6

GROUND TESTS

Tests were conducted with the rotor not rotating to measure the natural frequencies of various blade modes and the frequency and damping properties of the body modes on the landing gear and on the whirl tower. Pitch and roll moments of inertia of the unmodified XH-51A helicopter were also measured for reference.

6.1 SHAKE TESTS

6.1.1 Main Rotor

The test setup included the main rotor hub and two complete flexure and blade assemblies fastened at 90 degrees to each other, as shown in Figure 27. The assembly was fastened to a bench such that the rotor was in a horizontal plane. A dummy gyro hub was installed; its cyclic motion was restrained by blocks. Spacers were used to preset collective angles. A shaker was attached to the blade tip to provide flapping, chordwise, and torsional excitation.

Flapping, chordwise, and torsional frequencies were measured for three different blade angles. The out-of-phase chordwise modes were recorded (modes where the tips of the blades moved together or apart at the same time) to measure in-plane bending natural frequency without being influenced by yaw flexibility of the support. The measured frequencies were as expected, lower than calculated (and than would exist on the aircraft) due to the mass of the shaker and its attachment fittings, and to flexibility of the support. Measured frequencies are compared with analysis results in Table II.

A test was also conducted to determine the torsional frequency of the blade-flexure system with the pitch link disconnected. This test disclosed two modes: one had a natural frequency of 28 cps, the other a natural frequency of 8.3 cps. The higher frequency mode was similar to that with the pitch link connected (the torsion mode shown in Table II), probably due to the effect of bearing friction in linkage. The 8.3 cps mode corresponded to the calculated first torsional mode of the blade and flexure.

6.1.2 Fuselage

Vibration tests were performed on the XH-51A to determine body frequencies when completely supported by the gear, and when partially suspended (approximately half the weight supported by the gear). The vehicle was ballasted to represent the flight configuration.

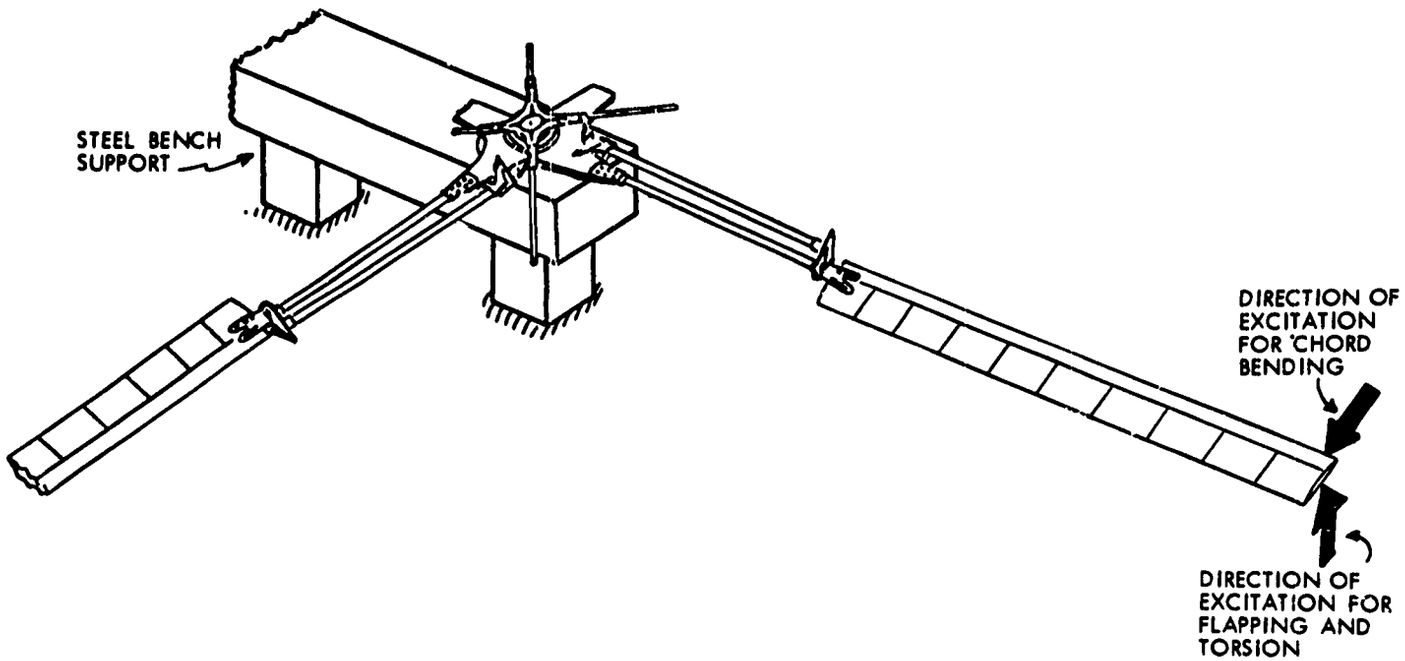

Figure 27. Main Rotor Shake Test Setup, Matched-Stiffness Flexure, Hub, and Blade.

TABLE II. NONROTATING FREQUENCIES OF MAIN ROTOR BLADES

MODE DESCRIPTION	FREQUENCY, cps					
	MEASURED			CALCULATED		
	$\Theta = 0$	$\Theta = 7.33^\circ$	$\Theta = 14.8^\circ$	$\Theta = 3.75^\circ$	$\Theta = 10.88^\circ$	$\Theta = 15.46^\circ$
1st Vertical Bending	1.26	1.26	1.25	1.35	1.35	1.35
2nd Vertical Bending	6.6	6.69	6.8	6.61	6.63	6.66
3rd Vertical Bending	16.8	16.9	17.3	17.74	17.86	18.06
1st In-plane Bending	1.78	1.74	1.76	1.93	1.93	1.92
2nd In-plane Bending	14.1	14.2	13.7	14.16	14.03	13.84
3rd In-plane Bending	38.3	38.0	37.2	34.19	33.81	33.36
1st Torsion	28.3	29.2	29.6	—	—	—

Θ is defined as blade angle at inboard end of blade relative to hub.

The tests were conducted in three parts:

(1) with soft-mounted transmission, gear dampers off, outriggers off

(2) with hard-mounted transmission, gear dampers on, outriggers off

(3) with hard-mounted transmission, gear dampers on, outriggers on

When these tests were made, the aluminum landing gear skids were on the aircraft. (The landing gear modification, which came after these tests, was estimated to have increased the pitch stiffness approximately 20%.)

The very low frequencies, approximately 2 to 3 cps, were excited by manually applied forces. Calidyne shaker equipment was used for higher frequencies. Locations of applied forces are shown on Figure 28. The measured frequencies are tabulated in Tables III, IV and V.

The shake tests showed that hard-mounting the transmission eliminated the undesirable high-mode rigid-body roll mode (therefore, this mode does not appear in Tables IV and V). This mode consists of transmission roll out of phase with fuselage roll.

The data in Table IV show decay rates that were measured with landing gear dampers installed (damping ratios are listed). The magnitude of the damping appears to be hardly more than might be expected from structural damping. This suggests that the damper design was not effective in increasing the on-the-ground mechanical stability margin. In fact, a comparison of the pitch and plunge frequencies in Tables III and IV shows the dampers to have a stiffening effect (this is explained in Section 10.2.2).

The mass added to the outriggers affected mostly the roll modes. Note that the roll frequencies in Table V are lower than in the preceding tables. This result was expected; the outriggers were included in the test plan as a means of lowering roll frequencies.

6.2 INERTIA DATA MEASUREMENTS

Center-of-gravity location and mass moments of inertia of the test aircraft about the pitch and roll axes were measured. Since calculated values were based on drawings, which can differ from hardware, it was decided that measured data would be appropriate for evaluating the tests.

The fore and aft center-of-gravity locations were determined by suspending the aircraft by a cable. The vertical location was calculated from data which included measuring the force in the suspension cable with a load sensor, applying known forces at the tail, and measuring the aircraft's attitude.

NOTES:

- DASHED ARROW INDICATES SHAKER PHASING FOR ROLL EXCITATIONS
- SHAKERS LOCATED AT FS 85

Figure 28. Shaker Locations for Ground Vibration Tests.

TABLE III. RIGID-BODY FREQUENCIES, AIRCRAFT ON LANDING GEAR (NO DAMPERS)

Means of Excitation	Description of Mode	Frequency, cps	
		Total Gross Weight on Skids	1/2 Gross Weight on Skids
Hand	Yaw	1.35	1.2
Hand	Pitch	2.5	2.0
Shaker	Plunge, forward and down (about 45°)	2.9	2.5
Shaker	Vertical, console and nose	7.7	-
Shaker	Roll, low node	5.68	5.0
Shaker	Roll, high node	6.95	6.05
Shaker	Roll, with aft-fuselage side bending	9.35	-

- Transmission was soft-mounted
- Aircraft gross weight = 3700 lb
- 1/2 gross weight on skids represents a partial lift condition

TABLE IV. RIGID-BODY FREQUENCIES, AIRCRAFT ON LANDING GEAR (WITH LANDING GEAR DAMPERS)

Means of Excitation	Description of Mode	Total Gross Weight on Skids (lb)		1905 lb on Skids	
		f	ζ	f	ζ
Hand	Yaw	1.34	.068	1.39	-
Hand	Pitch	2.63	.038	2.50	.055
Shaker	Plunge, forward and down (about 45°)	3.15	77.20	2.75	77.20
Shaker	Vertical, console and nose	7.8	-	-	-
Shaker	Roll, low-node	5.75	.036	5.91	.065
Shaker	Roll, with aft-fuselage side bending	9.3	-	8.8	-

- Transmission was hard-mounted
- Aircraft gross weight = 3875 lb
- The 1905-lb case represents a partial-lift condition
- f = frequency, cps
- ζ = damping ratio

TABLE V. RIGID-BODY FREQUENCIES, AIRCRAFT WITH OUTRIGGERS ON LANDING GEAR (WITH DAMPERS)

Means of Excitation	Description of Mode	Frequency, cps	
		Total Gross Weight on Skids	1905 lb on Skids
Hand	Yaw	1.42	1.3
Hand	Pitch	2.6	2.4
Shaker	Plunge, forward and down (about 45°)	3.4	3.3
Shaker	Vertical, console and nose	7.7	7.5
Shaker	Roll, low mode	5.22	5.3
Shaker	Roll, with aft-fuselage side bending	7.7	7.6

- Transmission was hard-mounted
- 100 lb on each outrigger, 5.5 ft from centerline
- Aircraft gross weight = 4145 lb
- The 1905-lb case represents a partial-lift condition

Mass moments of inertia were determined as follows. The fuselage was suspended using a universal joint at the top of the rotor mast, and swung in a pendular motion. Pitch and roll directions were examined separately. Frequencies of the oscillations were measured with an electronic counter. The frequency data were combined with the weight and center-of-gravity locations to determine moments of inertia. Results corresponding to a gross weight of 3,026 pounds were:

$$I_{PITCH} = 3{,}434 \text{ slug-feet}^2 \text{ (excluding rotor)}$$

$$I_{ROLL} = 304 \text{ slug-feet}^2 \text{ (excluding rotor)}$$

Section 7 shows that whirl tower tests were conducted with simulated moments of inertia different from those given above. The inertia frame and spring systems of the whirl tower had been fabricated prior to making the above measurements, so the inertia frame did not have the capability to simulate the proper pitch inertia. However, since the primary concern was the frequencies rather than moments of inertia, it was simply a matter of adjusting spring rates and inertia values in proper combinations to simulate the proper roll and pitch frequencies.

6.3 NONROTATING TESTS OF DYNAMIC CHARACTERISTICS OF THE WHIRL TOWER TEST SETUP

The gimbaled whirl tower frame was designed to accommodate various amounts of ballast so that mass moments of inertia could be varied. Adjustable springs were provided to restrain gimbal motion, to simulate landing gear stiffness, for example. Tests were made of the whirl tower/body system to establish roll and pitch frequencies and damping ratios.

The measured spring rates are listed in Table VI. The body frequencies and damping ratios are listed in Table VII. A range of frequencies and moments of inertia was established by these tests to determine the choice of arrangements that was available in the whirl tower test setup.

TABLE VI. MEASURED SPRING RATES ON WHIRL TOWER SPRINGS BETWEEN INERTIA FRAME AND GROUND (BASED ON STATIC DEFLECTION TESTS)

	Number of Spring Elements Connected	Spring Rate (ft-lb/radian)	
Roll Spring System	4	331,000	
	2	173,000	
(See note (1))	1	84,700	
		Pin at 29"	Pin at 20.5"
Pitch Spring System	4	226,000	407,000
	3	-	310,000
(See note (2))	2	133,000	226,800
	1	66,500	119,700

NOTES:

(1) The roll spring system consists of four torsion bars attached to the moving portion of the inertia frame and connected to the stationary part of the whirl tower through an arm and push rod.

(2) The pitch spring system consists of four leaf springs attached at one end to the stationary part of the whirl tower and at the other end to the moving portion of the inertia frame, through a push-pull rod (shown in Figure 30). The stiffness is adjustable by changing the distance between two pins which fasten the springs to the whirl tower. The "pin at 29 or 20.5" in the table refers to the location of one pin relative to the other. The lesser dimension represents the stiffer spring.

TABLE VII. WHIRL TOWER SHAKE TEST RESULTS

Excitation	Number of Elements Connected	Frequency (cps)	Damping Ratio ζ	Comment	Mass Moment of Inertia ($slug\text{-}ft^2$)
Pitch	4	2.30	.036	pin at 20.5"	1930
	2	1.67	.074	pin at 20.5"	2040
	1	1.27	.065	pin at 20.5"	1870
	1	.89	.130	pin at 29"	2100
Roll	4	3.33	.027		750
	2	2.43	.040	right push rod removed	735
	1	1.75	.060	left rear spring only	693
	1	1.73	.048	left rear spring only	710

NOTE:

(1) See notes on Table VI for description of spring systems and meanings of terms in "Comment" column above.

(2) Mass moments of inertia were determined from frequencies, damping ratios, and spring-rates listed in Table VI.

SECTION 7

WHIRL TOWER TESTS

The objective of these tests was to help define the best rotor configuration, particularly with respect to mechanical stability limits. The rotor was modified twice during these tests, once to eliminate a torsional flutter mode and again to incorporate mechanical control system coupling.

7.1 DESCRIPTION OF THE WHIRL TOWER

The whirl tower is shown in Figures 29 and 30. It is powered by a B1820 radial engine through a manually operated clutch. Power is transmitted by a driveshaft to a right-angle gearbox which transmits the power to a vertical shaft to rotate the rotor. The rotor system is installed on a gimbaled inertia frame which is free to move in pitch and roll. A constant-velocity universal joint located at the gimbal center is included in the drive line. Approximately ±10 degrees of roll and pitch attitude change are available with the gimbal. The gimbal point is 40 inches below the hub, which corresponds to the nominal center of gravity of the XH-51A.

A pneumatic locking device was provided to arrest all motion in the event of an emergency. The "caged" system becomes extremely stiff and thus provides a positive means of rapidly stabilizing a ground or air resonance condition at its inception.

Spring rates and mass moment of inertia of the frame are adjustable.

The collective control system was operated by an electric actuator which was controlled by a beeper switch on the cyclic stick. The cyclic control system was similar to that in the test aircraft except that a force-servo system was used in lieu of positive springs. The force-servo system consisted of a force sensor, a servo amplifier, a hydraulic actuator, and a pilot control input potentiometer. The system controlled the force at the load cell to a level commanded by the pilot through an input signal. A schematic of the cyclic control system is shown in Figure 31.

Instrumentation in the control room included indicators for body pitch and roll moments and angles, rotor lift, and flapping and in-plane bending moments at the blade root. The body attitudes were displayed on an oscilloscope in a manner similar to an artificial horizon.

The whirl tower equipment included a 50-channel oscillograph recording system on which blade loads, body motions, and control loads and motions were recorded. Motion picture cameras were provided to photograph the rotor system and the control panel. An emergency system was included. A single handle could cut the throttle, reduce the collective pitch, set the oscillograph to "fast record", cage the inertia frame, and activate the cameras.

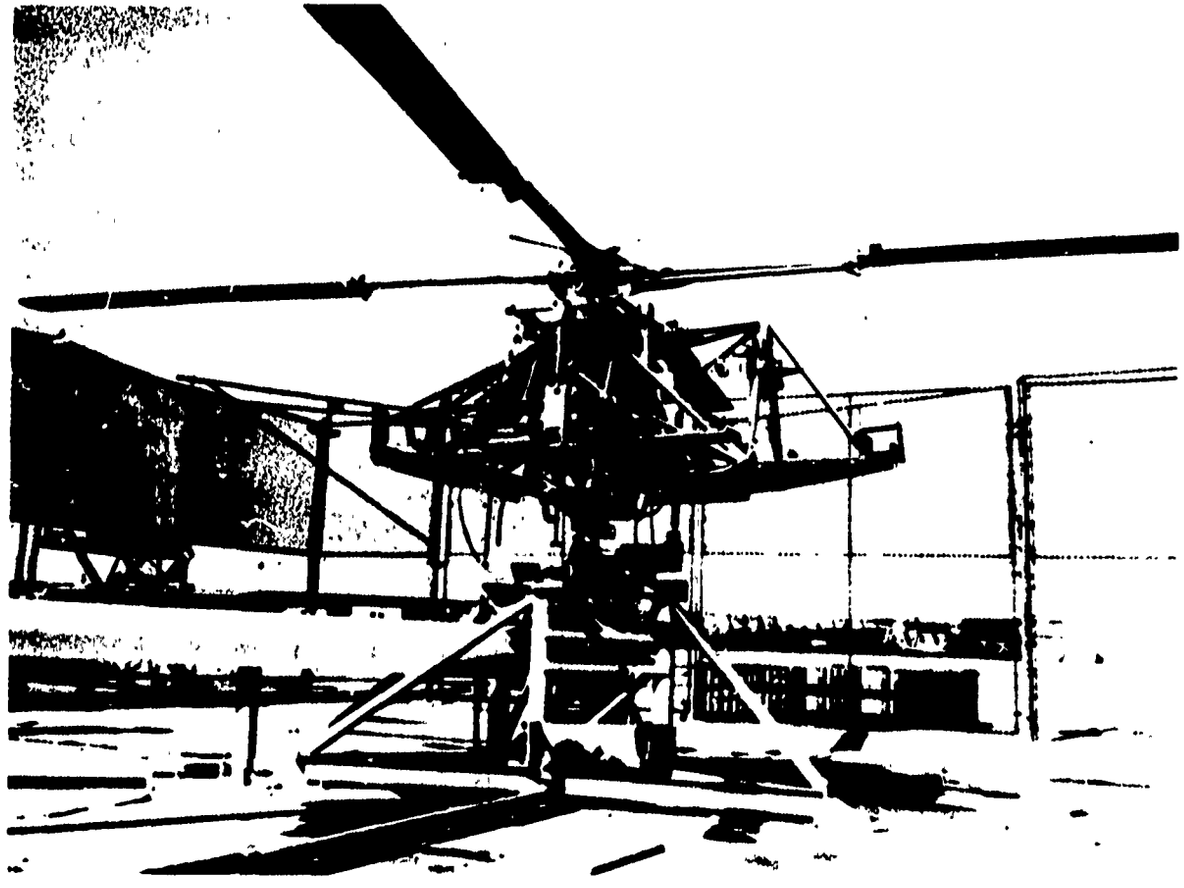

Figure 29. The Matched-Stiffness Test Rotor on the Whirl Tower.

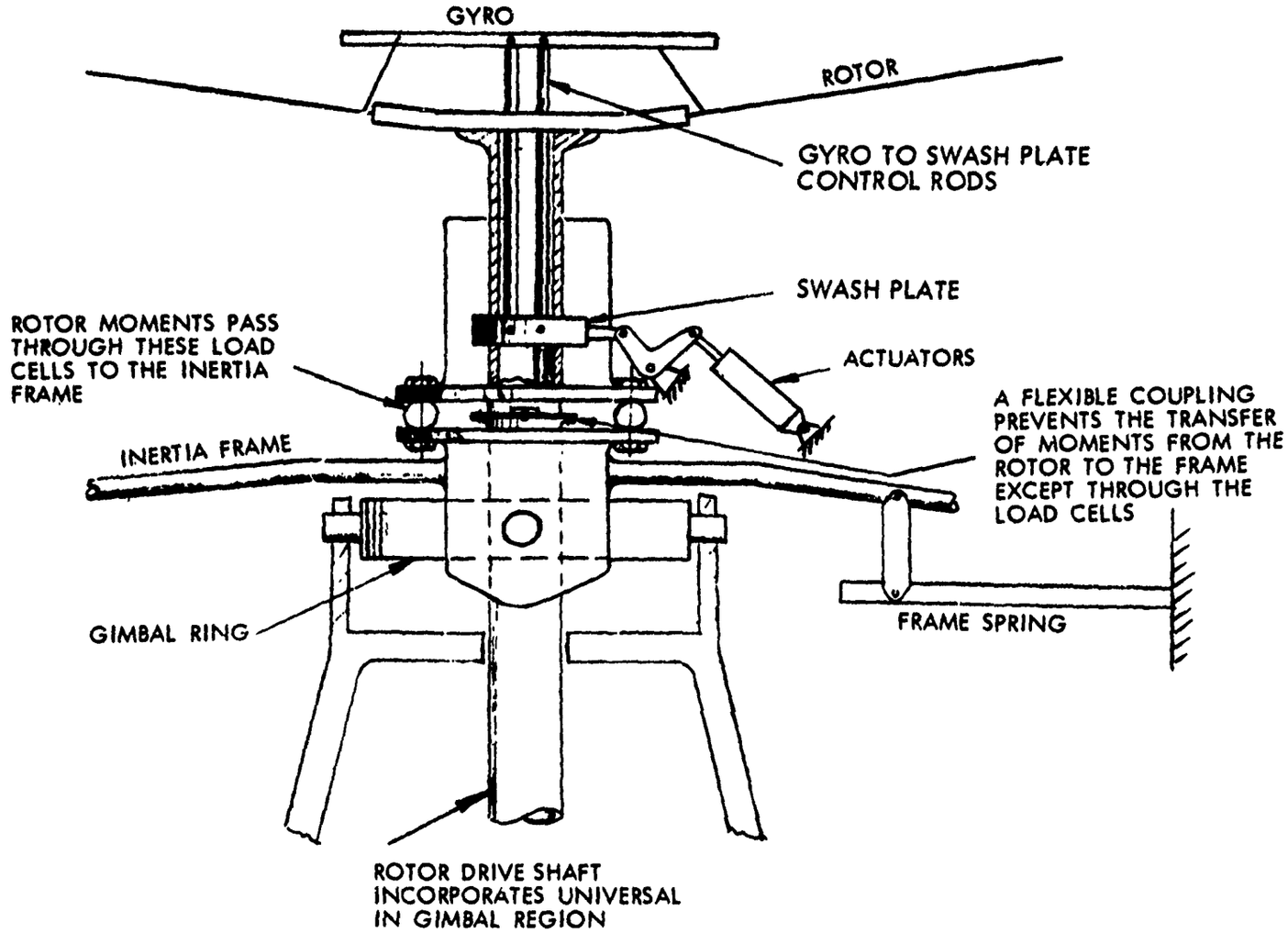

Figure 30. Schematic Diagram of Whirl Tower.

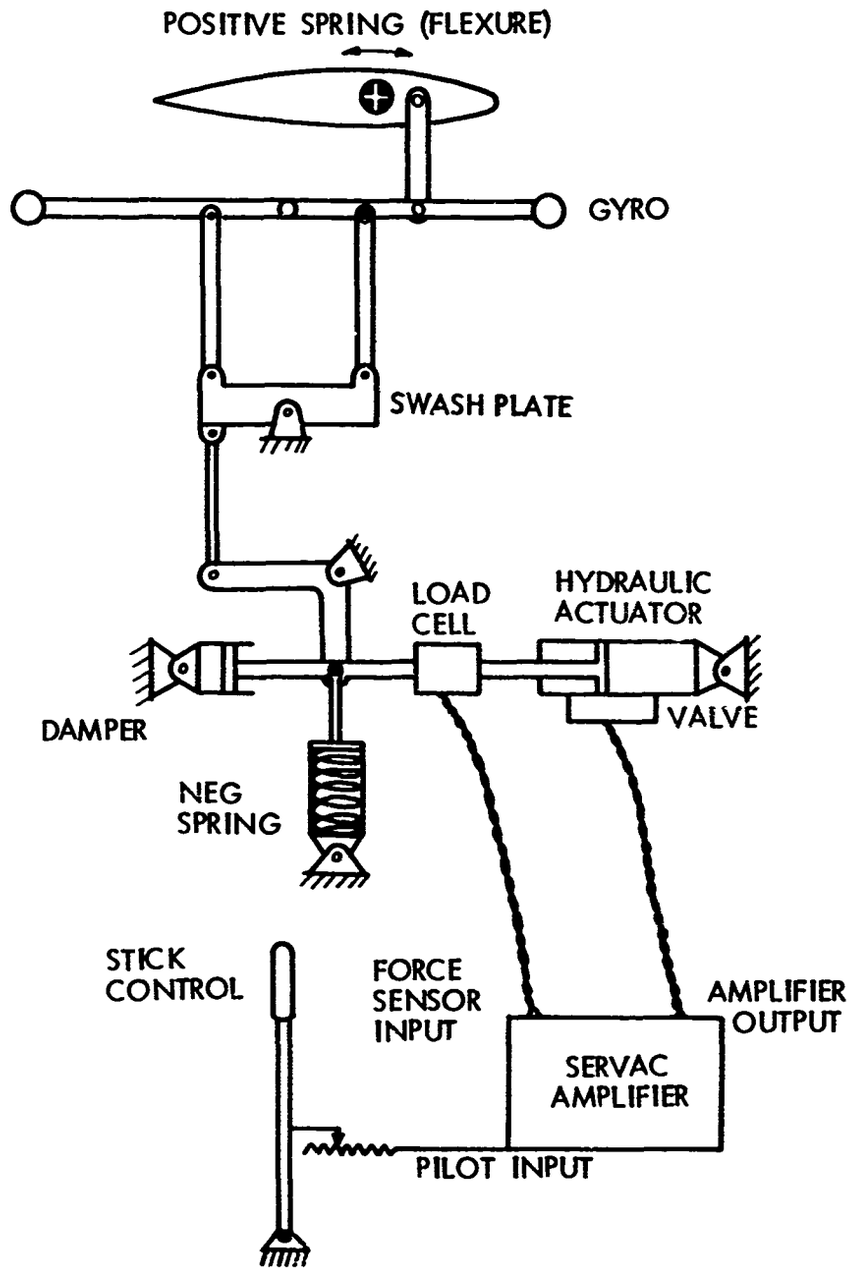

ONE CONTROL IS SHOWN. THE OTHER IS THE SAME EXCEPT DISPLACED 90° IN AZIMUTH

Figure 31. Schematic Diagram of Whirl Tower Cyclic Control System.

7.2 WHIRL TOWER TEST PROCEDURE

The first tests were conducted with the inertia frame caged. These tests were made to examine strain and motion data and to observe general stability characteristics of the rotor blades.

Tests were made to investigate on-the-ground rotor/body mechanical stability limits. Various combinations of springs and inertias were used to simulate body roll and pitch frequencies. In each test the frame was uncaged at a rotor speed below the predicted stability limit; then cyclic control motions ("stick stirring") were applied to excite the rotor/body motion coupling. Rotor speed was increased in small increments until either neutral stability or divergence tendencies were observed.

Tests were also made to investigate rotor/body mechanical stability limits that might be expected in flight. The frame was caged while the rotor was accelerated to a rotational speed predicted to be safely above the flight stability limit. Then it was uncaged and the system was "flown" by monitoring the frame's attitude on the oscilloscope and applying cyclic control to maintain a level attitude. Cyclic disturbances were introduced, and rotor speed was decreased incrementally until divergence characteristics were evident.

Tests were made to determine the effects of varying a number of configuration characteristics to provide data for considering the possibility of making changes to the rotor prior to flight tests. Variables which were tested are:

- Blade sweep
- Blade cone angle
- Control gyro size
- Blade tip weights
- Body roll and pitch inertia
- Body roll and pitch spring rates

7.3 WHIRL TOWER TEST RESULTS AND THEIR INFLUENCE ON THE FLIGHT TEST ROTOR SYSTEM

Early tests exhibited a divergent noise/vibration which was diagnosed as a high frequency (35 cps) flutter mode which involved coupling between the third flapping and the first torsional modes of the blades. This condition was corrected by adding weights at an aft chord location at blade Station 80. The "fix" is shown in Figure 32.

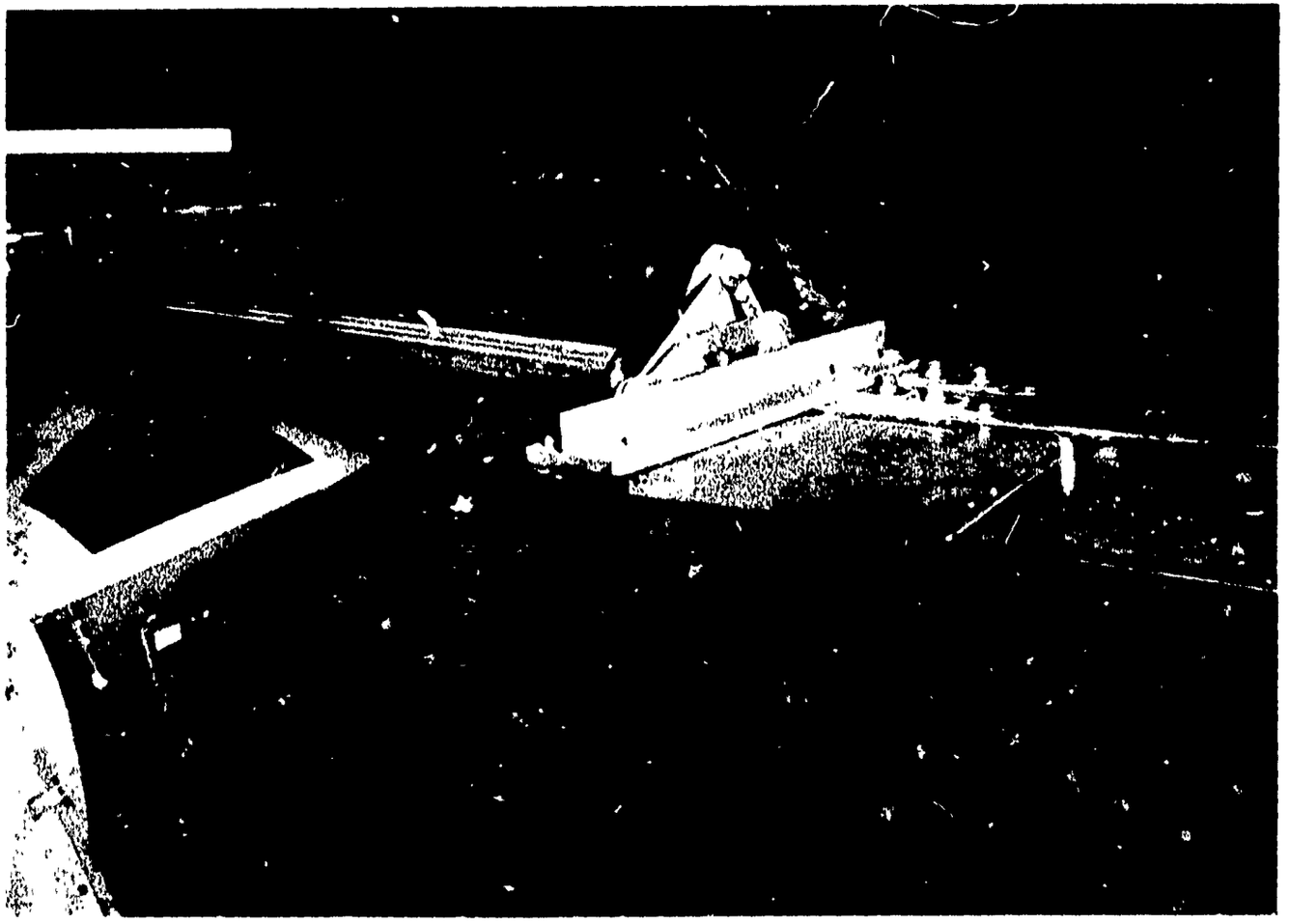

Figure 32. Chordwise Balance Weights at Inboard End of Blade.

A list of the tests is given in Table VIII. The table identifies configuration changes and rotor speeds where neutral stability tendencies were observed. The effects of varying configuration characteristics are summarized in Table IX. Data are shown in both tables for the flight case (zero landing skid stiffness), and the ground case (landing gear stiffness simulated).

Several hours of testing (approximately 7) were performed with the initial rotor control system; that is, the system which had no mechanical control coupling ($\alpha_3 = \delta_3 = 0$). The only one of these tests recorded in Table VIII is Test 29. All other data shown are for tests made after the rotor had been modified to include mechanical coupling.

It was originally intended that more extensive testing be made with $\alpha_3 = \delta_3 = 0$, but since the tests were interrupted by the bearing failure, and since the design team had become convinced that coupling was beneficial, it was decided to make the geometry change coincident with the bearing modification. Details of the change are shown in Figures 33 and 34 and in Figure 75 in the Appendix. The resulting geometry included mechanical coupling defined by the values tangent $\alpha_3 = 0.769$ and tangent $\delta_3 = -0.318$.

It is of interest to note that the modified test rotor had a positive α_3 and a negative δ_3, whereas analyses had been made with both values positive (for example, see Figure 14). It was rationalized that since the potential instability was characteristically due to in-plane motion, α_3 was the more influential parameter, so an α_3 value of the algebraic sign and general magnitude consistent with the analyses was selected for testing. It was thought at that time that δ_3 was much less influential than α_3, and that its effect was not strongly dependent on algebraic sign. The negative δ_3 was part of the control system modification selected for testing. Its choice was considered secondary to that of a proper α_3 value. It was decided not to delay the test program to perform an analytical optimization of an α_3 and δ_3 combination; that the whirl tower would be used to evaluate mechanical coupling. It was accepted that other combinations could be tested if need be, but since the $\alpha_3 = 0.716$ and $\delta_3 = -0.318$ combination indicated enough of a margin to encourage proceeding with the program, it was established as the flight test configuration; no others were tested. When viewed in light of the knowledge that vehicle roll inertia changes could be used to increase safety margins (discussed below), the decision to proceed to the flight test program without whirl tower testing other geometries appeared logical.

Flight tests and subsequent analyses later indicated that other combinations of α_3 and δ_3 may have resulted in improved rotor behavior. This is discussed further in Sections 10.2 and 10.5.

Expansion of the safe operating rotor speed range for the on-the-ground case by inclusion of mechanical coupling is seen by comparing Tests 29 and 31 (Table VIII); a favorable rotor speed limit change from 101 to 104 percent is indicated.

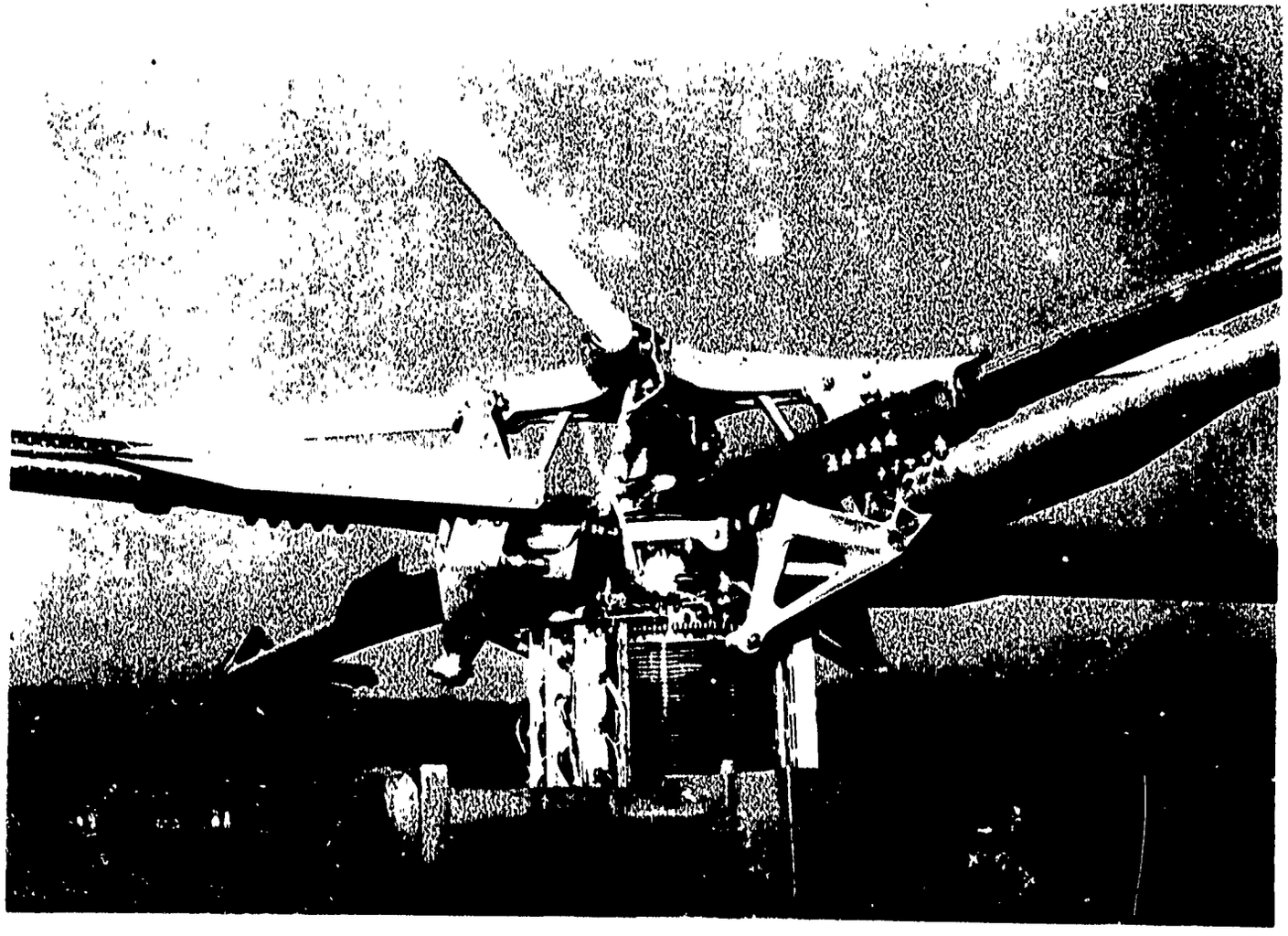

Figure 33. Original Configuration in Use Through Test 29.

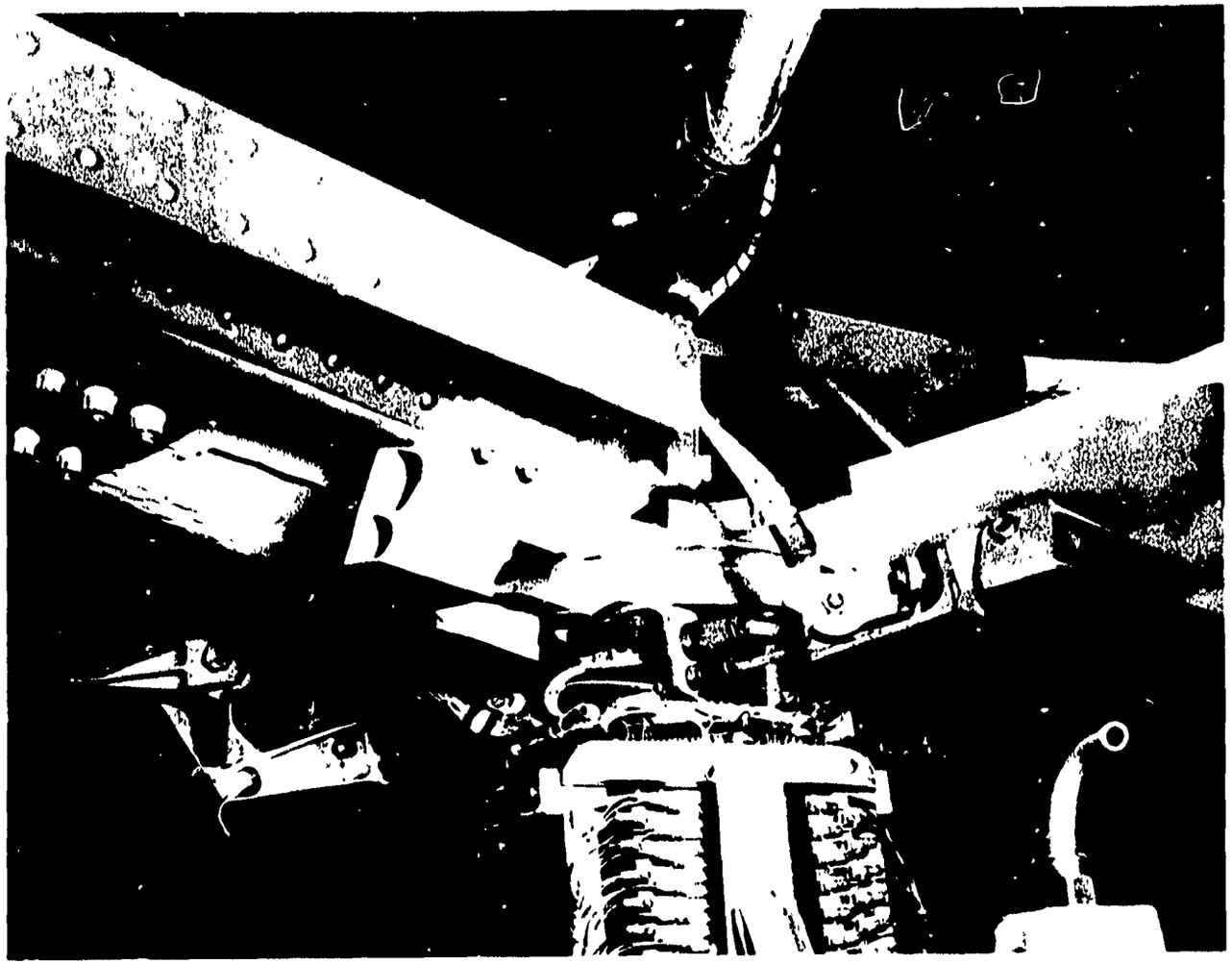

Figure 34. Modified Configuration, Used in Tests 30 Through 75.

TABLE VIII. WHIRL TOWER TEST DATA

TEST NO. (SEE NOTE 1)	FLIGHT OR GROUND Cond	GYRO SIZE (slug-ft^2)	ROTOR ANGLES (DEGREES)		TIP WEIGHT (lb)	INERTIA FRAME (SEE NOTES 2 AND 3)				LIFT (lb)	ROTOR SPEED FOR NEUTRAL STABILITY (% 355 rpm)
			SWEEP	CONE		SPRING		INERTIA (slug-ft^2)			
						PITCH	ROLL	PITCH	ROLL		
29	G	2	1 1/2	1	2	1/2	FULL	960	325	0	101
31	G	2	1 1/2	1	2	1/2	FULL	960	325	0	104
32	G	2	1 1/2	1	2	FULL	FULL	960	325	0	110
33	G	2	1 1/2	1	2	FULL	FULL	1960	525	0	96
34	G	2	1 1/2	1	2	1/2	FULL	1960	525	0	83
35	G	2	1 1/2	1	2	1/4	FULL	1960	525	0	76
36	G	2	1 1/2	1	2	1/8	1/2	1960	525	0	76
37	G	2	1 1/2	1	2	0	1/2	1960	525	0	94
39	F	2	1 1/2	1	2			1960	730	0	77
40	F	2	1 1/2	1	2			1960	525	0	91
44	F	2	2	1	2			1960	525	2000	90
45	F	2	2	1	2			1960	525	0	93
										2000	90
										4000	82
46	F	4	2	1	2			1960	525	0	91
47	F	1	2	1	2			1960	525	0	85
										2000	80
48	G	1	2	1	2	FULL	FULL	1960	525	0	97

TABLE VIII - Continued

TEST NO. (SEE NOTE 1)	FLIGHT OR GROUND Cond	GYRO SIZE (slug-ft^2)	ROTOR ANGLES (DEGREES)		TIP WEIGHT (lb)	INERTIA FRAME (SEE NOTES 2 AND 3)				LIFT (lb)	ROTOR SPEED FOR NEUTRAL STABILITY (% 355 rpm)
			SWEEP	CONE		SPRING		INERTIA (slug-ft^2)			
						PITCH	ROLL	PITCH	ROLL		
49	G	1	2	1	2	FULL	FULL	1960	325	0	100
										2000	104
50	G	1	2	1	2	FULL	FULL	1960	325	0	97
51	G	2	2	1	2	FULL	FULL	1960	325	2000	93
52	G	1	2	1	3.4	FULL	FULL	1960	325	0	89
										2000	91
56	F	1	2	1	3.4			1960	325	0	> 106
										2000	106
57	F	1	2	1	3.4			1960	525	0	85
										2000	83
58	F	1	3	1	2			1960	525	0	80
										2000	80
59	G	1	3	1	2	FULL	FULL	1960	525	0	94
61	G	1	2	0	2	FULL	FULL	1960	525	0	96
62	F	1	2	0	2			1960	525	0	85
										2000	82
63	G	1	2	0	2	FULL	FULL	1960	325	0	95
										2000	96

TABLE VIII - Continued

TEST NO. (SEE NOTE 1)	FLIGHT OR GROUND Cond	GYRO SIZE (slug-ft^2)	ROTOR ANGLES (DEGREES)		TIP WEIGHT (lb)	INERTIA FRAME (SEE NOTES 2 AND 3)				LIFT (lb)	ROTOR SPEED FOR NEUTRAL STABILITY (% 355 rpm)
			SWEEP	CONE		SPRING		INERTIA (slug-ft^2)			
						PITCH	ROLL	PITCH	ROLL		
64	G	1	2	0	0	FULL	FULL	1960	325	0	101
										2000	100
65	F	1	2	0	0			1960	525	0	85
										2000	82
67	F	1	3	1	0			1960	525	0	87
										2000	82
										4000	82
68	F	1	3	1	0			1960	525	2000	79
69	G	1	3	1	0	FULL	FULL	1960	525	0	99
70	G	1	3	1	0	FULL	FULL	1960	525	2000	99
										4000	97
71	G	1	3	1	0	FULL	FULL	1960	325	0	97
										2000	100
										4000	96
72	F	1	3	1	0			1960	325	0	106
										2000	97
										4000	92

TABLE VIII - Continued

TEST NO. (SEE NOTE 1)	FLIGHT OR GROUND Cond	GYRO SIZE (slug-ft^2)	ROTOR ANGLES (DEGREES) SWEEP	ROTOR ANGLES (DEGREES) CONE	TIP WEIGHT (lb)	INERTIA FRAME (SEE NOTES 2 AND 3) SPRING PITCH	SPRING ROLL	INERTIA (slug-ft^2) PITCH	INERTIA (slug-ft^2) ROLL	LIFT (lb)	ROTOR SPEED FOR NEUTRAL STABILITY (% 355 rpm)
73	G	4	3	1	0	FULL	FULL	1960	325	0	97
										2000	99
										4000	99
75	F	4	3	1	0			1960	525	0	92
										2000	93

NOTES:
1. Test 29 with $\alpha_3 = \delta_3 = 0$; all other tests with tan $\alpha_3 = 0.769$ and tan $\delta_3 = -0.318$
2. Full Spring Rates: ROLL = 234,000 ft-lb/rad; PITCH = 407,000 ft-lb/rad
3. Mass moment of inertia values shown do not include rotor or gyro.
   Rotor and gyro produce 220 slug-ft^2 about gimbal axis.
   The 325-slug-ft^2 value shown represents basic aircraft without rotor and without outriggers.
4. Total test time on whirl tower: 27.6 hours.

Referring to Table IX, it can be seen that of the configuration variables tested, other than control system coupling, a strong influence on in-flight stability margins were due to changes in control gyro size and changes in roll mass moment of inertia. For example, a reduction in gyro size from 4 to 1 slug-ft^2 expanded the safe operating rpm range by about 6 percent of the normal operating rpm. A 200-slug-feet^2 increase in roll moment of inertia expanded the range by 10 percent (at 4,000 pounds of lift; slightly more improvement at a lesser rotor lift); this is seen by comparing Tests 67 and 72, Table VIII.

The configuration change which showed a strong influence on on-the-ground stability margins was a reduction in blade tip weight. Each pound of tip weight influenced the stability margin by about 10 rpm (almost 3 percent).

A summary of the effects of the changes is given below.

Configuration Variable	Effect on Rotor Speed for Neutral Stability	
	In Flight	On the Ground
Blade Forward Sweep	Beneficial	Harmful
Blade Overcone	Nil	Beneficial
Blade Tip Weight	Nil	Harmful (when added)
Gyro Inertia	Harmful (when increased)	Nil
Body Inertia, roll	Beneficial (when increased)	Nil
Pitch Spring	Not Applicable	Beneficial (when increased)

The configuration selected as a result of the whirl tower tests included the following parameters:

3 degrees forward blade sweep

1 degree blade overcone

0 lb blade tip weight

1 slug-foot^2 gyro inertia

Mechanical coupling: tangent $\alpha_3 = 0.769$ and tangent $\delta_3 = -0.318$

Figure 35 presents the stability characteristics of this configuration

TABLE IX. EFFECTS OF CONFIGURATION VARIABLES ON ROTOR STABILITY LIMITS

VARIABLE TESTED	ROTOR SPEED FOR NEUTRAL STABILITY (% OF 355)					
	IN FLIGHT			ON THE GROUND		
BLADE SWEEP, deg						
1 1/2	91(40)					
2	93(45)		85(47)		97(48)	
3			80(58)		94(59)	
OVERCONE ANGLE, deg						
0		85(62)		96(61)		95(63)
1		85(47)		97(48)		97(50)
GYRO INERTIA, slug-ft^2						
1	85(47)		87(67)		96(71)	
2	93(45)					
4	91(46)		92(75)		97(73)	
BLADE TIP WEIGHTS, lb						
0	85(65)		87(67)	101(64)		99(69)
2	85(62)	85(47)	80(58)	95(63)	97(50)	94(59)
3.4		85(57)			89(52)	
ROLL INERTIA, slug-ft^2						
325	106(56)		106(72)		97(50)	
525	84(57)	91(40)	87(67)		97(48)	
730		77(39)				

Numbers in parentheses identify whirl tower tests; see Table VIII

TABLE IX - Continued

VARIABLE TESTED	ROTOR SPEED FOR NEUTRAL STABILITY (% OF 355)		
	IN FLIGHT	ON THE GROUND	
PITCH INERTIA, slug-ft^2			
960	-	110(32)	104(31)
1960	-	96(33)	83(34)
PITCH SPRING (See Note 2 of Table VIII)			
1/4	-		76(35)
1/2	-	104(31)	83(34)
FULL	-	110(32)	96(33)

Numbers in parentheses identify whirl tower tests; see Table VIII

based on data obtained from oscillograph records. The figure shows that mechanical instability in flight can be expected to occur at and below 80 percent of the normal operating speed, and on the ground at and above 100 percent. A ground resonance neutral speed of at least 105% was considered necessary for flight tests. It was rationalized that this margin would be the acceptable minimum for ground tests since there were unknown differences between whirl tower simulation and the aircraft, and it was likely that with additional knowledge, a way to increase the margin would be found.

7.4 INCIDENTS WHICH OCCURRED DURING WHIRL TOWER TESTS

In spite of precautions, body moments of approximately 100,000 inch-pounds were inadvertently developed on three separate occasions. The records of these incidents indicated that the number of cycles of high load was small and the corresponding cumulative fatigue damage was minimal. A posttest inspection revealed no structural damage.

On one occasion, the torque tubes contacted the flexures. No serious damage was incurred. The indentation in the end fitting was easily smoothed and did not limit subsequent testing. Figure 36 shows the contact location.

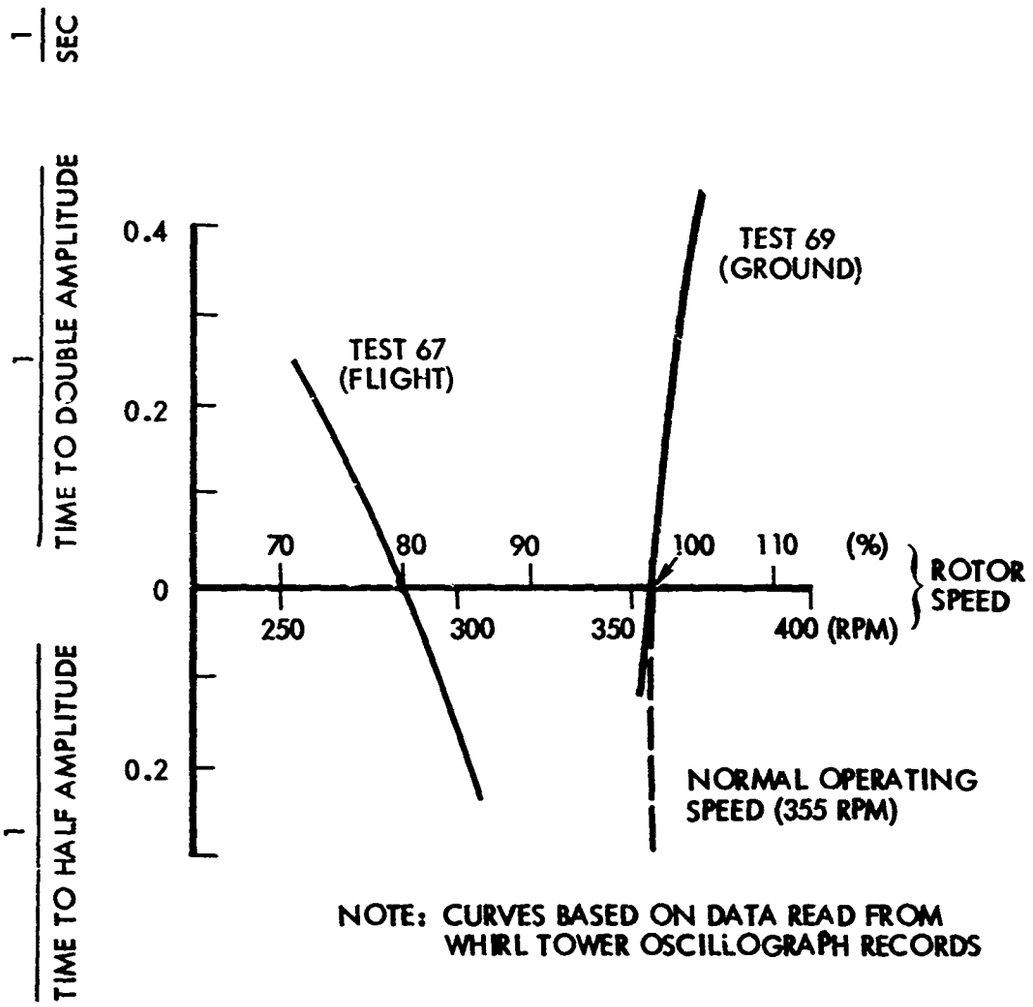

Figure 35. Stability Characteristics of Final Configuration Tested on Whirl Tower.

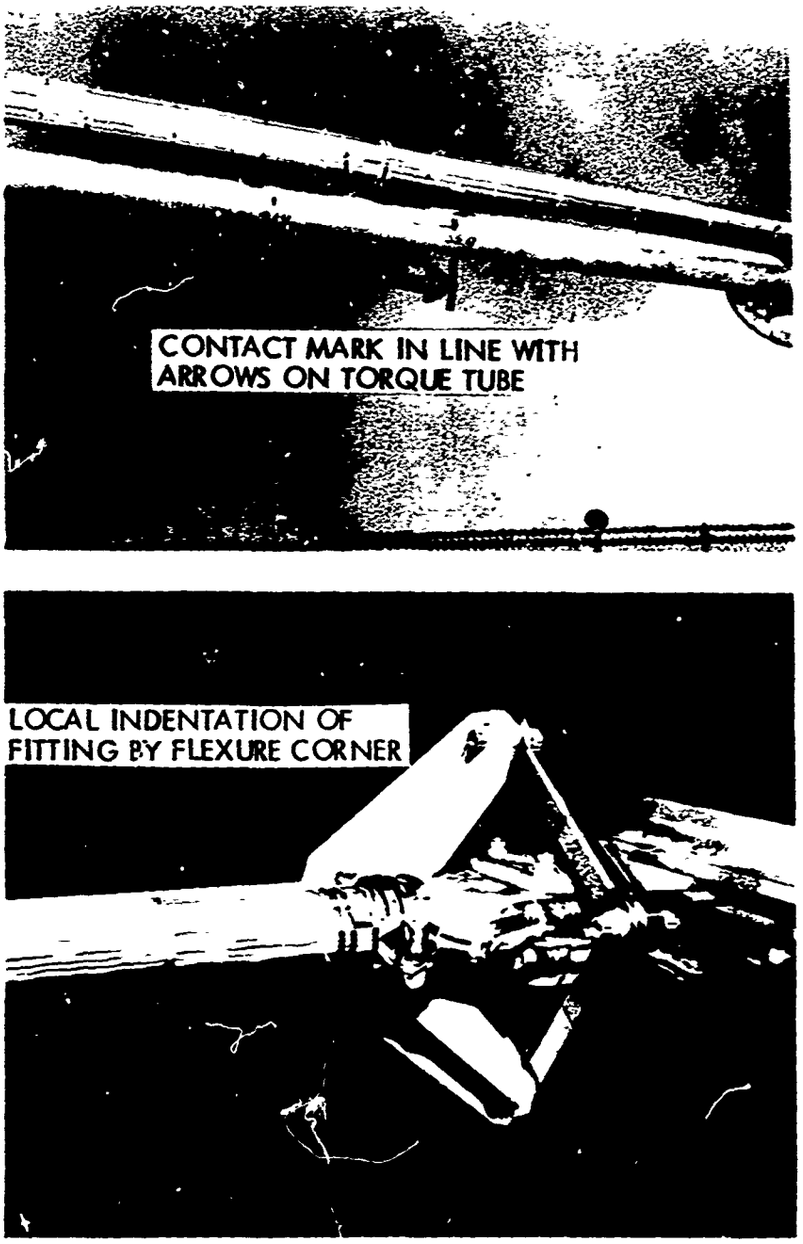

Figure 36. Contact Between Torque Tube End Fitting and Flexure.

SECTION 8

PREFLIGHT GROUND TESTS

Ground tests were conducted to establish that the vehicle was ready for flight. Tiedown tests included tracking and balancing the rotor on the aircraft, checking its control characteristics, evaluating on-the-ground rotor/body mechanical stability, and checking flight-readiness of the instrumentation.

8.1 DESCRIPTION OF TEST EQUIPMENT

The aircraft was placed on a rectangular frame which was fastened to the ground to provide a means of applying restraint. The aircraft on the tie-down frame is shown in Figure 37. A frame member was positioned laterally, above and clear of the landing gear skids, forward of the rear legs; this can be seen at the right-hand edge of Figure 38. During the first tests, wooden blocks were placed between this frame member and the skids such that the landing gear was effectively tied down at one point across the skids. This tiedown also provided vertical restraint during high-lift tests. One test was made with the gear tied down at three points across the skids to prevent the front from rising. Other tests were made with no tiedown.

Four cables from the fuselage were connected to hydraulic jacks (the jacks were operated by a switch in the cockpit) to tie the aircraft firmly to the ground. Later tests were conducted in a free mode where the cables were loosened.

The instrumentation included a visual display of the root in-plane bending moments located in the cockpit. This instrument provided an effective means of monitoring the approach to instability. Additional monitoring was provided by a remote recording oscillograph located in an adjacent building.

8.2 GROUND TEST PROCEDURE

Tests of control system were made by installing weights on the blades in a manner that produced maximum design feathering moments. The cyclic and collective controls were operated through their full ranges against these loads.

Since whirl tower tests had indicated that ground resonance would be at and above the normal operating rotor speed, tests were scheduled in a manner to approach the normal operating speed gradually.

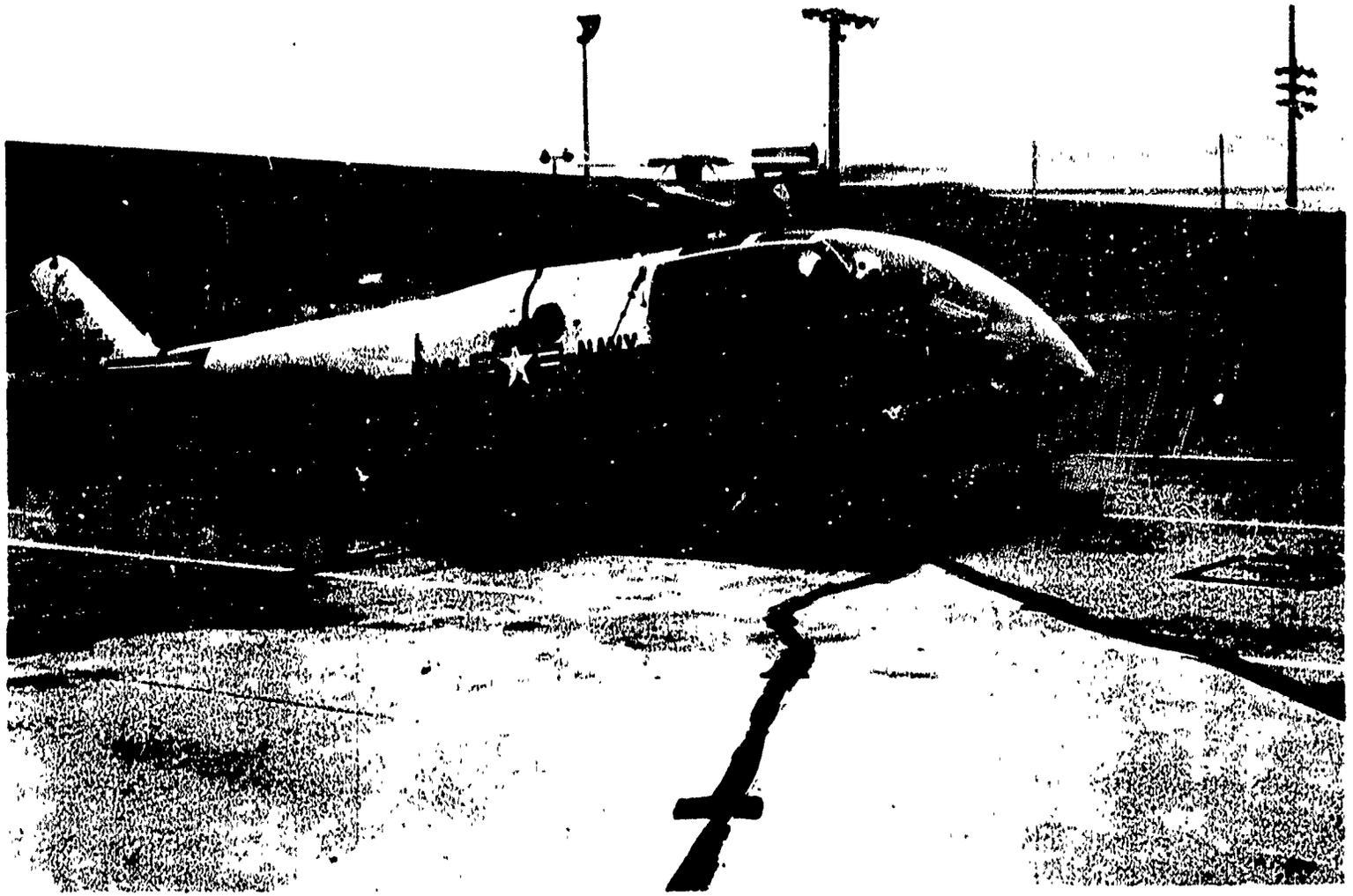

Figure 37. Preflight Ground Tests on Tiedown Frame.

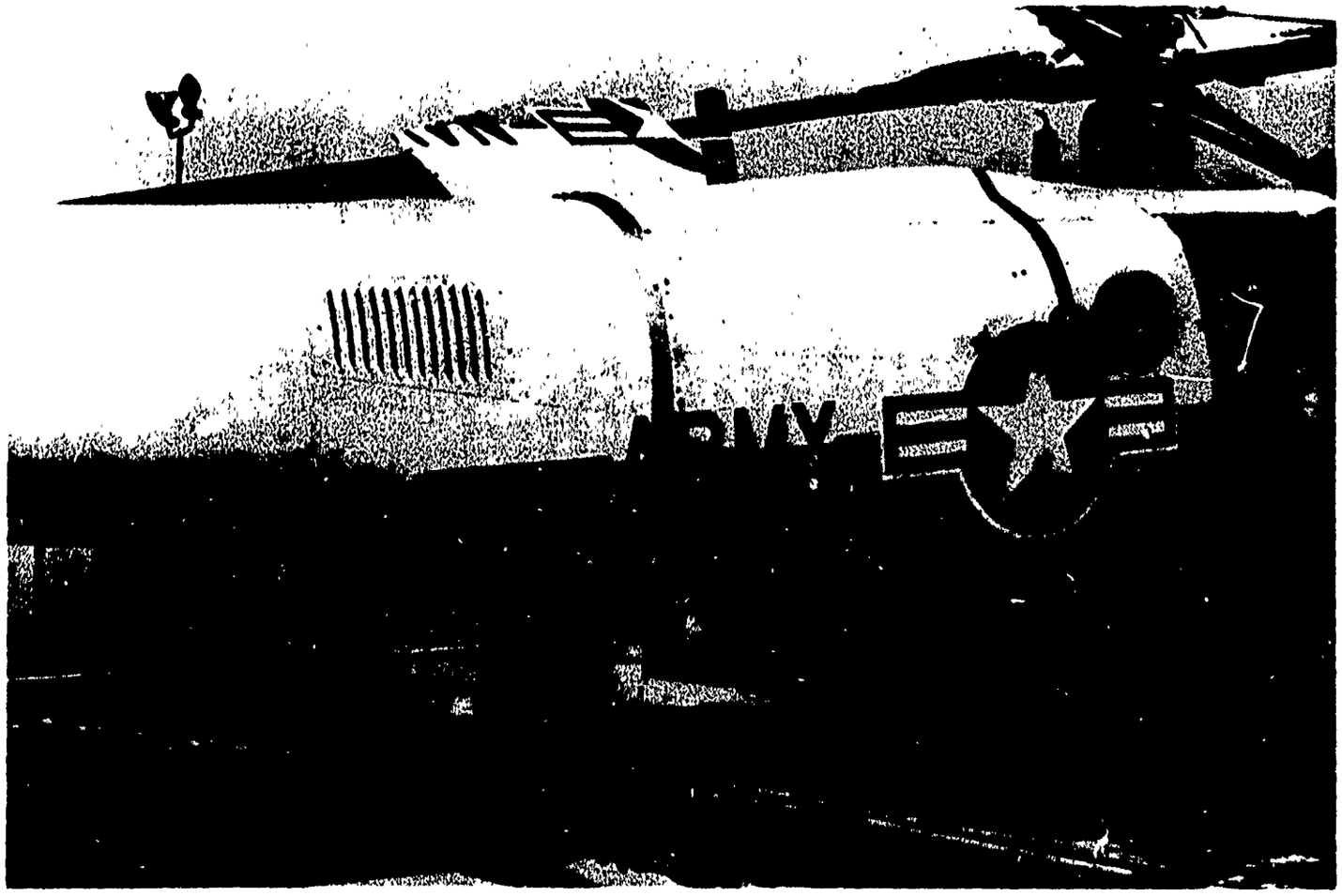

Figure 38. Tiedown Frame, Showing Fuselage and Skid Ties.

8.3 RESULTS OF GROUND TESTS

A log of ground tests is presented in Table X. The neutral stability values were estimated from observing first indications of instability on instrumentation gages. The tests listed in the table are separated into three groups: the first group of tests (through Test 664) was made with the aluminum skid landing gear; the second group (through Test 685) was with steel skids; and the third group was with extended and stiffened steel skids.

The data show that the neutral stability rotor speed can be as low as 90 percent of the normal operating speed with no landing gear modification (see Test 661). For a similar condition tested on the whirl tower, the neutral point had been estimated to occur at 99 percent (see Test 69, Table VIII).

Improvement was seen when viscous dampers were added to the aluminum-skid gear; comparison of Test 659 with Test 661 shows an improvement from 90 to 96 percent. However, increasing the damping by a factor of ten (Test 660) did not seem to help.

It was concluded that a more effective change could be made by increasing the landing gear stiffness by replacing the aluminum skids with steel skids. Tests 665 through 672 show that this change moved the neutral point to above 100 percent (102 to more than 106). Tests 670 to 672 show that a control system sensitivity change helped to move the neutral point to more than 106 percent. Tests 673 through 679 were conducted with partial skid contact conditions as depicted in Figure 39. As expected, the ground resonance margin deteriorated due to reduction of body pitch frequencies. This is seen in Test 676, where ground resonance occurred at 81 percent of normal operating rotor speed (with a single support point of each skid under the centerline of the main transmission). These observations led to the conclusion that a safe margin could be maintained during flight tests if takeoff and landing conditions were carefully controlled.

Torque tube balance weights were also tried during these tests. The objective was to lessen the effects of inertia loads on the gyro due to the center-of-gravity location of the torque tube assembly. The balance is shown in Figure 40. The net effect of these tests appeared to be a deterioration of the stability limit. (Tests 682, 683, 686, 687 of Table X.) However, balancing the torque tube was tried again during flight test for a different reason, to improve control characteristics (Section 9).

The configuration selected for flight test as a result of ground tests was that represented by Test 688. Although Test 689 shows that a slight improvement was seen when the gear damper was used, this improvement was viewed with question, in light of inconsistent indications (see Tests 676 through 679), and of the stiffening effect which had been observed earlier in the frequency measurements (Section 6.1.2). The dampers were left on the landing gear, but were arranged so that their use was optional.

The stability limit of the selected configuration is shown on Figure 41.

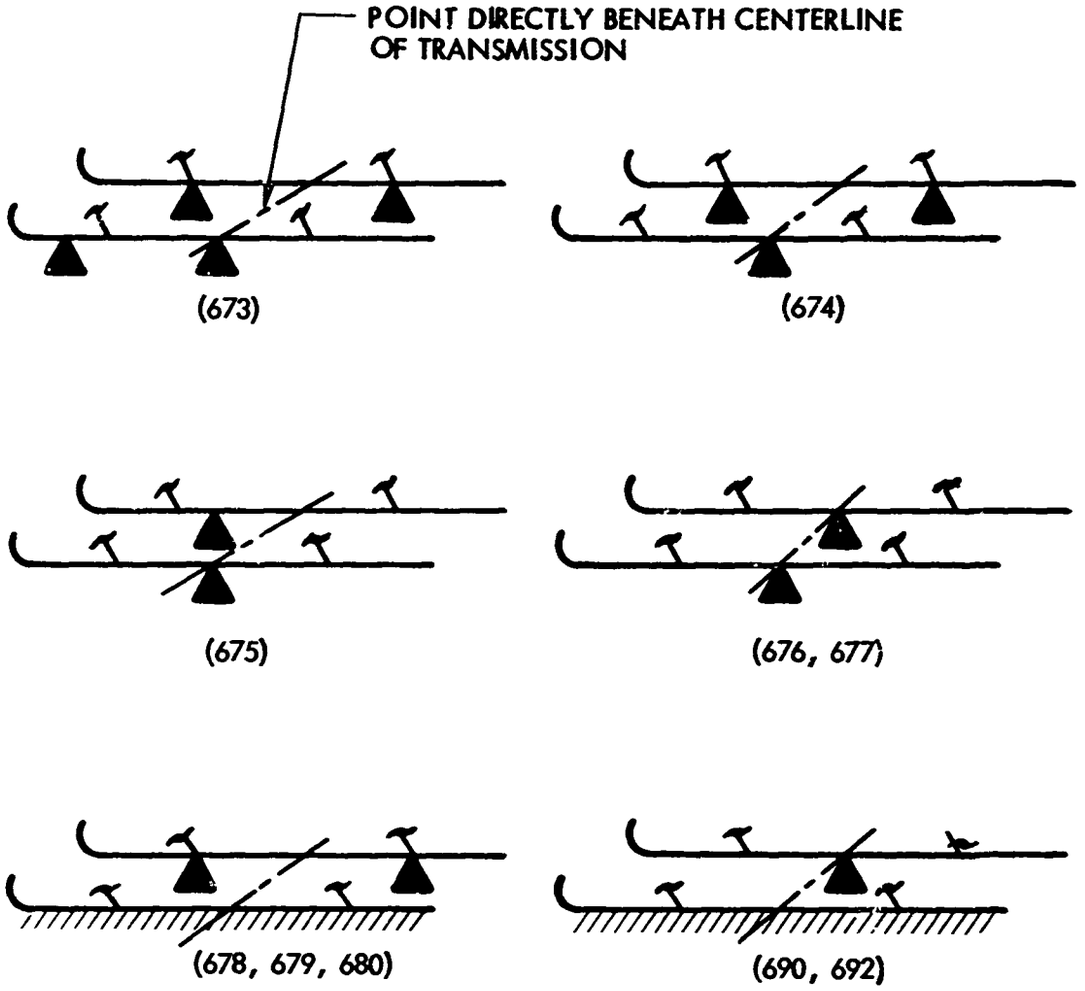

Figure 39. Schematic Diagrams Showing the Partial Skid Contact Conditions Tested.

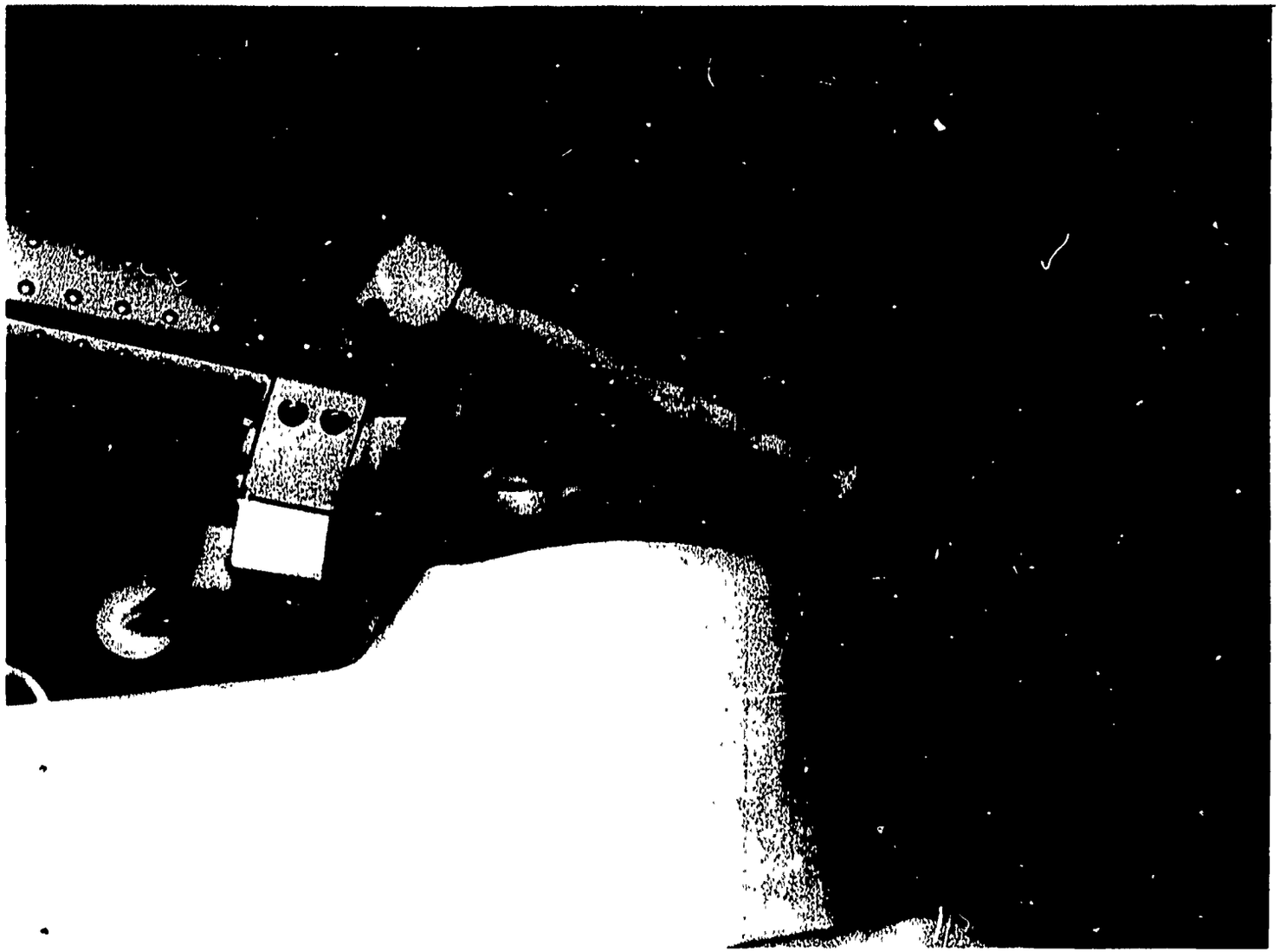

Figure 40. Torque Tube Balance Weights.

TEST 688

STIFFENED AND EXTENDED SKIDS
NO SKID DAMPERS
3° SWEEP, 1° OVERCONE
0 TIP WEIGHTS, 1 SLUG-FT^2 GYRO
NO TORQUE TUBE WEIGHTS

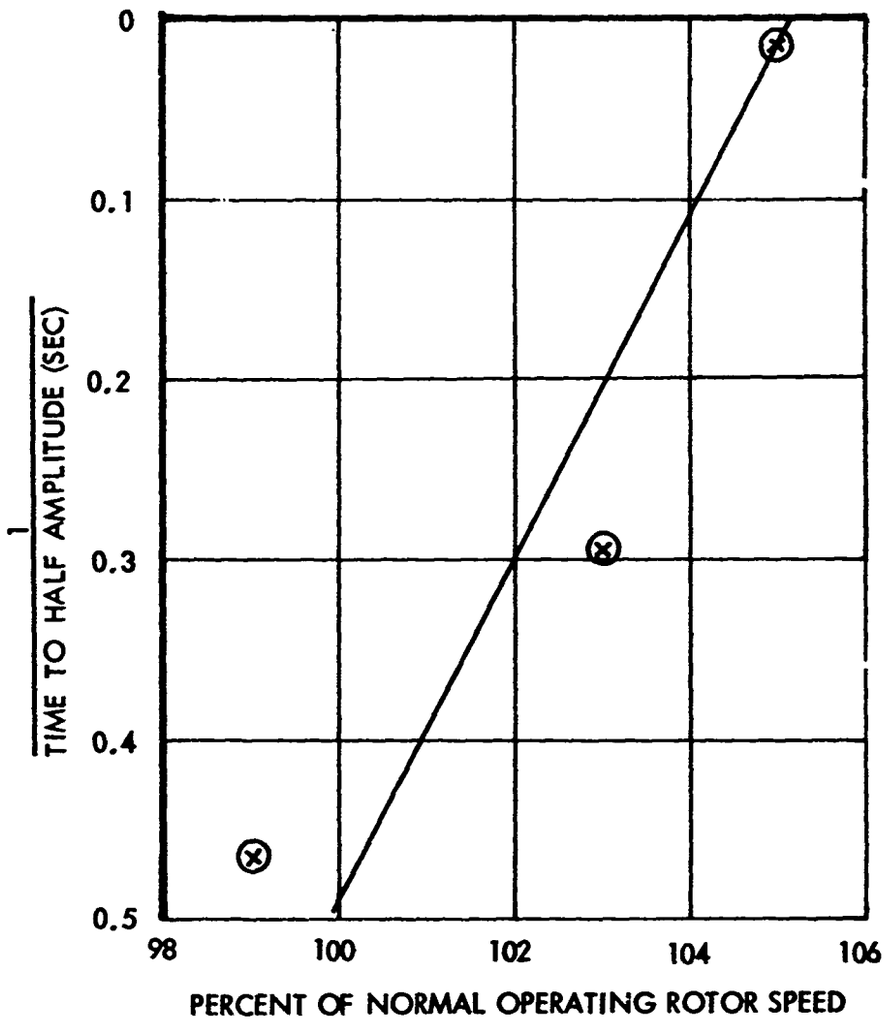

Figure 41. Ground Resonance Stability Limit of Configuration Selected for Flight – From Ground Test Data.

TABLE X. GROUND TEST DATA

TEST NO.	CONTROL SYSTEM SPRINGS		SWASH PLATE DAMPERS (lb/in/sec)	LANDING GEAR DAMPERS (see note 3)	INERTIA ADDED TO OUTRIGGERS (SLUG-FT^2)	SKID TIEDOWN (NO. OF PLACES)	TORQUE TUBE BALANCE WEIGHTS	NEUTRAL STABILITY ROTOR SPEED (% NORMAL)
	POSITIVE (see note 1)	NEGATIVE (see note 2)						
659	59	100	20	1	75	1	0	96
660	59	100	20	10	75	1	0	96
661	59	100	20	0	75	1	0	90
662	59	100	20	10	445	1	0	95
663	59	100	20	10	445	1	0	96
664	59	100	20	10	75	3	0	106
665	59	100	20	10	75	1	0	102
666	59	100	20	0	75	1	0	104
667	59	100	20	0	75	0	0	108
668	59	100	2	0	75	1	0	103
670	19	72	2	0	0	1	0	>106
671	19	72	2	0	0	1	0	>106
672	19	0	2	0	0	1	0	>106
673	19	72	2	0	0	0	0	96
674	19	72	2	0	0	0	0	94
675	19	72	2	0	0	0	0	84
676	19	72	2	0	0	0	0	81
677	19	72	2	1	0	0	0	77
678	19	72	2	1	0	0	0	101
679	19	72	2	0	0	0	0	103
682	19	72	2	0	0	0	3/4 lb	97
683	19	72 and 0	2	0	0	0	>3/4 lb	95
684	19	72	2	0	0	0	0	95
685	19	72	2	0	0	0	0	98

TABLE X - Continued

TEST NO.	CONTROL SYSTEM SPRINGS		SWASH PLATE DAMPERS (lb/in/sec)	LANDING GEAR DAMPERS (see note 3)	INERTIA ADDED TO OUTRIGGERS (SLUG-FT^2)	SKID TIEDOWN (NO. OF PLACES)	TORQUE TUBE BALANCE WEIGHTS	NEUTRAL STABILITY ROTOR SPEED (% NORMAL)
	POSITIVE (see note 1)	NEGATIVE (see note 2)						
686	19	72 and 0	2	0	0	0	>3/4 lb	106
687	19	72	2	0	0	0	>3/4 lb	105
688	19	72	2	0	0	0	0	105
689	19	72	2	1	0	0	0	106
690	19	72	2	0	0	0	0	99
691	19	72	2	0	0	0	0	100
692	19	72	2	1	0	0	0	97

NOTES:

1. Positive spring given in percent of original XH-51A control system spring rate 540 lb/in.
2. Negative spring given in percent of gyro spring rate of original XH-51A system, 5310 in.lb/rad.
3. Landing gear dampers listed thus: 1 indicates design damping strength
   10 indicates damping magnified by 10
   0 indicates damper removed.
4. Swash plate damper strength of 20 lb/in./sec is same as original XH-51A.
5. Tests 659 through 664 are with aluminum skids.
   Tests 665 through 685 are with steel skids.
   Tests 686 through 692 are with extended and stiffened steel skids.
6. Test 684 with 2 slug-ft^2 gyro (all other tests with 1 slug-ft^2 gyro).
7. Total ground test time: 19.2 hours.

The ground tests gave the first measured indication of rotor profile drag increase due to the flexure and blade control system. The 220 shp required, at zero lift and 100 percent rpm, compares with 150 shp for the standard XH-51A.

SECTION 9

FLIGHT TESTS

9.1 FLIGHT TEST PROCEDURES

The original plan was to perform flight tests of the matched-stiffness rotor system covering the full operating range of the XH-51A helicopter. However, flight tests were curtailed early in the program because the air resonance stability margin was judged to be incompatible with safe continuation of the program. Nineteen flights were performed in a total flight time of 3.5 hours. The first flight was performed on 7 June 1966. Although the flight test period was brief, sufficient data were obtained to evaluate mechanical stability margins of the matched-stiffness rotor and the general nature of flying qualities and structural load characteristics.

Safety-of-flight meetings were held to assess the airworthiness of the test aircraft. The aircraft was judged ready for flight testing, providing the following precautions were heeded:

- Takeoffs and landings were to be restricted to smooth, prepared surfaces.
- These lift-off and touchdown procedures were to be followed:

(1)	On ground	Flat pitch	N_R = 101 - 100%
(2)	Just prior to noseup	3/4 g	N_R = 99 - 98%
(3)	Airborne	Smooth rapid lift-off	N_R = 98 - 97%
(4)	Initial control check to be made at constant rpm		
(5)	Touchdown	Reduce rotor rpm	N_R = 96% in hover
(6)	Smooth, firm touchdown and reduction of collective to flat pitch	Normal shutdown	N_R = 100% (max)

The flight tests were conducted in a manner similar to the whirl tower tests; that is, the procedure involved starting in a conservatively safe set of conditions and gradually reducing the rotor speed, while monitoring the rotor's dynamic behavior, until an indicati. approaching the stability

limits was seen. Recovery from an impending air resonance condition was accomplished by increasing the rotor speed or by returning the aircraft to the ground.

9.2 FLIGHT TEST CONFIGURATION

The flight test aircraft contained the following configuration details:

- Mechanical couplings: tangent $\alpha_3 = 0.769$ and tangent $\delta_3 = -0.318$
- The main rotor transmission was rigidly mounted.
- Control system positive and negative springs were adjusted to provide a small net positive gyro spring rate.
- The landing gear had the stiffened steel skids; the dampers were arranged so that their use was optional.
- Outriggers with maximum practical amounts of mass were installed.

Weight and center-of-gravity restrictions for the first flight were:

- Pilot only; with capability for a quick change between flights to a two-man crew, at the same gross weight.
- Center of gravity not farther aft than during tiedown tests.
- Minimum fuel consistent with 12 minutes of hover.
- Weight not to exceed that consistent with 500 shp maximum continuous rating.

The maximum gross weight at takeoff was established as 4240 pounds. All flights were conducted within 80 pounds of this weight. The primary differences between the originally selected design gross weight, 3800 pounds, and the actual takeoff weight are attributed to the landing gear modifications, ballast, and the increased weight of the outriggers.

The first hovering flight of the matched-stiffness flight test aircraft was performed on 7 June 1966. The program continued until 3.5 hours of flight time had accumulated.

9.3 DESCRIPTION OF TESTS

The first flights were made using the largest practical roll inertia and a small control gyro. Tests were then made to study the effects of the following changes:

- Body roll inertia (reduced)
- Control gyro inertia (increased)
- Torque tube balance weights
- Changes in control system sensitivity by varying control spring rates and swash plate damper rates

Evaluation of flying qualities was qualitative. Control sensitivity, friction, gyro size, torque tube balance weights and swash plate damper rates were evaluated. Structural loads were measured for all flight conditions.

9.4 RESULTS OF FLIGHT TESTS

9.4.1 Air Resonance Tests

Flight tests indicated a lesser stability margin than had been estimated from the whirl tower tests. The whirl tower data had indicated a rotor speed for neutral stability of approximately 80 percent with a roll inertia increment of 200 slug-feet^2, whereas the flight test data indicated a neutral point at 89 percent with a roll inertia increment of 430 slug-feet^2. This was the reason for early curtailment of the flight program.

The results of several of the test flights (selected as representative of all data) are presented in Table XI. Figures 42 through 51 show data for the same tests listed in the table.

Time-to-half-amplitude values of the blade root in-plane bending and of the fuselage roll rate are selected as the response characteristics with which to assess stability. An extrapolation of a curve fitted to the scatter of points (by eye) is used to estimate the neutral stability rpm (Figures 42 through 51). The results of the extrapolation are listed in Table XI as "neutral stability rpm". The general result is that of all the variables tested, roll body inertia was the one that appreciably affected the stability margin. The effect of varying this parameter is summarized in Figure 52.

Although at the end of the preflight ground tests the recommended gyro size was 1 slug-foot^2, the flight test data shown in Table XI include a 3, 4, or 5 slug-feet^2 gyro. In early flight tests, for which data are not shown, 1 and 2 slug-feet^2 gyros were tried. Vehicle control with the small gyro proved to be sensitive (what the pilot referred to as "nervous hover"). The pilot-coupled oscillations in these tests with small gyros made it difficult to anticipate mechanical instability oscillations. Therefore, a larger gyro was considered mandatory.

Motions involved in air resonance are illustrated by time traces on Figure 53. These data show motions of body roll at 1.65 cps and blade in-plane bending at 3.7 cps. The swash plate roll angle shown is relative to the body

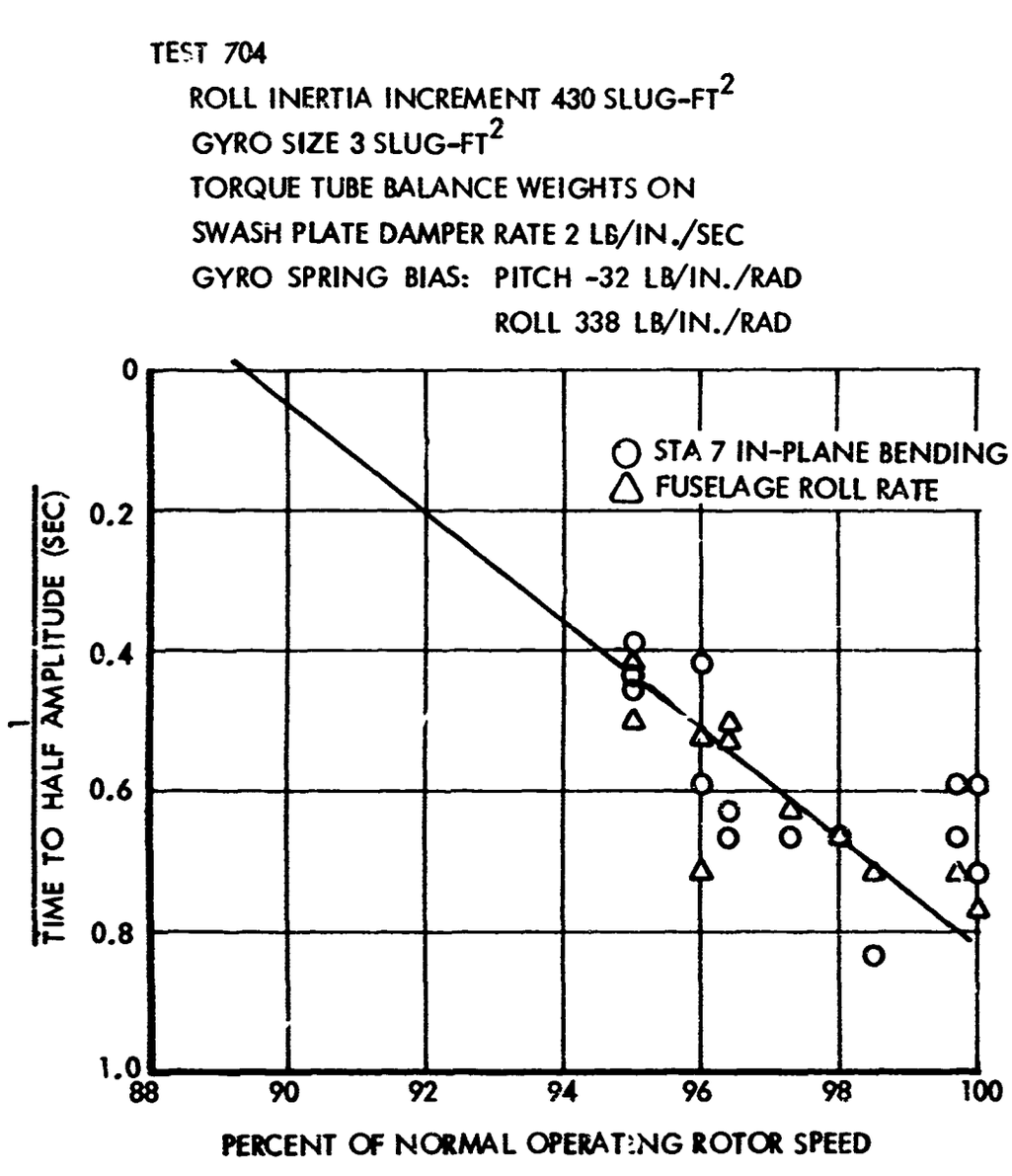

Figure 42. Air Resonance Stability, Test 704.

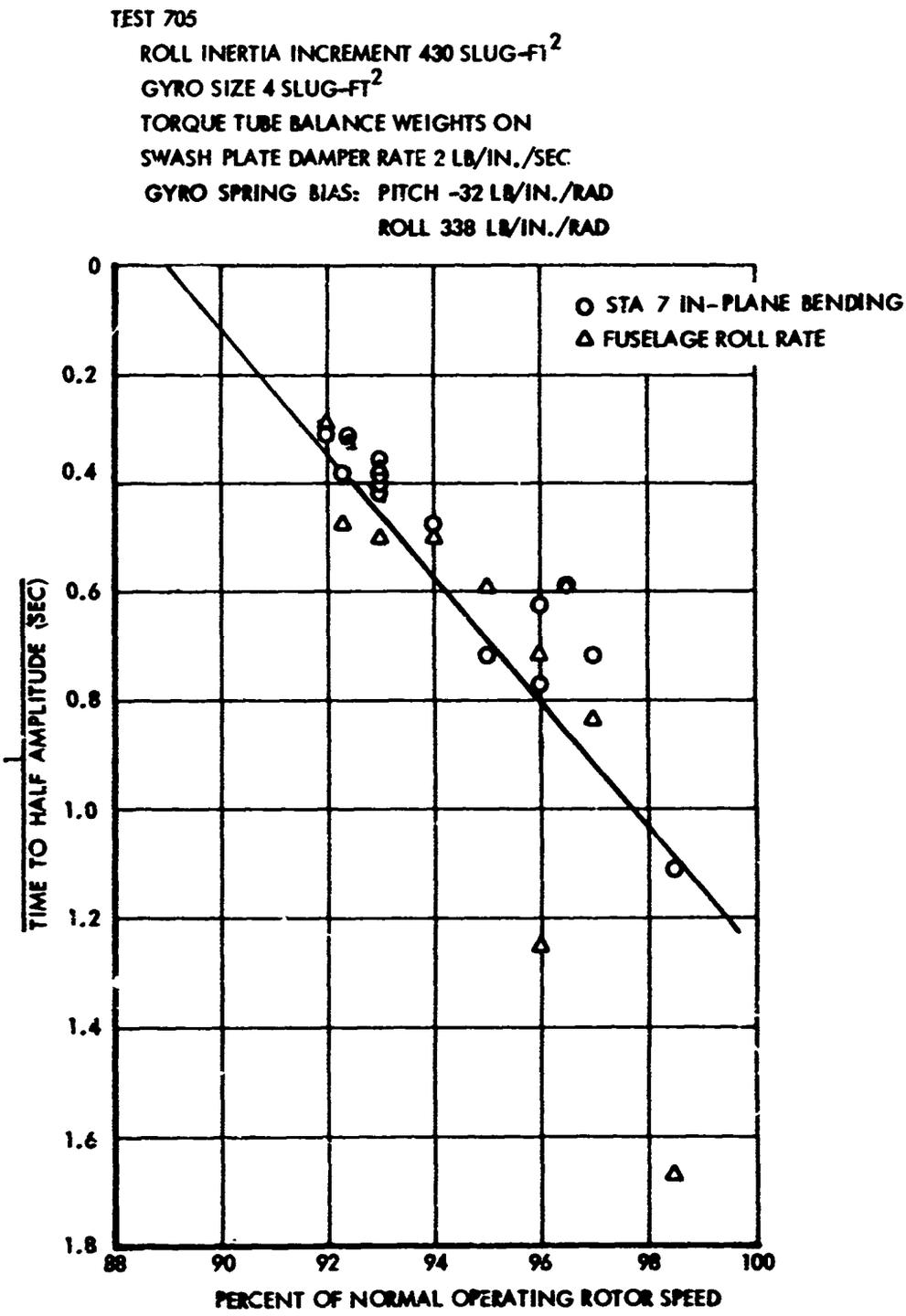

Figure 43. Air Resonance Stability, Test 705.

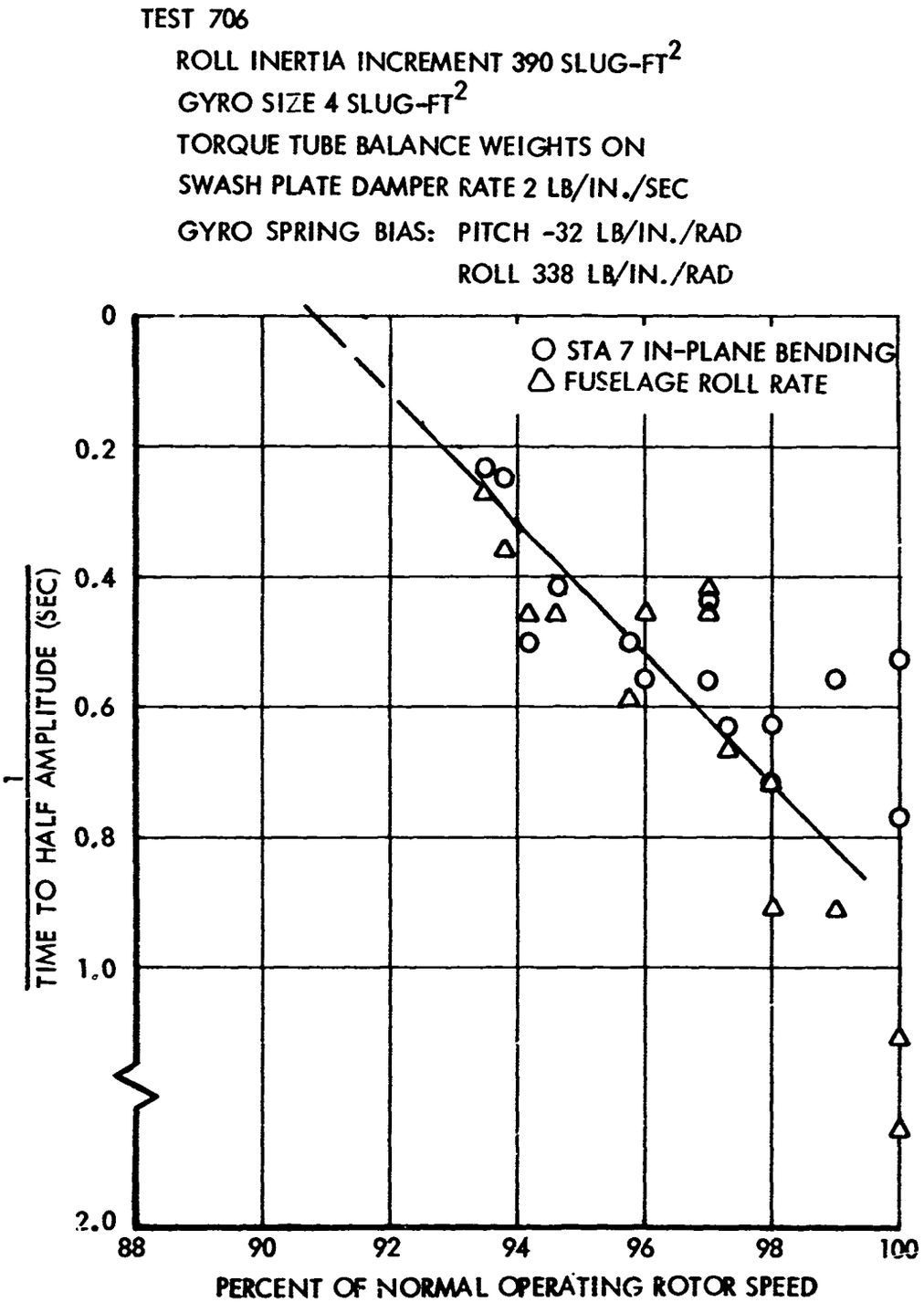

Figure 44. Air Resonance Stability, Test 706.

TEST 707

ROLL INERTIA INCREMENT 350 SLUG-FT^2

GYRO SIZE 4 SLUG-FT^2

TORQUE TUBE BALANCE WEIGHTS ON

SWASH PLATE DAMPER RATE 2 LB/IN./SEC

GYRO SPRING BIAS: PITCH -32 LB/IN./RAD

ROLL 338 LB/IN./RAD

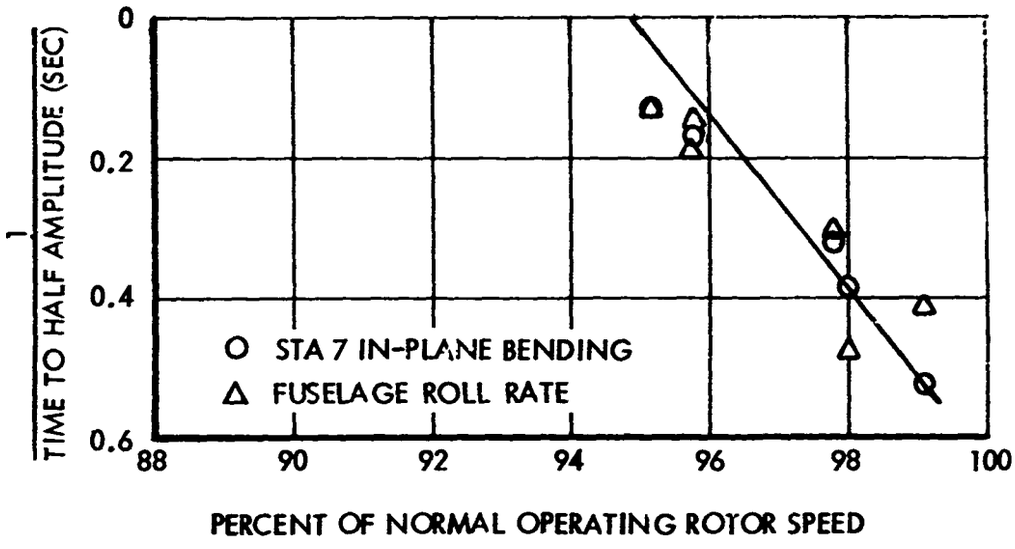

Figure 45. Air Resonance Stability, Test 707.

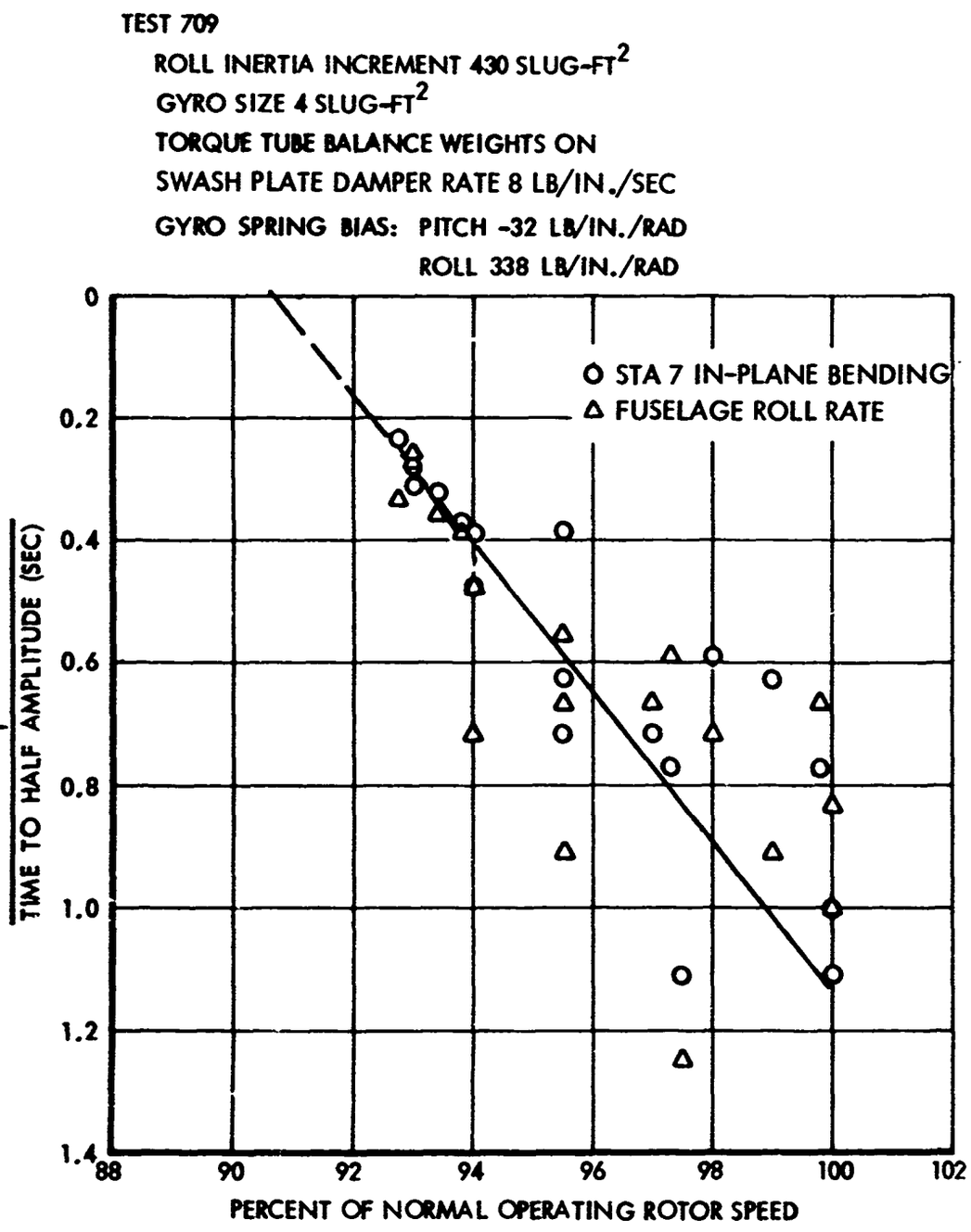

Figure 46. Air Resonance Stability, Test 709.

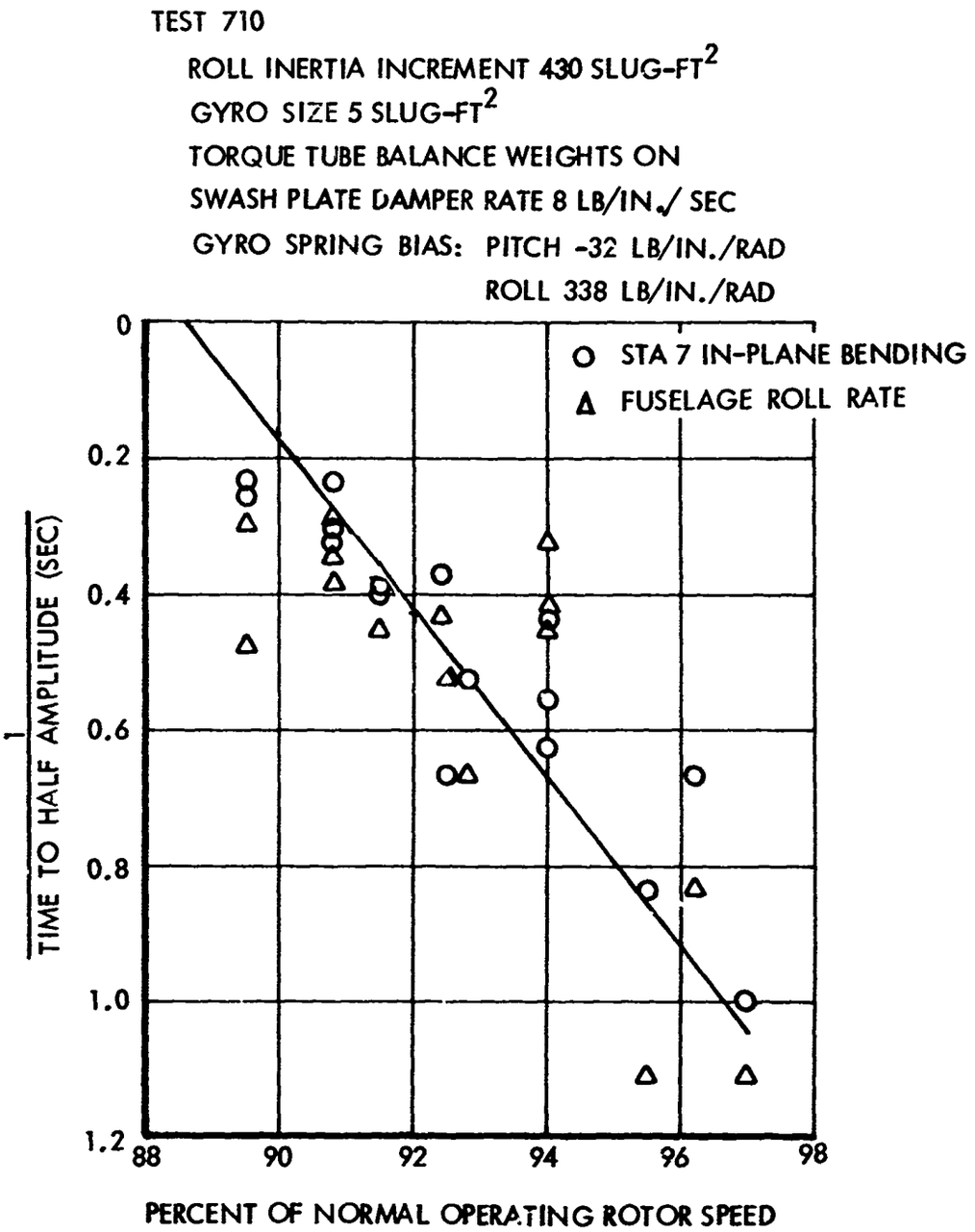

Figure 47. Air Resonance Stability, Test 710.

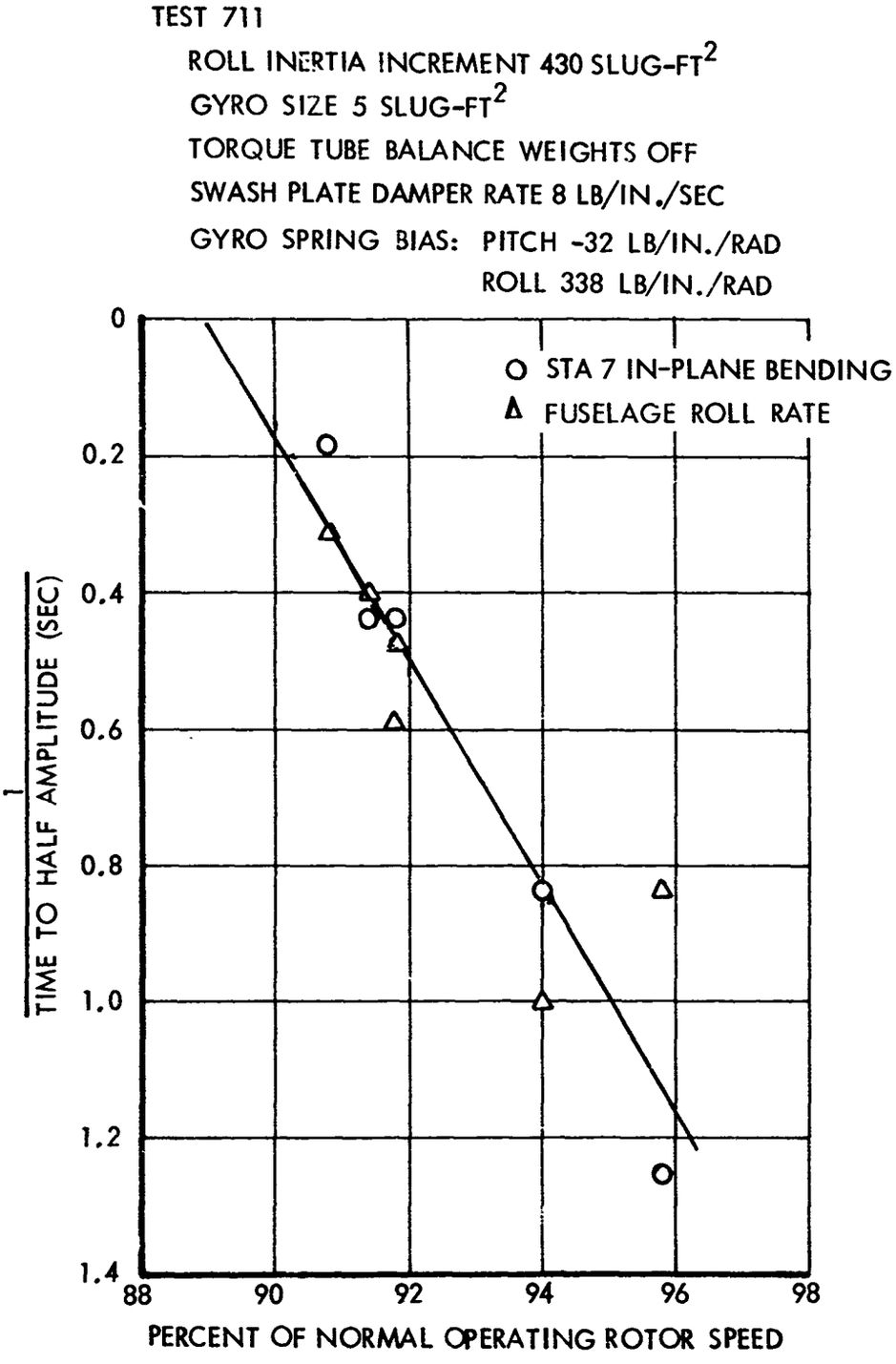

Figure 48. Air Resonance Stability, Test 711.

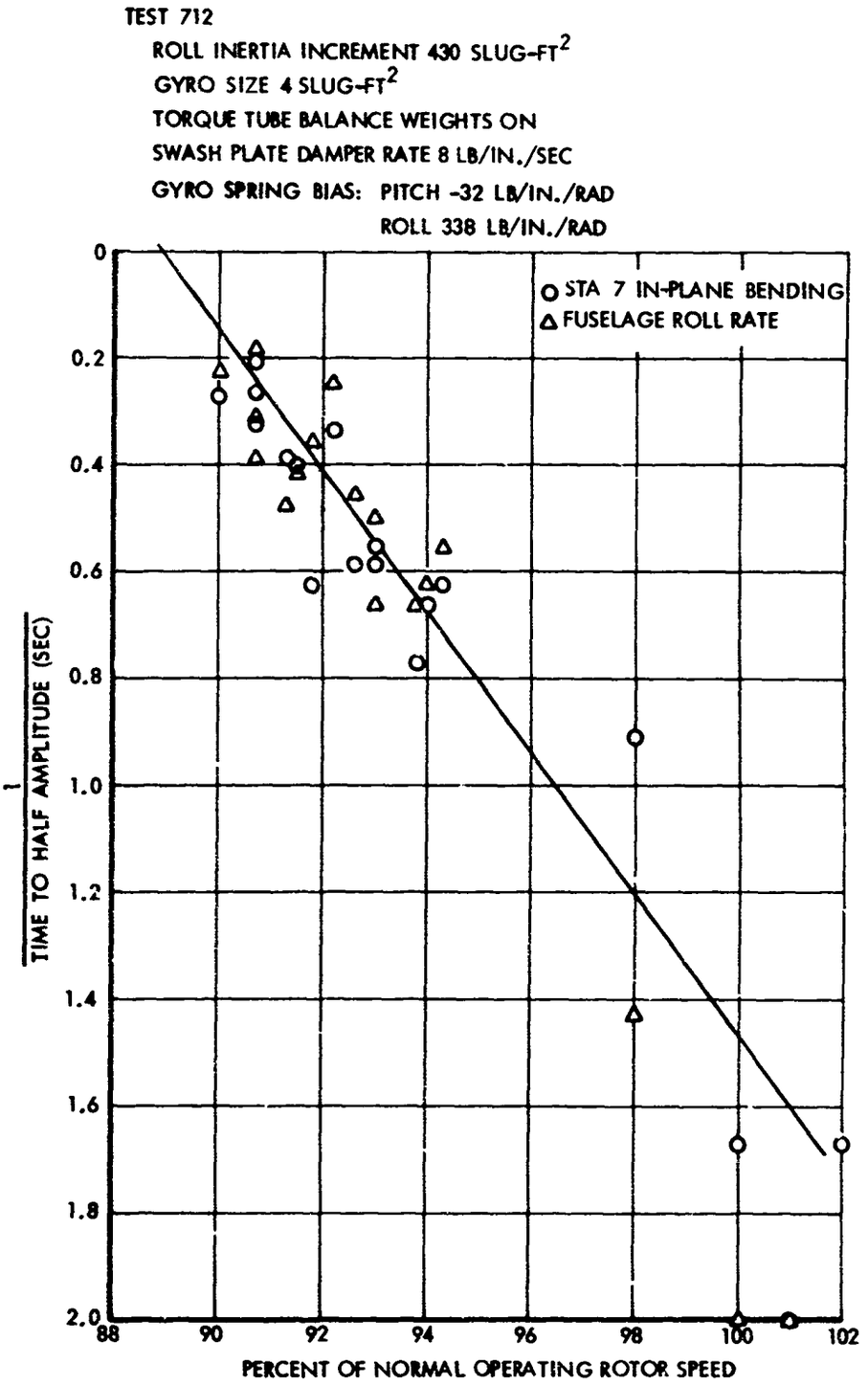

Figure 49. Air Resonance Stability, Test 712.

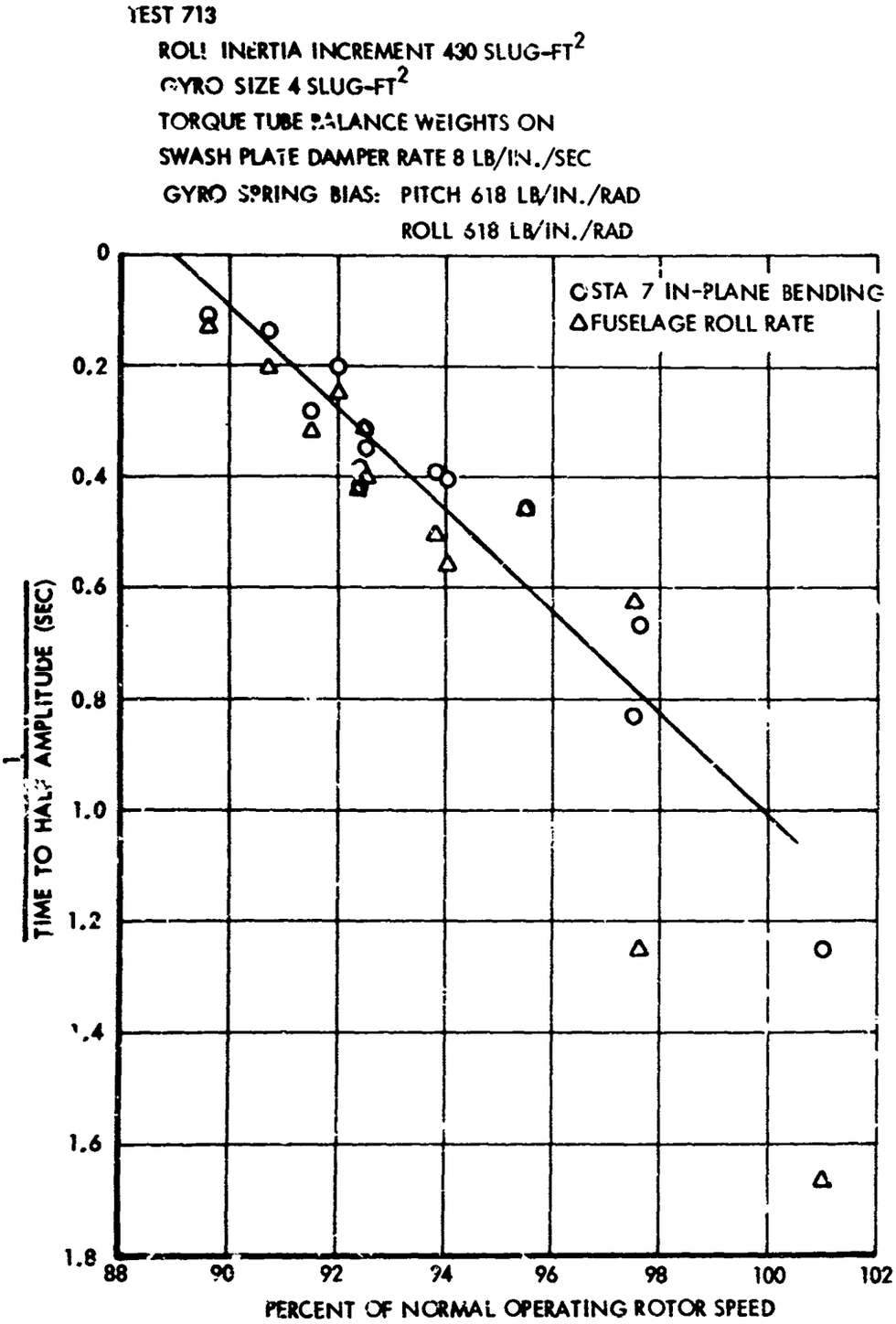

Figure 50. Air Resonance Stability, Test 713.

TEST 714

ROLL INERTIA INCREMENT 430 FLUG-FT^2

GYRO SIZE 2 SLUG-FT^2

TORQUE TUBE BALANCE WEIGHTS ON

SWASH PLATE DAMPER RATE 8 LB/IN./SEC

GYRO SPRING BIAS: PITCH 618 LB/IN./RAD

ROLL 618 LB/IN./RAD

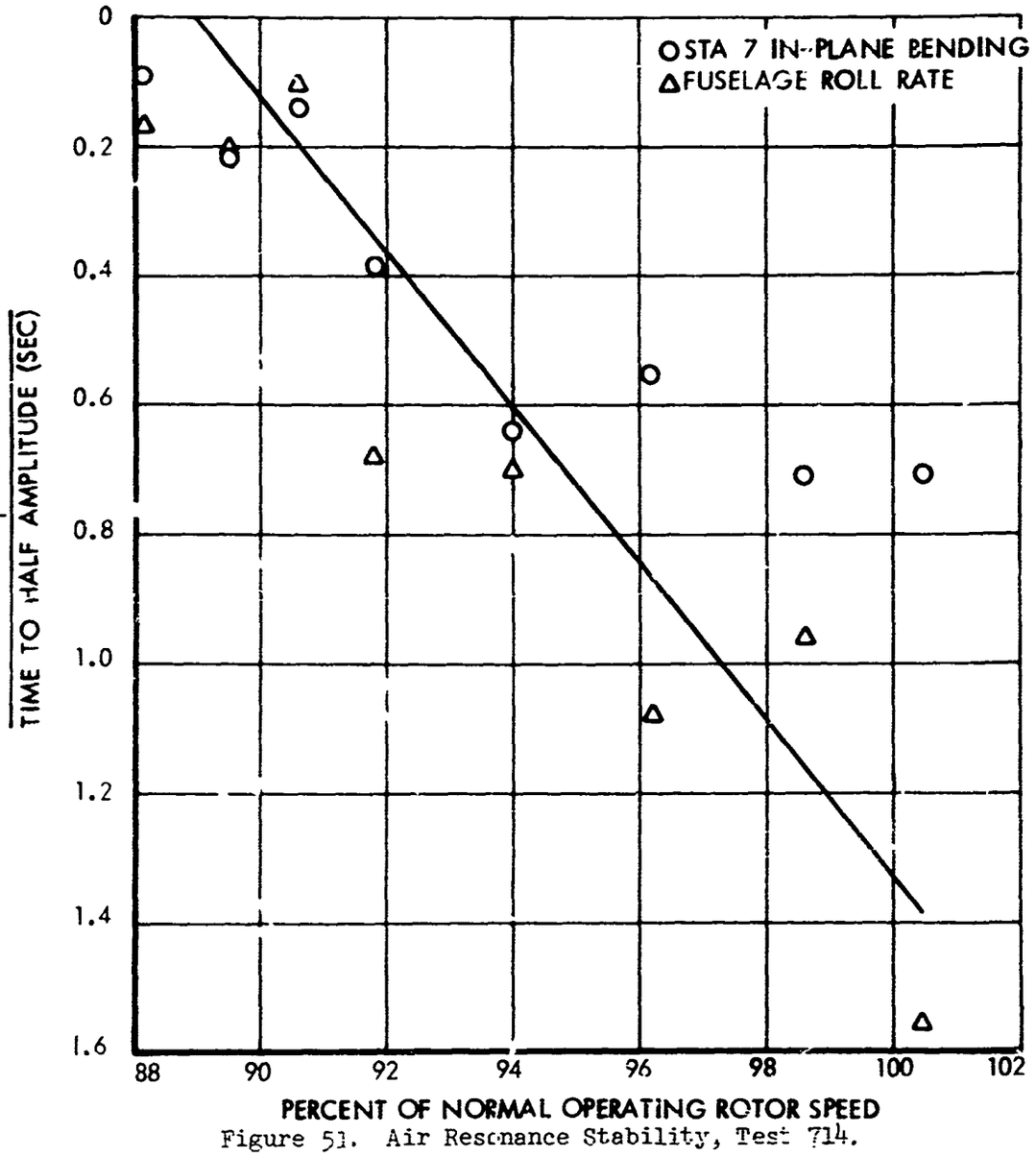

Figure 51. Air Resonance Stability, Test 714.

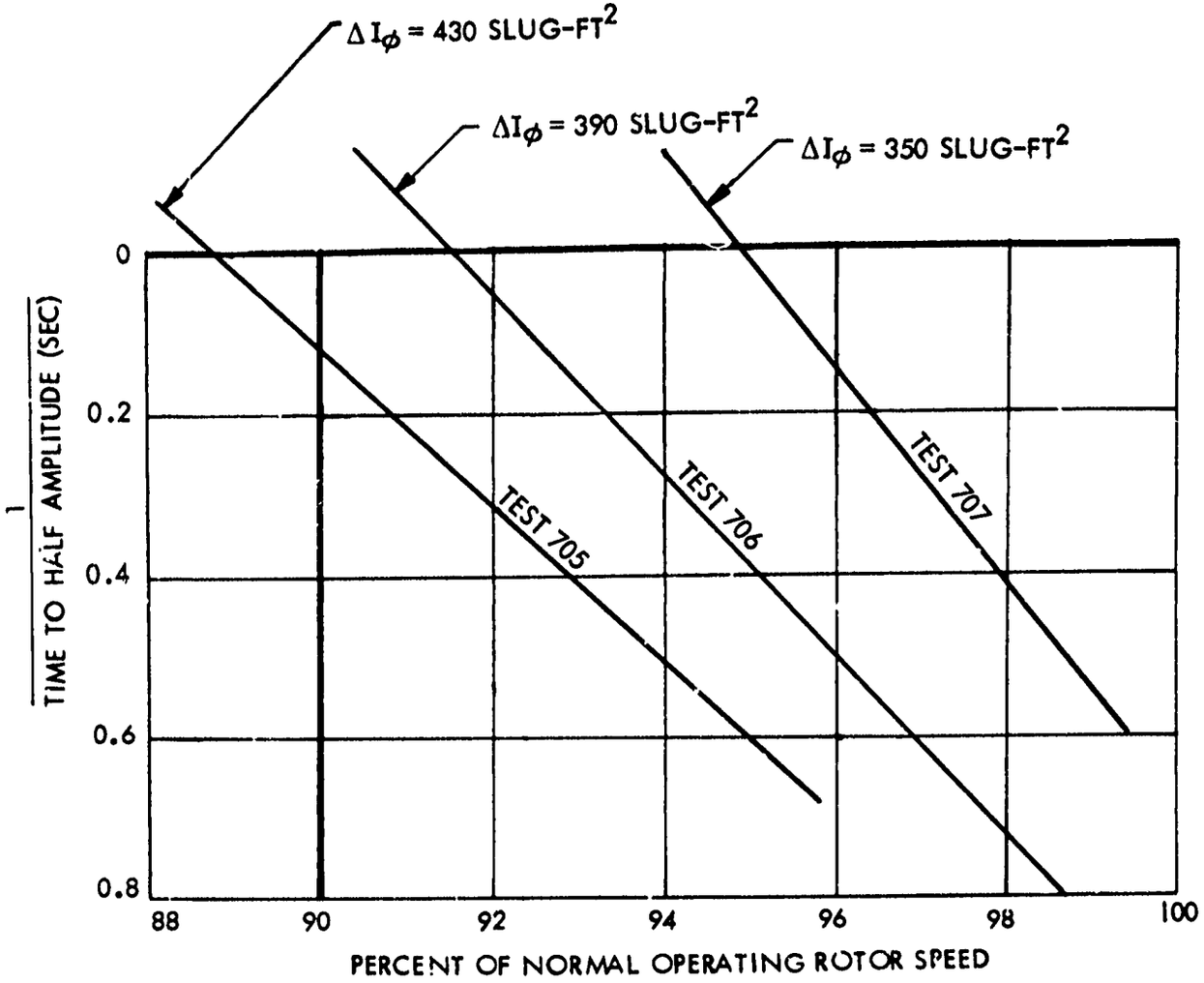

Figure 52. Summary of Air Resonance Flight Tests.

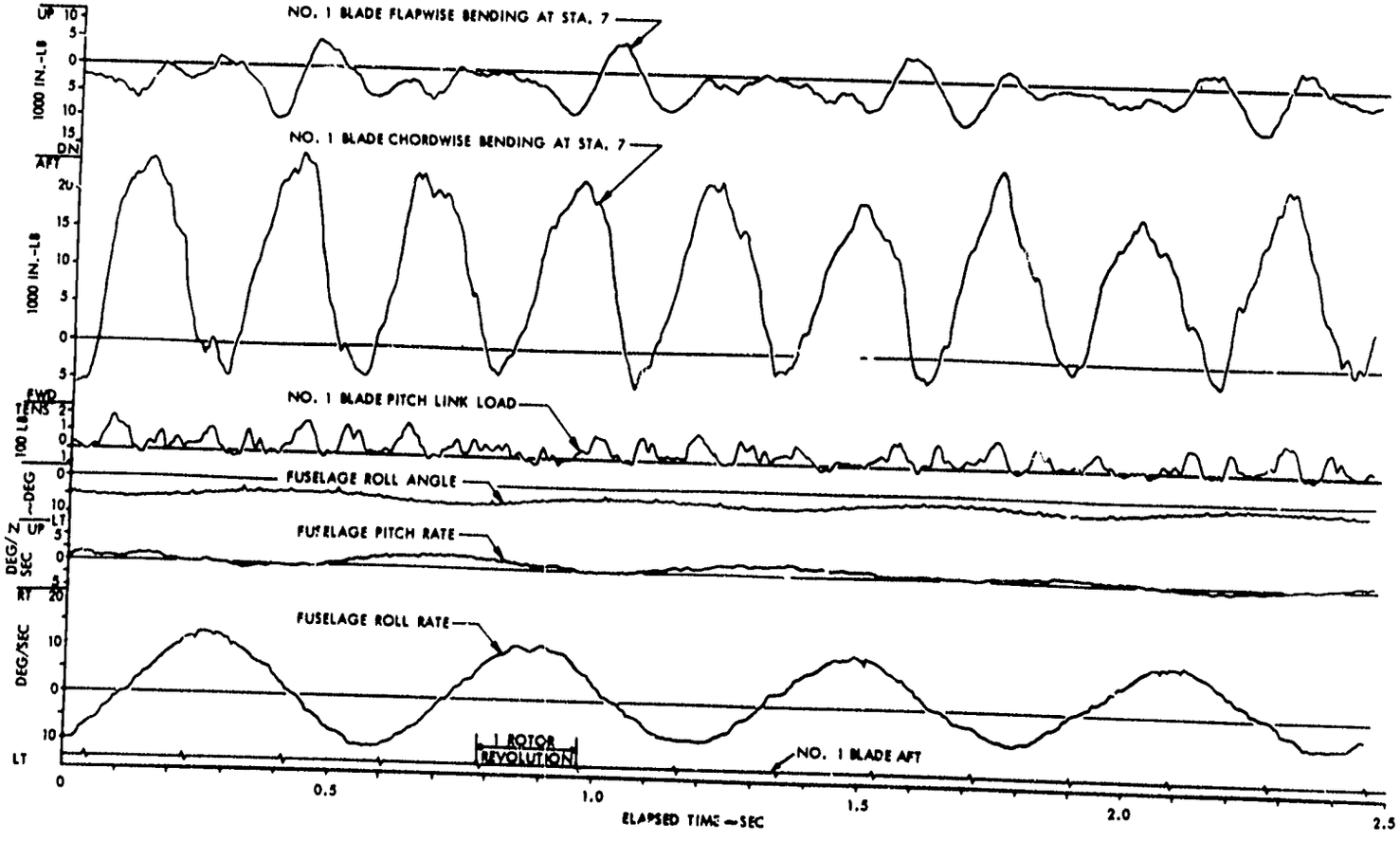

Figure 53. Time History of Air Resonance.(1 of 2)

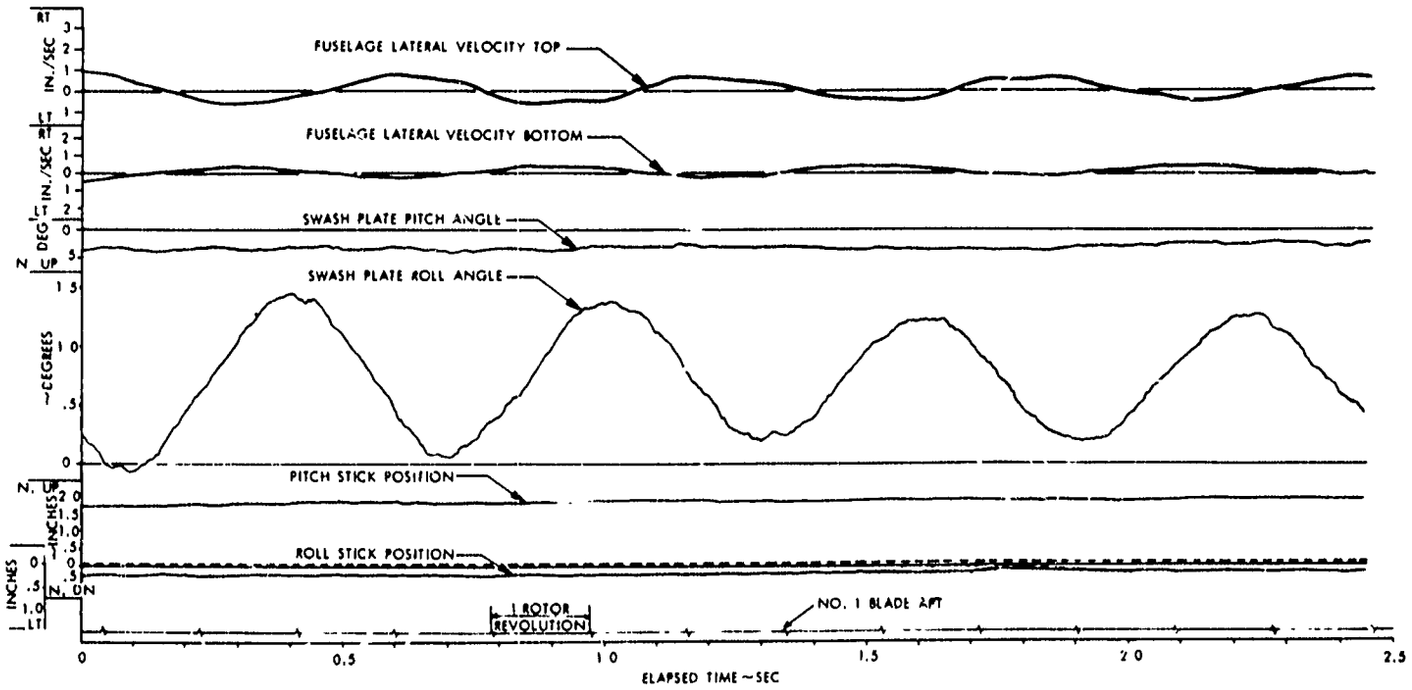

Figure 53. Time History of Air Resonance.(2 of 2)

TABLE XI. FLIGHT TEST DATA

TEST NO.	ROLL INERTIA INCREMENT (Slug-Ft^2)	GYRO SIZE (Slug-Ft^2)	TORQUE TUBE BALANCE (On/Off)	SWASH PLATE DAMPER RATE (Lb/In./Sec)	GYRO SPRING BIAS (in.lb/rad)		ROTOR RPM FOR NEUTRAL STABILITY (% OF 355)
					PITCH	ROLL	
704	430	3	ON	2	-32	338	89
705	430	4	ON	2	-32	338	89
706	390	4	ON	2	-32	338	91
707	350	4	ON	2	-32	338	95
709	430	4	ON	8	-32	338	91
71[illegible]	430	5	ON	8	-32	338	89
711	430	5	OFF	8	-32	338	89
712	430	4	ON	8	-32	338	89
713	430	4	ON	8	618	618	89
714	430	2	ON	8	618	618	89

and is almost entirely due to body motion. Little or no absolute motion of the swash plate occurred. The data in Figure 53, for a case where the rotor speed was 323 rpm (91 percent), show a lightly damped oscillation. No pilot inputs are present; the motion is self-sustained.

Figure 54 shows the pilot control input used to excite air resonance. As shown, the pilot applied the control in opposite phase with the body roll rate. After the oscillations are self-sustaining, the pilot input can be removed.

9.4.2 Handling Qualities Test

An objective of the program was to demonstrate that the matched-stiffness rotor can be controlled by a small gyro. This was demonstrated to a limited degree, but was abandoned in favor of a 4 slug-feet^2 gyro, as discussed above. This larger gyro is still much smaller than used in a standard XH-51A.

Torque tube balance weights used on some of the flight tests appeared to have a beneficial effect on handling qualities even though they had been judged as ineffective in the whirl tower tests.

Vibration levels were exceptionally low (qualitative evaluation by the pilot). The low vibration levels are due to low in-plane stiffness, which transmits lower in-plane loads to the hub than a stiff in-plane blade.

9.4.3 Characteristics of Rotor Loads

Rotor loads were measured in flight. Flapping and in-plane loads were measured at Blade Stations 7, 50, 73, and 95. Bending moments at Station 7 are shown among the time history traces in Figures 53 and 54. Figures 55 and 56 show measured rotor bending moments at various forward speeds. Pitch link loads are shown in Figure 57.

Only a small amount of load data was permanently recorded. Therefore, comparison of the measured and calculated data would not be conclusive. The data do show, however, that loads did not approach maximum allowables.

The measured loads were analyzed to examine harmonic components of flapwise bending moments. The results are shown in Figure 58. The results of a similar analysis for the stiff in-plane blades of the original XH-51A rotor are shown in Figure 59 for comparison. The comparison shows that for speeds below 50 knots the matched-stiffness blades have lower 2P and 3P components. Extrapolation of the matched-stiffness data to higher speeds suggests that the two sets of data would be in agreement.

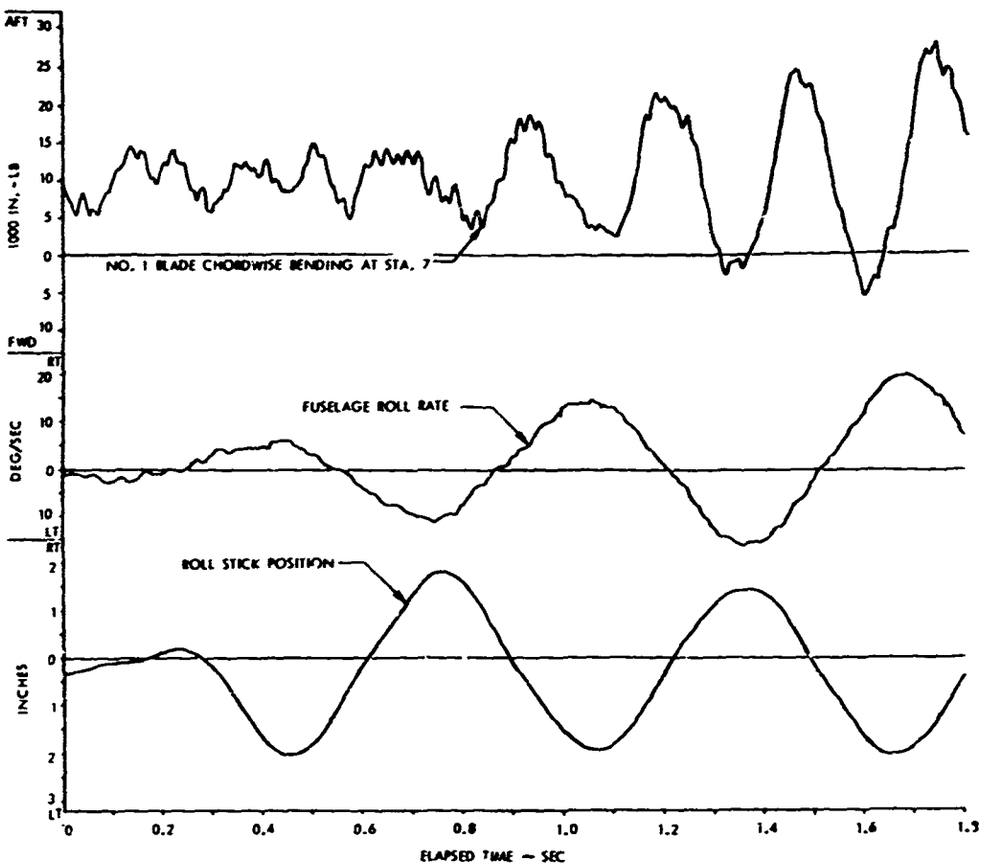

Figure 54. Time History of Air Resonance Excitation.

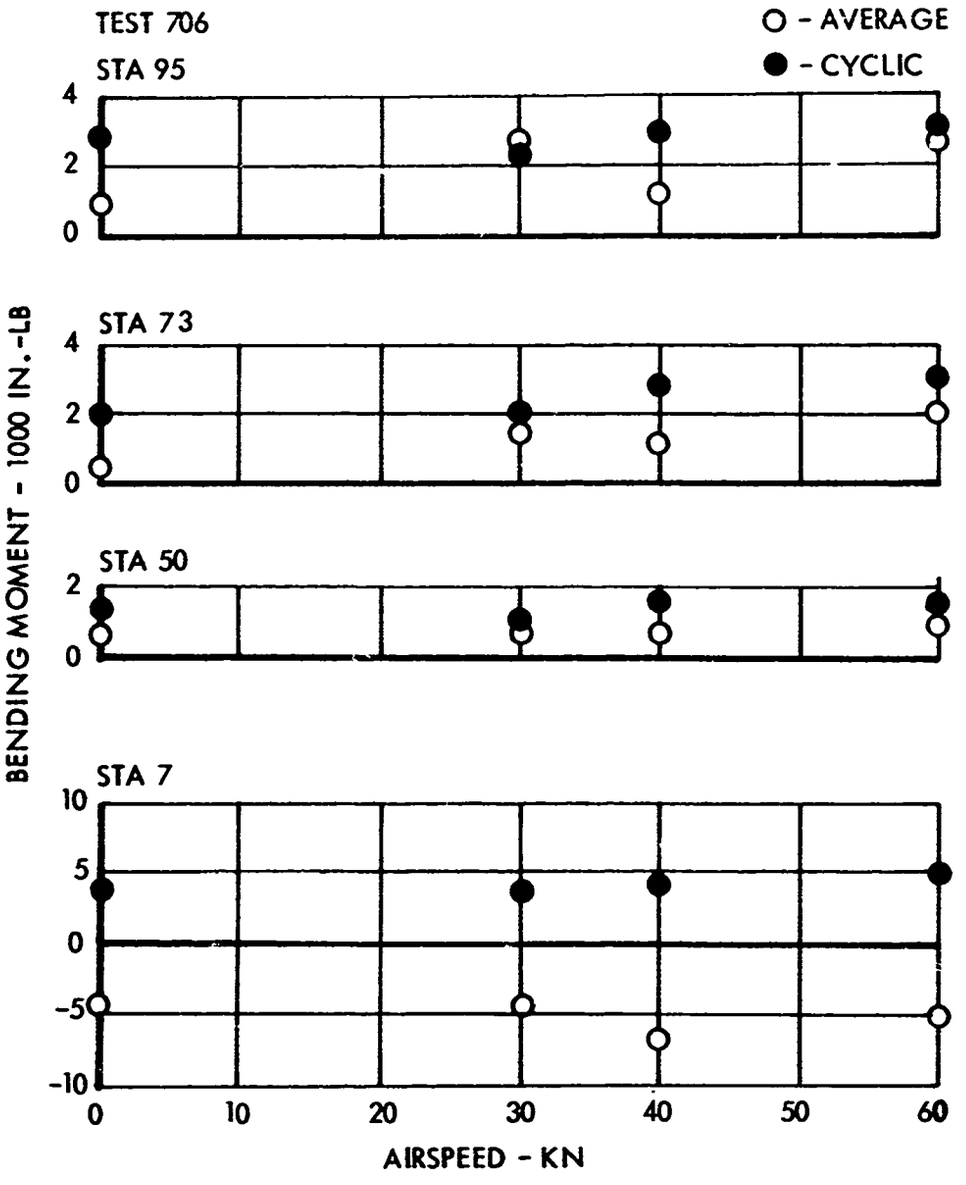

Figure 55. Flapwise Bending Moments Measured in Flight Tests.

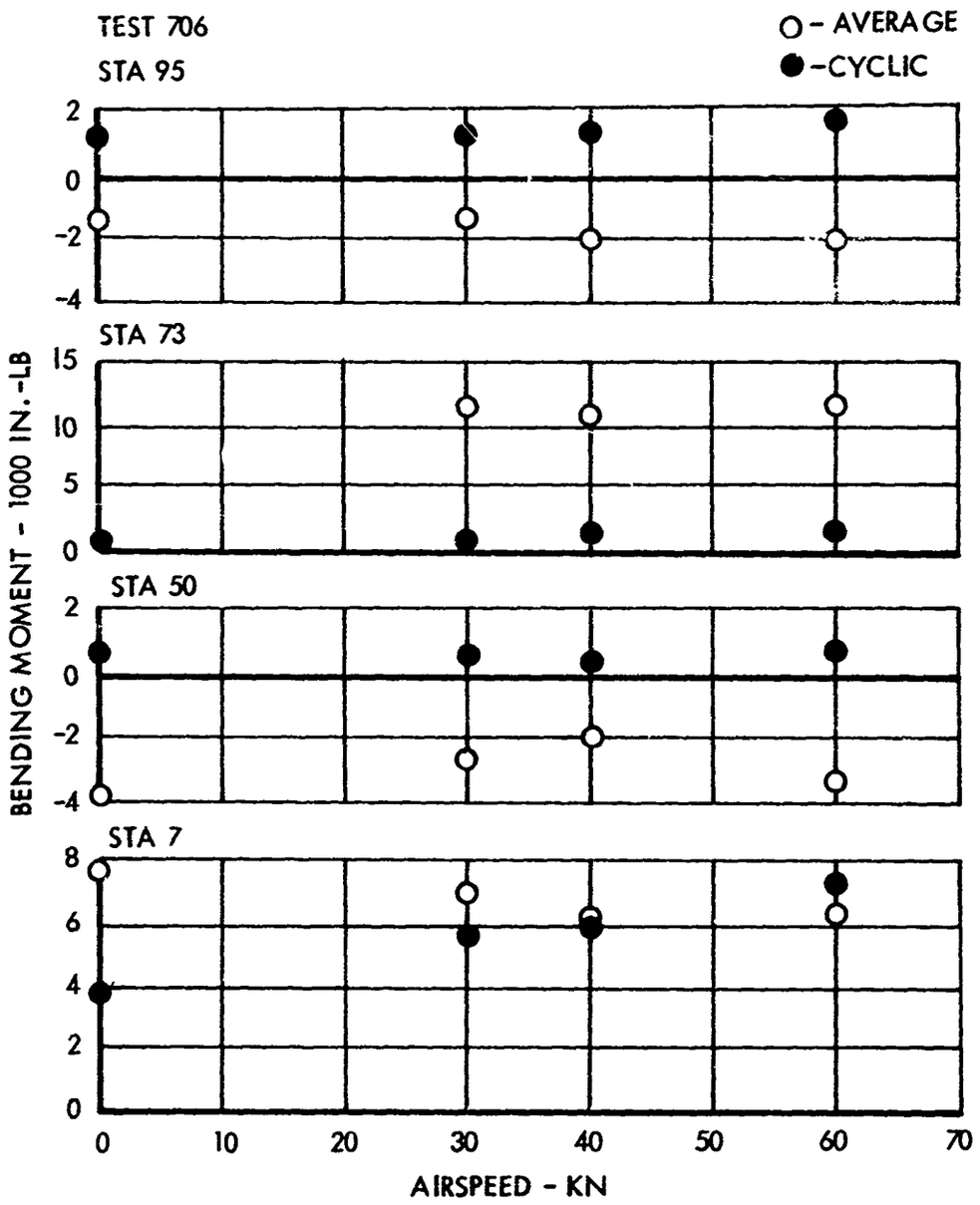

Figure 56. Chordwise Bending Moments Measured in Flight Tests.

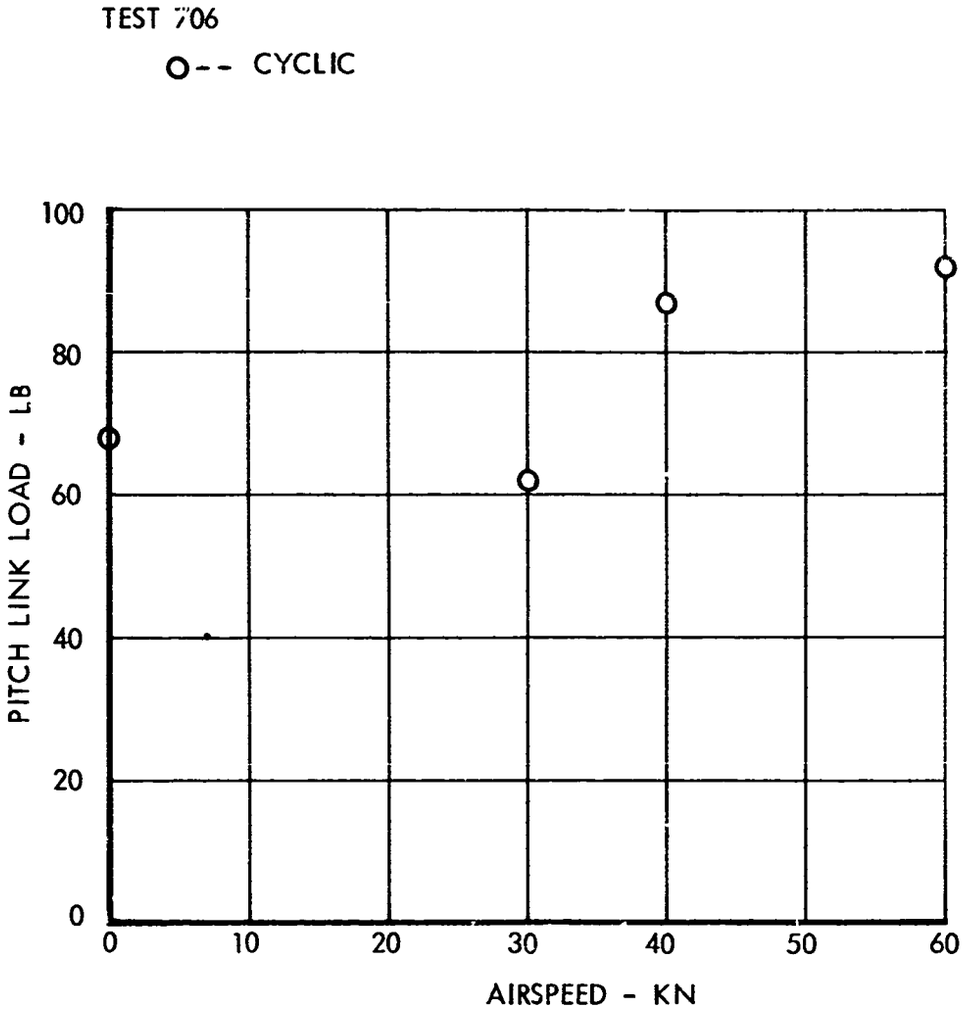

Figure 57. Blade Pitch Link Loads Measured in Flight Tests.

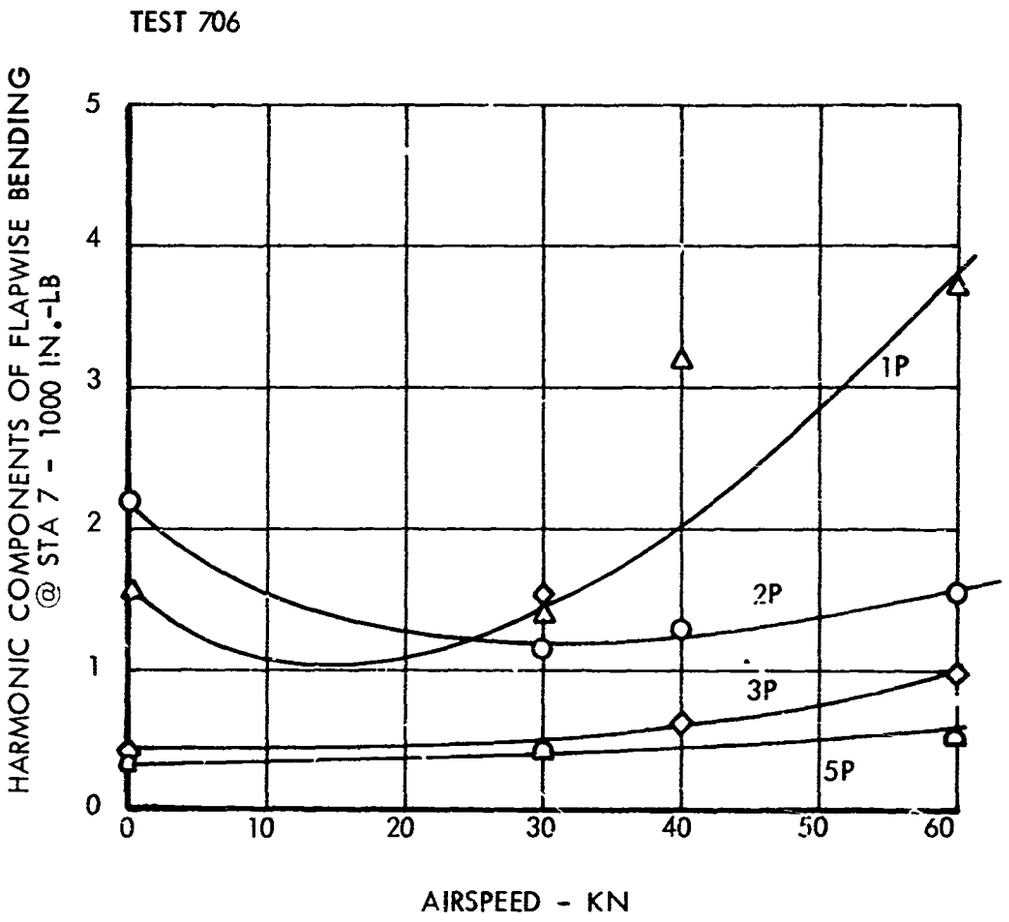

Figure 58. Harmonic Components of Blade Flapwise Bending at Blade Root.

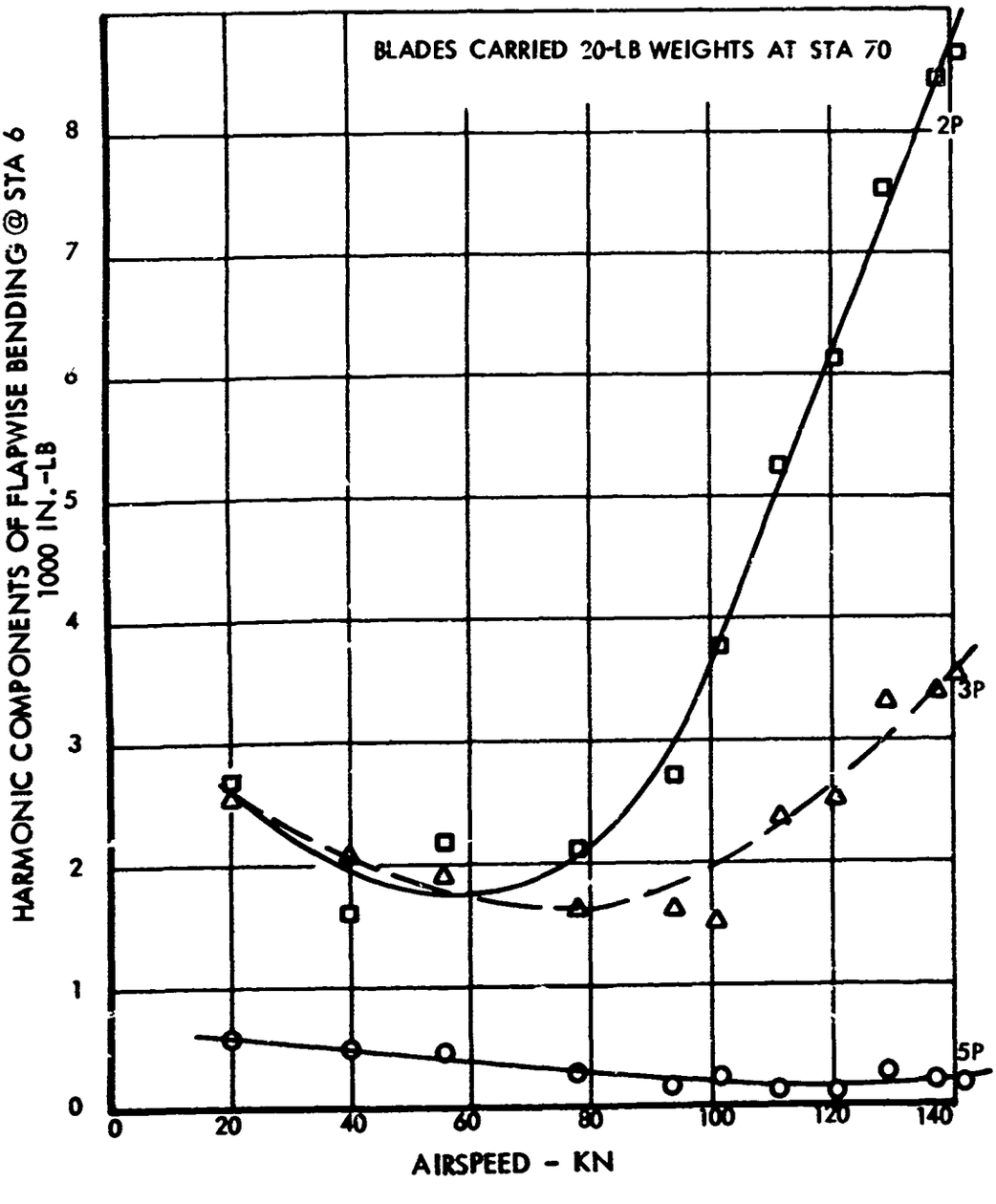

Figure 59. Harmonic Components of Flapwise Bending at Blade Root of a Standard XH-51A 4-Blade Rotor.

SECTION 10

REVIEW OF PROGRAM AND DISCUSSION OF RESULTS

The analytical studies had indicated that the aircraft with the soft in-plane matched-stiffness flexure-root rotor and with 200 slug-feet^2 added to the roll inertia (over that of the original XH-51A) would be mechanically stable in flight at the normal operating rpm and at overspeed, but that it must be restricted in rotor rpm reduction to avoid air resonance. Analyses of the effects of control system couplings and the knowledge that conservative assumptions had been made in preliminary analyses relative to structural damping provided encouragement that a wider range of rotor rpm might be achieved in flight tests than was predicted from preflight analyses and tests.

10.1 BRIEF REVIEW OF CONFIGURATION EVOLUTION

The rotor configuration was modified during whirl-tower tests. The changes included the addition of aft-chord balance at blade Station 80 and the incorporation of in-plane/feathering and flap/feathering mechanical coupling. At th conclusion of the whirl tower tests the configuration had the following characteristics:

- 3 degrees forward sweep
- 1 degree blade overcone
- 0 lb blade tip weight
- 1 slug-foot^2 gyro inertia
- More roll inertia than the standard XH-51A aircraft (up to 430 slug-feet^2 was added to the basic 304 slug-feet^2)
- Control system mechanical coupling: tangent α_3 = 0.769 and tangent δ_3 = -0.318

Preflight ground tests indicated that the configuration would be satisfactory. It was judged necessary to increase the landing gear stiffness to improve the ground resonance margin; the landing gear skids were changed from aluminum to steel, and additional stiffening was included.

10.2 TECHNICAL EVALUATION OF PROGRAM

10.2.1 Whirl Tower Tests

Since mechanical instability is not detectable unless body pitch and roll frequencies are permitted to occur, a whirl tower which had a gimbaled

inertia frame to permit rotational freedom, and a spring system to simulate the effects of landing gear in contact with the ground was used for testing the matched-stiffness rotor system. The gimbal center location simulated the center-of-gravity location of the XH-51A vehicle.

An analysis was made of a rotor configuration used in whirl tower tests (the rotor used in Test Number 75, Table VIII) to correlate theoretical procedures with test results. Results of the analysis are shown in Figure 60. The damping levels ascribed to the gimbal were based on measurements. The calculated rotor speed for air resonance using $\zeta = 0.06$ is 309 rpm (87 percent). For this condition, whirl tower measurements showed air resonance at 92 percent. Good correlation between analytical and test results is indicated.

10.2.2 Preflight Ground Tests

The ground tests showed need to stiffen the landing gear skids to improve the on-the-ground mechanical stability margin sufficiently to allow flight testing. The margin proved to be marginally adequate without gear dampers.

Several stages of landing gear modification occurred during ground testing. The original aluminum landing gear skids, in combination with dampers, did not appear to affect the ground resonance margins. Similar performance of the dampers was observed when the dampers were used in combination with the stiffened steel skids, except this time satisfactory margins were seen due to the stiffness change. A review showed that the landing gear geometry and flexibility allowed very little motion for proper actuation of the dampers. Alternate damper arrangements were examined, but since minimally acceptable margins had been attained with the stiffened gear without dampers, the dampers were not used.

Comparison of whirl tower tests results with preflight ground test results indicates fair correlation with respect to ground resonance rotor speeds. For the original aluminum skids with dampers, ground resonance rotor speeds were determined to be 90 percent in Test 661 and 99 percent in Test 69. Part of the difference is attributed to whirl tower gimbal friction.

10.2.3 Flight Tests

Since the configuration which had been tested on the whirl tower was shown to be only marginally acceptable, with respect to the rotor speed safe operating range, and since the influence of vehicle roll moment of inertia had been shown to be very strong, it was decided to fly with as much roll inertia as practical in order to provide the maximum margin of safety. The whirl tower tests had been made with a roll moment of inertia increment (over the original XH-51A roll moment of inertia) of 200 slug-feet^2, whereas a 430 slug-feet^2 increment was used for flight test. It was expected that the aircraft would then have a better margin against air resonance than the 80 percent of normal operating speed value that had been estimated from the whirl tower tests and the analyses. The results of the flight tests were disappointing, however, even with the added roll inertia,

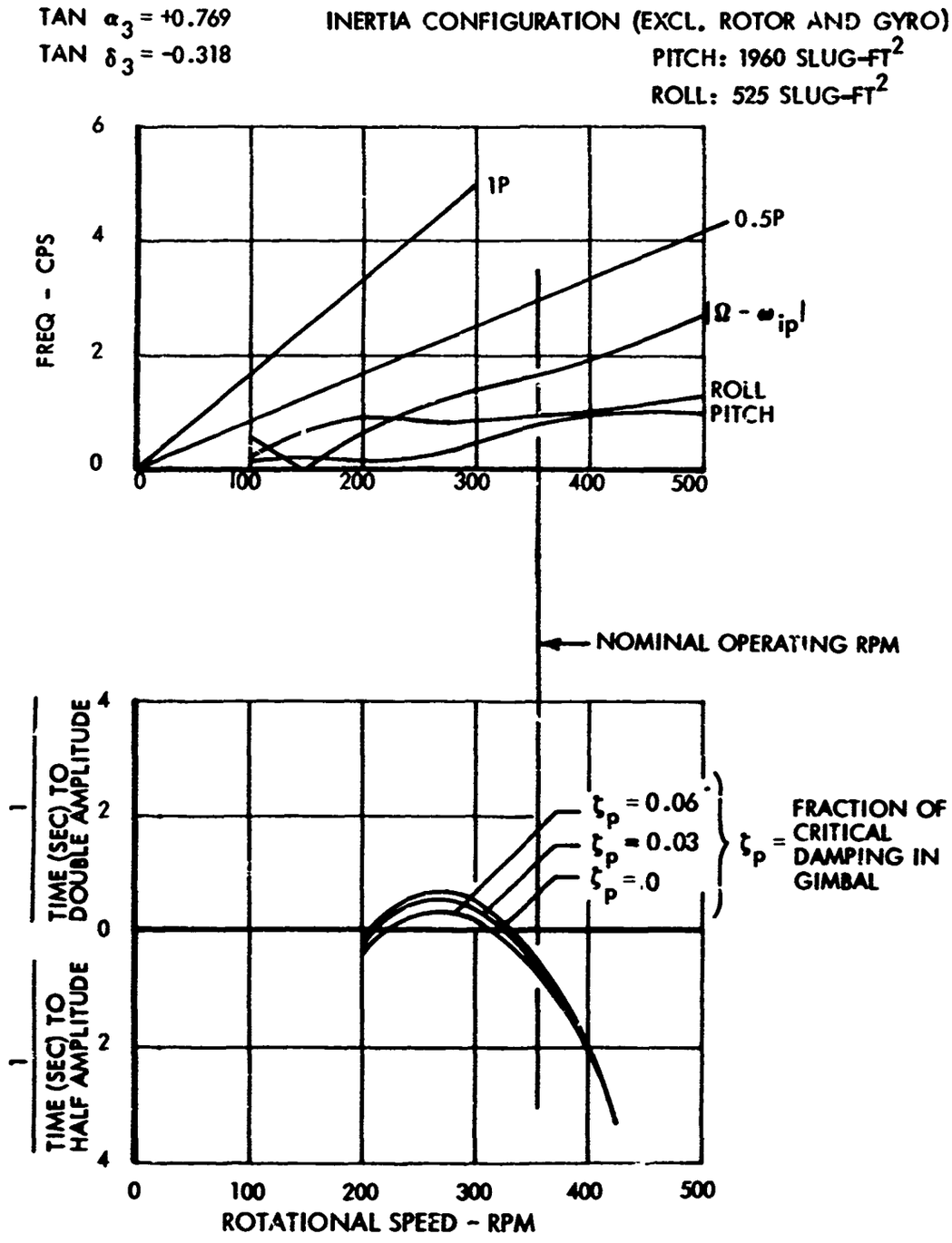

Figure 60. Analysis Results of Air Resonance From Whirl Tower Data, Gyro = 4 Slug-Ft^2.

the air resonance margin was established at 89 percent of the operating rpm. Therefore, the analyses, the whirl tower tests, or both were suspected as not properly predicting flight test behavior.

10.2.4 Analytical Studies of Flight Test Results

Analyses were made to study two of the configurations flown (different gyro sizeswere used). Data for these flights are included in Table XI as Tests 713 and 714 and results of the analyses are shown in Figures 61 and 62. The analyses indicated neutral stability to occur at about 305 rpm (86 percent) for both configurations. Estimates of the neutral stability speed from the flight test data plotted in Figures 50 and 51 show that these same configurations are neutrally stable at 315 rpm (89 percent). The analytical and flight test results are therefore reasonably close. In view of this corroboration of the analytical method by flight test, and a similar correlation between analysis and whirl tower results (Section 10.2.1), it was concluded that the analytical method is good, and that the whirl tower does not simulate flight adequately, perhaps due to gimbal friction, and the lack of freedom in translational motion. However, it can also be concluded that the gimbaled whirl tower and the analytical technique can be used together to predict in-flight mechanical instability, air resonance, quite well.

The confidence gained in the method led to an extension of the analytical study to try to improve the knowledge of the effects of α_3 and δ_3, and perhaps lead to a combination of these parameters that would significantly improve the in-flight stability margin. This extended study effort is discussed in Section 10.5.

Analyses also yielded knowledge of a rotor behavior characteristic which had not been seen in preliminary design analyses. Analyses with the 4 and 2 slug-feet^2 gyro showed a slight instability at 0.8 and 0.9 cps at the nominal operating rpm. Figures 63 and 64 show this lightly damped mode (the dashed lines on the lower chart). The only confirmation of the existence of this characteristic is a pilot report of "nervous hover". The mode is principally gyro-rotor-body motion, in that order of importance of the relative amplitudes. There is analytical evidence that adding a small amount of swash plate damping or friction in the stationary system will damp this mode with essentially no effect on mechanical stability. It is interesting to note by comparing Figures 63 and 65 that the 2 slug-feet^2 gyro system is more stable than the 4 slug-feet^2 gyro system for this type of instability. The pilot confirmed this trend.

The analysis was also extended to examine the effect of altitude. An analysis was made for flight at 16,000 feet. Results, shown in Figure 66, indicate very little effect of altitude when compared with the sea level case shown in Figure 63. The effects of altitude have not yet been systematically examined, however, so caution should be exercised in generalizing this result.

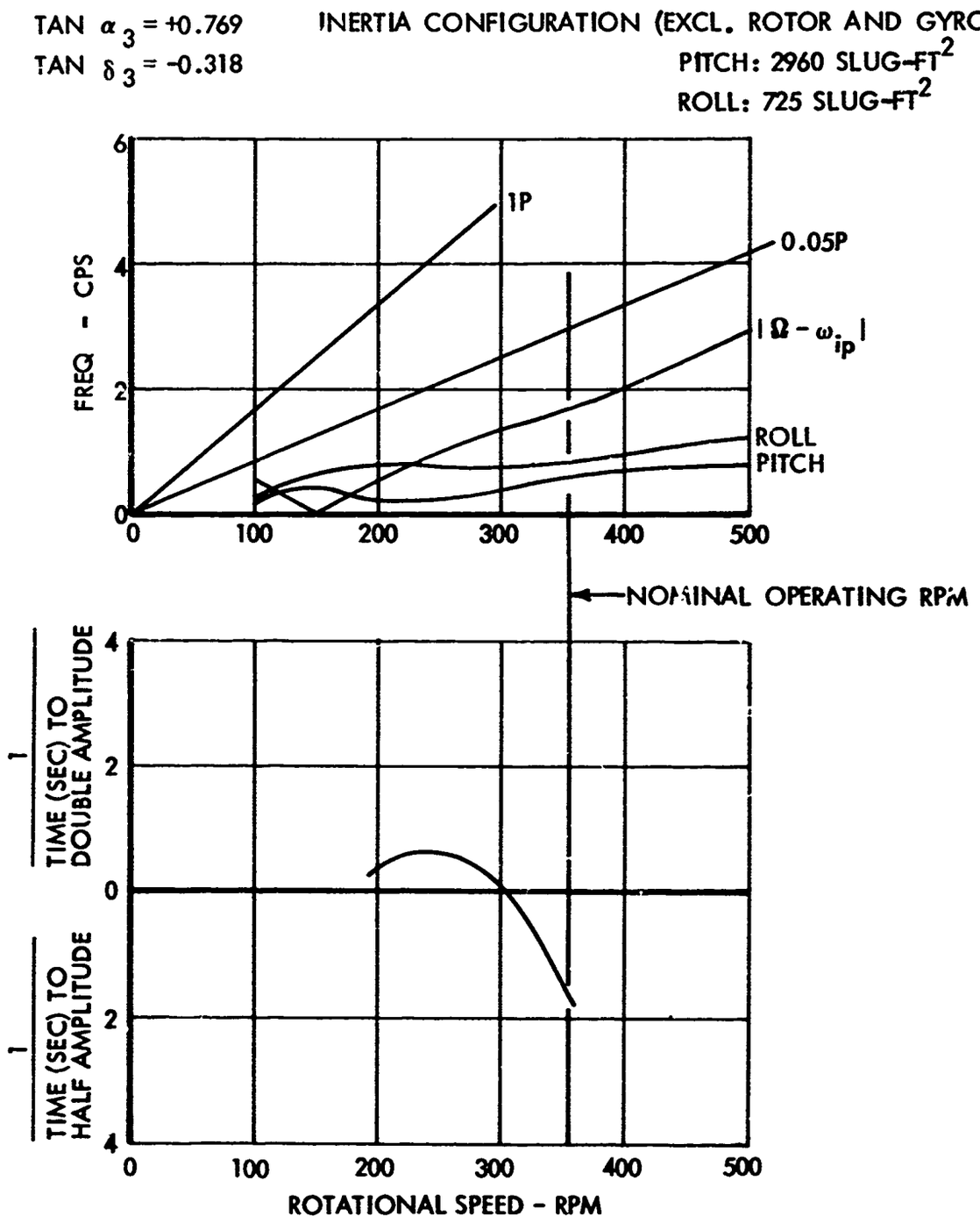

Figure 61. Analysis Results of Air Resonance From Flight Test Data, Gyro = 4 Slug-Ft^2.

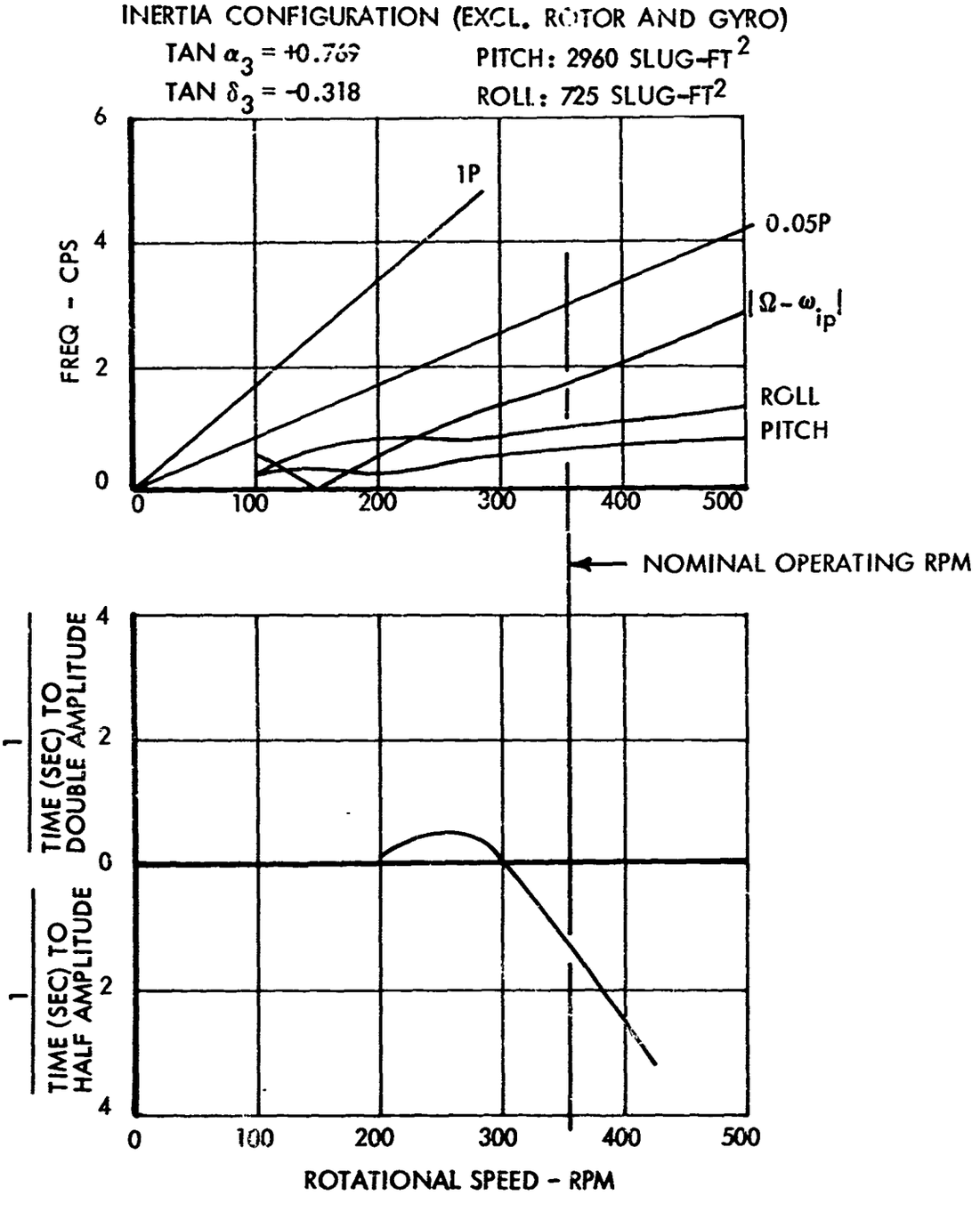

Figure 62. Analysis Results of Air Resonance From Flight Test Data, Gyro = 2 Slug-Ft^2.

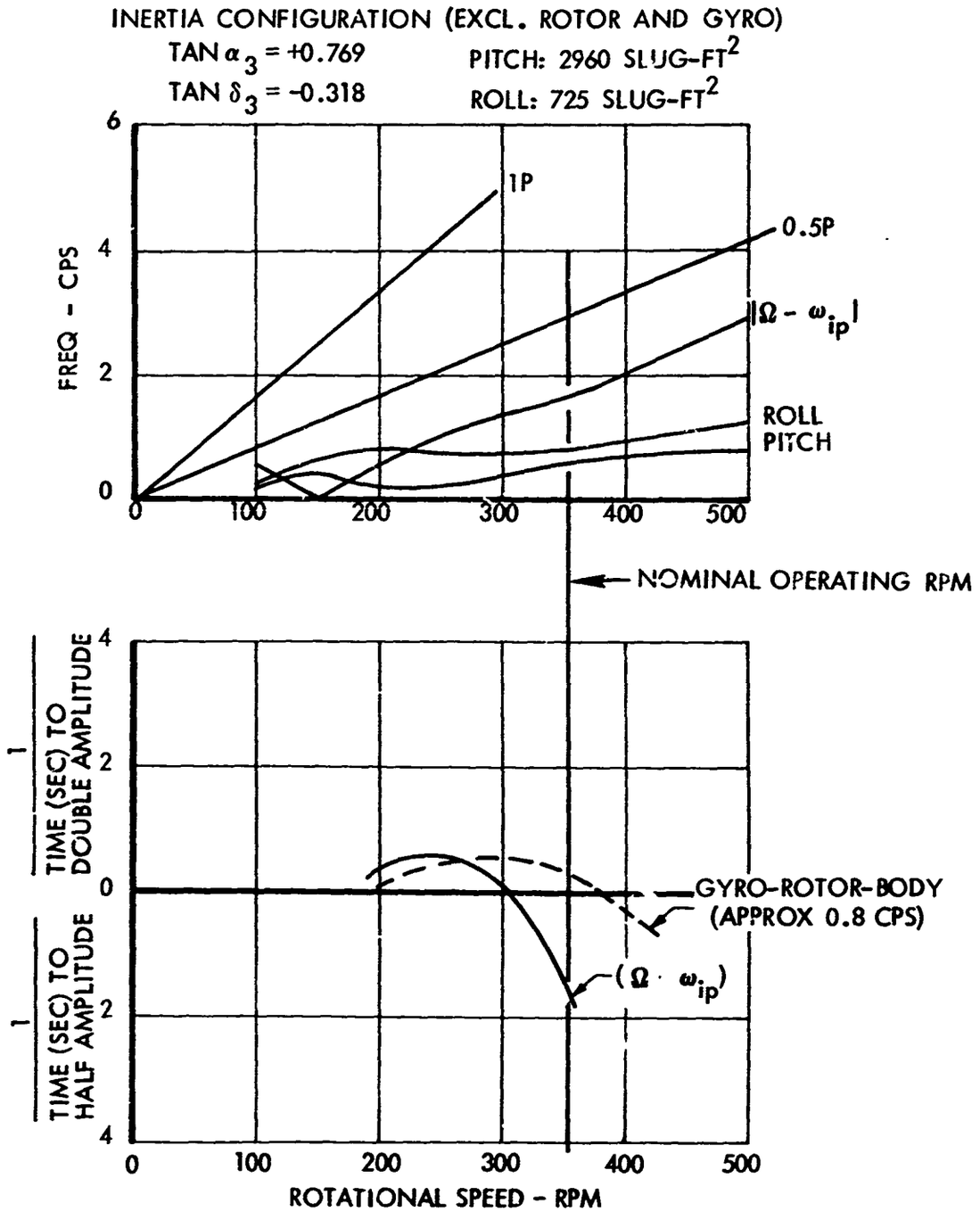

Figure 63. Results of Cyclic Stability Analysis for an In-Flight Configuration With a 4-Slug-Ft^2 Gyro.

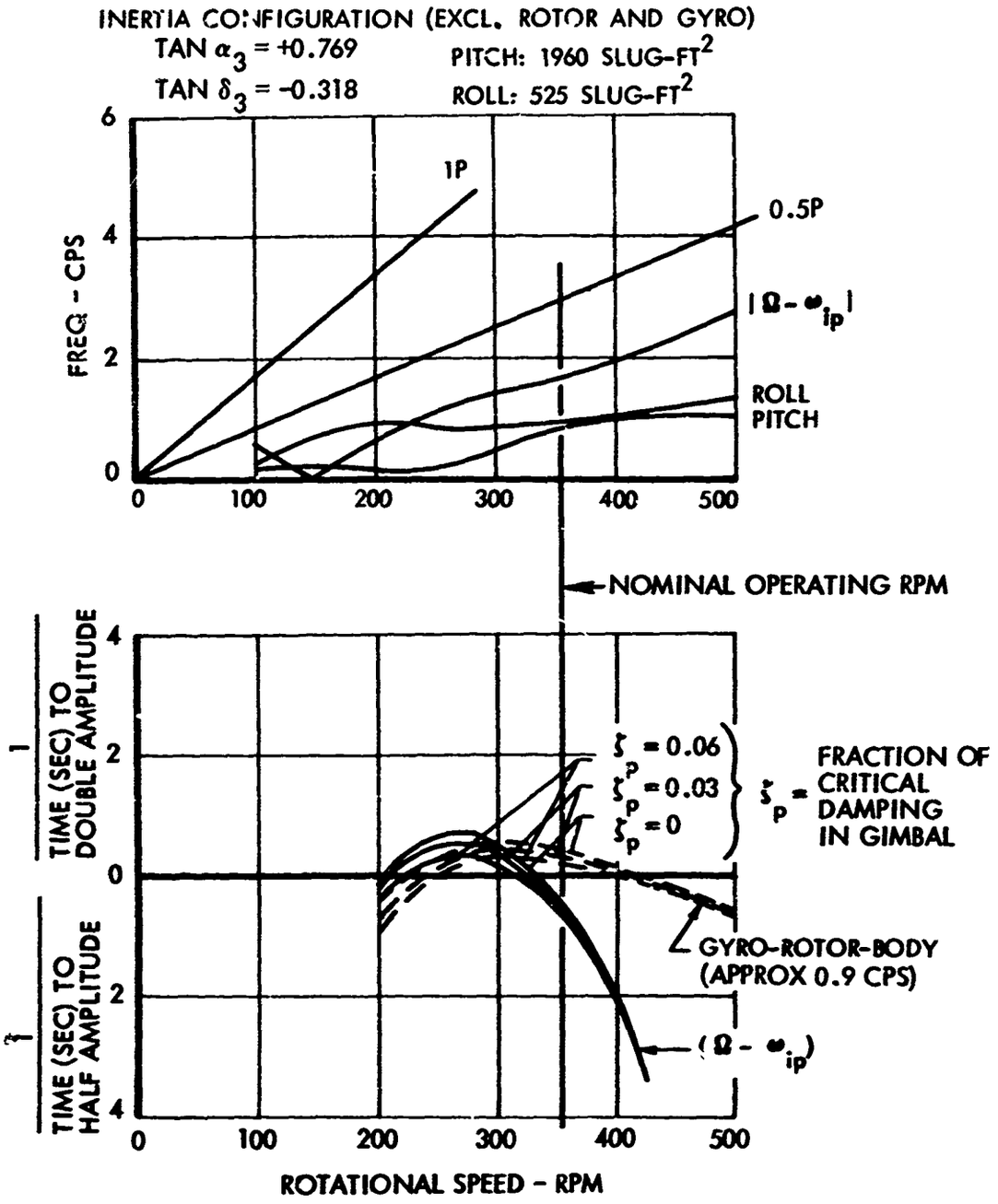

Figure 64. Results of Cyclic Stability Analysis for a Whirl Tower Configuration (Gimballed) With a 4-Slug-Ft^2 Gyro.

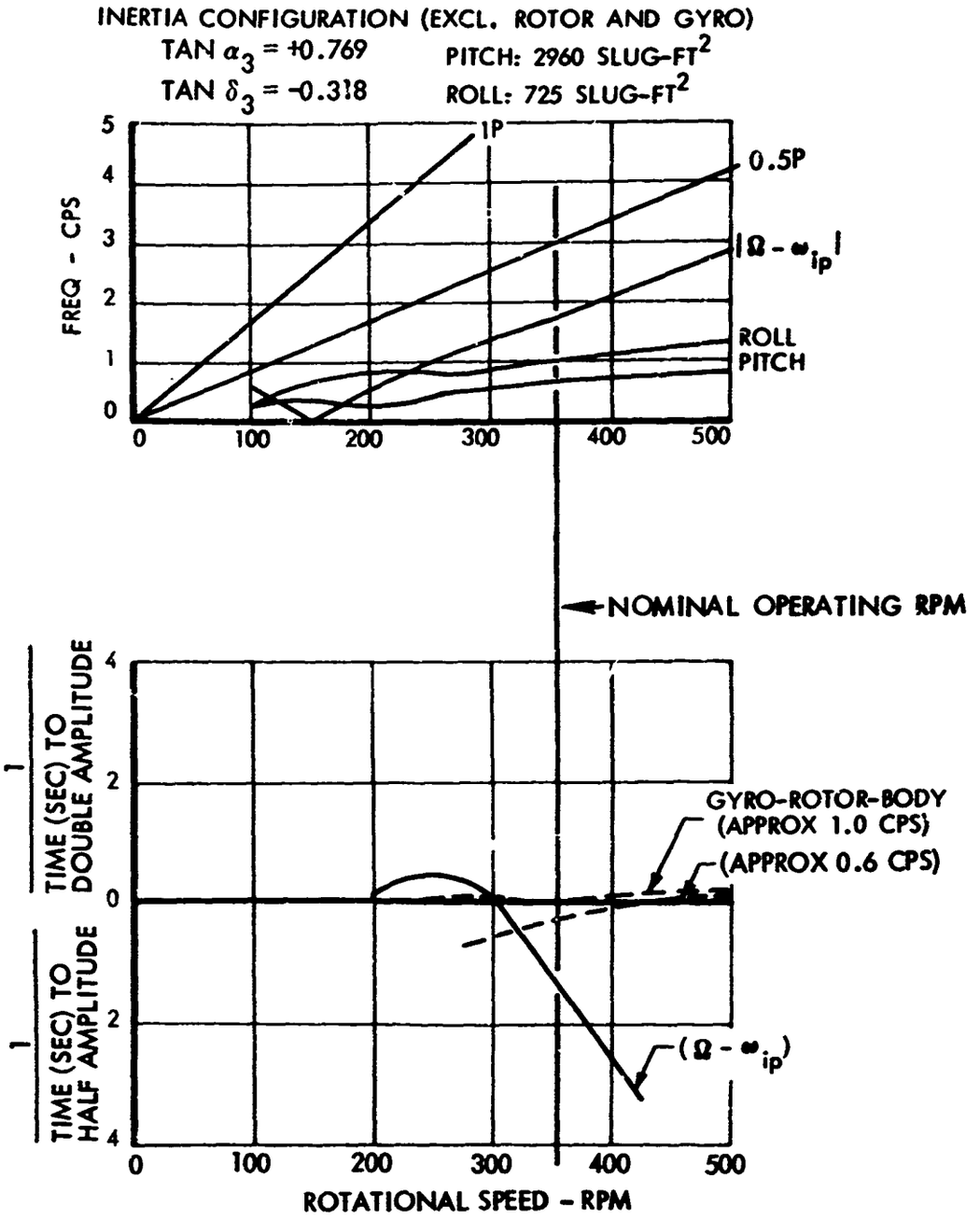

Figure 65. Results of Cyclic Stability Analysis for an In-Flight Configuration With a 2-Slug-Ft^2 Gyro.

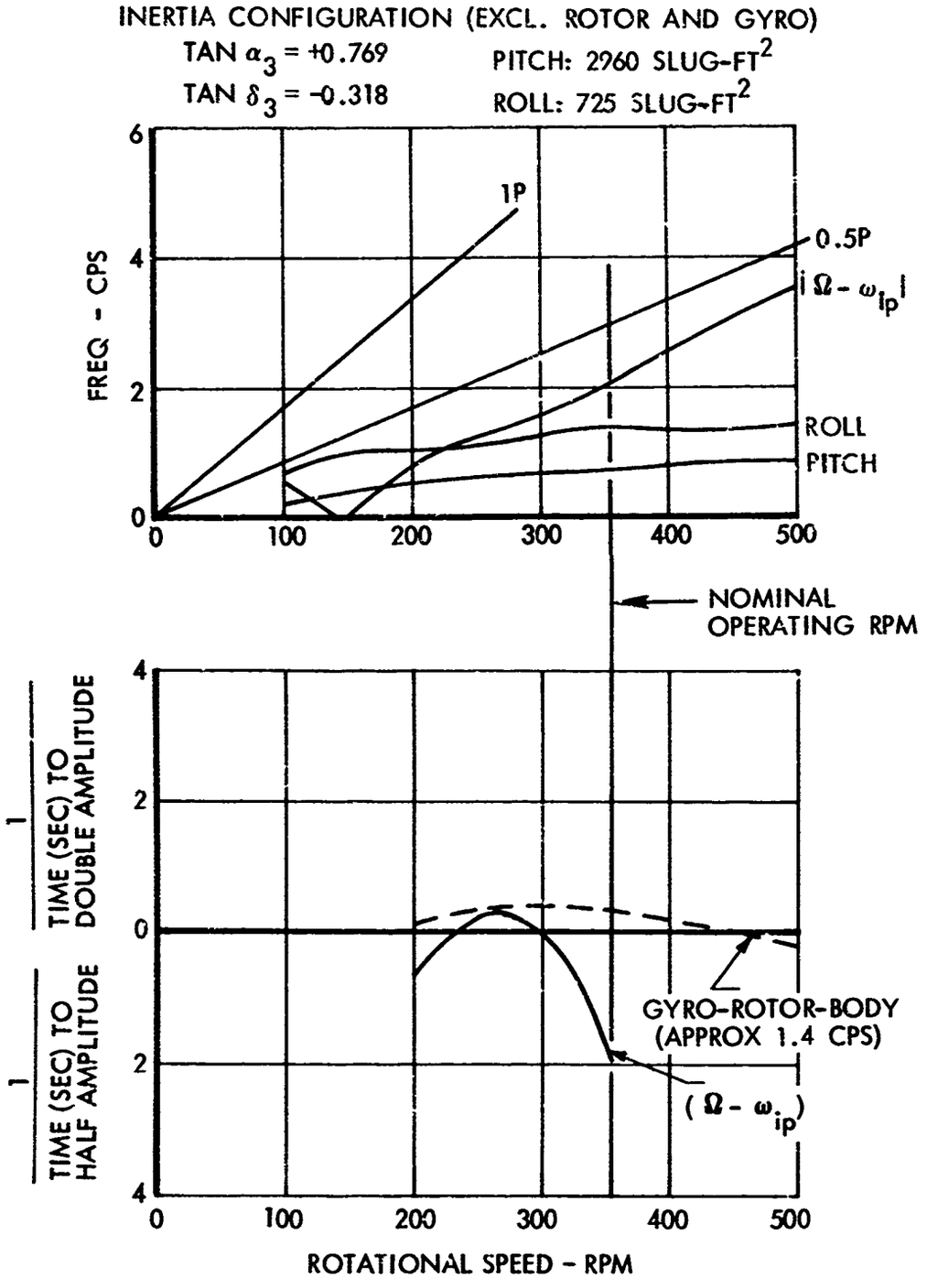

Figure 66. Results of Cyclic Stability Analysis for Flight at 16,000 Feet With a Configuration Having a 4-Slug-Ft^2 Gyro.

10.3 COMMENTARY ON ANALYTICAL TECHNIQUES

The analysis methods used yielded results which were in good agreement with whirl stand and flight test data measurements. Good correlation of the analyses with both whirl tower and flight test results is viewed as substantiation for concluding that the gimbaled inertia frame is a valuable experimental technique for studying air/ground resonance.

10.4 GENERAL OBSERVATION REGARDING THE ONSET OF INSTABILITY

The onset of mechanical instability in all of the experimental work was easily detected and was very mild. For example, in one hovering flight case, reduced rpm resulted in a slow in-plane bending moment divergence which was seen by the pilot on the flight panel instrument (was also seen on the oscillograph recordings). The pilot elected to fly out of this condition simply by increasing the rotor rpm. An alternate choice would have been to immediately land the aircraft, where contact with the ground would have caused an immediate change to a stable condition.

Ground resonance cases were observed to be equally mild, both on the aircraft and in the simulations made on the whirl tower. Hovering tests where the skid gear was in partial contact with the ground did not show any observable rotor in-plane bending moment activity.

10.5 EXTENDED ANALYTICAL STUDY

The observation that mechanical coupling does affect in-flight stability, and that the effects of relative magnitudes of α_3 and δ_3 were not fully understood, led to an extension of the analysis effort beyond curtailment of the flight test program. The objective was to seek a better understanding of the influence of mechanical coupling on in-flight stability.

Several configurations were analyzed, in which α_3, δ_3, and the roll inertia increment were varied. Results of these analyses are summarized in Figure 67, where they are compared with the flight test configuration.

Note that a curve (dashed line on figure) has been estimated, a curve connecting results of the "extended" study with the calculated result of an analysis of the flight-tested configuration. The α_3 values of the points connected by the curve are not identical, so the estimated curve suggests that the α_3 difference is of small significance. The validity of this suggestion is open to question; however, based on the overall picture presented by the figure, the curve indicates a plausible trend. It is felt that the algebraic sign and general magnitude of α_3 is important, and that the two values, 0.50 and 0.76, are of the proper general magnitude to produce beneficial damping.

Generally, Figure 67 shows how the stability boundary tends to vary with changes of roll moment of inertia and δ_3. Care must be applied in forming conclusions from this figure. Each point on the figure represents an analysis which yielded a set of stability plots such as those shown in Figures 13 and 14. Interpretation of these plots, to identify a single rotor speed value as a stability boundary, involves consideration of all aspects of the rotor's dynamic behavior. This last statement makes reference to the fact that the analytical model contains many variables which were set at fixed values in the analyses (examples of these "fixed variables" are: blade sweep, blade droop, rotor-to-gyro mechanical advantage, rotor spring, and gyro spring), and that these parameters appear to interact strongly with α_3 and δ_3 when used in certain combinations. To summarize this point, it should be made clear that in the cases which resulted in the points shown in Figure 67, all modes other than those representing mechanical stability were stable. Whereas in many other cases (other combinations of α_3 and δ_3 and/or the "fixed variables"), modes other than those directly attributable to mechanical stability showed signs of instability and therefore made it difficult to interpret the results in terms of a mechanical stability boundary. For these cases no "boundary point" was identified for inclusion in Figure 67.

It was hoped that a sufficient number of "boundary points" could be determined to expand Figure 67 into a data map which would offer conclusions regarding optimum combinations of α_3 and δ_3. However, since other modes did become involved, it appeared that experimenting with changes in the "fixed variables" would be the next logical step. It is important at this point to be reminded that changing the "fixed variables" could affect the handling qualities and the control characteristics of the rigid-rotor vehicle. Thus, it became evident that a meaningful continuation of the extended study could grow into an analytical effort beyond the scope of the program. Therefore, the extended study was terminated.

It is noteworthy that inspection of Figure 67 leads to the conclusion that varying δ_3 while holding α_3 fixed has a pronounced effect on the neutral stability rotor speed. This conclusion is in contrast with the results shown in Figures 13 and 14, where the effects of adding mechanical coupling appeared to be primarily a change in the level of instability, with little change in the neutral stability rotor speed.

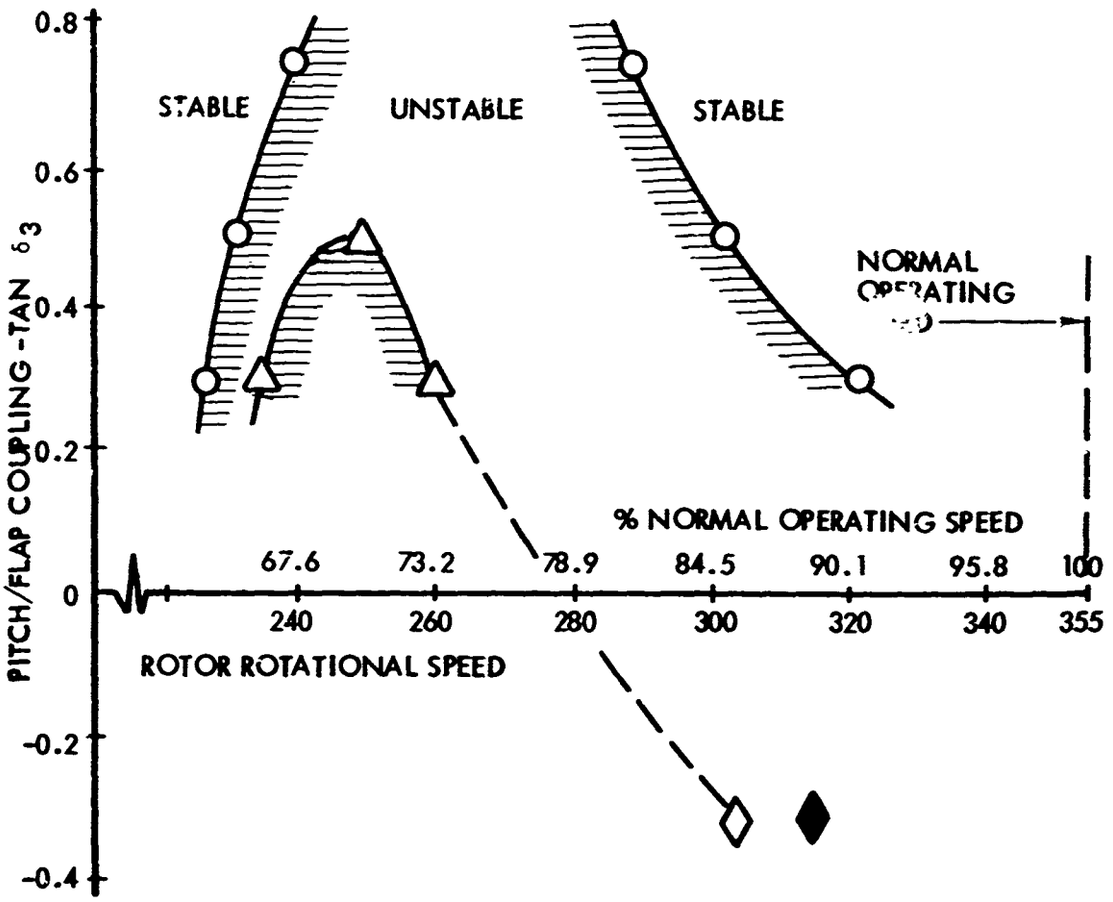

VARIABLES REPRESENTED BY POINTS				
LEGEND	TAN α_3	ΔI_{ROLL} SLUG-FEET^2	J_{GYRO} SLUG-FEET^2	COMMENT
○	0.5	0	2	EXTENDED STUDY
△	0.5	400	2	EXTENDED STUDY
◇	0.76	400	2, 4	FLIGHT CONFIG-URATION, ANALYSIS
◆	0.76	430	2, 4, 5	FLIGHT CONFIG-URATION, TEST

Figure 67. Results of Air Resonance Analyses.

SECTION 11

CONCLUSIONS

The soft in-plane matched-stiffness flexure-root rotor system was investigated to explore its full-scale feasibility and operational limitations. Primary benefits derived from this rotor concept are a direct result of the elimination of undesirable feedback signals from the rotor to the control gyroscope, such as occur in the control system of a more conventional stiff in-plane nonmatched-stiffness rigid rotor. These benefits would include lowering the size of the control gyro and rotor system weight, and an overall simplification of the control system. A soft in-plane configuration was selected for the study because it introduced the added benefit of eliminating the need for rotor blade feathering bearings.

Analyses, ground tests, and flight tests demonstrated that the concept is feasible, but in its present stage of development, the existing rotor system is limited in the range of rotor speeds (rpm) in which it can operate safely.

Pilot comments indicated that the XH-51A test aircraft experienced lower crew station vibration levels when flown with the matched-stiffness rotor than when flown with a standard stiff in-plane rotor. These comments applied to flight from hover to forward speeds up to 60 knots, which was the speed range flown in this program.

The matched-stiffness rotor system flown in this test program was 11 percent lighter than the original rotor used on the test aircraft. An operational matched-stiffness rotor would likely be even lighter, since the test rotor was designed conservatively and was fitted with provisions for varying geometric characteristics for experimental purposes.

The operational limitations revealed by this study/test program arise from the fact that two modes of rotor-body mechanical instability were encountered, depending upon whether the rotor was allowed to "overspeed" or "underspeed". If the rpm was increased from normal (approximatly 6 percent) while the vehicle was in contact with the ground, the aircraft was exposed to developing an on-the-ground rotor-body mechanical instability, "ground resonance". Further, if the rpm was decreased from normal (approximately 11 percent) while in the air, the aircraft was exposed to developing an in-flight rotor body mechanical instability, "air resonance". Thus it was determined that the overall safe operating range was of the order of 17 percent of the normal operating speed. In view of this restricted operating rpm range, it was concluded that continuation of the flight test program would produce no additional engineering data pertinent to the matched-stiffness concept; the program was thus curtailed after 3.5 hours of flight testing.

The operational limitations were identified in the analyses and whirl tower tests that preceded the flight tests. However, it was concluded that, due to conservatisms recognized to exist in the analyses and whirl tower tests, the operational envelope could be enlarged in flight test, but this proved not to be the case. This fact was identified very early in the flight program, so testing was limited to speeds not greater than 60 knots, and the flight program was redirected to obtain engineering information pertinent to the in-flight mechanical instability.

It is noteworthy that this program demonstrated the feasibility of controlling "ground resonance" without recourse to rotor in-plane dampers or landing gear dampers. However, the flight rotor speed range for which this was accomplished is not considered to be adequate for extended safe operation.

It is also important to note that the rotor system tested, although it proved to be marginal with respect to air resonance, performed very satisfactorily in all other respects. Extensive variations of rotor rpm, thrust, body moments, and applied control moments were examined in the early fixed-shaft whirl tower tests. The results were entirely satisfactory.

Analysis of the work conducted in this program indicates that the mechanical instability problem is amenable to solution by the use of inherent aerodynamic damping in the rotor without recourse to the use of mechanical dampers. Appropriate pitch/flap and pitch/in-plane coupling in the rotor system is seen as a means of producing satisfactory operating rpm ranges for many rotary-wing configurations. Pursuit of this means of solution will require additional research to determine optimum combinations of mechanical coupling and to assure that this approach will not lead to detrimental effects on control characteristics of the rotor system.

Analytical methods were developed which satisfactorily correlate whirl stand, ground, and flight test dynamic data measurements. Consequently, these methods can be used to predict air and ground resonance phenomena with acceptable quantitative accuracy. The development of these methods represents a major step toward understanding the mechanical instability phenomena which can occur in soft in-plane rotor systems. These methods also provide a means for exploring the use of rotor aerodynamics to inhibit mechanical instabilities.

LITERATURE CITED

1. Lockheed-California Company, MATCHED-STIFFNESS/FLEXURE-ROOT-BLADE ROTOR SYSTEM ANALYTICAL STUDIES REPORT, LR 19057, Burbank, Calif., Oct. 1, 1965; revised Jan. 28, 1966.

2. National Advisory Committee for Aero, THEORY OF SELF-EXCITED MECHANICAL OSCILLATIONS OF HELICOPTER ROTORS WITH HINGED BLADES, by R. P. Coleman and A. M. Feingold, Report 1351, 1958.

3. Princeton University, THE MECHANICAL INSTABILITY AND FORCED RESPONSE OF ROTORS ON MULTIPLE-DEGREE-OF-FREEDOM SUPPORTS, by G. W. Brooks, doctoral dissertation, New Jersey, 1961.

4. Princeton University, Department of Aeronautical Engineering, AN EXPERIMENTAL AND ANALYTICAL STUDY OF THE MECHANICAL INSTABILITY OF ROTORS ON MULTIPLE-DEGREE-OF-FREEDOM SUPPORTS, by R. L. Bielawa, Report No. 612, New Jersey, 1962.

5. U.S. Army Transportation Research Command, WIND TUNNEL TESTS OF AN OPTIMIZED MATCHED-STIFFNESS RIGID ROTOR, TRECOM Technical Report 64-56, Fort Eustis, Virginia, Nov. 1964.

6. R. J. Roark, FORMULAS FOR STRESS AND STRAIN, McGraw-Hill, Third Edition, 1954.

7. METALLIC MATERIALS AND ELEMENTS FOR FLIGHT VEHICLE STRUCTURES, MIL-HDBK-5, Revised June 1, 1965.

8. S. Timoshenko, STRENGTH OF MATERIALS, Part I, D. Von Nostrand Co., Inc., New York, N.Y., Second Edition, 1940.

9. Lockheed-California Company, FATIGUE AND STATIC TESTS OF THE DYNAMIC COMPONENTS OF THE MODEL CL-864 MATCHED-STIFFNESS HELICOPTER, LR 19551, Burbank, Calif., August 15, 1966.

APPENDIX

REFERENCE DATA

TABLE XII. DESCRIPTION OF XH-51A TEST AIRCRAFT AS MODIFIED FOR MATCHED-STIFFNESS ROTOR FLIGHT TEST PROGRAM

General	
Design Gross Weight	3800 lb
Maximum Flight Test Gross Weight	4240 lb
Maximum crew	2
Overall length	42.6 ft
Maximum tail-low ground altitude	6 deg
Design Level Flight Speed	140 kn
Design Dive Speed	150 kn
Mass Moments of Inertia	–
Excluding rotor and outriggers, at GW =	3026 lb
Pitch	3434 slug-ft^2
Roll	304 slug-ft^2
Yaw (not determined; estimated approx. same as pitch)	–
Maximum added increment due to outriggers, mass on outriggers, and 54 slug-ft^2 due to heavier skids, Roll	430 slug-ft^2
Main Rotor	
Type	rigid, matched-stiffness
First in-plane frequency @ 355 rpm	0.66r
Diameter	35 ft
Number of blades	4
Blade chord	13.5 in
Airfoil section	modified NACA 0012
Blade taper	0
Blade twist (root to tip)	-5 deg
Rotational axis tilt	6 deg forward
Hub precone	3 deg
Blade overcone (variable)	0 to 1 deg
Blade forward sweep (variable)	0 to 3 deg (forward)
Solidity	.0818
Disc area	962 sq ft
Rotor weight	515 lb
Polar moment of inertia	803 slug-ft^2
Normal operating speed	355 rpm
Tan α_3	0.769
Tan δ_3	-0.318

TABLE XII - Continued

Control Gyro	
Diameter	Variable
Number of arms	4
Polar moment of inertia (variable)	1 to 5 slug-ft^2
Tail Rotor	
Diameter	72 in
Number of blades	2
Blade chord	8.5 in
Hub type	teetering
Airfoil section	NACA 0012
Blade taper	0
Blade twist (root-to-tip)	-4.35
Feathering moment balance weights at 3 in. arm	2.25 lb per blade
δ_3	15 deg
Disc area	28.27 sq ft
Solidity	.1503
Pitch change travel	27 deg to -8 deg
Normal operating speed	2085 rpm
Horizontal Stabilizer	
Area	7.58 sq ft
Span	84 in.
Chord	13 in.
Airfoil section	NACA 0015
Aspect ratio	6.46
Vertical Stabilizer	
Area	12.58 sq ft
Span	41.75 in.
Chord (tip)	38.5 in.
(root)	51.5 in.
Taper ratio	0.70
Aspect ratio	0.95
Airfoil section	modified NACA 4424
Power Plant	
Type	Turboshaft PT6B-9
Maximum power	500 SHP @ SL
Fuel	JP-4
Oil	Turbo 35

TABLE XIII. WEIGHT-EMPTY BALANCE DATA

	Weight (lb)	Horizontal Arm (FS, in.)	Vertical Arm (WL, in.)
Rotor Group	523	100.4	95.4
Tail Group	57	343.8	87.1
Body Group	502	103.8	43.8
Alighting Gear Group	164	87.7	16.2
Flight Controls Group	271	81.9	43.4
Engine Section Group	13	125.2	47.9
Propulsion Group	867	139.8	62.4
Instrument and Navigational Equipment Group	46	63.2	42.8
Hydraulic Group	42	98.4	51.6
Electrical Group	92	33.4	28.7
Electronics Group	14	70.7	30.6
Furnishings & Equip. Group	106	57.7	38.8
Air-Conditioning Group	3	56.3	53.7
Weight Empty*	2700	111.49	58.32

*Weight Empty Shaft Moment=+20,034 in.-lb

TABLE XIV. DESIGN GROSS WEIGHT BALANCE DATA

	Weight (lb)	Longitudinal Arm (FS, in.)	Vertical Arm (WL, in.)
Weight Empty, Gear Down	2700	111.49	58.32
Useful Load	(1100)	(92.10)	(38.14)
Crew, Pilot	200	56.0	44.0
Fuel, Unusable	3	110.0	35.0
Fuel, Usable	220	108.5	25.6
Oil, Unusable	3	193.4	59.4
Oil, Engine	24	165.0	55.9
Flight Test Equipment	450	91.5	43.2
Outriggers with Ballast	200	101.0	32.3
Gross Weight*	3800	105.88	52.48

*GROSS WEIGHT SHAFT MOMENT = +4,674 in.-lb

TABLE XV. COORDINATES OF 80-DEGREE-OF-FREEDOM SYSTEM

1	X_o		Hub Fore and Aft Translation
2	Y_o		Hub Lateral Translation
3	ϕ_o		Hub Roll
4	θ_o		Hub Pitch
Blade No. 1	Blade No. 2		
5	39	Z 5.78	Vertical Deflection at Rotor Station 5.78
6	40	Z 21	Vertical Deflection at Rotor Station 21
7	41	Z 42	Vertical Deflection at Rotor Station 42
8	42	Z 63	Vertical Deflection at Rotor Station 63
9	43	Z 84	Vertical Deflection at Rotor Station 84
10	44	Z105	Vertical Deflection at Rotor Station 105
11	45	Z126	Vertical Deflection at Rotor Station 126
12	46	Z147	Vertical Deflection at Rotor Station 147
13	47	Z168	Vertical Deflection at Rotor Station 168
14	48	Z189	Vertical Deflection at Rotor Station 189
15	49	Z210	Vertical Deflection at Rotor Station 210
16	50	X 5.78	Chordwise Deflection at Rotor Station 5.78
17	51	X 21	Chordwise Deflection at Rotor Station 21
18	52	X 42	Chordwise Deflection at Rotor Station 42
19	53	X 63	Chordwise Deflection at Rotor Station 63
20	54	X 84	Chordwise Deflection at Rotor Station 84
21	55	X105	Chordwise Deflection at Rotor Station 105
22	56	X126	Chordwise Deflection at Rotor Station 126
23	57	X147	Chordwise Deflection at Rotor Station 147
24	58	X168	Chordwise Deflection at Rotor Station 168
25	59	X189	Chordwise Deflection at Rotor Station 189
26	60	X210	Chordwise Deflection at Rotor Station 210

TABLE XV - Continued

Blade No. 1	Blade No. 2		
27	61	θ 5.78	Torsional Deflection at Rotor Station 5.78
28	62	θ 21	Torsional Deflection at Rotor Station 21
29	63	θ 42	Torsional Deflection at Rotor Station 42
30	64	θ 63	Torsional Deflection at Rotor Station 63
31	65	θ 84	Torsional Deflection at Rotor Station 84
32	66	θ105	Torsional Deflection at Rotor Station 105
33	67	θ126	Torsional Deflection at Rotor Station 126
34	68	θ147	Torsional Deflection at Rotor Station 147
35	69	θ168	Torsional Deflection at Rotor Station 168
36	70	θ189	Torsional Deflection at Rotor Station 189
37	71	θ210	Torsional Deflection at Rotor Station 210
38		ϕ G	Gyro Roll
	72	θ G	Gyro Pitch
73	X_T	Transmission Fore and Aft Translation	
74	Y_T	Transmission Lateral Translation	
75	ϕ_T	Transmission Roll	
76	θ_T	Transmission Pitch	
77	X_F	Fuselage Fore and Aft Translation	
78	Y_F	Fuselage Lateral Translation	
79	ϕ_F	Fuselage Roll	
80	θ_F	Fuselage Pitch	

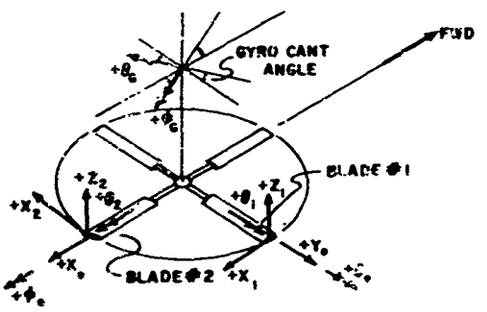

TABLE XVI. COORDINATES OF 22-DEGREE-OF-FREEDOM SYSTEM

1	X_o	Rotor Fore and Aft Translation	
2	Y_o	Rotor Lateral Translation	
3	ϕ_o	Rotor Roll	
4	θ_o	Rotor Pitch	
5	X_{11}	First In-Plane Bending	Blade #1
6	Z_{11}	First Flap Bending	
7	θ_{11}	Feathering	
8	Z_{12}	Second Flap Bending	
9	X_{12}	Second In-Plane Bending	
10	X_{21}	First In-Plane Bending	Blade #2
11	Z_{21}	First Flap Bending	
12	θ_{21}	Feathering	
13	Z_{22}	Second Flap Bending	
14	X_{22}	Second In-Plane Bending	
15	X_T	Transmission Fore and Aft Translation	
16	Y_T	Transmission Lateral Translation	
17	ϕ_T	Transmission Roll	
18	θ_T	Transmission Pitch	
19	X_F	Fuselage Fore and Aft Translation	
20	Y_F	Fuselage Lateral Translation	
21	ϕ_F	Fuselage Roll	
22	θ_F	Fuselage Pitch	

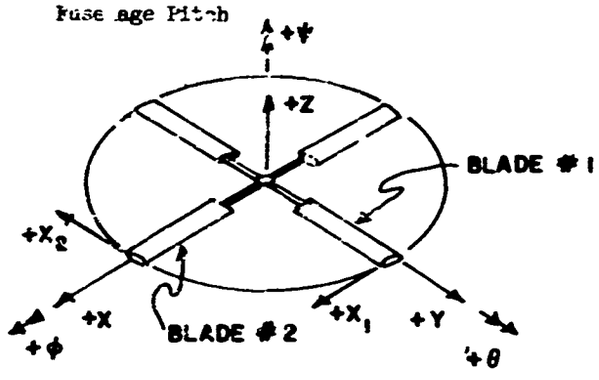

TABLE XVII. SYMBOLS FOR 10 X 10
EQUATIONS OF TABLE XVIII

X	Fore and aft translation of entire system, positive forward
Y	Lateral translation of entire system, positive right
θ_R	Pitch attitude of rotor plane relative to horizontal, positive nose up; the rotor plane is defined by the plane joining the 0.75R stations
ϕ_R	Roll attitude of rotor plane, positive right side down
θ_G	Pitch attitude of control gyro, positive nose up
ϕ_G	Roll attitude of control gyro, positive right side down
θ_F	Pitch attitude of fuselage and shaft, positive nose up
ϕ_F	Roll attitude of fuselage and shaft, positive right side down
ϵ_X	Angular deflection component of all blades toward front of rotor
ϵ_Y	Angular deflection component of all blades toward right side of rotor
M_R	Mass of rotor
M_F	Mass of fuselage, transmission and shaft system
J_R, J_G	Polar moment of inertia of rotor or gyro
I_R, I_G	Diametral moment of inertia of rotor or gyro
e	Distance of effective in-plane pivot location from centerline of hub
I_{eb}	Moment of inertia of one blade about effective pivot location
S_{eb}	Blade static unbalance about effective pivot location

TABLE XVII - Continued

S_β	Blade static unbalance in flapping
W_F	Weight of fuselage, transmission and shaft system
I_{θ_F}, I_{ϕ_F}	Pitch or roll moment of inertia of fuselage, transmission, and shaft system about its center of gravity
K_β	Stiffness of rotor plane relative to shaft
K_ϵ	In-plane structural stiffness about effective pivot location
M_A	Aerodynamic effectiveness of cyclic feathering in producing moment
$M_{\dot{\theta}}$, $M_{\dot{\phi}}$	Rotor aerodynamic damping in pitch and roll
K_G	Control spring stiffness as seen by control gyro swash plate
M_G	Swash plate damper
h_F	Distance of fuselage, transmission, shaft system center of gravity from hub
β_o	Blade precone angle
ψ_o	Control gyro cant angle to blade
K	Control gyro mechanical advantage (gyro angle/blade angle)
λ	Blade sweep forward, net angle between blade quarter chord and feathering axis as seen in-plane view
C_m	Moment coefficient to account for spanwise location of sweep angle
Ω	Rotational speed of rotor, counterclockwise as viewed from above
P	Laplace operator

TABLE XVIII. DYNAMIC EQUATIONS OF EQUILIBRIUM FOR MATCHED-STIFFNESS/FLEXURE-HUB ROTOR

$$
\begin{Bmatrix} F_X \\ F_Y \\ M_{\theta_R} \\ M_{\phi_R} \\ M_{\theta_G} \\ M_{\phi_G} \\ M_{\theta_F} \\ M_{\phi_F} \\ M_{\epsilon_X} \\ M_{\epsilon_Y} \end{Bmatrix} =
\begin{bmatrix}
-(M_R+M_F)P^2 & & & & & & (M \\
 & -(M_R+M_F)P^2 & & & & & \\
 & & -I_RP^2 & -J_R\Omega P & & & \\
 & & +M\dot{\theta}P & -M_A & +M_A\frac{\cos\psi_o}{K} & +M_A\frac{\sin\psi_o}{K} & +2K\beta-M_A c \\
 & & -2K\beta & & & & \\
 & & & -I_RP^2 & & & \\
 & & +J_R\Omega P & +M\dot{\phi}P & & & \\
 & & +M_A & -2K\beta & -M_A\frac{\sin\psi_o}{K} & +M_A\frac{\cos\psi_o}{K} & -M_A\left(1-\frac{\sin}{K}\right. \\
 & & & & -I_GP^2 & & \\
 & & & & -M\dot{G}P & -J_G\Omega P & +M\dot{G}P \\
 & & +c_m2K\beta\frac{\cos\psi_o}{K}\lambda & -c_m2K\beta\frac{\sin\psi_o}{K}\lambda & -K_G & & +K_G-c_m2K\beta \\
 & & & & & -I_GP^2 & \\
 & & & & +J_G\Omega P & -M\dot{G}P & \\
 & & +c_m2K\beta\frac{\sin\psi_o}{K}\lambda & +c_m2K\beta\frac{\cos\psi_o}{K}\lambda & & -K_G & -c_m2K\beta\frac{\sin}{K} \\
(M_Fh_F)P^2 & & & & & & -(I_{\theta_F}+M_Fh \\
 & & & & +M\dot{G}P & & -M\dot{G}P \\
 & & +2K\beta & & +K_G & & -2K\beta-K_G \\
 & (M_Fh_F)P^2 & & & & & \\
 & & & & & +M\dot{G}P & \\
 & & & +2K\beta & & +K_G & \\
-2S_{ee}P^2 & & & & & & \\
 & & & & & & \\
 & -2S_{ee}P^2 & & & & & \\
 & & & & & &
\end{bmatrix}
$$

$$
\begin{bmatrix}
 & & (M_F h_F)P^2 & & -2S_{ob}P^2 & \\
 & & & (M_F h_F)P^2 & & -2S_{ob}P^2 \\
+M_A\frac{\cos\psi_o}{K} & +M_A\frac{\sin\psi_o}{K} & +2K\beta - M_A\frac{\cos\psi_o}{K} & +M_A\left(1-\frac{\sin\psi_o}{K}\right) & & \\
-M_A\frac{\sin\psi_o}{K} & +M_A\frac{\cos\psi_o}{K} & -M_A\left(1-\frac{\sin\psi_o}{K}\right) & +2K\beta - M_A\frac{\cos\psi_o}{K} & & \\
-I_G P^2 & & +M_{\dot{G}}P & & & \\
-M_{\dot{G}}P & -J_G\Omega P & & & & \\
-K_G & & +K_G - c_m 2K\beta\frac{\cos\psi_o}{K}\lambda & +c_m 2K\beta\frac{\sin\psi_o}{K}\lambda & & \\
 & -I_G P^2 & & +M_{\dot{G}}P & & \\
+J_G\Omega P & -M_{\dot{G}}P & & & & \\
 & -K_G & -c_m 2K\beta\frac{\sin\psi_o}{K}\lambda & +K_G - c_m 2K\beta\frac{\cos\psi_o}{K}\lambda & & \\
 & & -\left(I_{\theta_F}+M_F h_F^2\right)P^2 & & & \\
+M_{\dot{G}}P & & -M_{\dot{G}}P & & & \\
+K_G & & -2K\beta - K_G & & & \\
 & & & -\left(I_{\phi_F}+M_F h_F^2\right)P^2 & & \\
 & +M_{\dot{G}}P & & -M_{\dot{G}}P & & \\
 & +K_G & & -2K\beta - K_G & & \\
 & & & & -2I_{ob}P^2 & \\
 & & & & & +4\Omega I_{ob}P \\
 & & & & -2K_c + 2\Omega^2\left[I_{ob} - eS_{ob}\right] & \\
 & & & & & -2I_{ob}P^2 \\
 & & & & -4\Omega I_{ob}P & \\
 & & & & & -2K_c + 2\Omega^2\left[I_{ob} - eS_{ob}\right]
\end{bmatrix}
\begin{Bmatrix} X \\ Y \\ \theta_R \\ \phi_R \\ \theta_G \\ \phi_G \\ \theta_F \\ \phi_F \\ \epsilon_X \\ \epsilon_Y \end{Bmatrix}
$$

B

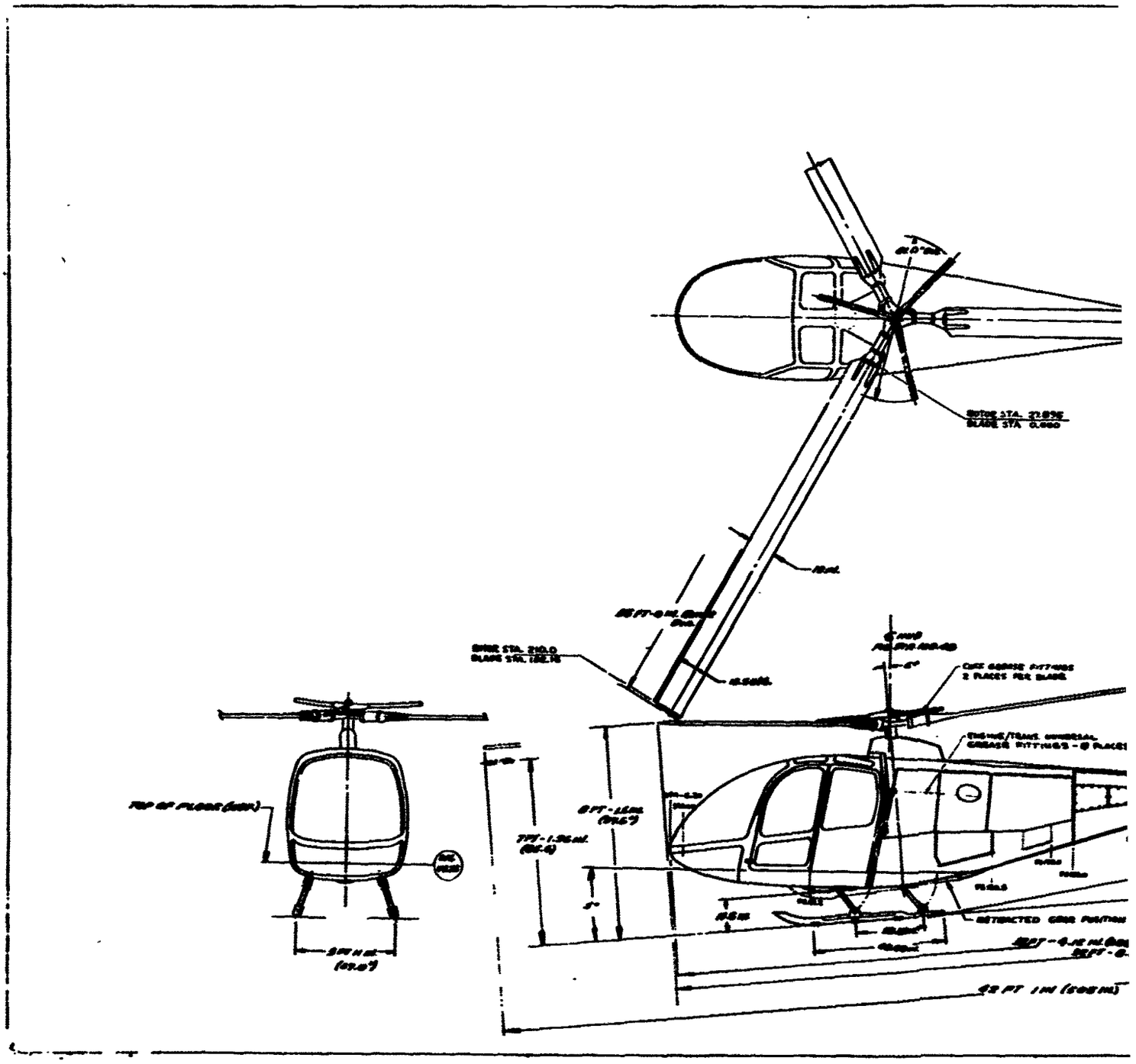

Figure 68. XH-51A General Arrangement.

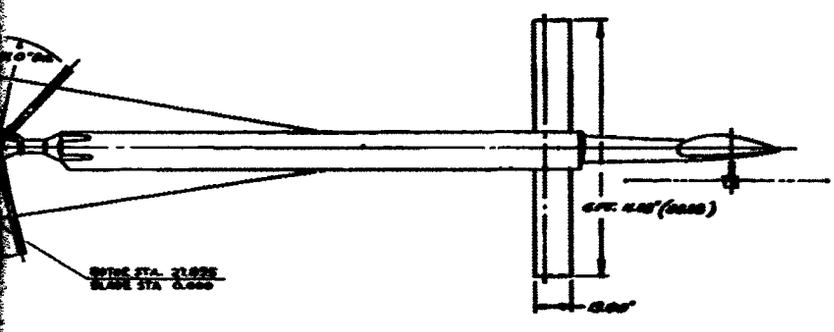

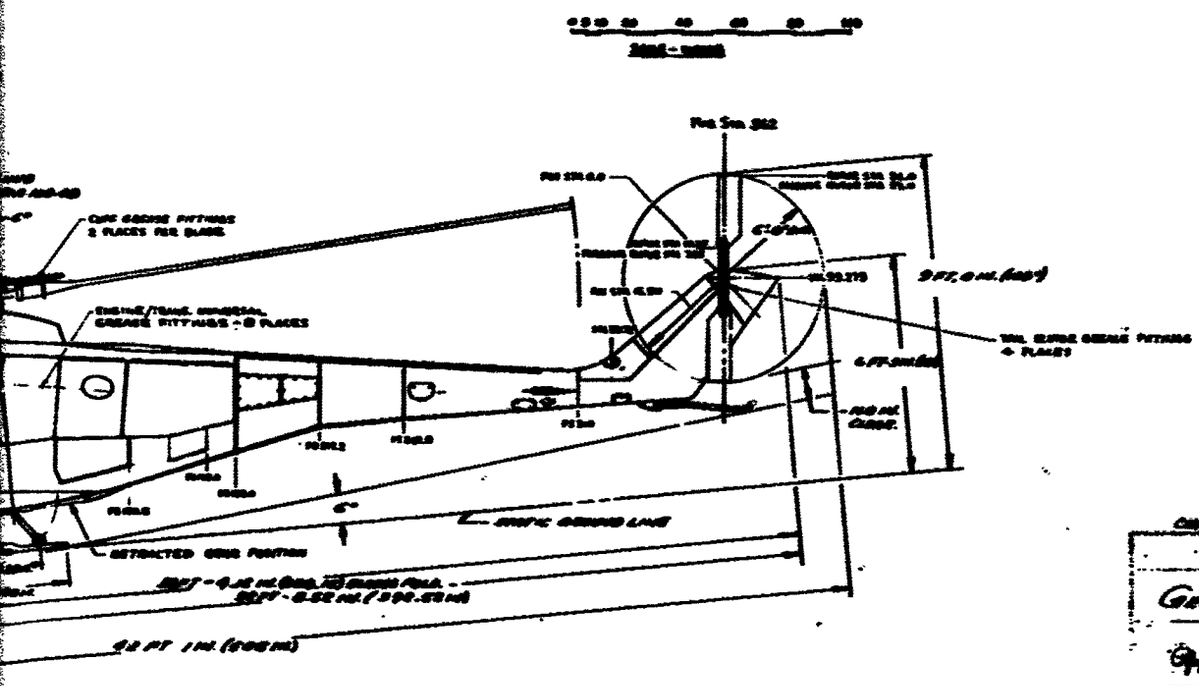

GENERAL ARRANGEMENT

186

540189

B

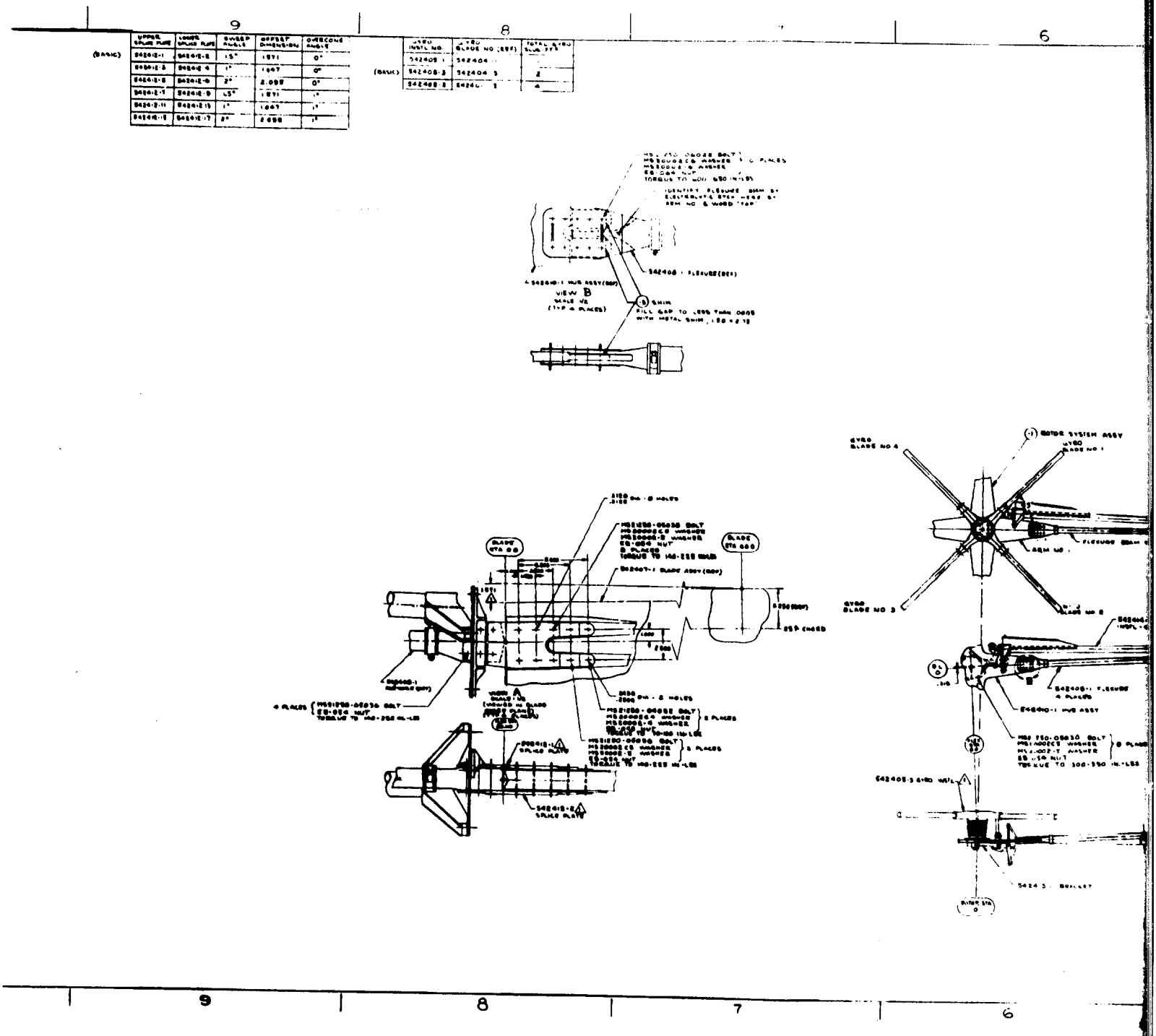

Figure 69. Rotor Assembly.

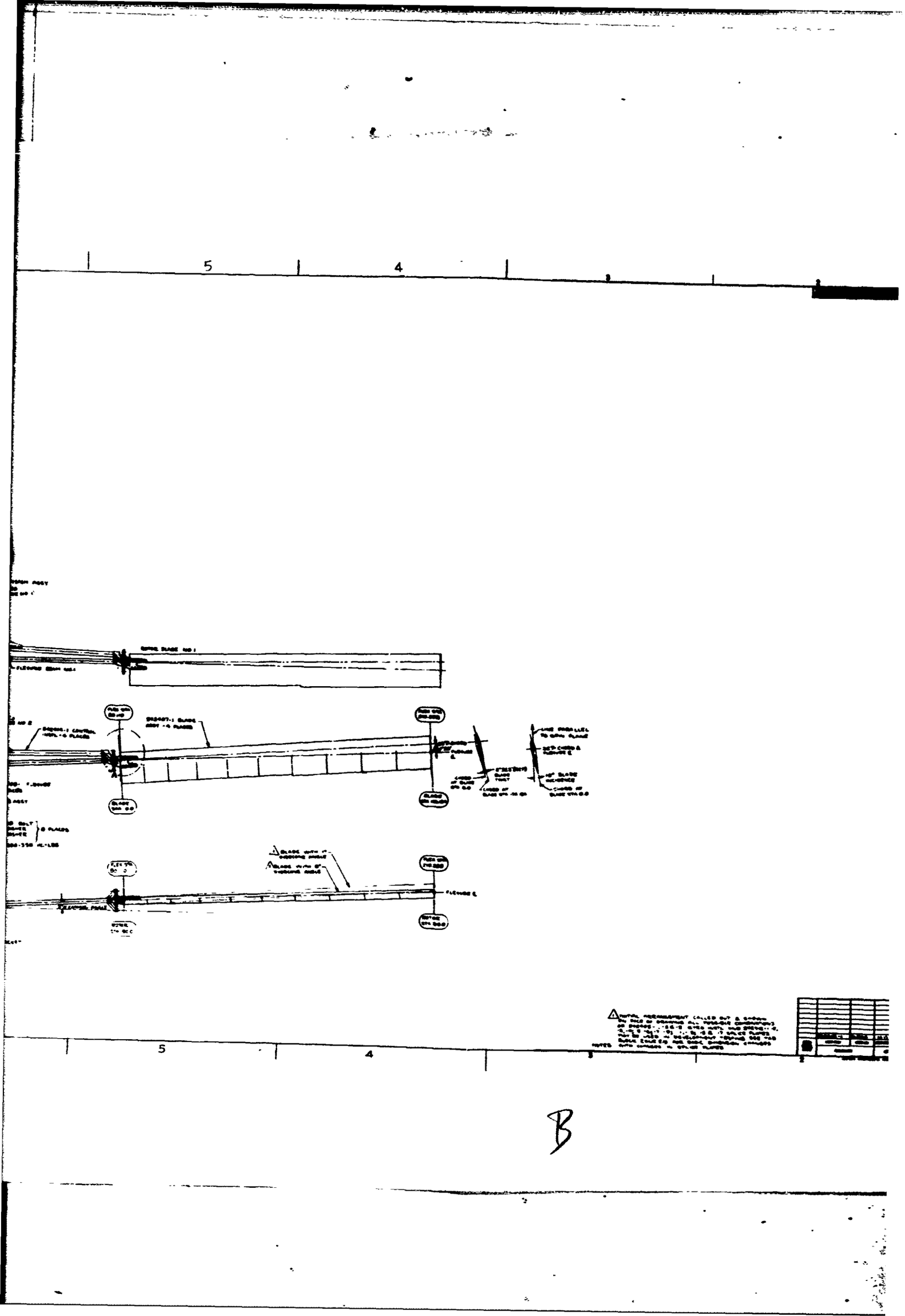
5
4
5
4
B

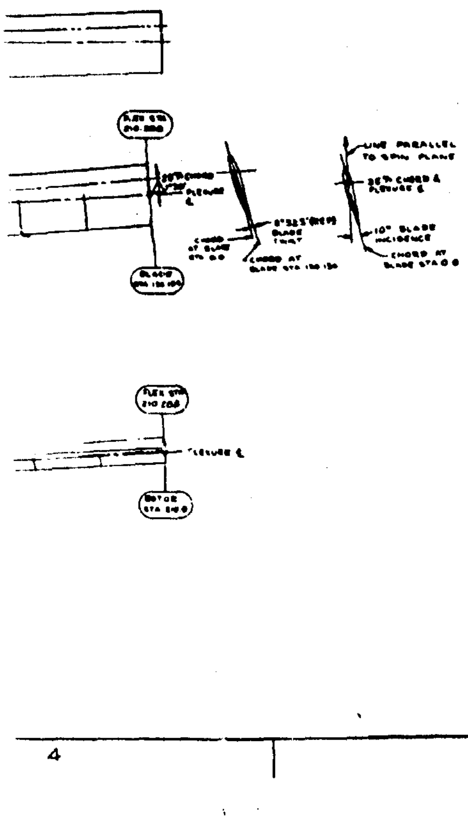

8	NUT	[illegible]	ELASTIC STOP NUT CO.
40	NUT	[illegible]	ELASTIC STOP NUT CO.
64	NUT	[illegible]	ELASTIC STOP NUT CO.
8	BOLT	[illegible]	
40	BOLT	[illegible]	
[illegible]	BOLT	[illegible]	
[illegible]	BOLT	[illegible]	
8	BOLT	[illegible]	
40	WASHER	[illegible]	
48	WASHER	[illegible]	
40	WASHER	[illegible]	
48	WASHER	[illegible]	
8	WASHER	[illegible]	
8	WASHER	[illegible]	
8	SHIM	-8	
1	BRACKET	[illegible]	
4	CONTROL HORN	[illegible]	
4	SPLICE PLATE	[illegible]	
4	SPLICE PLATE	[illegible]	
4	SPLICE PLATE	[illegible]	
4	SPLICE PLATE	[illegible]	
4	SPLICE PLATE	[illegible]	
4	SPLICE PLATE	[illegible]	
4	SPLICE PLATE	[illegible]	
4	SPLICE PLATE	[illegible]	
4	SPLICE PLATE	[illegible]	
4	SPLICE PLATE	[illegible]	
4	SPLICE PLATE	[illegible]	
4	SPLICE PLATE	[illegible]	
1	HUB ASSY	[illegible]	
4	FLEXURE	[illegible]	
4	BLADE ASSY	[illegible]	
1	GYRO ASSY	[illegible]	
1	GYRO ASSY	[illegible]	
1	GYRO ASSY	[illegible]	
	ROTOR SYS ASSY	-1	

NOTES: 1. INITIAL ARRANGEMENT CALLED OUT & SHOWN ON FACE OF DRAWING. ALL POSSIBLE COMBINATIONS [illegible] MAY BE USED IN DEVELOPMENT TESTING [illegible] WITH CHANGES IN SPLICE PLATES

LOCKHEED-CALIFORNIA COMPANY

ROTOR SYSTEM ASSY-MATCHED STIFFNESS

K 542411

Best Available Copy

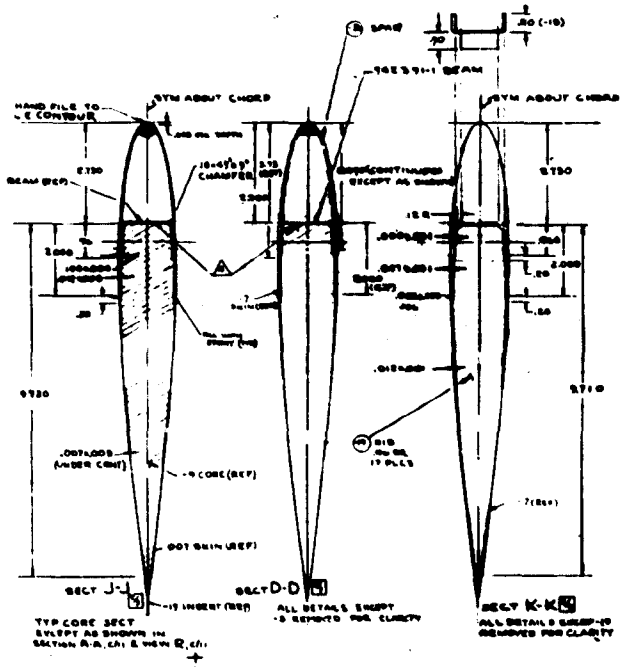

Figure 70. Blade Assembly.

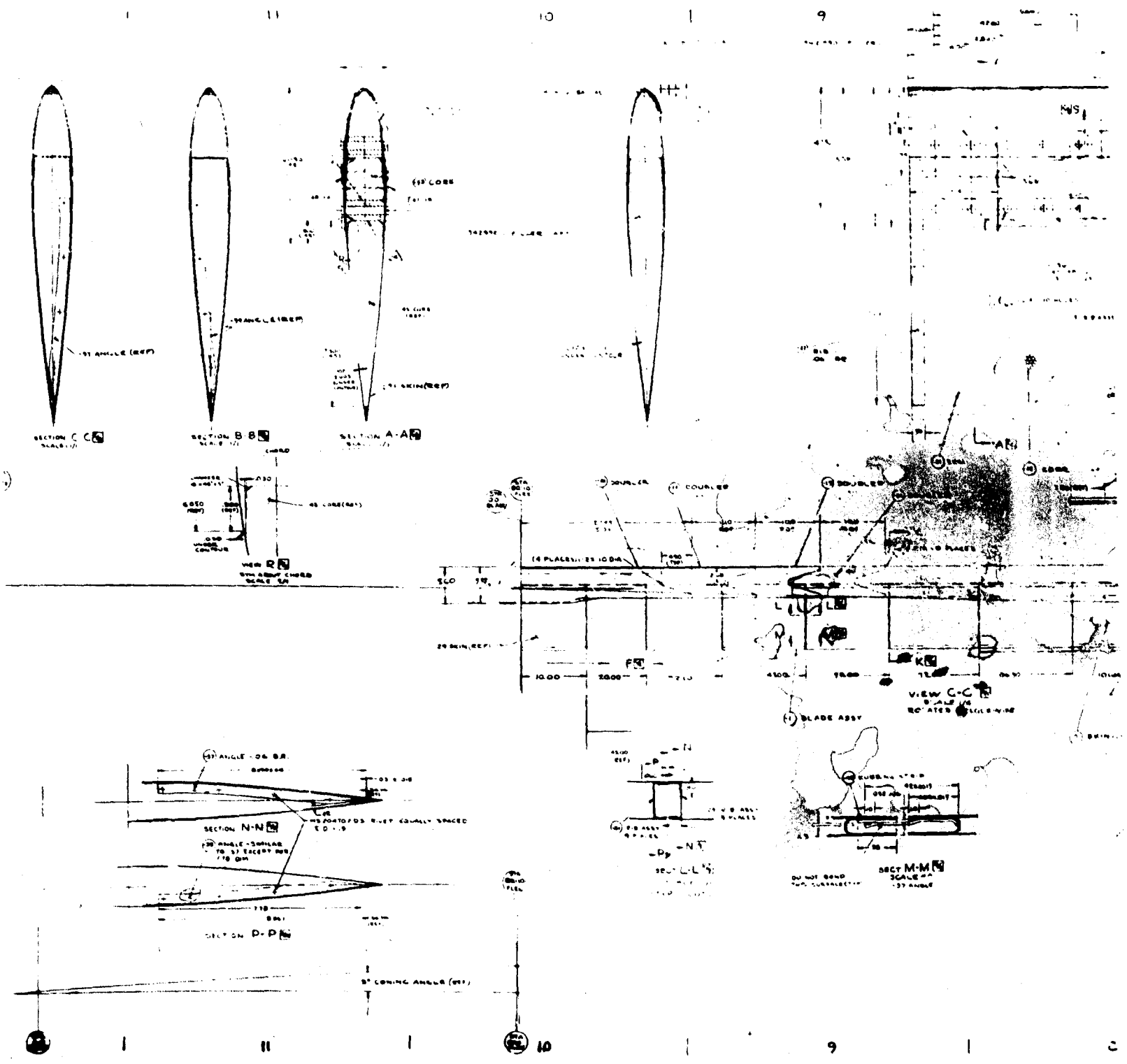

Boat Anchors Copy

B

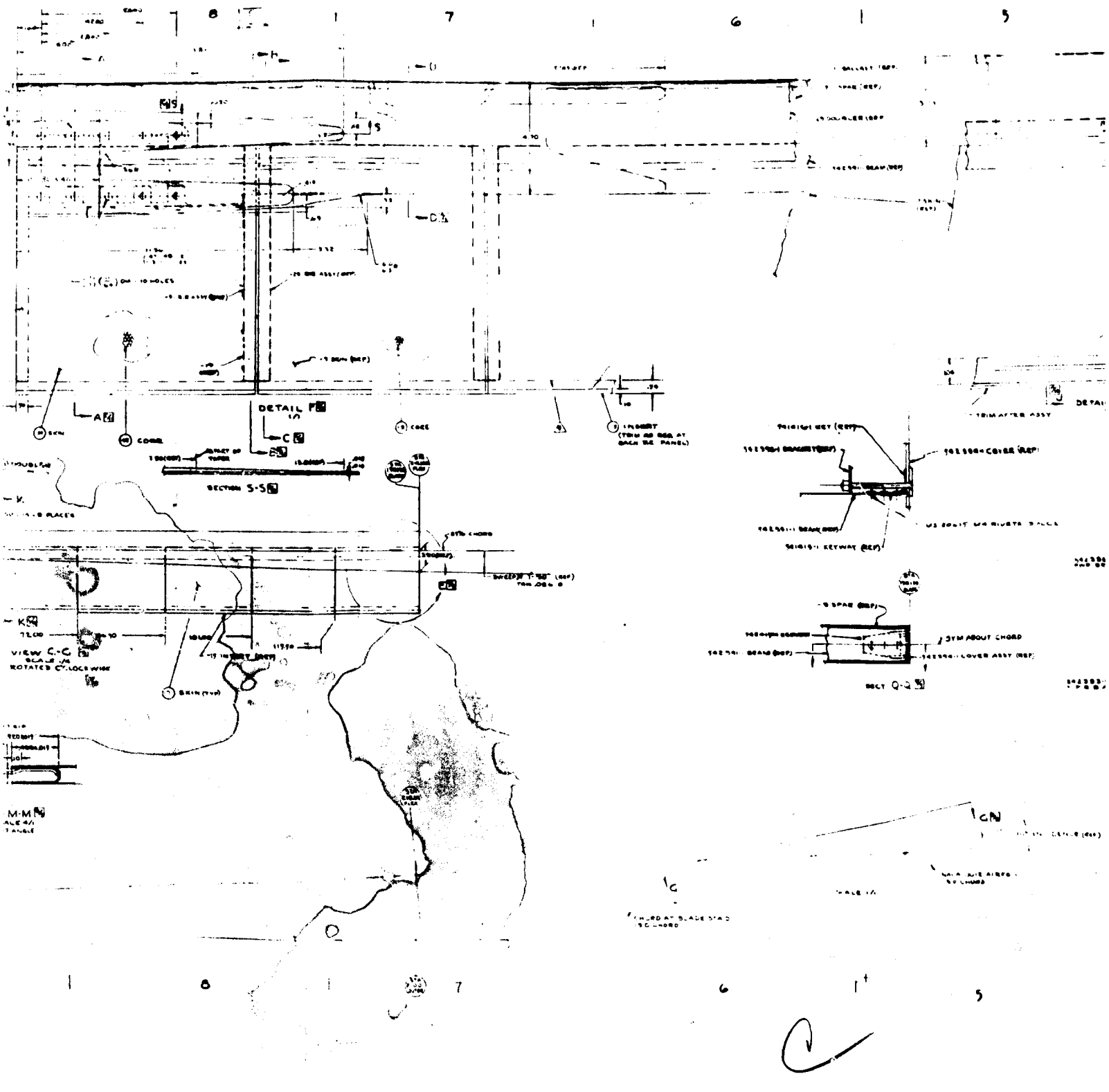
DETAIL F
SECTION S-S
VIEW C-C
SECT Q-Q

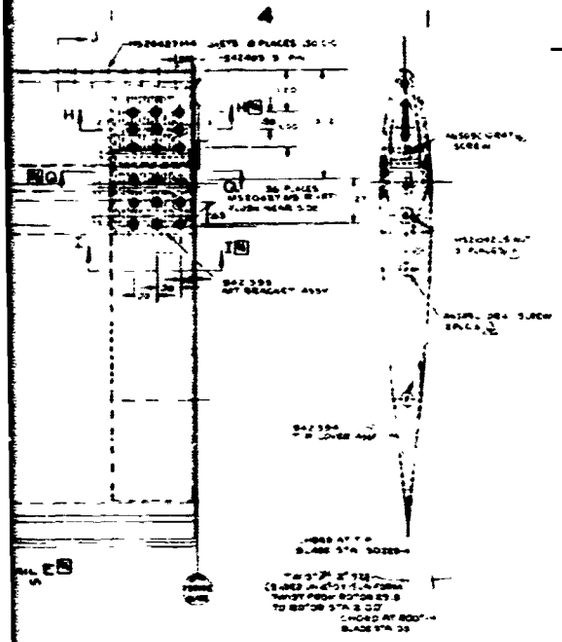

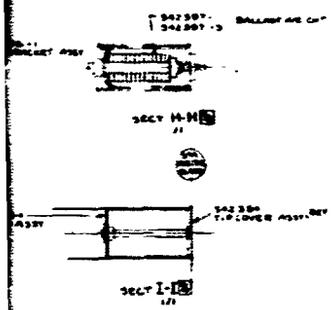

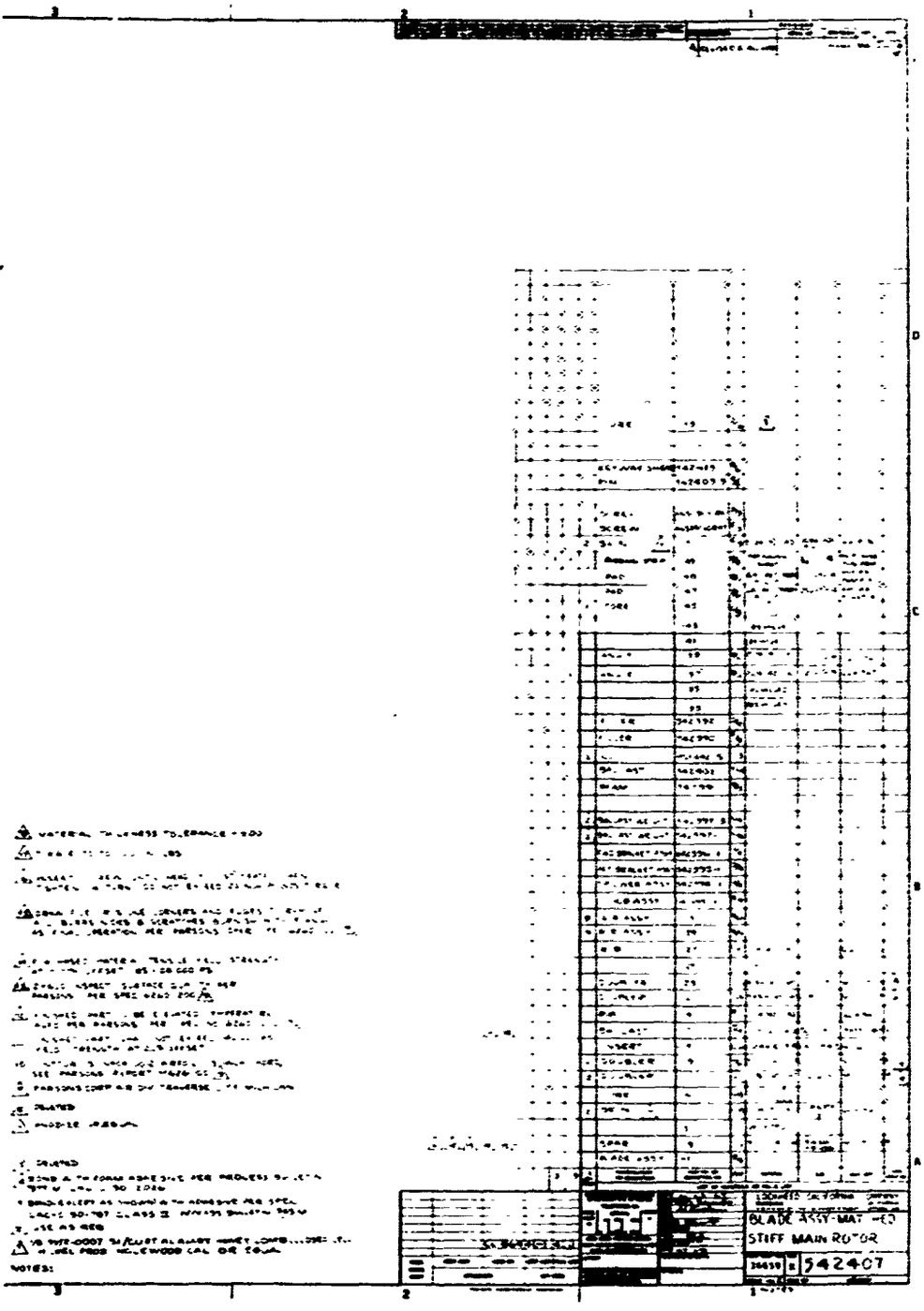

BLADE ASSY-MAT -ED
STIFF MAIN ROTOR
SIZE 36439 542407

D

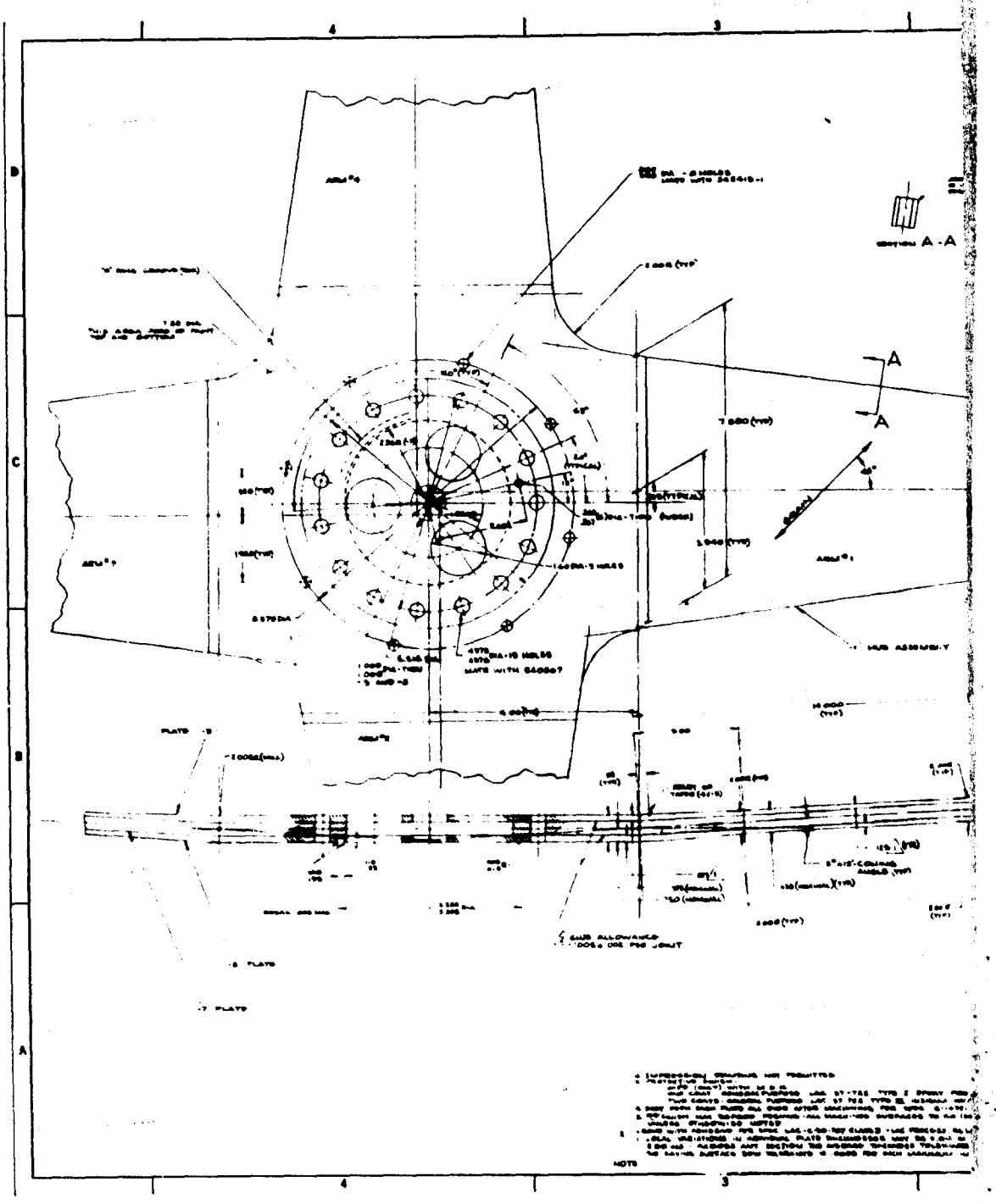

Figure 71. Rotor Hub Assembly.

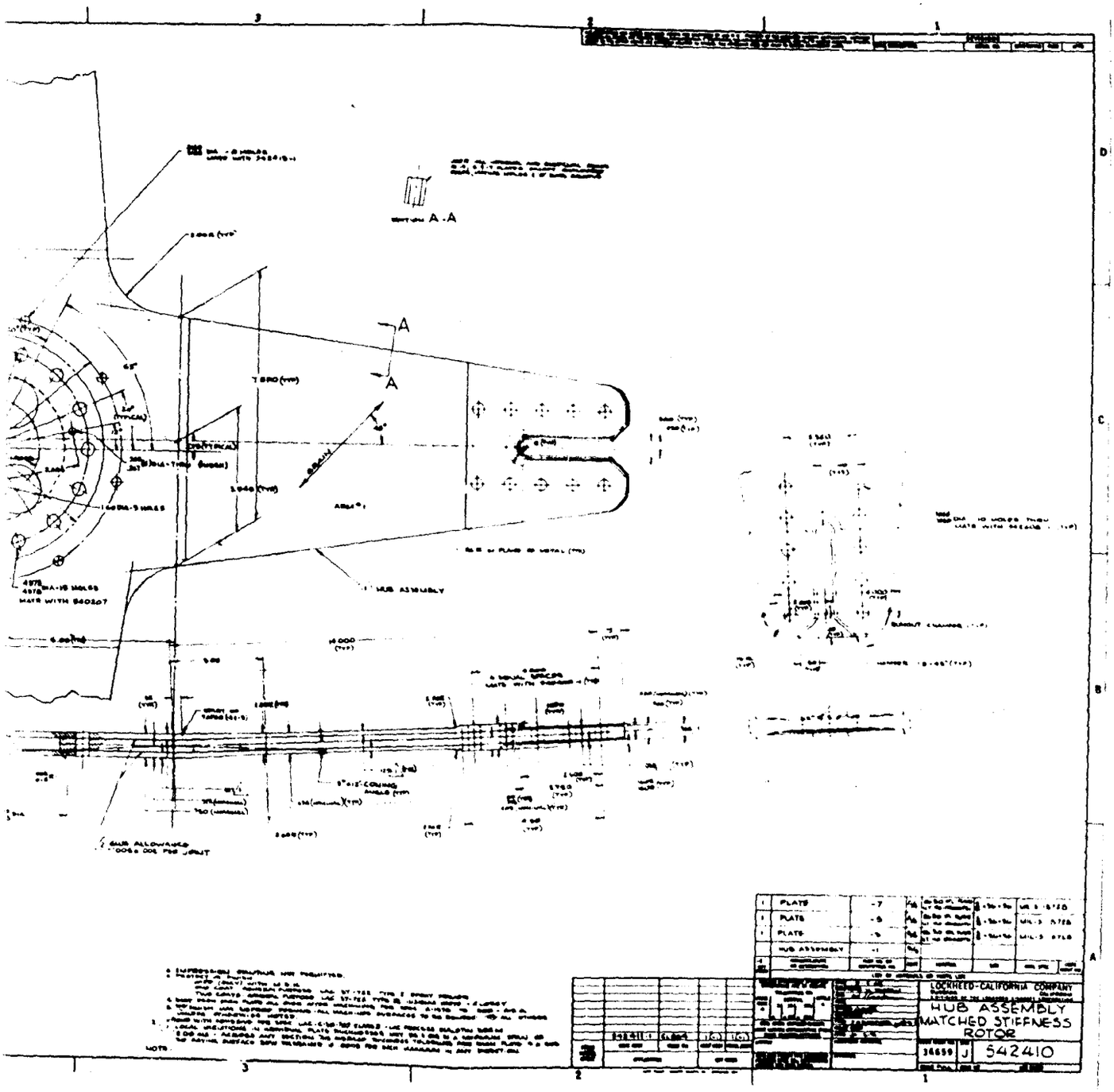

Rotor Hub Assembly.

B

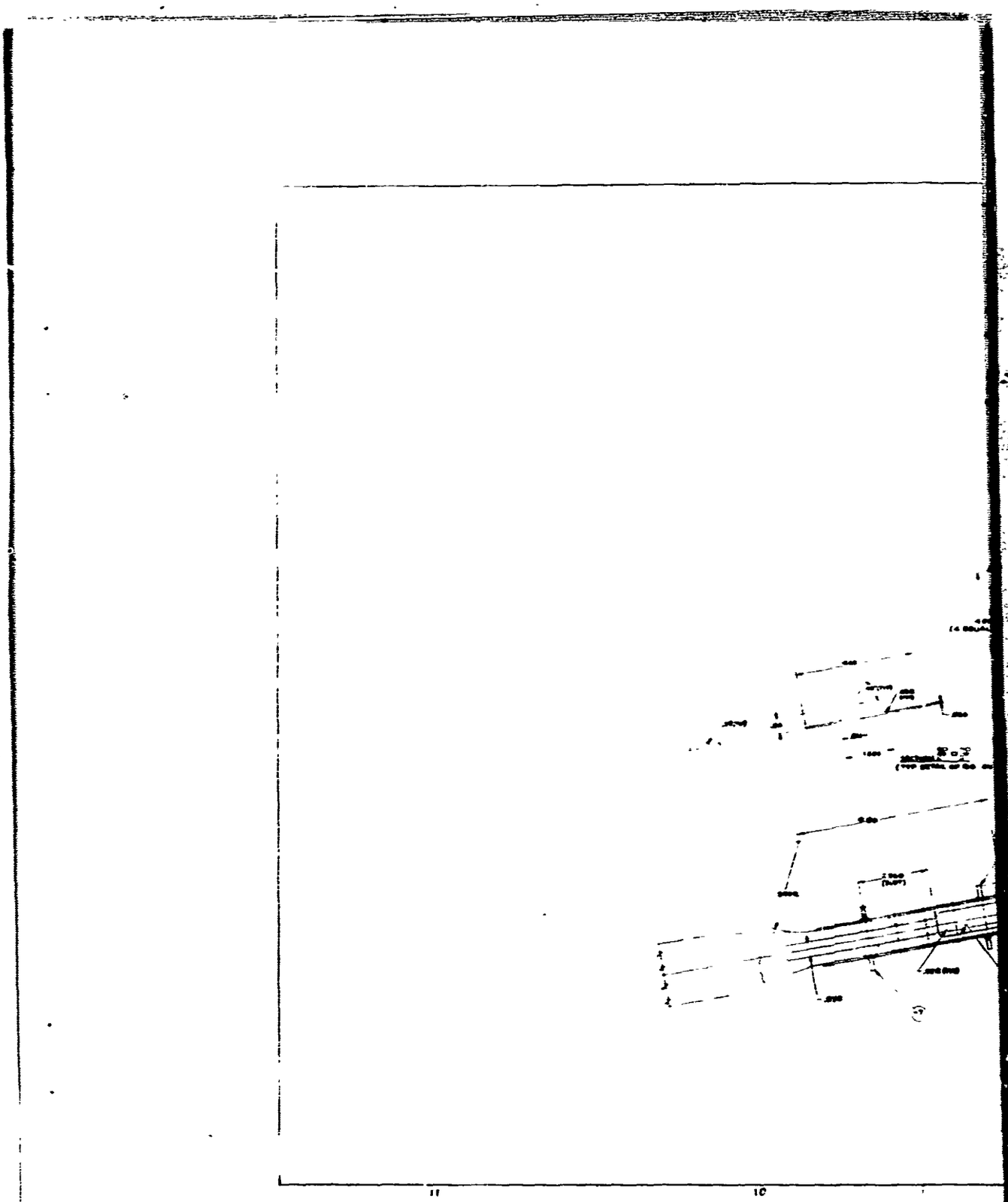

Figure 72. Flexure Beam Assembly.

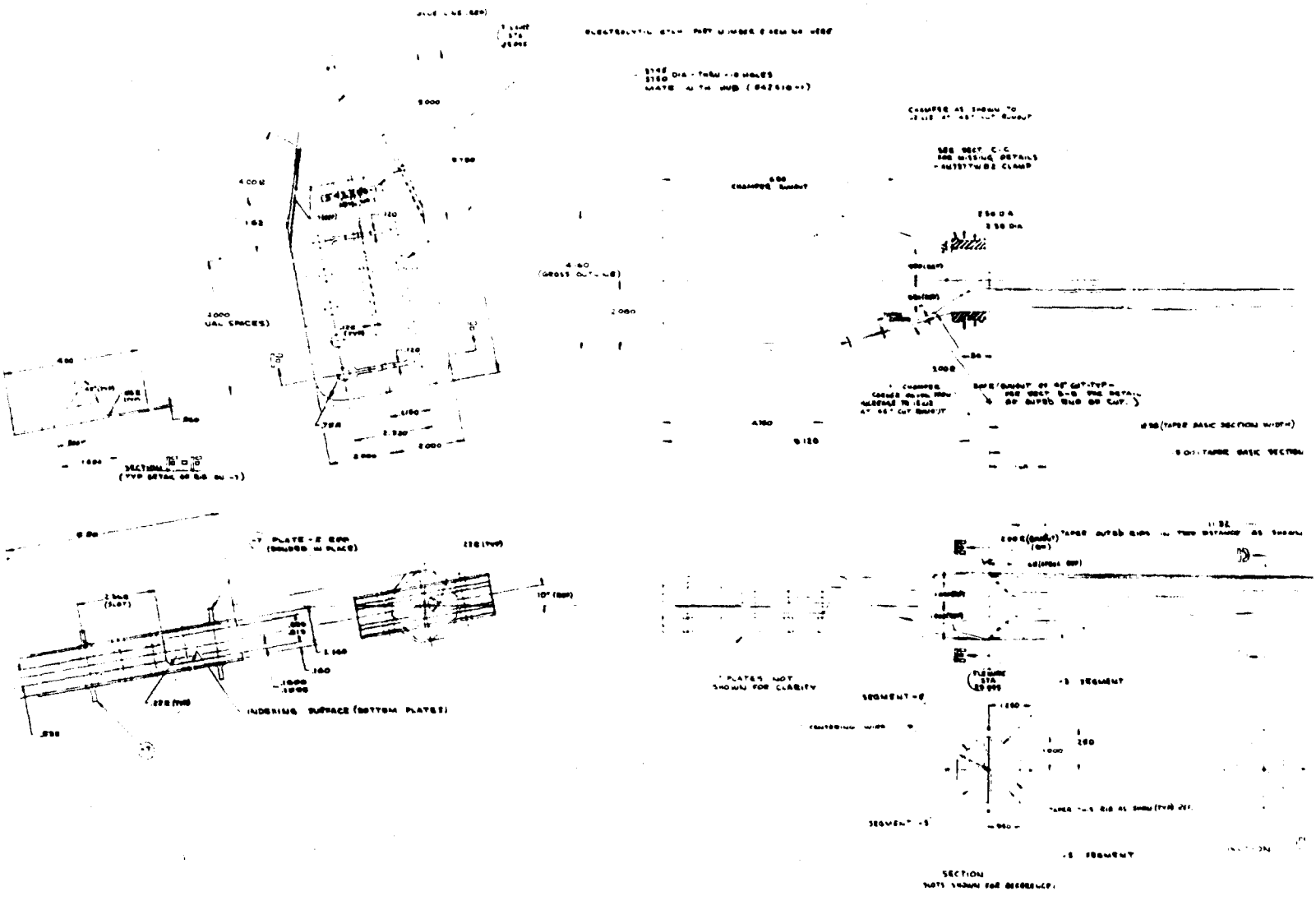

9 8 7

mbly.

B

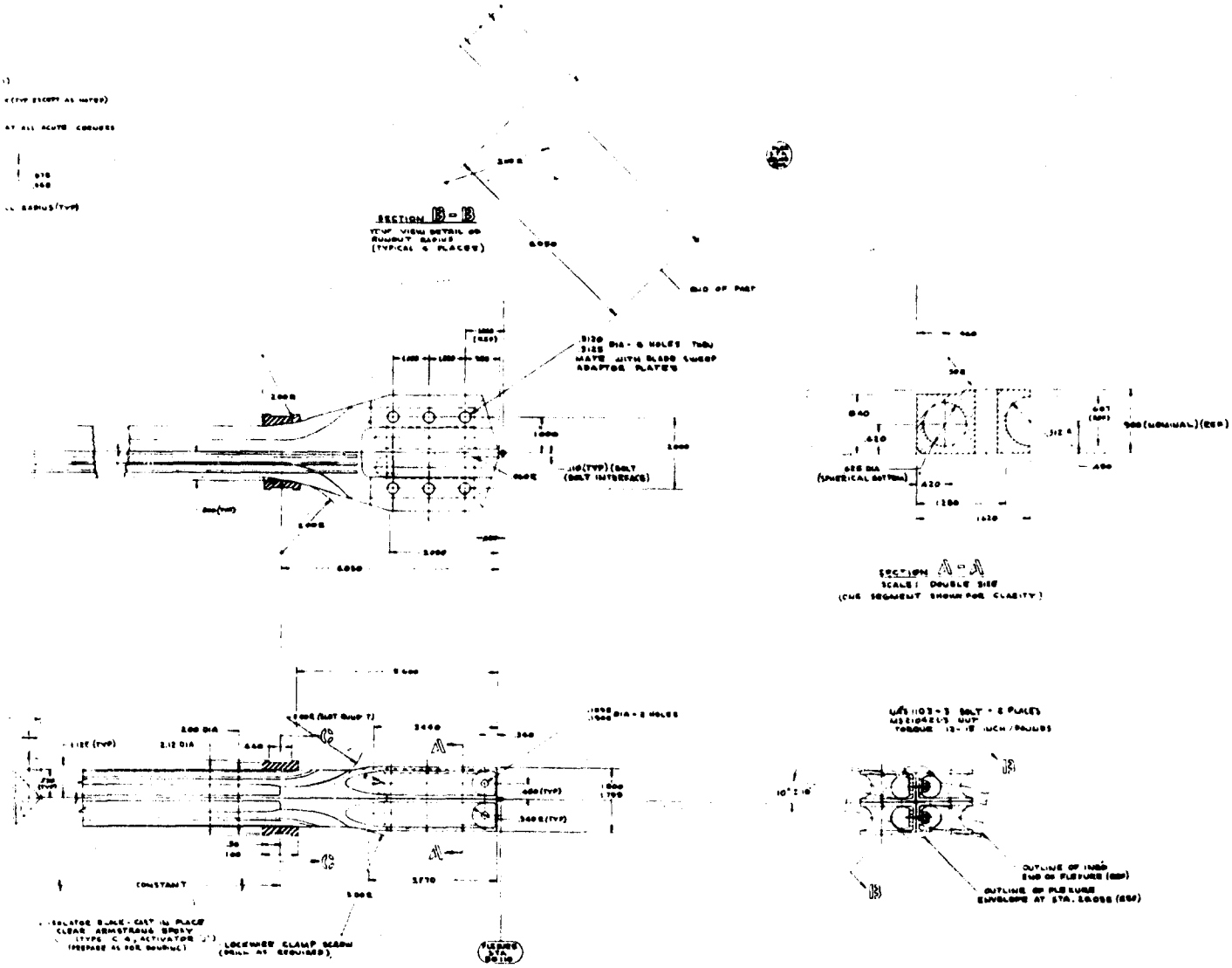

NOTES:

5. INFUSION STAMPING NOT PERMITTED
4. SHOT PEEN COMPLETED ASSY ALL OVER PER SPEC C-1614 TO .005-.012 A, BEFORE INSTALLING EPOXY CLAMP BLADES
3. BOND WITH ADHESIVE PER SPEC. LAC-C-50-787 CLASS II, LAC PROCESS BULLETIN 500 M
2. FINISH ALL MACHINED SURFACES - 63
1. HT TEST COND H-900

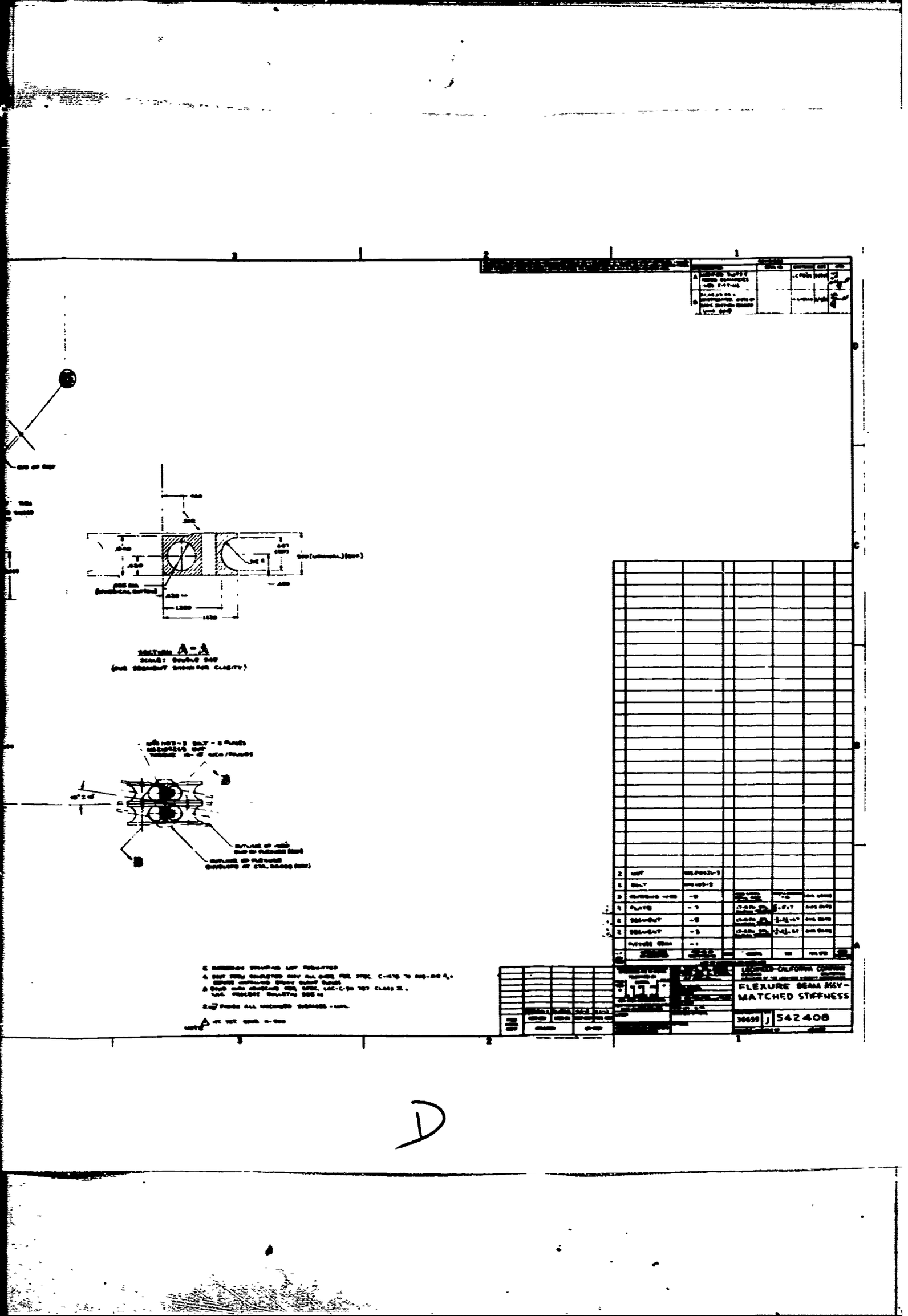
SECTION A-A
SCALE: DOUBLE SIZE
FLEXURE BEAM MAY-
MATCHED STIFFNESS
542408

D

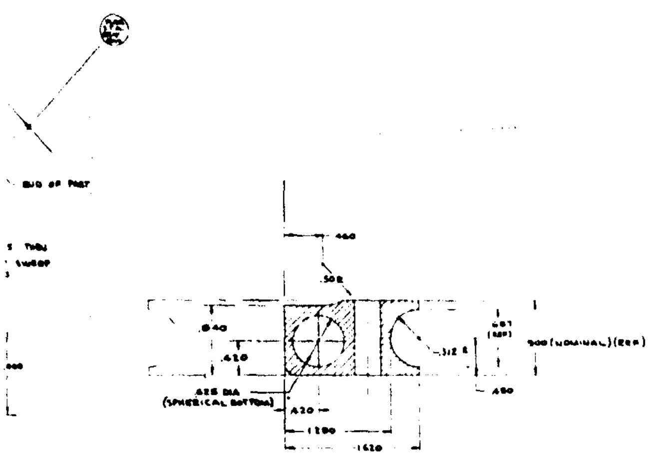

SECTION A-A
SCALE: DOUBLE SIZE
(ONE SEGMENT SHOWN FOR CLARITY)

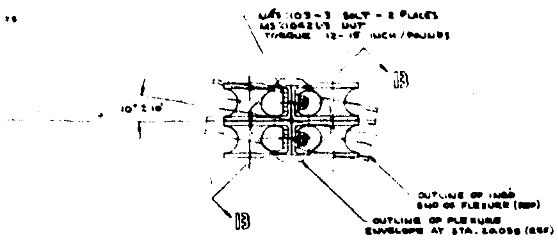

2	NUT	MS21042L-3				
	BOLT					
	CENTERING WIRE	-9				
	PLATE	-7	17-4 PH STL		AMS 5643	
	SEGMENT	-5	17-4 PH STL		AMS 5643	
	SEGMENT	-3	17-4 PH STL		AMS 5643	
	FLEXURE BEAM	-1				

5. IMPRESSION STAMPING NOT PERMITTED
4. SHOT PEEN COMPLETED ASSY ALL OVER PER SPEC
BEFORE INSTALLING EPOXY CLAMP BLOCKS
3. BOND WITH ADHESIVE PER SPEC. LAC-C-30-787 CLASS II,
LAC PROCESS BULLETIN
2. FINISH ALL MACHINED SURFACES
NOTE

LOCKHEED-CALIFORNIA COMPANY
CALIFORNIA

FLEXURE BEAM ASSY - MATCHED STIFFNESS

36650 J 542408

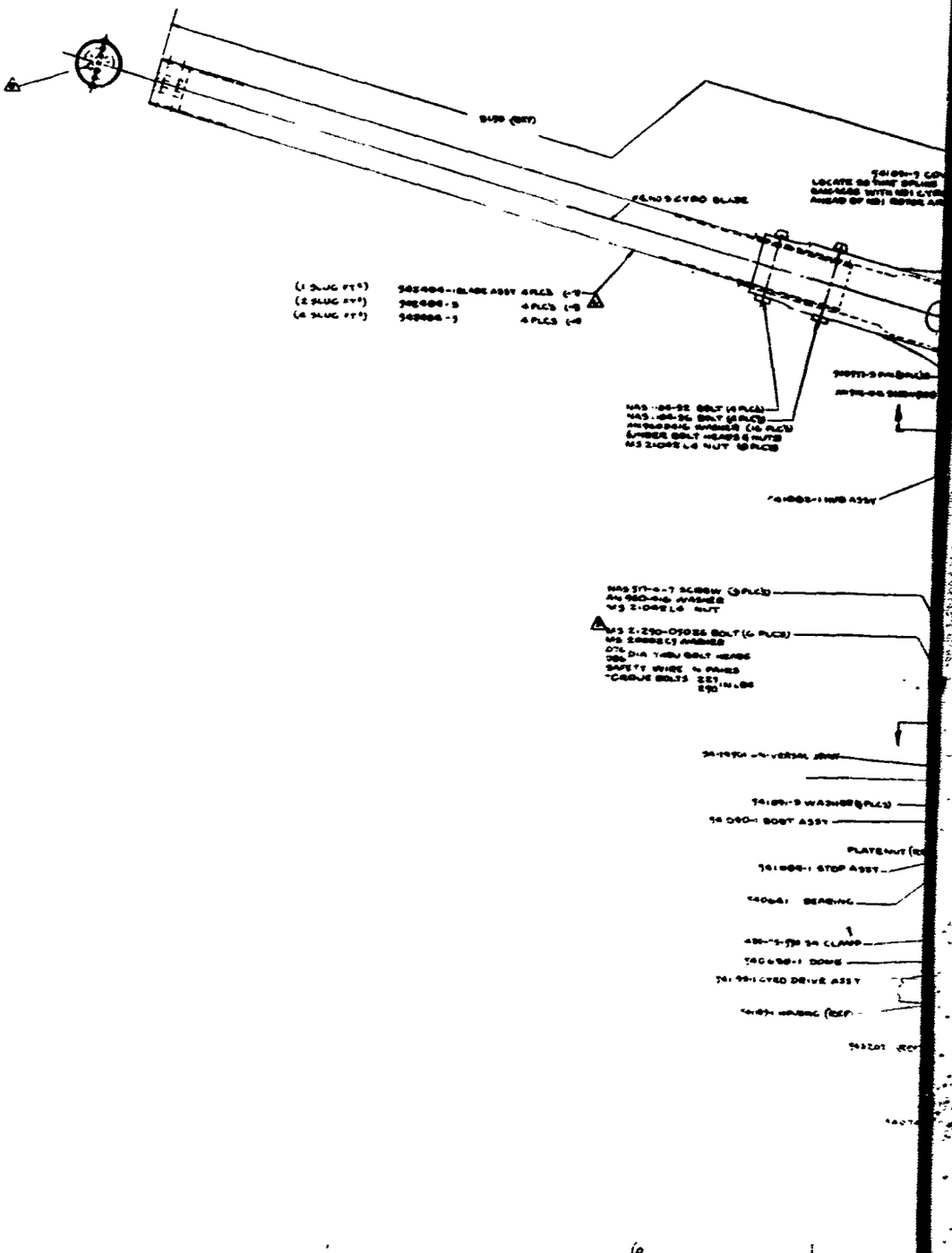

Figure 73. Gyro Assembly.

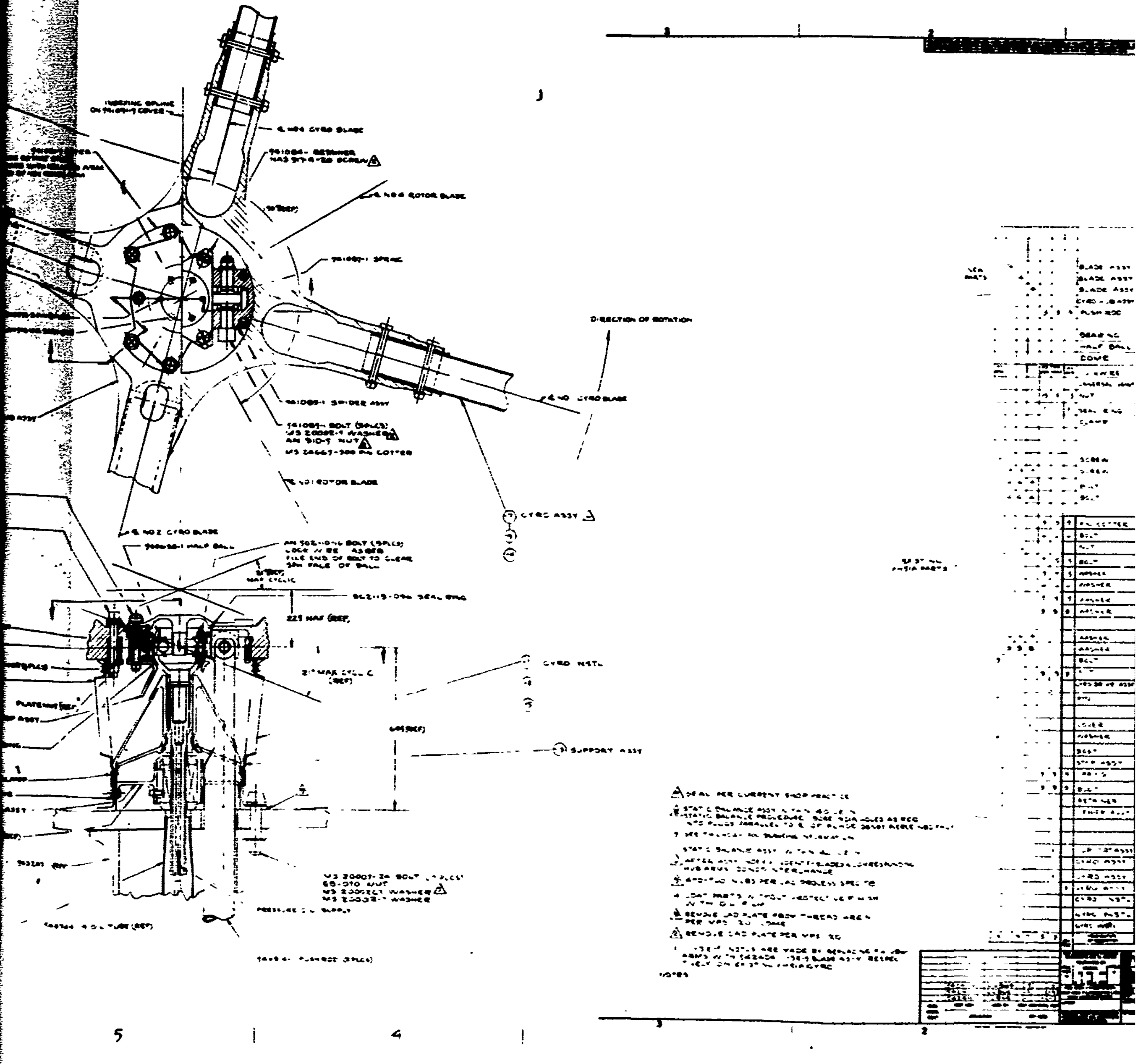
DIRECTION OF ROTATION
GYRO ASSY
GYRO INSTL
SUPPORT ASSY
NOTES
5
4
3
2

B

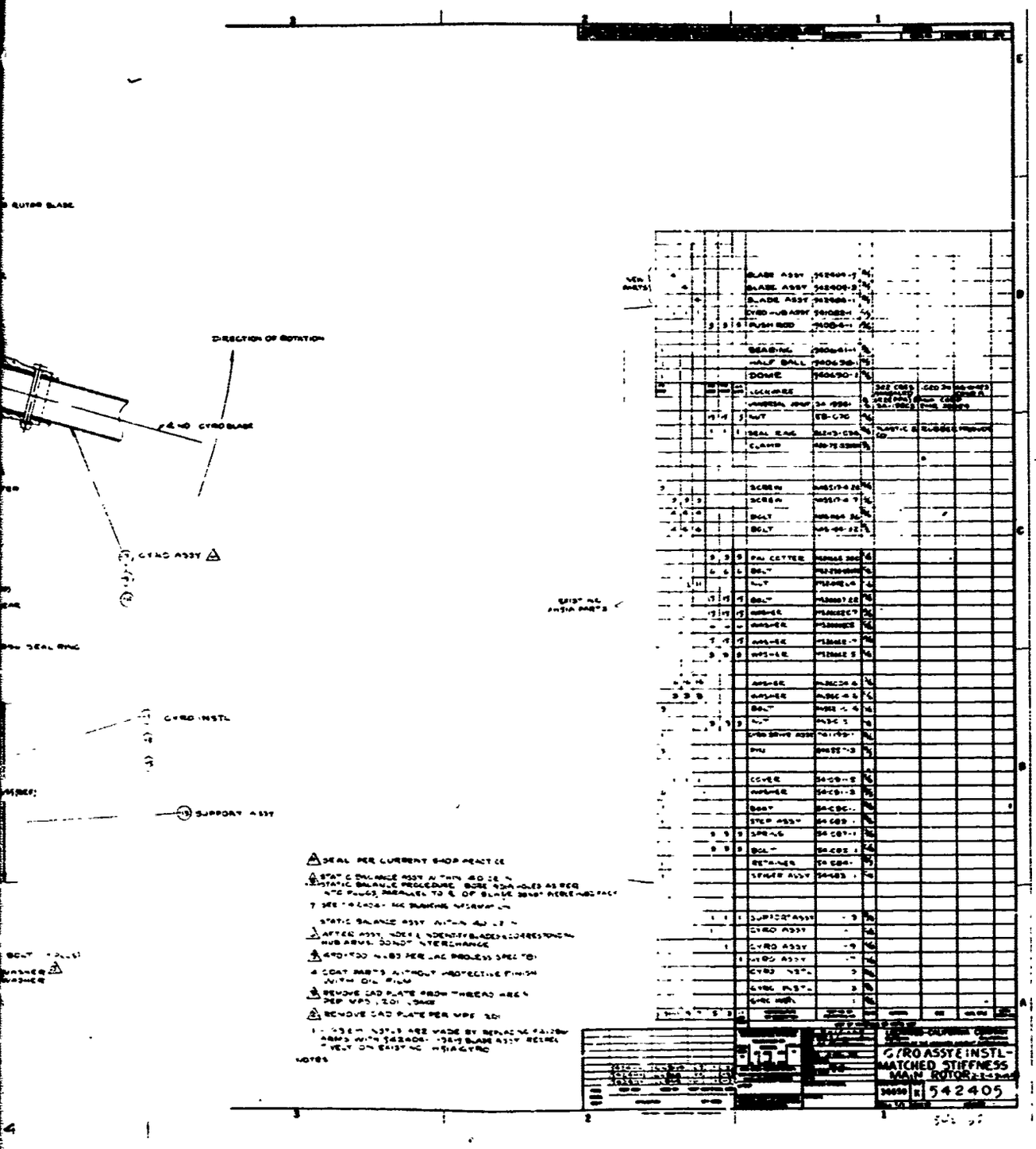
DIRECTION OF ROTATION
CYRO ASSY
CYRO INSTL
SUPPORT ASSY
SEAL PER CURRENT SHOP PRACTICE
AFTER ASSY, MARK IDENTIFY BLADES CORRESPONDING HUB ARMS TO PREVENT INTERCHANGE
4 COAT PARTS WITHOUT PROTECTIVE FINISH WITH OIL FILM
REMOVE LAD PLATE FROM THREAD AREA PER VPS
REMOVE LAD PLATE PER VPS
NOTES
GYRO ASSY INSTL-
MATCHED STIFFNESS
MAIN ROTOR
542405

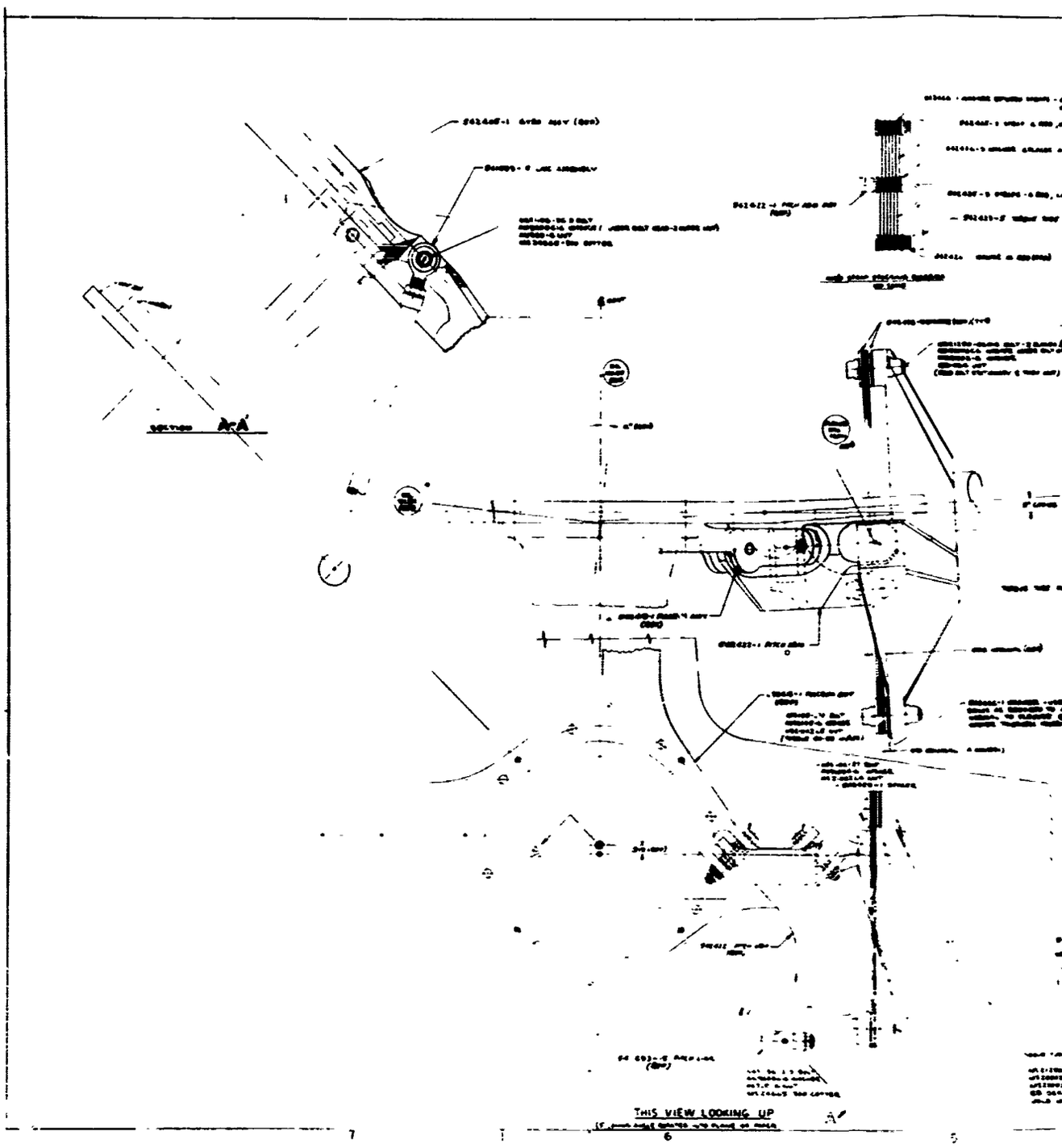

Figure 74. Controls Assembly.

A

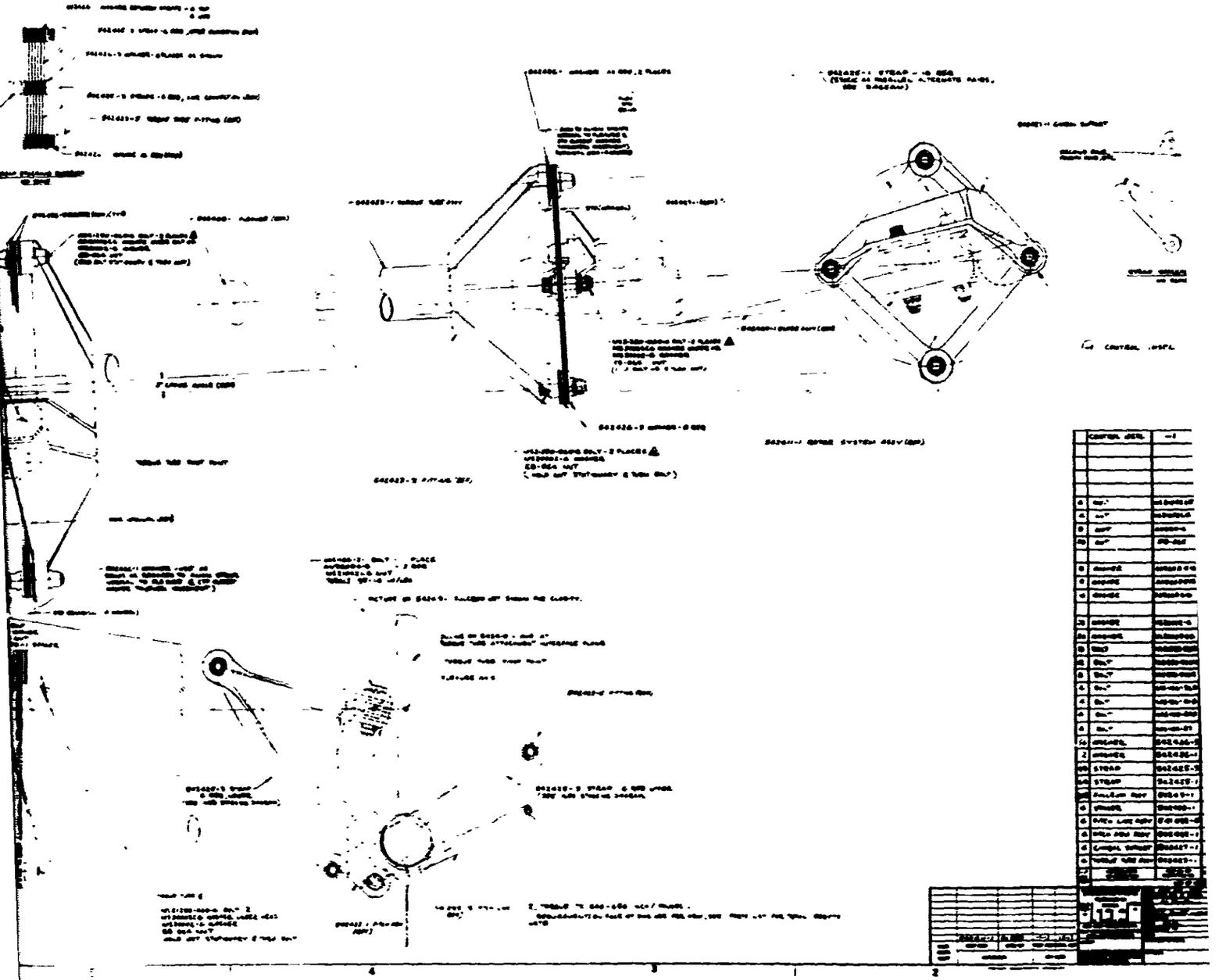

B

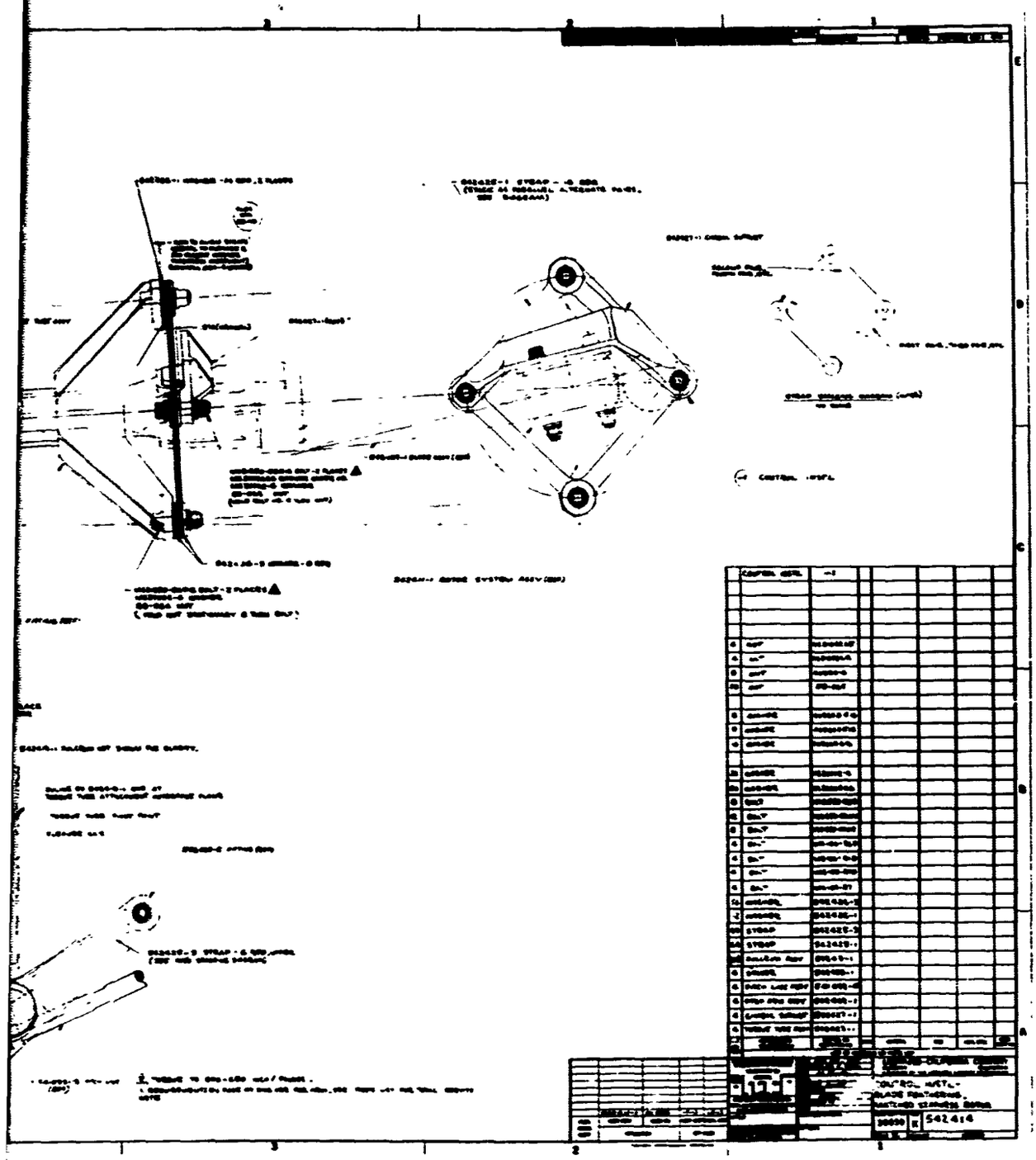

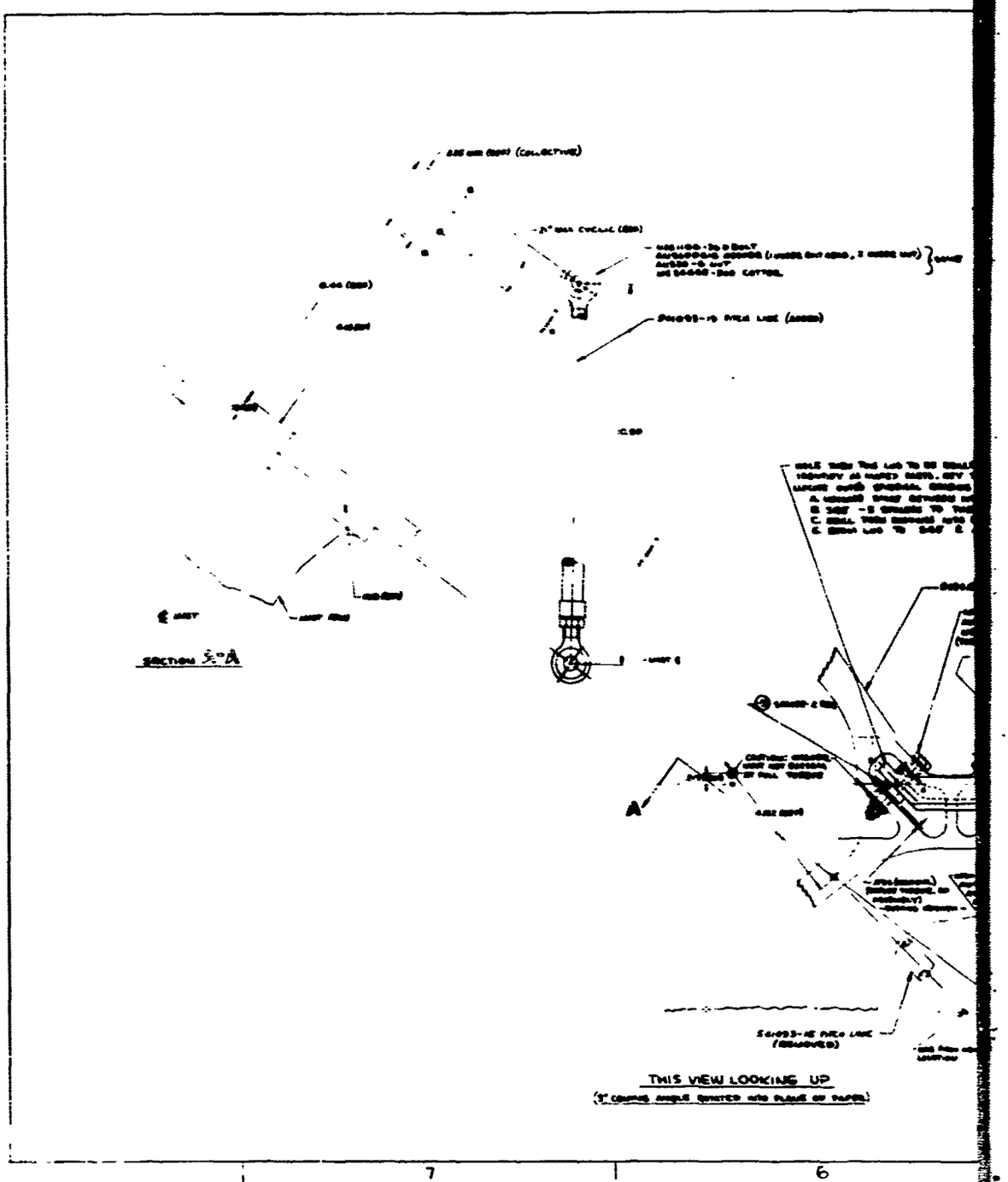

Figure 75. Rework - Control Installation, Blade Feathering/Coupling.

A

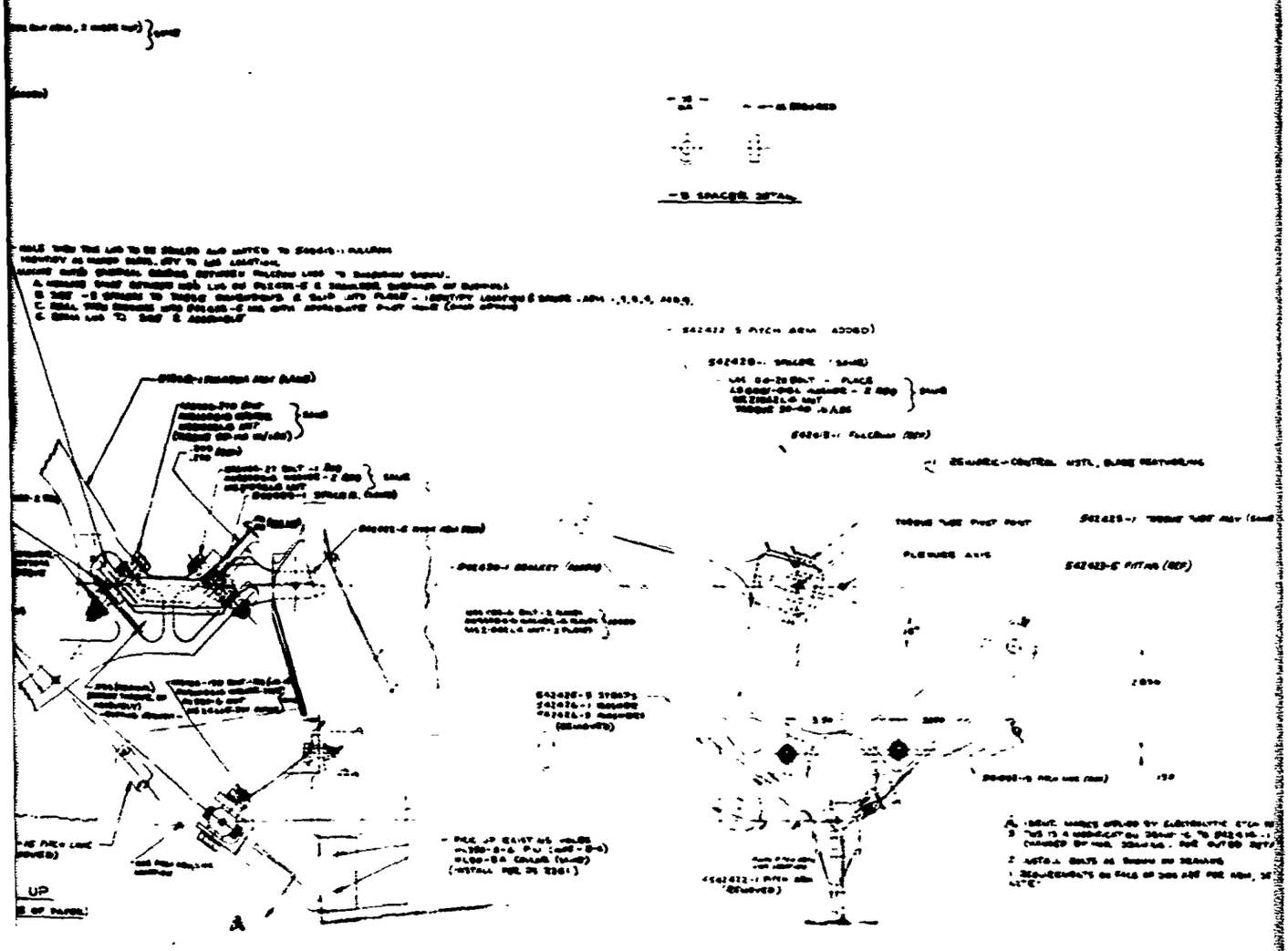

6 5 4 3

B

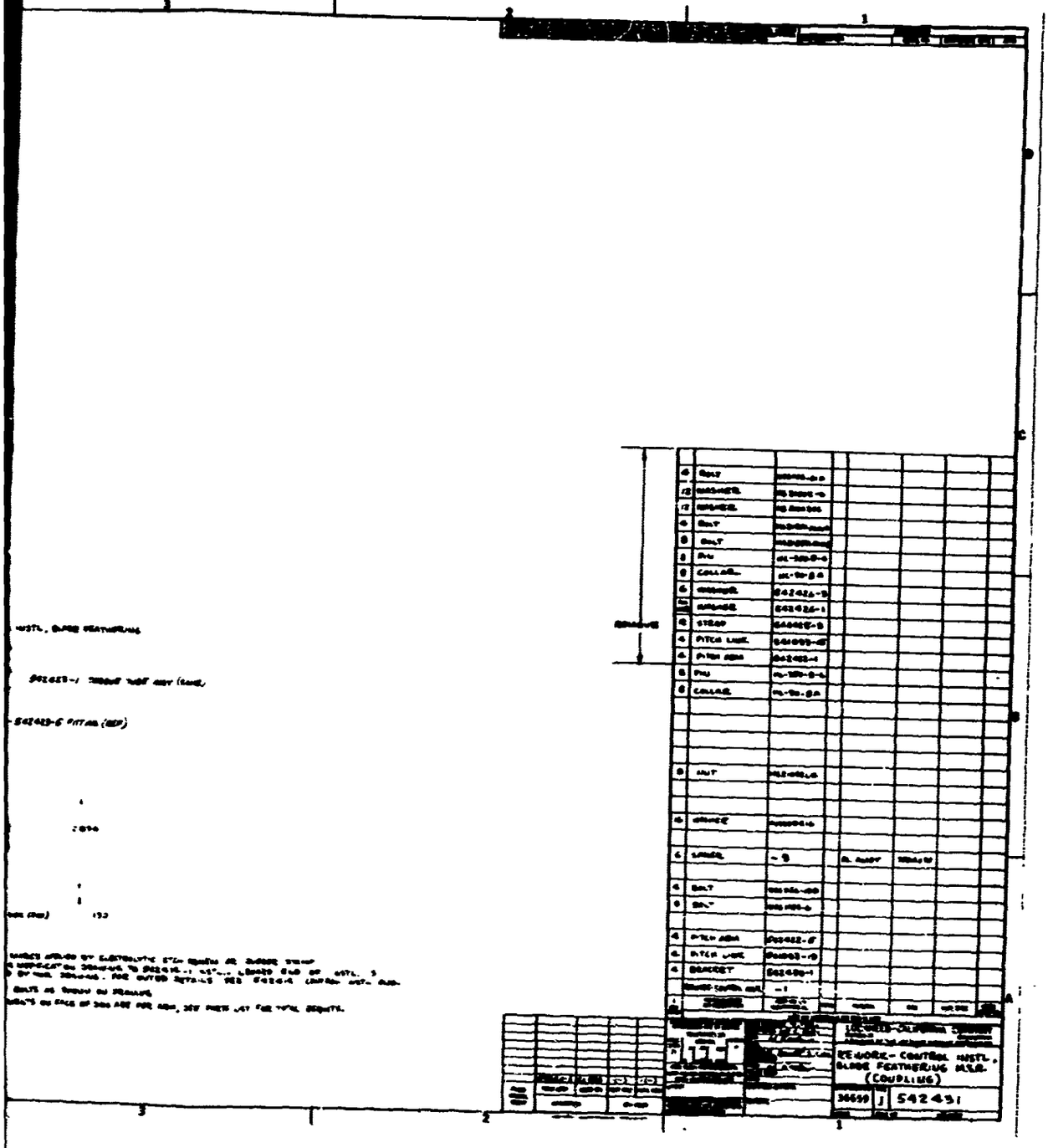
REQUIRED - CONTROL INSTL., BLADE FEATHERING MECH. (COUPLING)
30659
542431

UNCLASSIFIED

Security Classification

DOCUMENT CONTROL DATA - R & D

(Security classification of title, body of abstract and indexing annotation must be entered when the overall report is classified)

1. ORIGINATING ACTIVITY (Corporate author) Lockheed-California Company A Division of Lockheed Aircraft Corporation Burbank, California	2a. REPORT SECURITY CLASSIFICATION UNCLASSIFIED 2b. GROUP

3. REPORT TITLE

SOFT IN-PLANE MATCHED-STIFFNESS/FLEXURE-ROOT-BLADE ROTOR SYSTEM SUMMARY REPORT

4. DESCRIPTIVE NOTES (Type of report and inclusive dates)

Final Report

5. AUTHOR(S) (First name, middle initial, last name)

Salvatore V. Cardinale

6. REPORT DATE	7a. TOTAL NO. OF PAGES	7b. NO. OF REFS
August 1969	173	9

8a. CONTRACT OR GRANT NO. DA 44-177-AMC-244(T) b. PROJECT NO. Task 1F162204A13903 c. d.	9a. ORIGINATOR'S REPORT NUMBER(S) USAAVLABS Technical Report 68-72 9b. OTHER REPORT NO(S) (Any other numbers that may be assigned this report) Lockheed Report 19556

10. DISTRIBUTION STATEMENT

This document is subject to special export controls and each transmittal to foreign governments or foreign nationals may be made only with prior approval of US Army Aviation Materiel Laboratories, Fort Eustis, Virginia 23604.

11. SUPPLEMENTARY NOTES	12. SPONSORING MILITARY ACTIVITY
	U.S. Army Aviation Materiel Laboratories Fort Eustis, Virginia

13. ABSTRACT

A flight research program was conducted to explore feasibility and operating characteristics of a matched-stiffness rigid rotor which was designed to have sufficient torsional flexibility to eliminate the need for feathering bearings. The desired stiffness characteristics involved the use of low in-plane stiffness. An analytical and experimental research program was conducted in which the test rotor was flown on an XH-51A helicopter. The report discusses design, analysis, ground testing, and flight testing aspects of the program. The report also includes a review of features that make a matched-stiffness rotor attractive.

Mechanical instability characteristics of the soft-in-plane rotor were analyzed and tested for both in-flight and on-the-ground conditions. The effects of pitch-flap and pitch-lag mechanical coupling were analyzed and tested. Some promise is indicated for significant benefit to be gained from the use of mechanical coupling, but will involve additional research, beyond the scope of this program, to provide conclusive data.

The limited range of safe operating rotor speeds established by this program is reason to conclude that the safe in-plane matched-stiffness concept is not yet ready for practical use.

DD FORM 1 NOV 68 1473 REPLACES DD FORM 1473, 1 JAN 64, WHICH IS OBSOLETE FOR ARMY USE.

UNCLASSIFIED

Security Classification